AIRESEARCH MANUFACTURING COMPANY OF CALIFORNIA
A DIVISION OF THE GARRETT CORPORATION
2525 WEST 190TH STREET • TORRANCE, CALIFORNIA 90509

HYPERSONIC RESEARCH ENGINE PROJECT - PHASE II AEROTHERMODYNAMIC INTEGRATION MODEL (AIM) TEST REPORT

DATA ITEM NO. 63.06
NASA CONTRACT NO. NAS1-6666

Document No. AP-74-10784

Number of pages 201

Original date 19 May 1975

Prepared by W. L. Andersen and L. Kado

Edited by L. F. Jilly

Approved by E N Harris
Edward N. Harris
HRE Program Manager

Revision	Date	Pages Affected (Revised, Added, Eliminated)

CONTENTS

CONTENTS (Continued)

CONTENTS (Continued)

ILLUSTRATIONS

ILLUSTRATIONS (Continued)

ILLUSTRATIONS (Continued)

TABLES

I. INTRODUCTION

This report describes the test performed on the Hypersonic Research Engine - Aerothermodynamic Integration Model (HRE-AIM) in the Hypersonic Tunnel Facility (HTF) located at NASA Lewis Research Center (NASA/LeRC), Plum Brook Station, Sandusky, Ohio.

The HRE-AIM was designed, fabricated, and tested under contract NAS 1-6666 for NASA Langley Research Center (NASA/LaRC), Hampton, Virginia, by AiResearch Manufacturing Company division of The Garrett Corporation, Los Angeles, California.

The design of the HRE-AIM was initiated with the intention of utilizing the wind tunnel facility located at the Ordnance Aerophysics Laboratory (OAL) in Dangerfield, Texas. However, prior to the time the design and the fabrication of the HRE-AIM was completed, OAL facility was closed and NASA/LeRC was selected as an alternate source. Use of NASA/LeRC test facility resulted in some compromises in terms of installation, recording of pressure and temperature data and to test operational procedures.

A total of 52 test runs was made, 36 runs at Mach 6, 11 runs at Mach 7 and 5 runs at Mach 5, with an accrued time of 111 min, 44 sec in the hypersonic environment.

The objective of this report is to describe the HRE-AIM, its installation in the wind tunnel facility, test conditions to which the HRE-AIM was subjected, and observation made during tests. Analysis of the extensive data obtained will be submitted under a separate report.

Test data, as such, is not presented in this report since all data obtained were transmitted to NASA/LaRC and are on file at the Hypersonic Research Engine Project office.

I.1 OBJECTIVE AND SCOPE

The objective of the HRE-AIM program was to verify the feasibility of integrating the various analytical and experimental data available for the design of the Hypersonic Ramjet Engine and to evaluate the overall engine performance, component interaction,and ignition limits for the design selected. The scope of the test program was to determine the following:

(a) Evaluate and optimize supersonic and subsonic combustion mode utilizing heated hydrogen fuel.

(b) Determine ignition limits.

(c) Demonstrate capability to make a transition from subsonic combustion to supersonic combustion and return to subsonic combustion mode.

(d) Evaluate combustion hysteresis.

(e) Determine effect of engine performance when the centerline of the HRE-AIM is at a 3-deg nose-up attitude in respect to the hypersonic slipstream.

1.2 APPLICABLE DOCUMENTS

(a) NASA Statement of Work L-4947B, revised 3 September 1968.

(b) HRE/AIM Test Plan, Data Item 2-2.01 AiResearch Report No. AP-71-7877.

(c) HRE/AIM Measurement Plan, Data Item 2-1.01 AiResearch Report No. AP-70-6216.

1.3 SUMMARY DESCRIPTION OF HRE-AIM AND TEST SUPPORT EQUIPMENT

The aerodynamics design of the HRE-AIM was based on information obtained from research programs performed by AiResearch and government-sponsored activities. The HRE-AIM measured approximately 90 in. long and 27.5 in. in diameter and weighed approximately 2,400 lb. The design incorporated an axisymmetric inlet and utilized a translating spike assembly to control mass flow of air through the engine to optimize performance of the engine over speed range of Mach 3 through Mach 8. The inlet was followed by a fixed-geometry annular combustor and nozzle. Desired subsonic or supersonic combustion modes were obtained by sequential heat addition (staged combustion) through eight fuel injector stations.

The basic construction of the AIM utilized a double wall, wherein the aerodynamic surfaces (hot wall) were fabricated from Nickel-200 or Zirconium-copper and cooled by water. This surface was supported by a structural member (cold wall) fabricated from CRES 321 steel. Six separate cooling circuits were used to satisfy heat transfer requirements within the HRE-AIM. The HRE-AIM was instrumented with 266 pressure-sensing ports and 138 thermocouples from which performance can be calculated.

Special equipments included for test were electronic inlet spike position controller, a water-cooled instrumentation rig, and an air-metering duct. The instrumentation rig incorporated five pressure probes and five temperature probes. The pressure probes measured total pressure as well as cone static pressures so that air flow direction could be determined. The temperature probe measured total temperature and it also incorporated provision for gas sampling of the combustion products. The air-metering duct was fabricated and was available for use to determine air mass flow through the HRE-AIM at various test conditions. Testing was not performed with the air-metering duct attached because of restrictions imposed by the limited life of the test facility.

1.4 SUMMARY DESCRIPTION OF THE TEST INSTALLATION

The wind tunnel facility located at NASA/LeRC Plum Brook station was a free-jet blow-down tunnel. The synthesized hot hypersonic airstream was obtained by passing the gaseous nitrogen through the hot carbon bed heated by induction coils, and then adding cold gaseous oxygen and nitrogen to obtain the desired composition and inlet gas temperatures. The mixture of tunnel gas and the combustion products of the HRE-AIM was then cooled and expelled to the atmosphere by the steam-ejector system.

The coolant supply required for both the HRE-AIM and the sections of the facility was supplied by a closed-circuit coolant pumping system and by a supplementary pressurized reservoir system.

The hot hydrogen fuel required for testing of the HRE-AIM was obtained by passing cold gaseous hydrogen through a heated pebble-bed heater. The heated hydrogen was then transferred to the HRE-AIM through heated and insulated supply lines.

1.5 SUMMARY OF TESTS

Objectives of the test program were achieved; namely, ignition limits established, supersonic and subsonic combustion obtained, and ability to make a smooth transition from subsonic- to supersonic-combustion mode was demonstrated. The ability to operate the AIM satisfactorily when the engine centerline was at 3 deg nose-up attitude with respect to the hypersonic freestream, was also demonstrated.

Valuable information regarding the operation and performance of this type of propulsion was obtained and is described in length in a separate report.

2. DESCRIPTION OF HRE-AIM

2.1 DESIGN REQUIREMENTS

The HRE-AIM was designed with emphasis directed toward evaluating the aerothermodynamics and defining the operational cycle of the hypersonic ramjet engine without major concern for the structural life of the engine. The design incorporated all applicable analysis and experimental data available through the year 1970 for operation of a ramjet engine over flight Mach number range from Mach 3 to Mach 8.

The significant design requirements set forth in the NASA Statement of Work for the HRE-AIM are listed below:

(a) The engine to be designed to operate and maintain structural integrity over test flight Mach number range of 3 to 8.

(b) A means to be provided for inlet start and maintaining combustion from Mach 3 to 8.

(c) The engine to be designed to withstand inlet unstart over the entire operating range.

(d) The engine to be designed to operate in supersonic combustion mode over test Mach numbers 5 to 8.

(e) The engine to be designed for minimum of 100 operational cycles.

(f) An ignition system to be provided to obtain positive ignition during subsonic and supersonic combustion mode.

(g) The engine to be designed to withstand the following environmental conditions:

1. Total temperature (clean air) $3820^{0}R$
2. Total pressure (clean air) 1000 psia
3. Stagnation heat flux, $Btu/ft^2/sec$:

(a)	Spike tip	632
(b)	Cowl support	1900
(c)	Cowl leading edge	4300
(d)	Strut leading edge	2200

2.2 AERODYNAMIC CONTOUR

The selected contour was arrived at from tests performed by AiResearch and from government sponsored research programs.

The centerbody spike assembly was composed of a 10-deg (half angle) cone with a tip section radius of 0.125 in. This section was followed by two isotropic compression surfaces with a total external angular turning of 22 deg. The inlet section incorporated an up-sloping throat of 5.65 deg with respect to the engine centerline.

The inlet cowl section incorporated a leading edge tip radius of 0.03 in. followed by a 37-deg conical section on the external side. The inlet cowl on the internal side was designed to close off the inlet airflow when the translating spike assembly was in the fully extended position in order to reduce heating and drag when the engine was not operating. The overall inlet contraction ratio at Mach 8 and 6 test conditions was 14 and 8 respectively.

2.3 COMBUSTOR SECTION

The combustor section was designed to operate in either supersonic or subsonic combustion mode as the inlet conditions may dictate. The design permitted operating in (1) the supersonic combustion mode for test in freestream Mach number of 5 to 8 at a fuel equivalence ratio of 0.5 to 1.5, and (2) in the subsonic combustion mode for tests in freestream Mach number of 3 through 6 at a fuel equivalence ratio of 0.3 to 1.3. Four locations along the outerbody and on the centerbody, for a total of eight fuel injection stations, were selected to evaluate optimum fuel injection configuration and sequence (see Figure 2-1 for locations of these fuel injectors).

Fuel injectors designated 1A and 1B were selected for first-stage supersonic combustion; fuel injectors 2A and 2C were selected for second-stage supersonic combustion mode; fuel injectors 1C and 4 were selected as an intermediate fuel injector to be used as either first-stage injectors or as second-stage fuel injectors to optimize supersonic combustion; and fuel injectors designated 3A and 3B were selected for subsonic combustion.

2.4 NOZZLE

The nozzle consists of a shroud and a plug. The contour selected was obtained from experimental tests performed by AiResearch and was designed for optimum performance under simulated flight conditions of Mach 8 at a dynamic pressure of 1800 psf. The trailing edge radius of both the shroud and plug was selected to facilitate fabrication.

2.5 MECHANICAL DESIGN

The mechanical design of the HRE-AIM incorporated a double-wall construction. The aerodynamic surface (hot shell) fabricated from Nickel 200 or Zirconium-copper, was cooled by water and supported by a structural member (cold shell). AiResearch Drawing No. 950501, Sheet 2 (attached at the end of this report), presents a cross-sectional view of the unit.

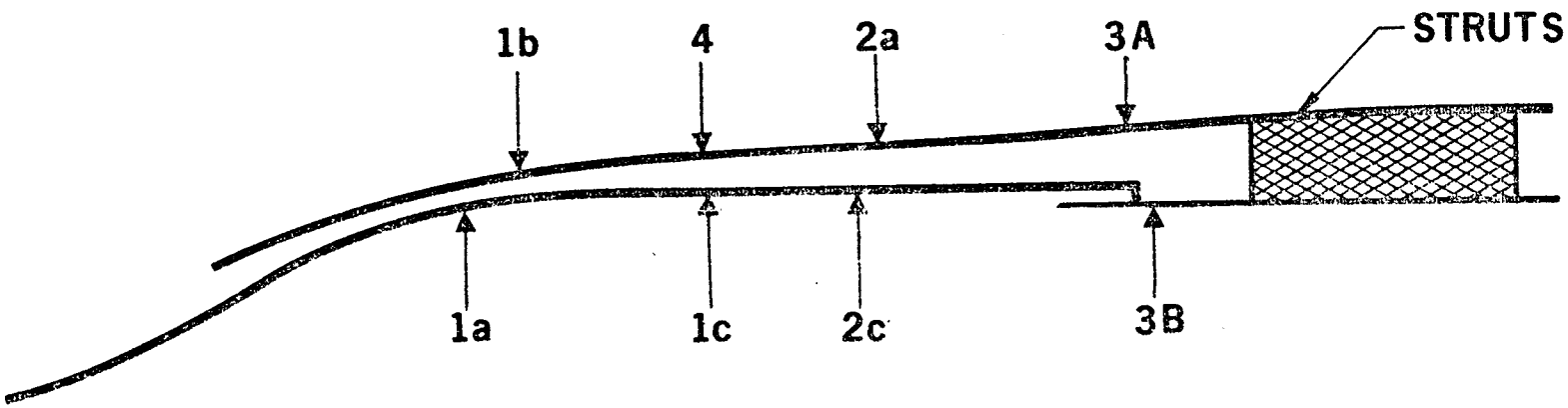

Figure 2-1. Fuel Injector Locations

Conventional metal joining procedures such as furnace brazing, welding, and bolted mechanical joints were used. In areas requiring special heat transfer requirements, use of gold-base alloys and complex mechanical joints were used. Pure nickel (Nickel 200) and Zirconium-copper were selected for their relatively high heat transfer characteristics, together with relatively high mechanical strength at metal temperatures anticipated. Difficulties encountered in heliarc-welding thick sections of nickel (0.200 in. thick) lead to almost exclusive use of electron-beam welding. Use of electron-beam welding minimized the problem of excessively low mechanical properties resulting from excessive heat-affected zones and associated large grain growth. However, the affinity of nickel to a magnetic field and its ability to hold the magnetic field introduced a problem of deflecting the electron-beam from its target. Special shields were fabricated from Mu metal to minimize the problem of deflected beam and the resultant partially welded joint. After series of experiments and analysis, it was determined that the probable cycle life of the weld joint developed would exceed the minimum value established.

2.6 HEAT TRANSFER

Heat transfer analysis performed for the HRE-AIM included effects of shock interaction, surface protuberances and upstream air-turbulence effects, in addition to those normally considered. The change to utilize the NASA/LeRC facility necessitated reassessment of these analyses since the hypersonic freestream conditions and operational characteristics of NASA/LeRC and OAL were different.

The test facility at OAL was basically a continuously operated wind tunnel, and its high-temperature inlet conditions were obtained from an in-line vitiated heater. The wind tunnel at NASA/LeRC was a clean air blow-down tunnel with a maximum operating time of approximately 3 min.

The analysis indicated that the maximum heat flux was about equal for the two facilities although the maximum heat flux condition occurred under different test conditions. The reason for the above is attributed to the fact that under test conditions of NASA/LeRC the level of the gas enthalpy is reduced although the air mass flow rate is increased. Results of this analysis are shown in Figure 2-2.

2.7 COOLANT SYSTEM

The basic coolant circuit was selected to satisfy the structural and operational requirements of HRE-AIM. Target maximum gas side temperature of the hot shell was 1525°F, as shown in Figure 2-3. This maximum temperature was selected by physical requirements of Nickel 200 material to insure attaining minimum cycle life targeted.

Five coolant circuits were selected for the HRE-AIM and four coolant circuits for the outer cowl body assembly. Figures 2-4 through 2-7 show these circuits schematically. Table 2-I presents the pressure drops of these circuits and the calculated coolant outlet bulk temperature.

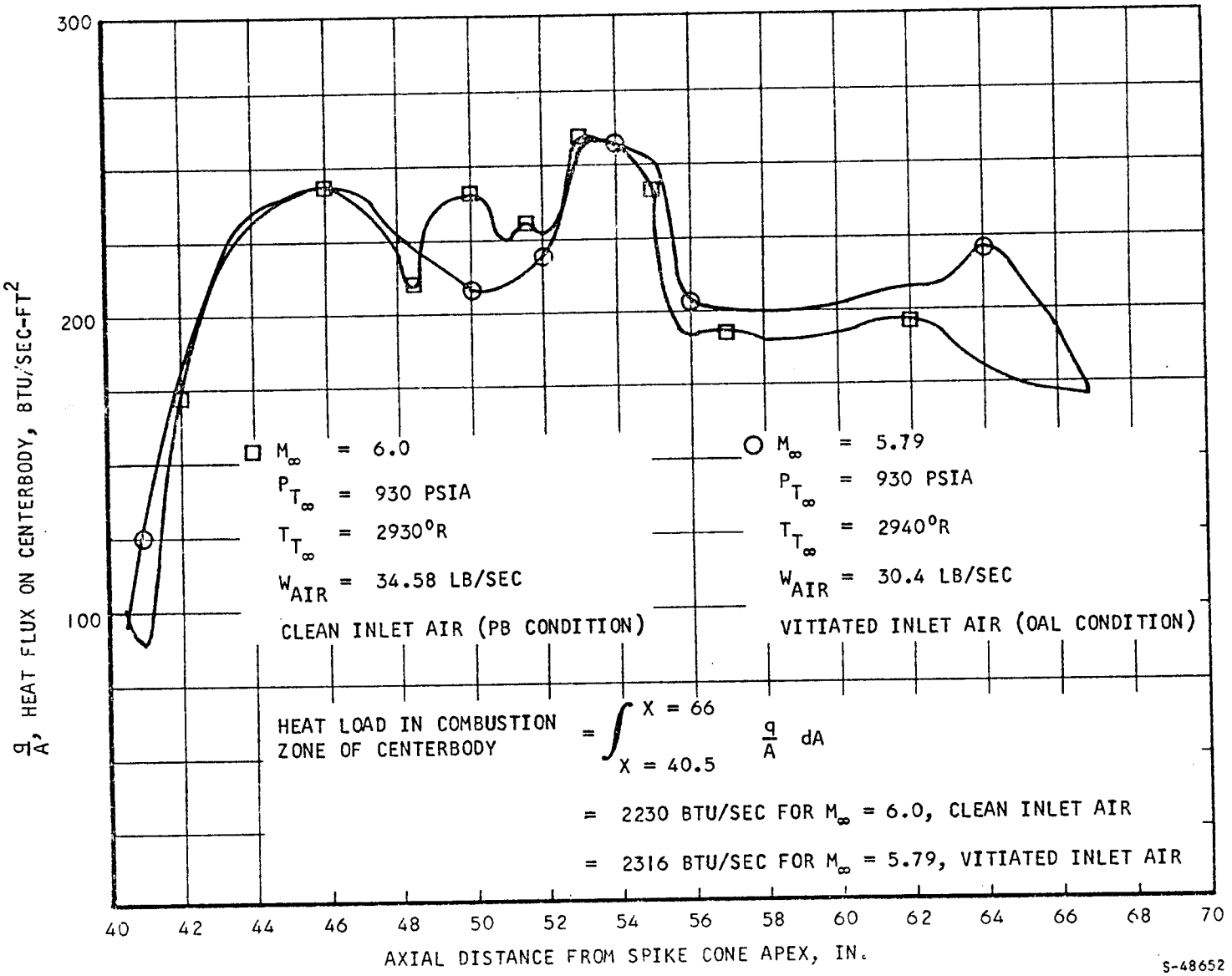

Figure 2-2. Comparison in Heat Flux Between Plum Brook and OAL Gas Conditions

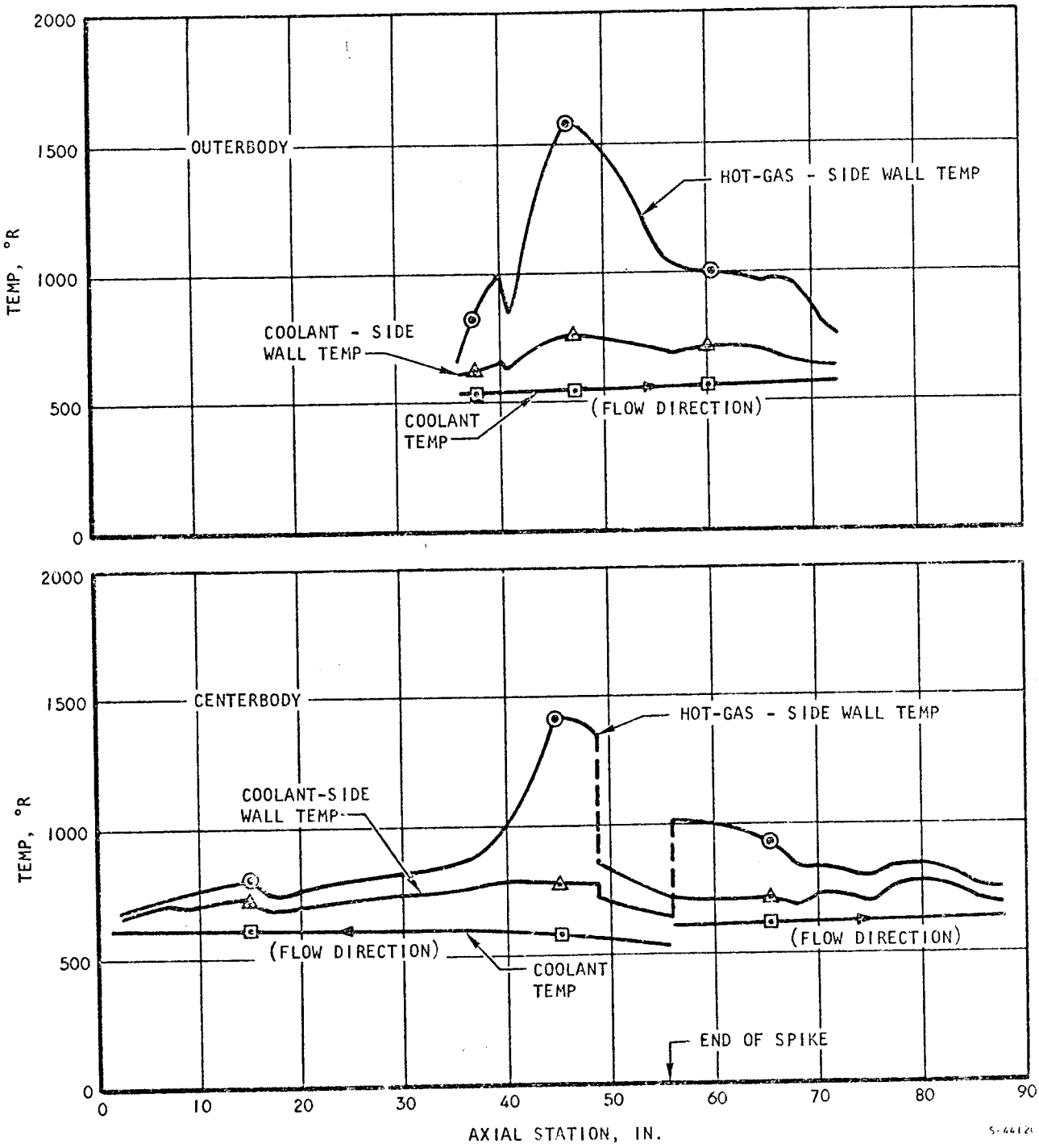

Figure 2-3. Wall and Coolant Temperatures for $M_\infty = 6.65$

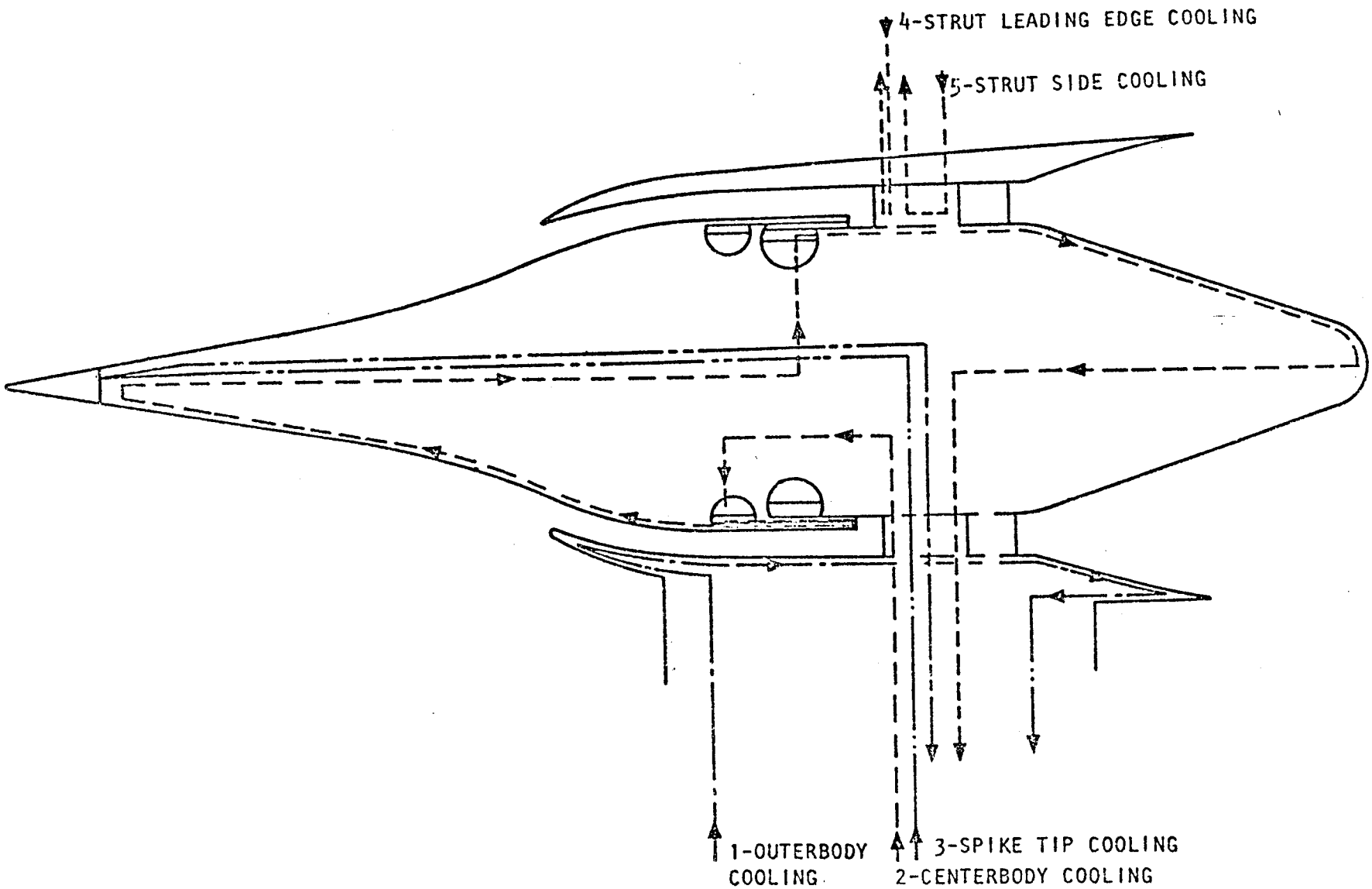

Figure 2-4. AIM Cooling Circuits

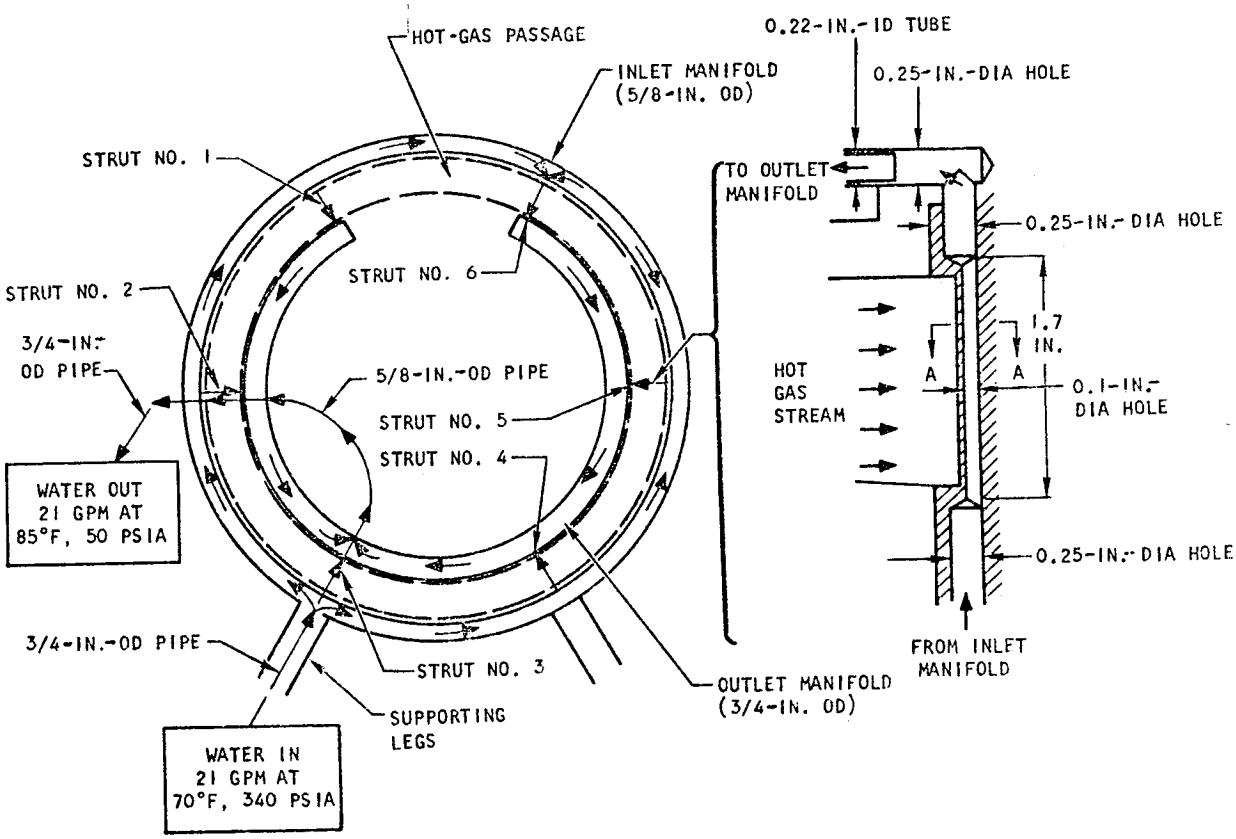

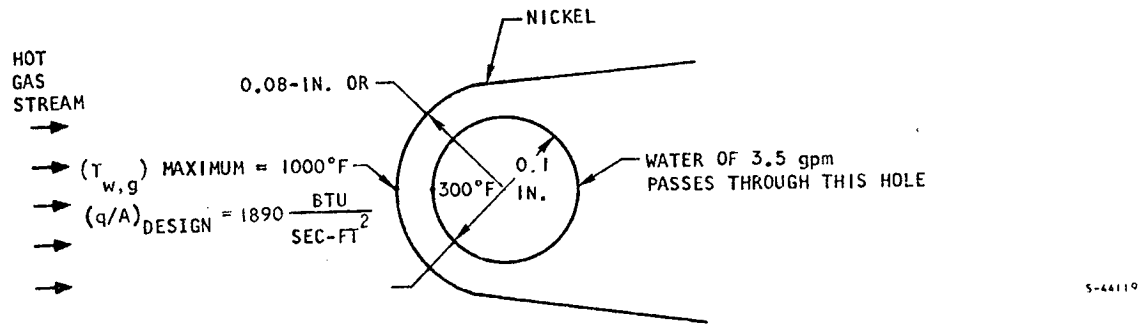

SECTION A-A

NOTE:
THE DESIGN HEAT FLUX FOR THE LEADING EDGE WAS TAKEN 1.15 TIMES THE FAY-RIDDELL STAGNATION HEAT FLUX (SEE FIGURE 5-37).

Figure 2-5. Strut Leading Edge Cooling

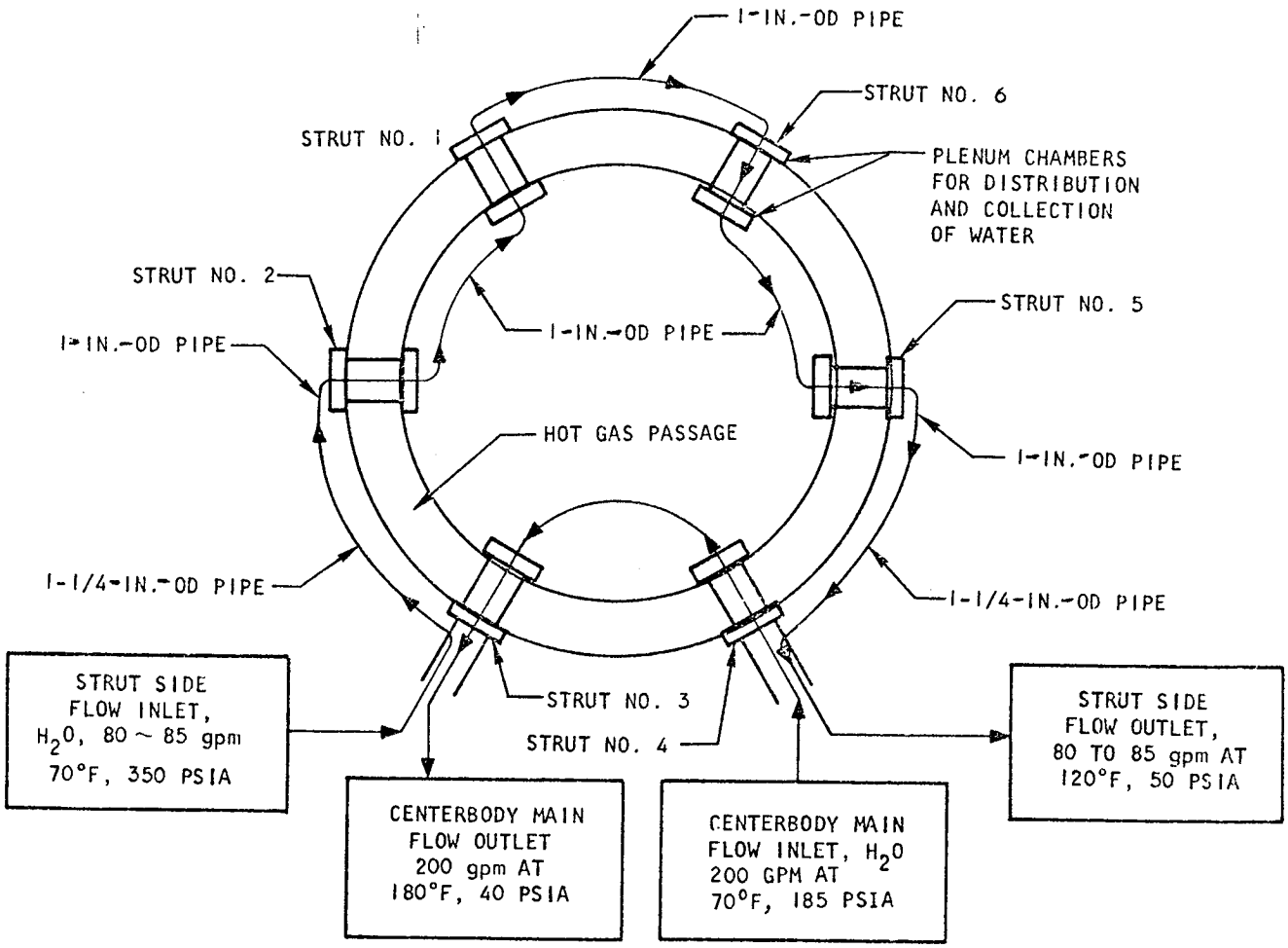

NOTES:

(a) STRUT SIDE SURFACES ARE COOLED BY WATER FLOWING THROUGH A NUMBER OF HOLES AND ANNULAR PASSAGES ALONG THE CIRCUMFERENCE OF THE STRUTS. DETAILED FLOW GEOMETRIES ARE SHOWN IN DRAWING L-950983.
(b) HEAT FLUX DISTRIBUTION ON THE STRUT SIDE SURFACE IS SHOWN IN FIGURE 5-37.
(c) MAXIMUM COOLANT SIDE METAL TEMPERATURE IS 300°F.
(d) MAXIMUM HOT GAS SIDE METAL TEMPERATURE IS 1100°F.
(e) FREE FLOW AREA AT STRUTS = 0.63 $IN.^2$ FOR STRUTS NO. 1, 2, 5, 6.
= 1.7 $IN.^2$ FOR STRUTS NO. 3, 4.
(f) STRUTS NO. 3 AND 4 ARE COOLED BY MAIN CENTERBODY COOLANT FLOW.

S-44117

Figure 2-6. Strut-Side Surface Cooling

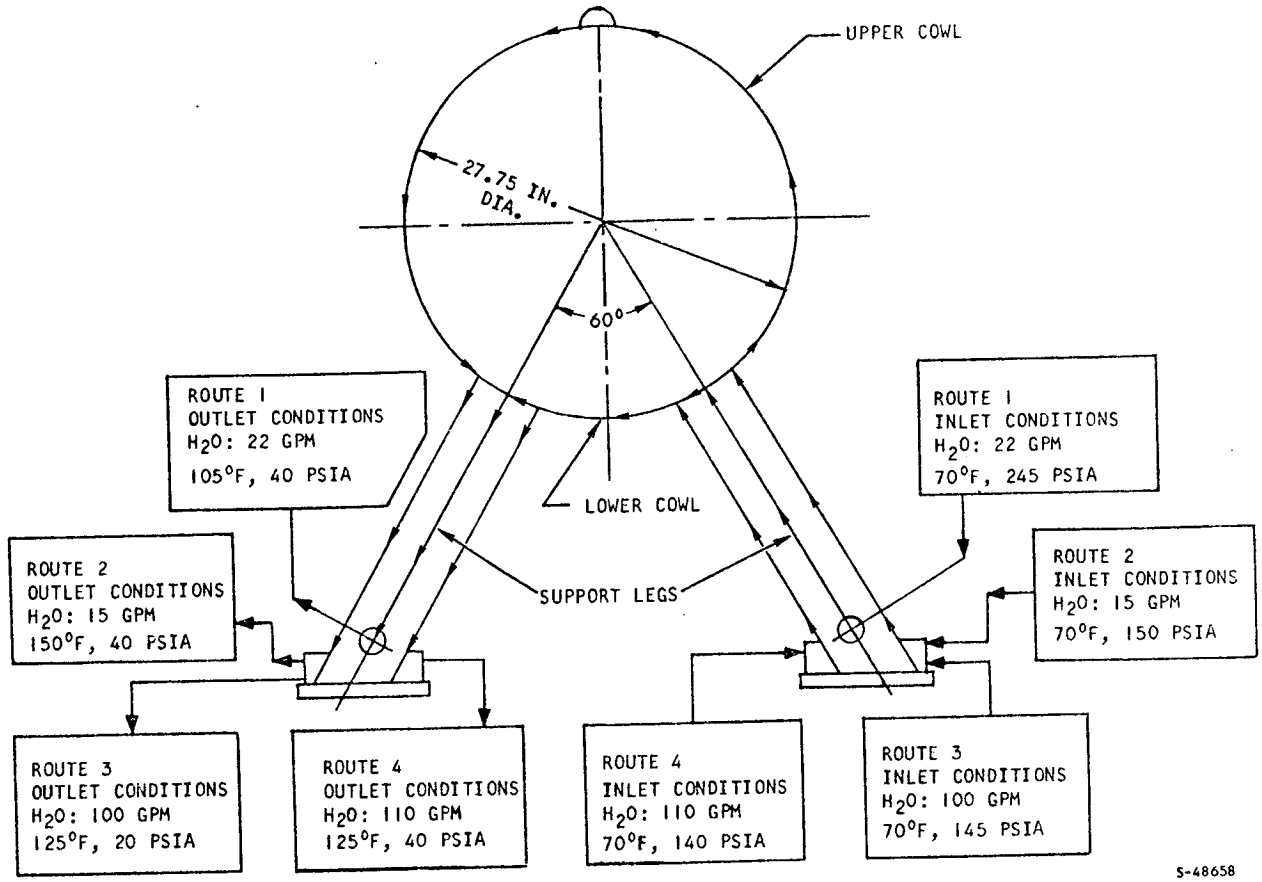

NOTES:

1. ROUTE 1 - LEG LEADING EDGE → FORWARD PORTION OF LOWER COWL (3.6 IN. LONG) → LEG LEADING EDGE
2. ROUTE 2 - FORWARD PORTION OF LEG OUTER SIDE SURFACE (3 IN. LONG) → FORWARD PORTION OF UPPER COWL (3.6 IN. LONG) → FORWARD PORTION OF LEG OUTER SIDE SURFACE (3 IN. LONG)
3. ROUTE 3 - MAIN LEG OUTER SIDE SURFACE → MAIN UPPER COWL → MAIN LEG OUTER SIDE SURFACE
4. ROUTE 4 - LEG INNER SIDE SURFACE → MAIN LOWER COWL → LEG INNER SIDE SURFACE
5. DETAILED FLOW GEOMETRIES ARE SHOWN IN DRAWING L-950994
6. HOT-GAS CONDITIONS ARE $M_\infty = 7.0$, $P_{T_\infty} = 1200$ PSIA, $T_{T_\infty} = 3820°R$

Figure 2-7. Cooling System of the Outer Cowl and Support Legs

TABLE 2-1

HRE-AIM COOLANT SYSTEM

Item No.	Coolant Circuit	Coolant Flow, gpm		Inlet Press, psia		Outlet Press, psia		Calculated Coolant Temp, °F	
		Calc	Actual	Calc	Actual	Calc	Actual	Inlet	Outlet
1	Centerbody	200	197	210	200	40	42	70	180
2	Outerbody	660	645	235	205	40	40	70	115
3	Strut Leading Edge	21	20.3	360	415	50	41	70	85
4	Strut Body	85	78	350	350	50	46	70	125
5	Spike Tip	7	9.2	225	248	70	78	70	150
6	Outer Cowl Body Forward Section	15	15	135	140	40	38	70	150
7	Outer Cowl Body Center Section	110	110	110	130	40	43	70	125
8	Outer Cowl Body Leg Leading Edge	22	22	260	192	40	52	70	105
9	Outer Cowl Body Aft Section	100	86	130	145	40	38	70	150

2.8 STRUCTURAL

The mechanical and the structural design of the HRE-AIM was primarily directed toward satisfying the aerothermodynamic requirements as directed by the Statement of Work. The design cycle life of the critical components of the HRE-AIM in all cases exceeded the minimum set forth by the Statement of Work. Figure 2-8 and its associated table lists the design cycle life of these components. The HRE-AIM mount structure was originally designed to mount to a floor plate at OAL facility. Utilizing NASA/LeRC facility required mounting the HRE-AIM from an overhead "H" frame. To facilitate installation at NASA/LeRC, the handling and the transport fixture was designed to hold the HRE-AIM in this attitude. Analysis was made to determine the structural integrity of the mount structure. Figure 2-9 and its associated tables list the structural capability of this structure.

2.9 INSTRUMENTATION

The HRE-AIM was instrumented with 266 pressure-sensing ports and 138 thermocouples. All pressure and temperature sensing lines were not recorded due to limited recording capability of the Plum Brook facility. Hence, selected parameters were recorded for each series of tests. Parameters provided and recorded are noted in "Measured Data" section.

2.10 TEST SUPPORT EQUIPMENT

2.10.1 Inlet Spike Actuation Control System

The inlet spike actuation control system (ISACS) was designed to provide position control for the inlet spike assembly, the translating member of the centerbody.

The ISACS utilized a closed loop voltage feedback signal, from a linear voltage differential transducer (LVDT), to continuously monitor and to position the inlet spike assembly at the commanded position.

The ISACS was fabricated in two sections; (a) control panel section, and (b) signal conditioning section (see Figure 2-10). The control panel section consisted basically of (a) position set-point pots, (b) a computer interface circuit, (c) the time delay and lock-up protection circuit, and (d) control switches. The signal conditioning section consisted of a LVDT signal conditioner, error signal amplifier, and other signal conditioning modules necessary to control position of the inlet spike assembly. A schematic of the various components is shown in Figure 2-11.

The operation of the ISACS can be briefly described as follows:

The position command is obtained by entering a set-point voltage into the input side of the error monitor and amplifier, initially obtained from adjusting the pots. In the error monitor circuit, the entered set-point voltage is compared with the position feedback voltage (obtained from the LVDT signal conditioner). The difference, or the error, was then amplified and filtered to remove noise, and then conditioned through the output driver

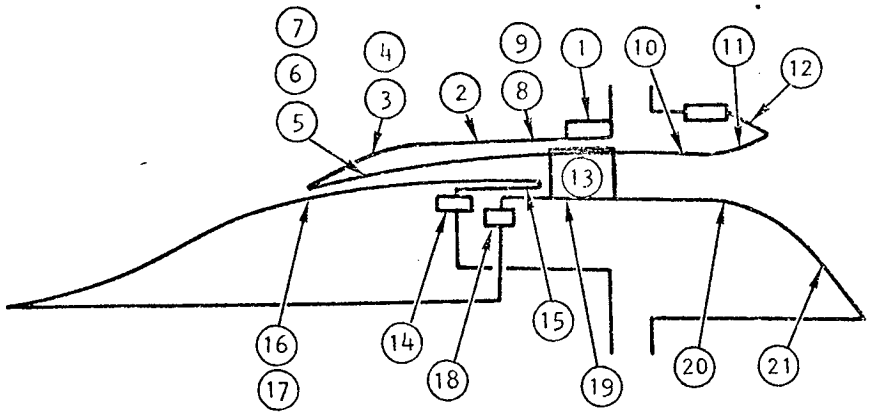

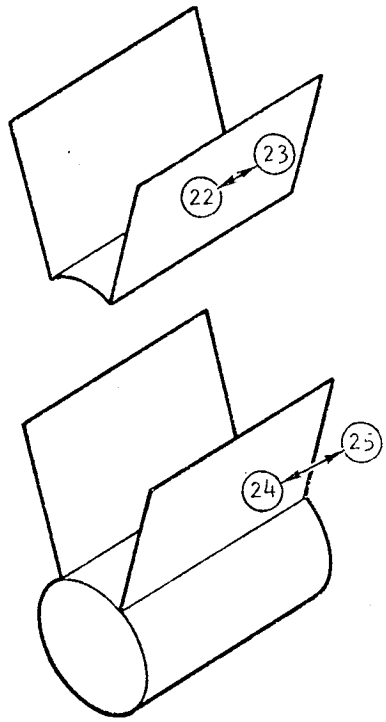

Location No.	Station (Ref)	Description	No. Cycles
1	51.0 to 46.0	Coolant Inlet Manifold	330
2	46.0 to 41.5	Outerbody Finned Shell	>1000
3	40.5 to 39.5	CLE Outer Shell	500
4	38.5 to TIP	CLE Outer Shell	300
5	TIP to 35.7	CLE Inner Hot Shell	300
6	36.5 to 38.5	CLE Inner Hot Shell	240
7	39.6 to 40.5	CLE Inner Hot Shell	>500
8	40.5 to 41.3	Outerbody Hot Shell	>500
9	41.3 to 66.4	Outerbody Hot Shell	350
10	66.4 to 67.3	Outerbody-Nozzle Hot Shell	500
11	68.2 to TIP	Nozzle Hot Shell	250
12	TIP to 64.4	Nozzle Outer Shell	350
13		Strut Cover	>500
14	48.25	Coolant Inlet Manifold	>500
15	48.8 to 55.8	Inlet Spike Finned Shell	>425
16	48.8 to 40.6	Inlet Spike Hot Shell	225
17	40.3 to TIP	Inlet Spike Hot Shell	250
18	53.0	Innerbody Coolant Manifold	>500
19	49.9 to 66.0	Innerbody Hot Shell	225
20	66.0 to 67.1	Nozzle Plug Hot Shell	>300
21	68.0 to End	Nozzle Plug Hot Shell	225
22		Leading Edge and Inner Cowl Fwd	>300
23		Inner Cowl Aft and Support	200
24		Outer Cowl Fwd and Support	200
25		Outer Cowl Aft and Support	225

S-89671

Figure 2-8. Structural Components

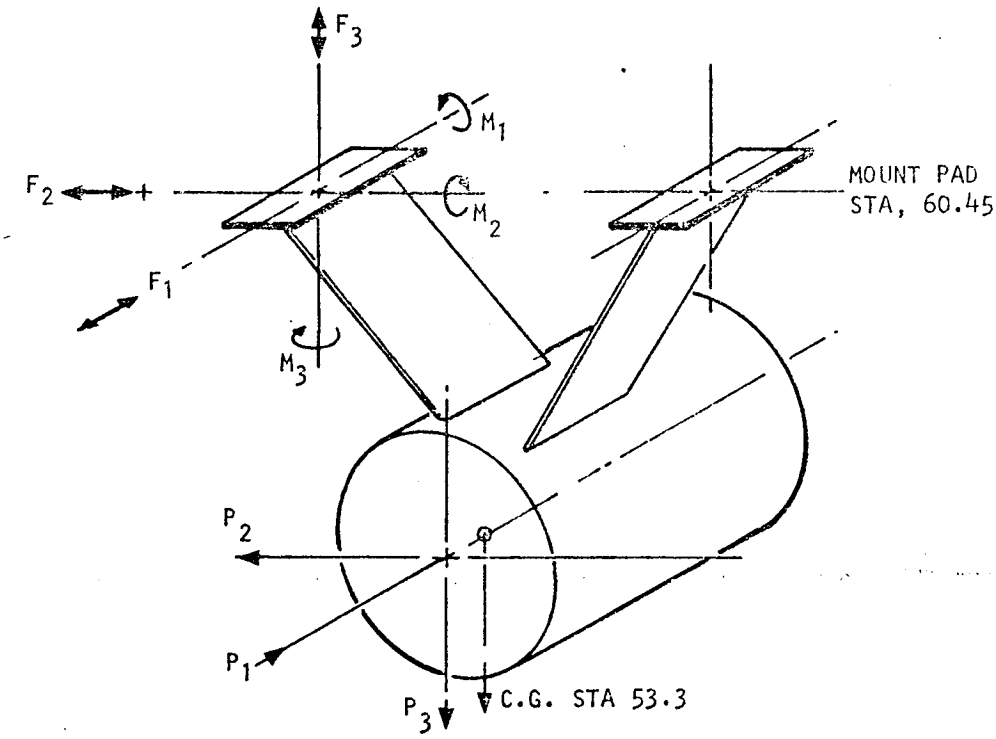

Design load of mount based on worst condition, either due to aero-operational maximum load or transport.

Load	Aero Load, lb	Oper. Load, lb	Transport Load, lb	Max. Load Each Leg lb	Based on
P_1	8,400	(3g) (3000)	(5g) (3000)	17,460/2	Aero + Oper.
P_2	Negli.	(3g) (3000)	(5g) (3000)	15,000/2	Transport
P_3	Negli.	(4g) (3000)	(6g) (3000)	18,000/2	Transport

Reaction load at each leg due to test.

Load Direction	Reaction Load, lb	Reaction Moment, in.-lb
P_1	F_1 = +8800	M_2 = -410,000
P_2		
P_3	F_3 = -6000	M_2 = +42,600

Cowl Mount

Load	Aero Load, lb	Oper. Load, lb	Transport Load, lb	Max. Load Each Leg lb	Based on
P_1	6,325	(3g) (800)	(5g) (800)	8,725/2	Aero + Oper.
P_2	N/A	--	(5g) (800)	4,000/2	Transport
P_3	14,840	(4g) (800)	(5g) (800)	18,040/2	Aero + Oper.

Reaction Load at Each Cowl Mount Due to Test

Load Direction	Reaction Load, lb	Reaction Moment, in-lb
P_1	F_1 = +4,400	M_2 = -125,000
P_2		
P_3	F_3 = -9,000	M_2 = Negligible

S-89557

Figure 2-9. Structural Loads

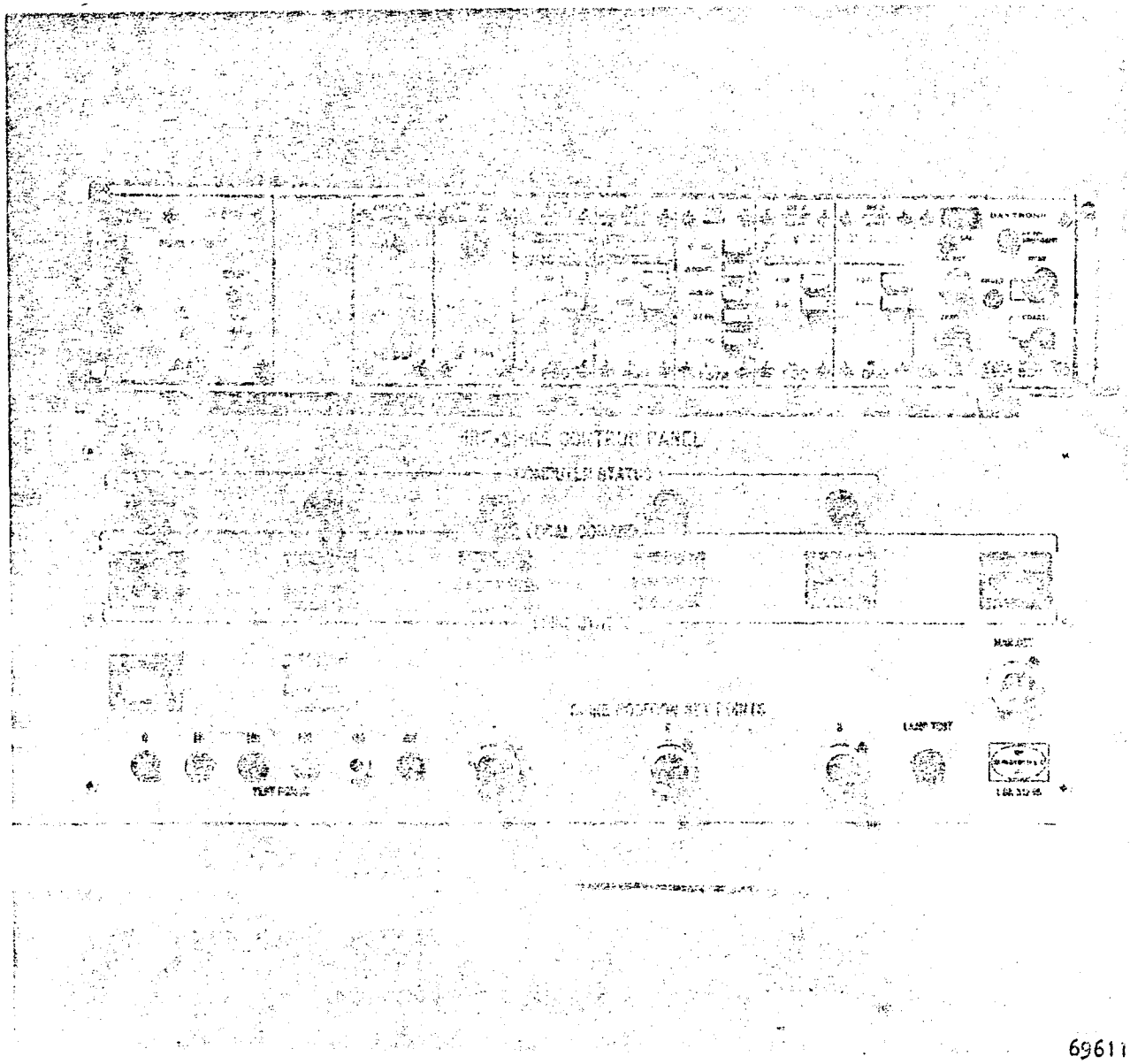

Figure 2-10. ISAACS Control Panel

ORIGINAL PAGE IS
OF POOR QUALITY

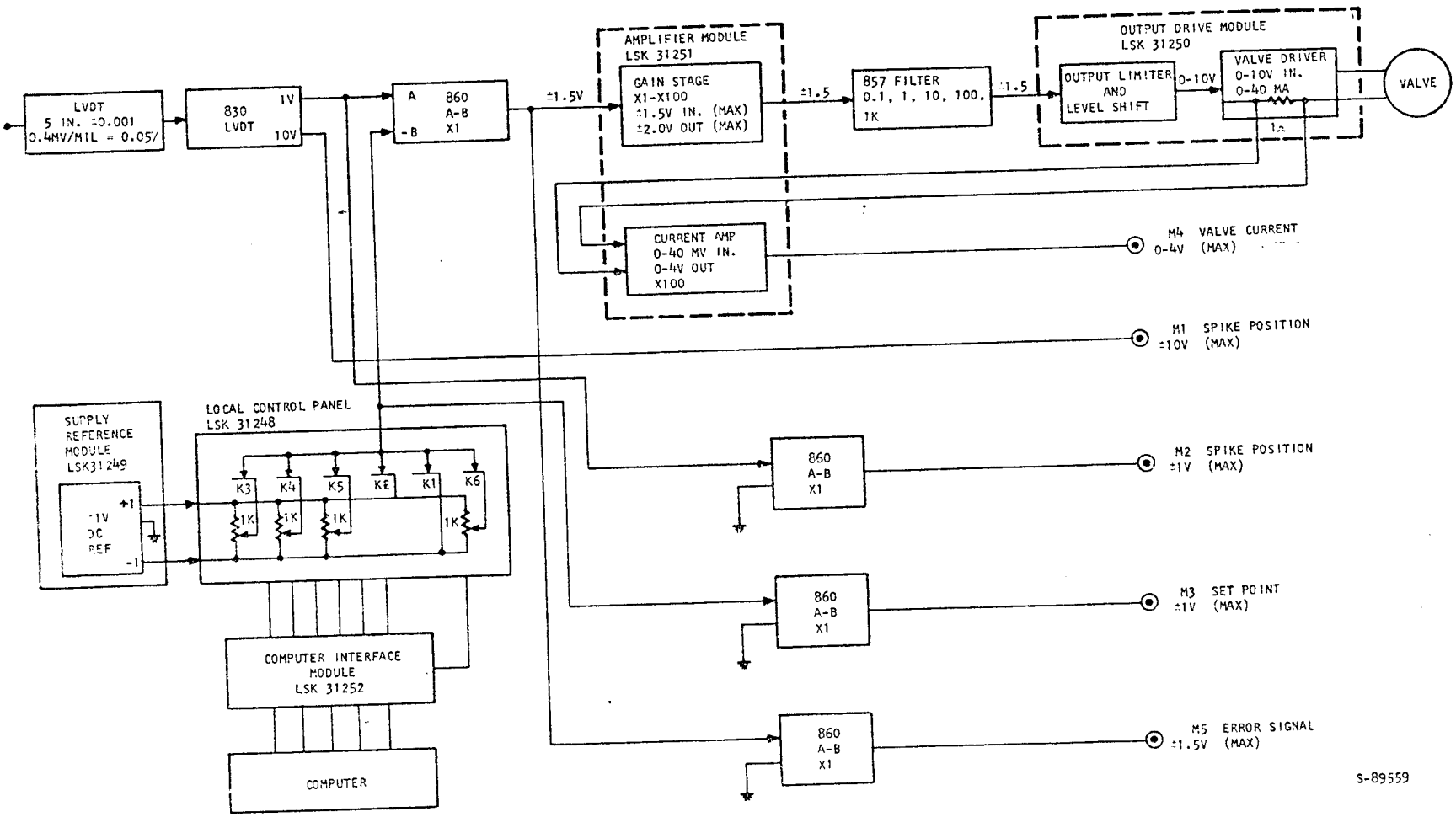

Figure 2-11. Block Diagram - HRE ISAACS System

module to operate a 4-way hydraulic servo valve. The inlet spike assembly was then positioned by the hydraulic actuator.

The ISACS was designed such that three different spike positions could be commanded from a remote source. As a fail-safe feature, the ISACS was designed to close the inlet of the HRE-AIM in the event the command signal was lost or a power failure experienced.

2.10.2 Instrumentation Rig

The instrumentation rig was fabricated to determine the quality of the combustion and the direction of the combustion products at the exit of the combustor zone. The instrumentation rig consisted of a large annular ring upon which five gas sampling-total temperature probes and five pressure sensing probes were mounted. The configuration of both probes was obtained from requirements set forth by NASA. (See Figures 2-12, 2-13, and 2-14).

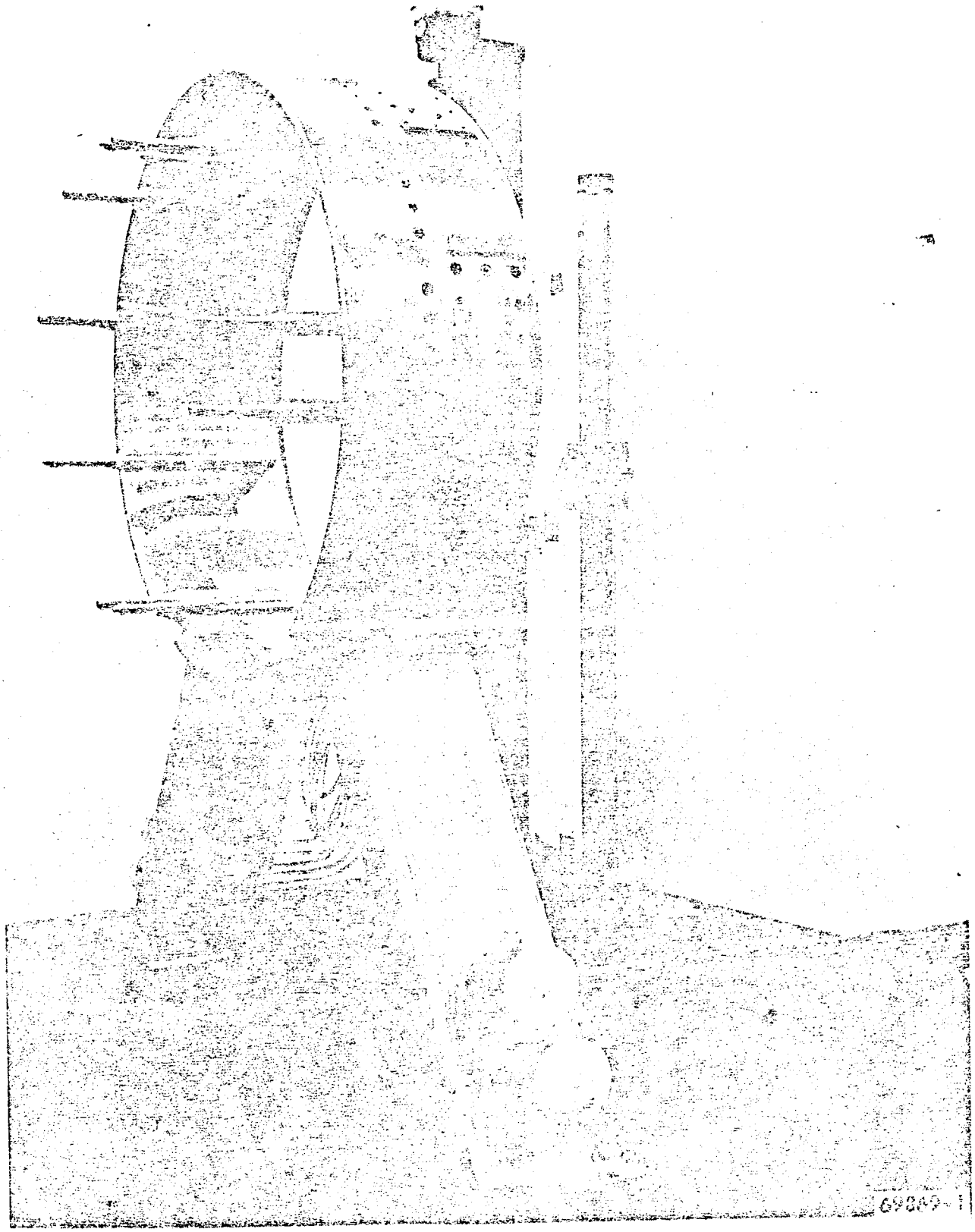

Figure 2-12. Instrumentation Rig

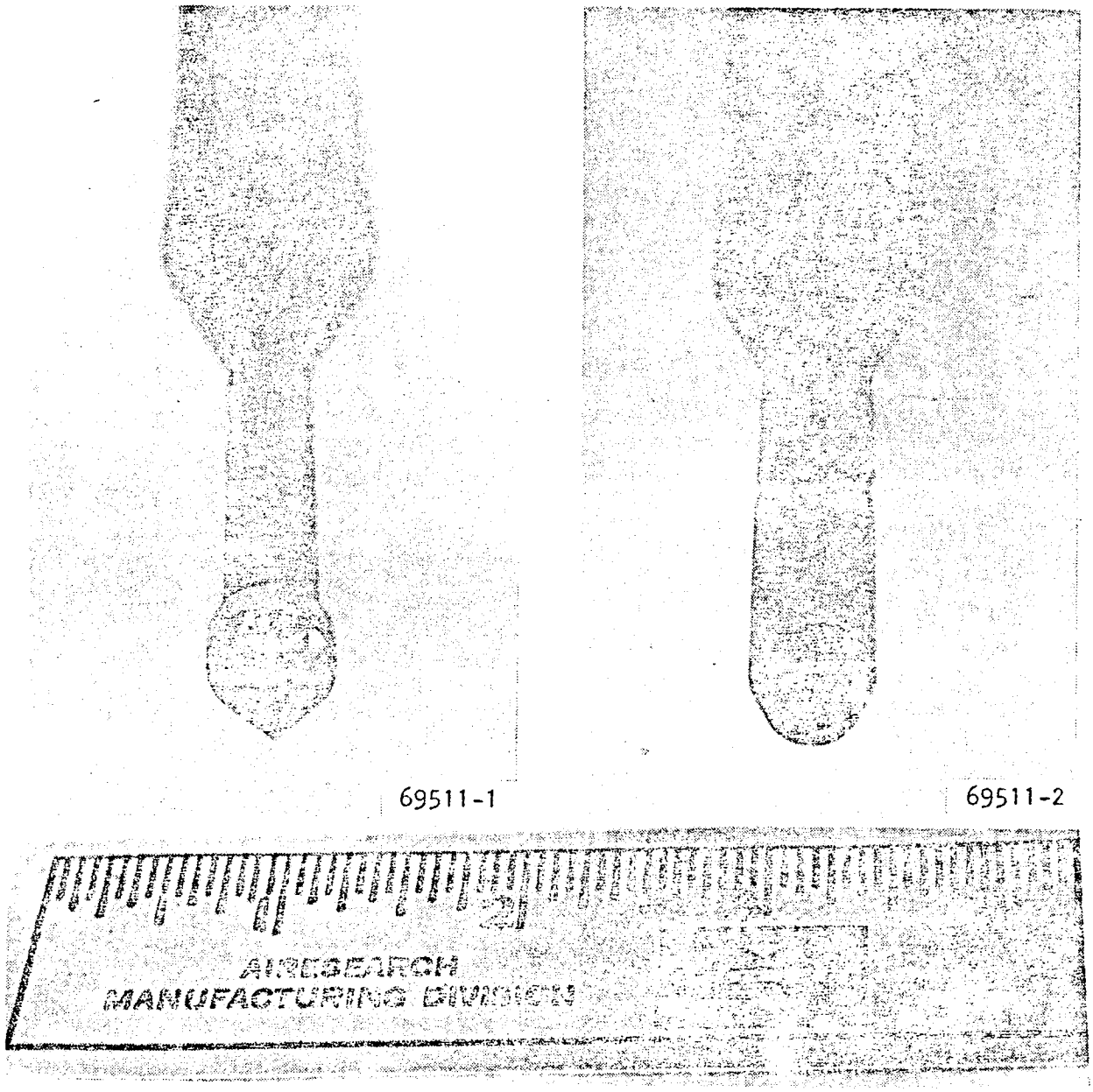

Figure 2-13. Instrumentation Rig Temperature and Pressure Probe Tips

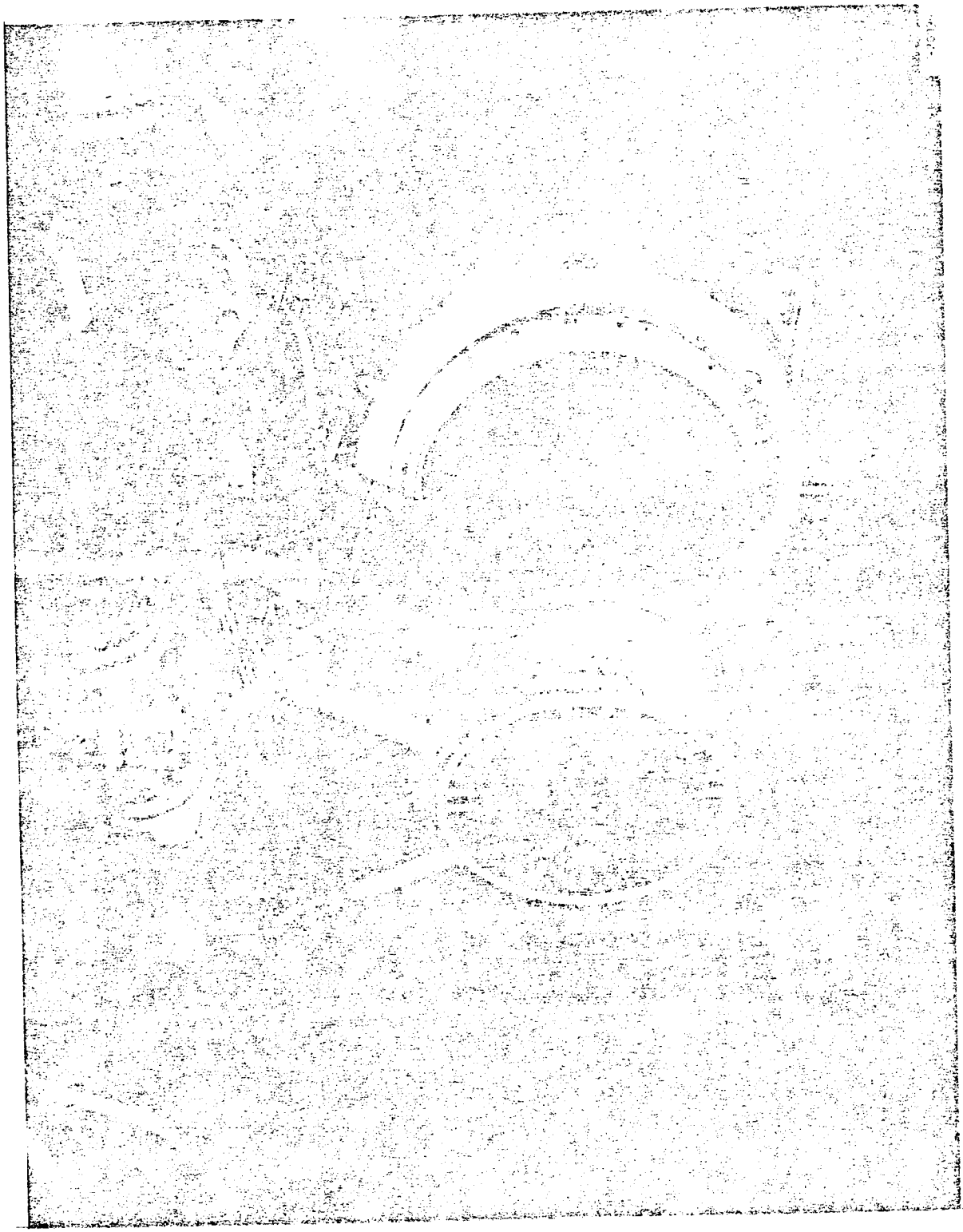

Figure 2-14. Aft View of AIM Showing Instrumentation Rig

3. TEST FACILITY AND INSTALLATION

The hypersonic tunnel facility (HTF) at NASA/LeRC, Plum Brook Station, was designed for research, development and acceptance testing of engines at simulated flight conditions of Mach 5, 6, and 7. The wind tunnel incorporated interchangeable hypersonic nozzles with an exit diameter of 42 in., and a boundary layer energizer which permitted free-jet testing of engines up to two feet in diameter. Figures 3-1, 3-2, 3-3, and 3-4 show the installation, and Figure 3-5 depicts schematically the supporting equipment necessary for operation. AiResearch Drawing 950500, Sheet 1 attached at the end of this report, shows the initial installation of the HRE-AIM in the HTF.

The source for the hypersonic air stream was heated gaseous nitrogen augmented by cold gaseous oxygen and nitrogen to obtain desired synthesized freestream conditions. A schematic of this control system is shown in Figure 3-6.

3.1 FACILITY SUPPORT

Equipment and sources of energy required for operation of the facility are described below.

3.1.1 Gaseous Nitrogen

The source of gaseous nitrogen (GN_2) was obtained from three systems:

(a) A portable rail car with a capacity of 726,000 scf at 5000 psig. This system was the basic source of the heated hypersonic freestream, diluent gas (GN_2) for the hypersonic freestream, and the source for the purge gas necessary for operation of the HRE-AIM.

(b) A portable rail car with a capacity of 240,000 scf at 2400 psig. This system was the source of GN_2 for the facility wedge nozzle (boundary layer energizer).

(c) A fixed storage tank with a capacity of 227,000 scf at 2400 psig. This system was used to purge the various oxygen and hydrogen systems before and immediately following the test and to pressurize the supplementary coolant reservoir system.

3.1.2 Gaseous Oxygen

The oxygen necessary to augment the heated GN_2 gas to obtain the desired synthesized hypersonic freestream, and GO_2 necessary for operation of the

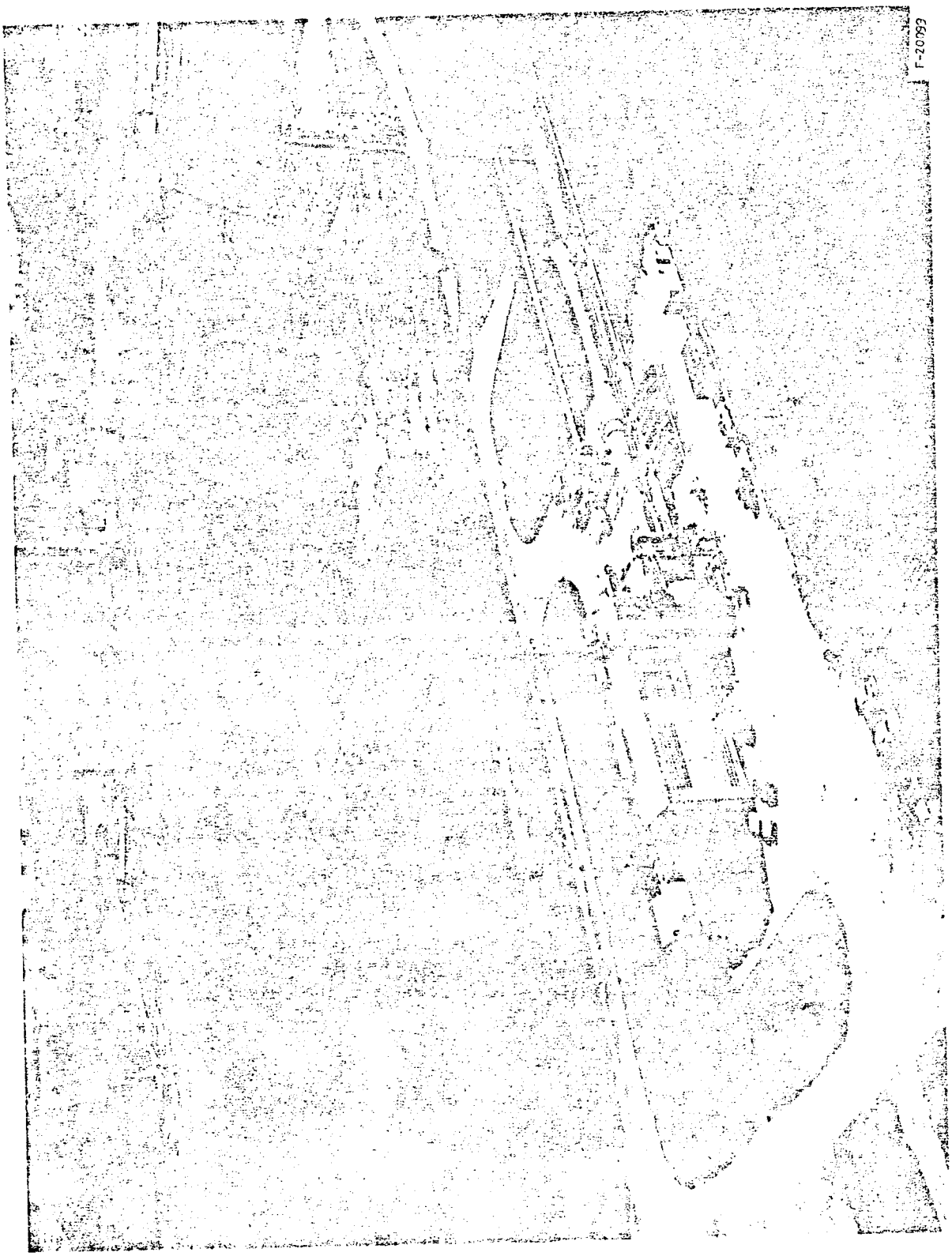

Figure 3-1. Hypersonic Wind Tunnel Facility at NASA/LeRC Plum Brook Station

ORIGINAL PAGE IS
OF POOR QUALITY

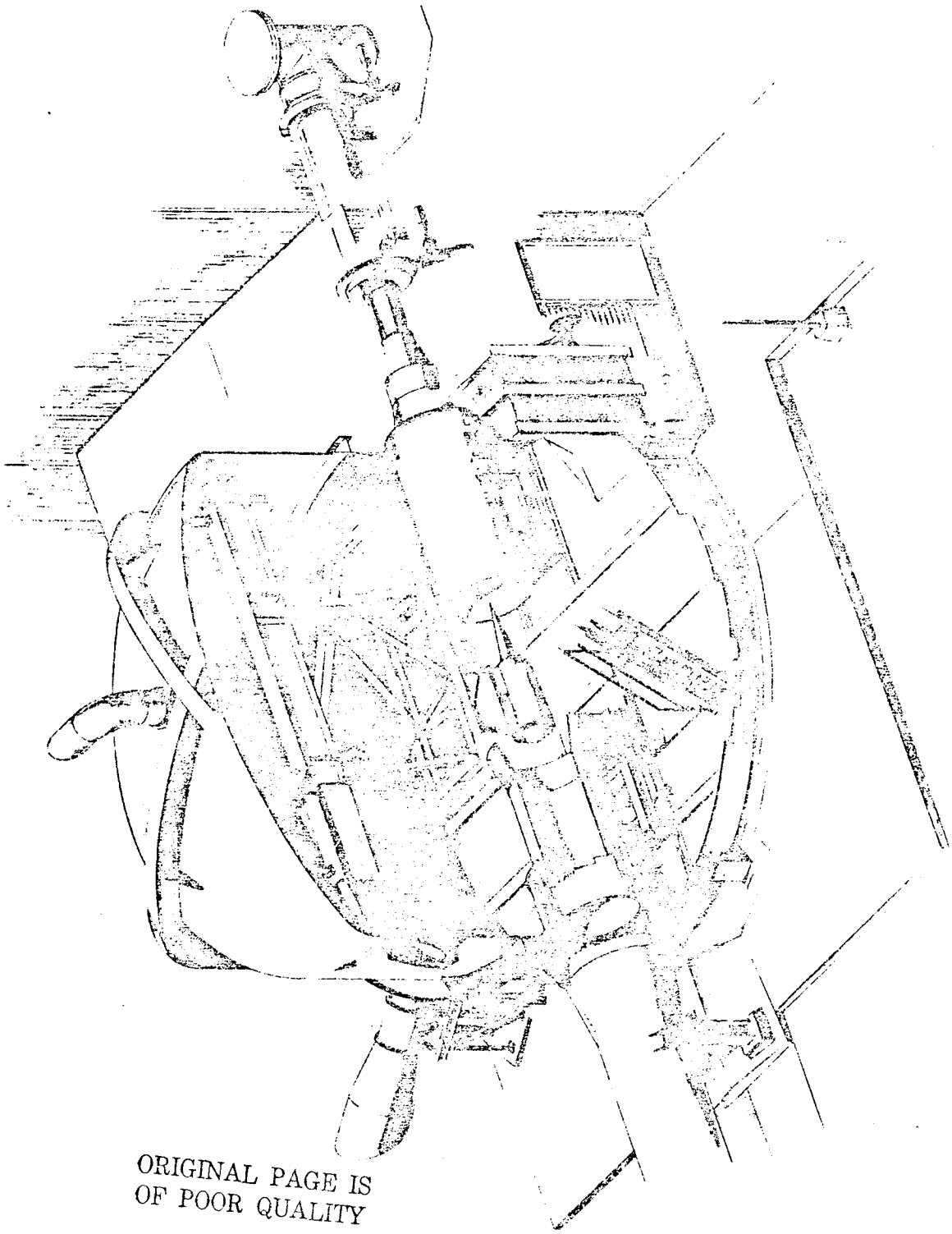

ORIGINAL PAGE IS
OF POOR QUALITY

Figure 3-2. AIM Test Installation

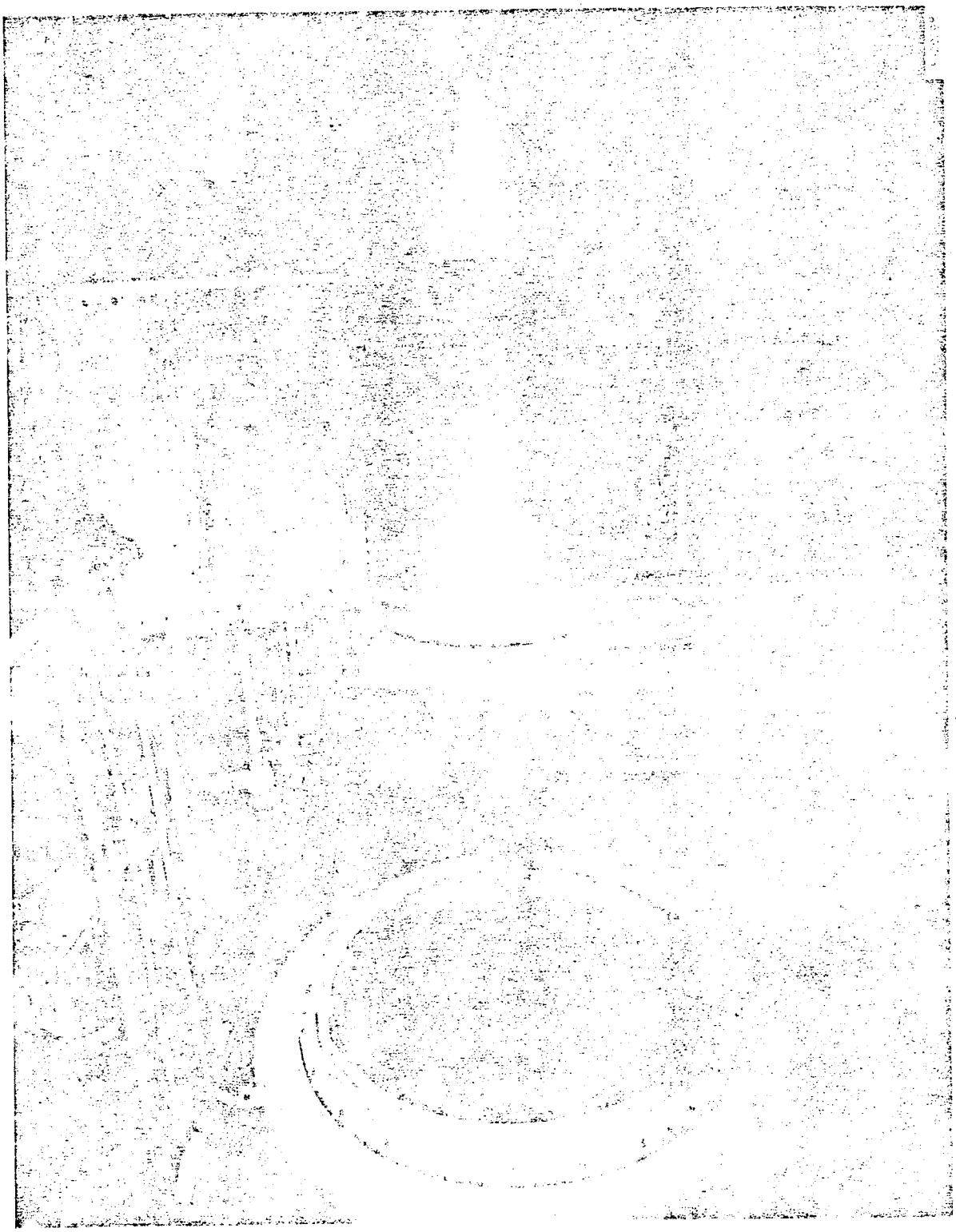

Figure 3-3. HRE-AIM Wing Tunnel Installation

ORIGINAL PAGE IS
OF POOR QUALITY

Figure 3-4. HSR-AIM Wind Tunnel Installation

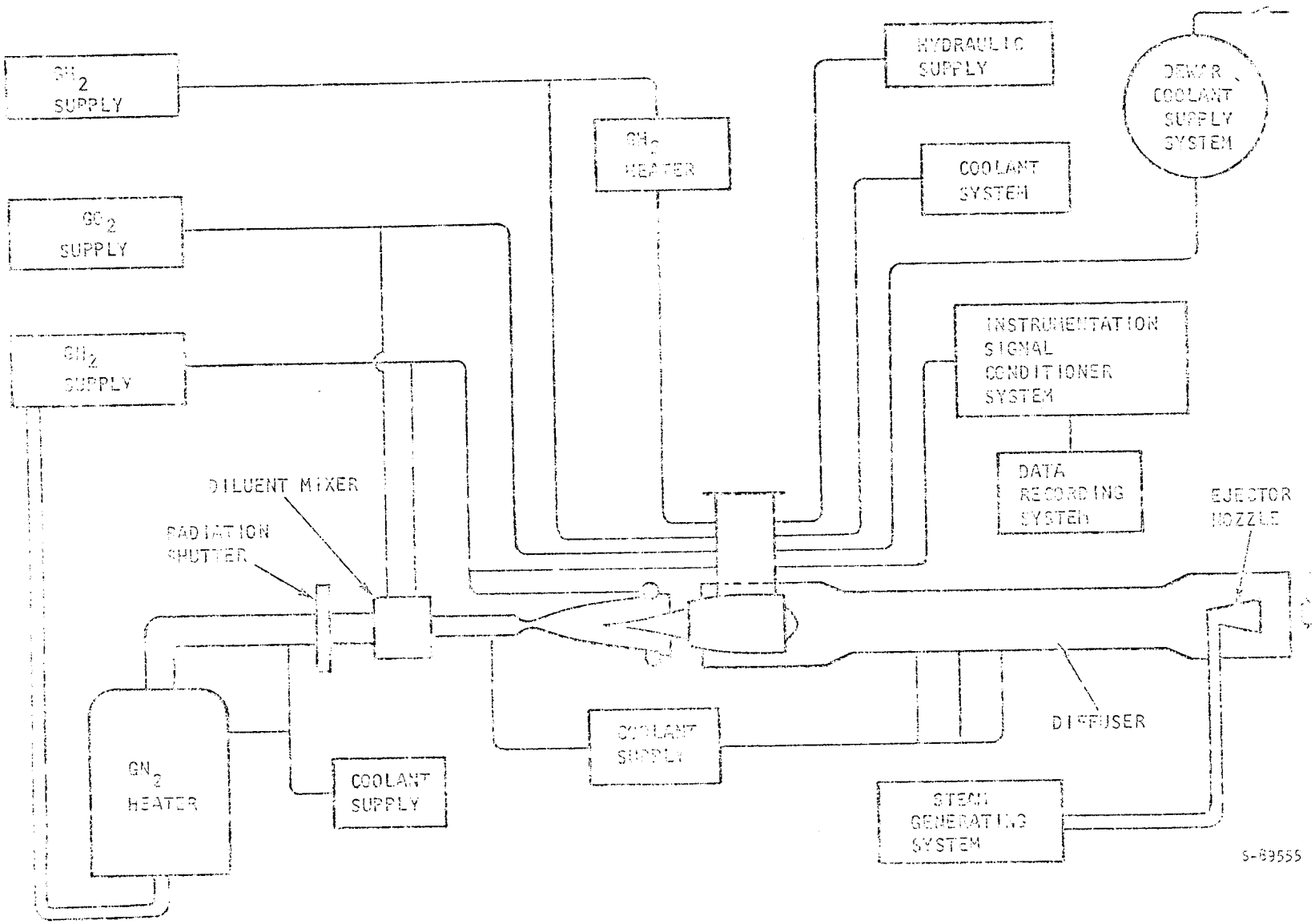

Figure 7-5. Test System Schematic

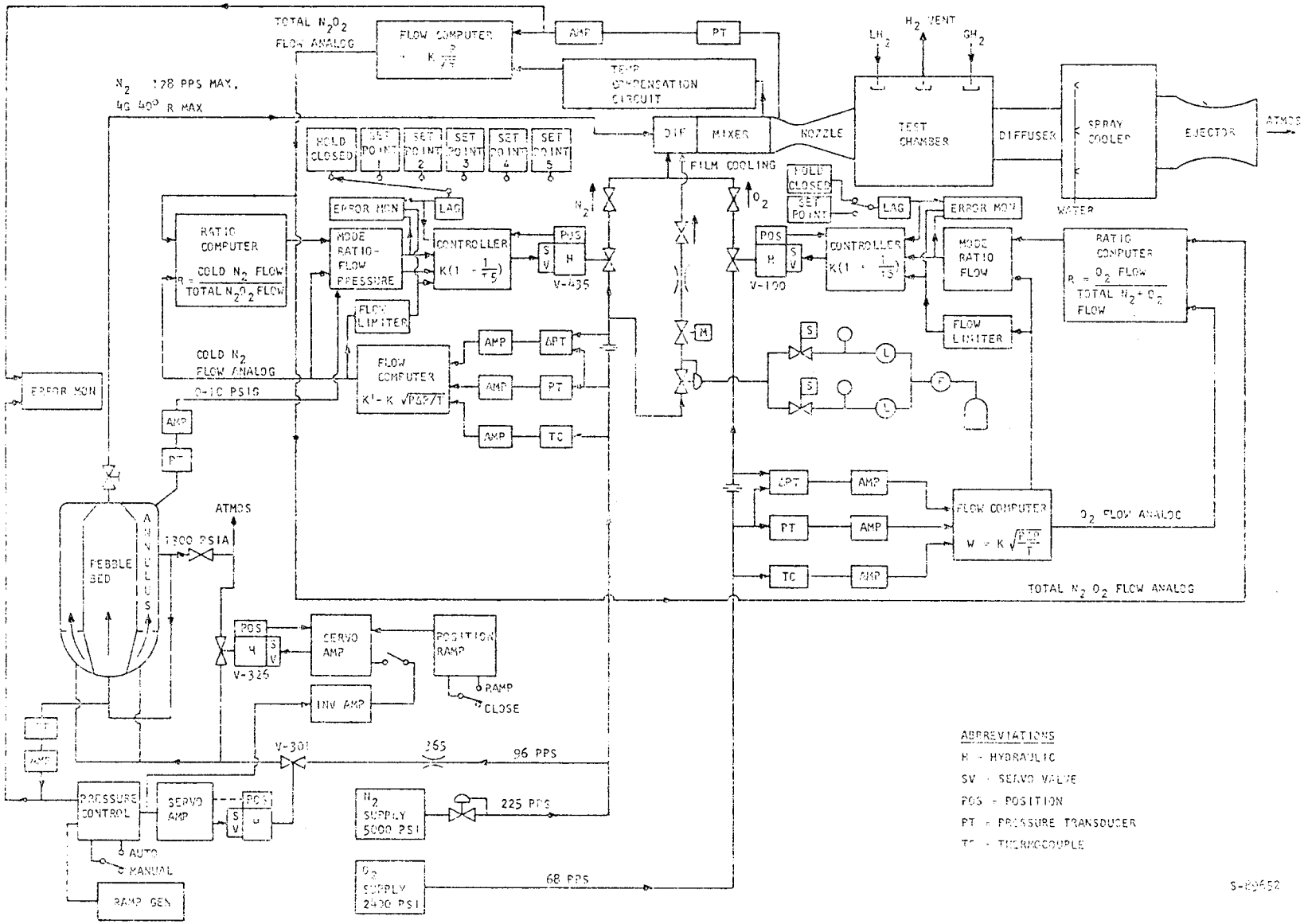

Figure 3-6. Fuel Control System

ignitors installed on the HRE-AIM was obtained from a fixed storage tank with a capacity of 500,000 scf of GO_2 at 2400 psig.

3.1.3 Gaseous Hydrogen

Gaseous hydrogen used as fuel for the HRE-AIM and source of GH_2 necessary for operation of the ignitors installed on the HRE-AIM was obtained from five portable tubers with a total capacity of 350,000 scf at 2400 psig.

3.1.4 Heater Systems

3.1.4.1 Gaseous Nitrogen Heater

This heater system was used to furnish heated nitrogen source for the hypersonic freestream air. It was capable of supplying 128 lb/sec of gas at 4540°F and 1200 psig. The GN_2 was heated by passing through a series of perforated carbon discs approximately 5 ft in diameter and 2 ft high. These carbon discs were heated to 4540°F by series of water-cooled induction coils and were insulated by a felt blanket. Rated operating pressure of the water-cooled pressure vessel enclosing the carbon discs was 1200 psig. Control of this complex heater system was accomplished by a mini-computer.

3.1.4.2 Gaseous Hydrogen Heater

This heater was used to heat the hydrogen gas to the fuel manifolds of the HRE-AIM. The heater was capable of heating 2.5 lb/sec of gas from ambient temperature to 2100°F for 90 sec. The gas was heated by passing through a pebble bed heated by induction coils.

3.1.4.3 Fuel Supply Line Heater

Cal-rod type heaters were installed on each of the fuel supply lines from the GH_2 heater to the HRE-AIM to insure that the hydrogen gas supplied to the HRE-AIM was at 1000°F. Electrical power to these heaters was initiated well in advance of the scheduled test time to insure line temperatures were at maximum allowable to minimize heat loss. Power to these heaters was cut off prior to injecting hydrogen.

3.1.5 Fuel Control System

The operation of the HRE-AIM required injecting the hydrogen fuel from various fuel manifolds (see Figure 3-7 for schematic of this system). The control system used to supply desired amount of fuel to specific fuel manifolds is shown in Figures 3-6 and 3-8. The specific information relating to the venturi, measuring range, and method of calculation is shown in Appendix A.

3.1.6 Coolant Supply System

The coolant system for the HTF consisted of four closed-loop pumping systems and one open-loop pressurized dewar coolant supply system. All of

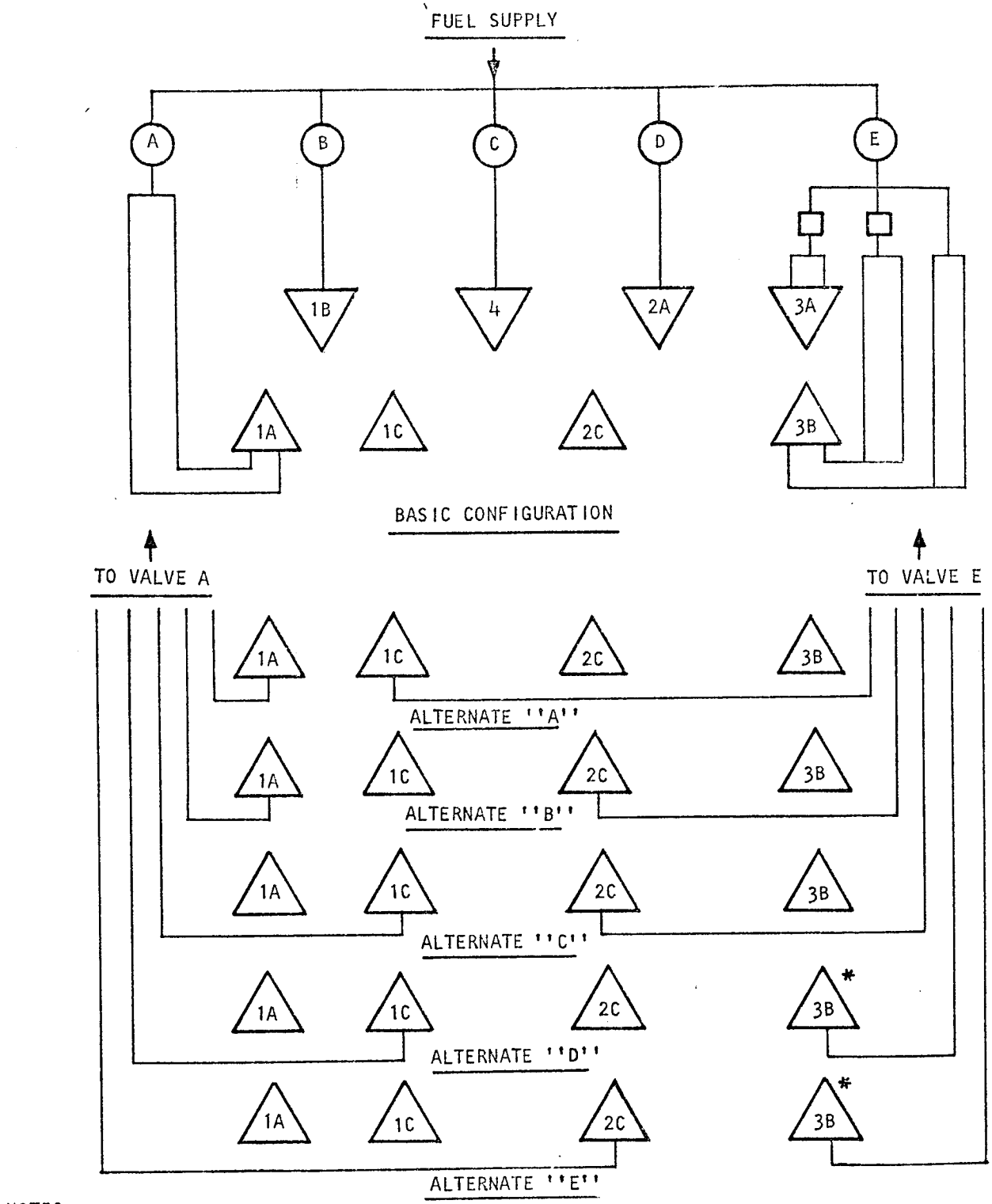

NOTES:

*SHUTOFF VALVE OPEN

○ FUEL FLOW CONTROL VALVE

□ SHUTOFF VALVE

△ FUEL MANIFOLD IDENT. CODE

Figure 3-7. AIM Fuel System Schematic

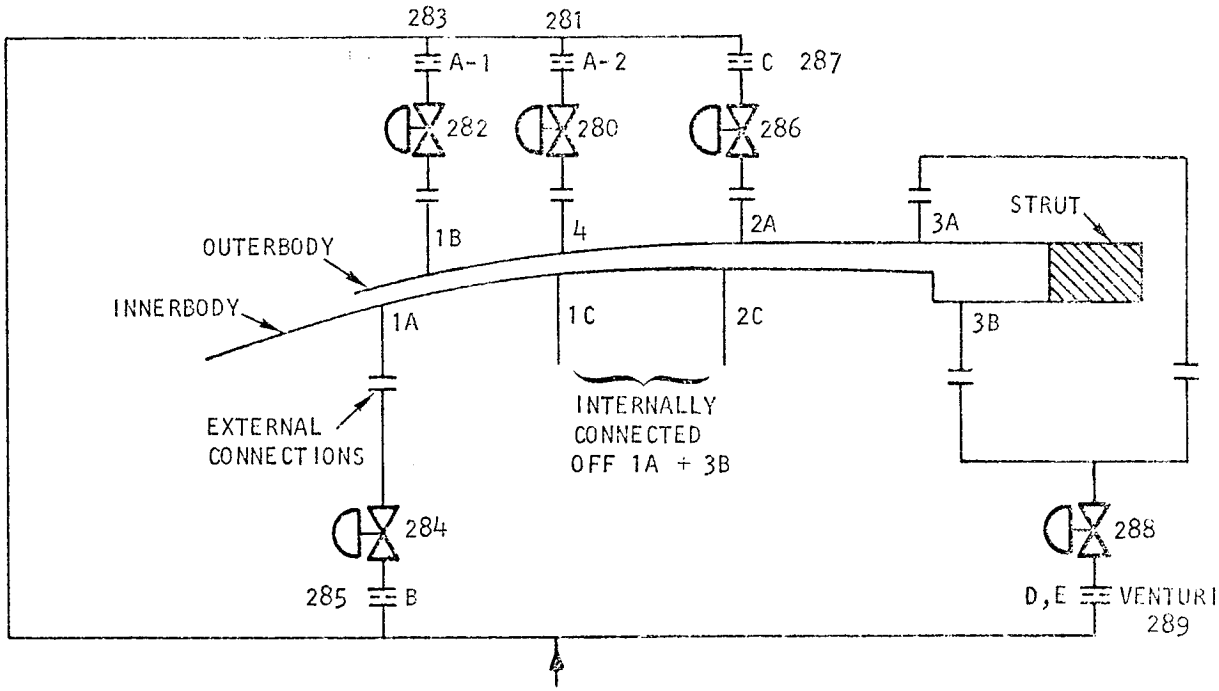

INJECTOR COMBINATIONS

OUTERBODY - ANY COMBINATION WITH ALLOWABLE INNERBODY COMBINATION

INNERBODY - ANY TWO INJECTORS WITH ANY OUTERBODY COMBINATION
EXCEPT → INJECTORS 3A + 3B USED TOGETHER FOR SUBSONIC COMB

Ser. No.	Sta No.	Req Flow Range, lb/sec		Venturi Range, lb/sec		Diameters, In.		Inlet Press, psig	Inlet Temp, °R
						Inlet	Throat		
B	1A	0.021	0.580	0.008	0.752	1.5	0.750	900	1600
A-1	1B	0.026	0.152	0.008	0.247	1.5	0.450	900	1600
C	2	0.021	0.520	0.0078	0.736	2.3	0.750	900	1600
D	3 (Sub)	0.021	0.580	0.0078	0.736	2.3	0.750	900	1600
E	3 (Sub)	0.158	1.518	0.068	2.00	2.3	1.220	900	1600
A-2	4	0.026	0.152	0.008	0.247	1.5	0.450	900	1600

S-89073

Figure 3-8. HTF GH_2 Fuel System

these systems utilized demineralized water. The rated capability of each system and it's primary use is listed below:

(a) A 600 gpm, 100 psig pumping system was used for the nitrogen heater system.

(b) A 1000 gpm, 120 psig pumping system was used to cool the mixer and the diffuser.

(c) A 300 gpm, 400 psig pumping system used to cool the hypersonic nozzle.

(d) A 1200 gpm, 400 psig pumping system used to cool the HRE-AIM.

(e) A 6000 gallon dewar pressurized to 400 psig used to augment cooling systems on the HRE-AIM, and cooling requirements of the hot nitrogen supply system.

3.1.7 Hydraulic Supply System

Hydraulic supply utilizing MIL-L-5606 oil capable of furnishing 34.0 gpm at 3000 psig was available to operate various components of the facility and the inlet spike actuator installed on the HRE-AIM.

3.1.8 Instrumentation Recording System

The instrumentation signal generated at the test site was conditioned and processed at three separate buildings A schematic of this system is shown in Figure 3-9.

The instrumentation signal generated in the test cell was initially conditioned at the instrument room at the test site and sent by wire to "B" control building. Here the signal was routed to four areas--control area, control computer area, support equipment area, and data-acquisition area. Only parameters pertaining to the status of the test was processed at this location. Pertinent operational parameters and remaining data was sent to "H" building for process and permanent recording.

At "B" control building an XDS-9300 data computer was used to display parameters and calculated data in engineering units for assessment during the test period. This computer was also used to reduce specific data to engineering units immediately following the test so that success of the test and plans for the following test could be determined.

Equipments available for use at the "B" control building in addition to the XDS-9300 computer with a 32,000 word memory were:

(a) Four tape transports

(b) 250,000 word rapid-access disk (RAD)

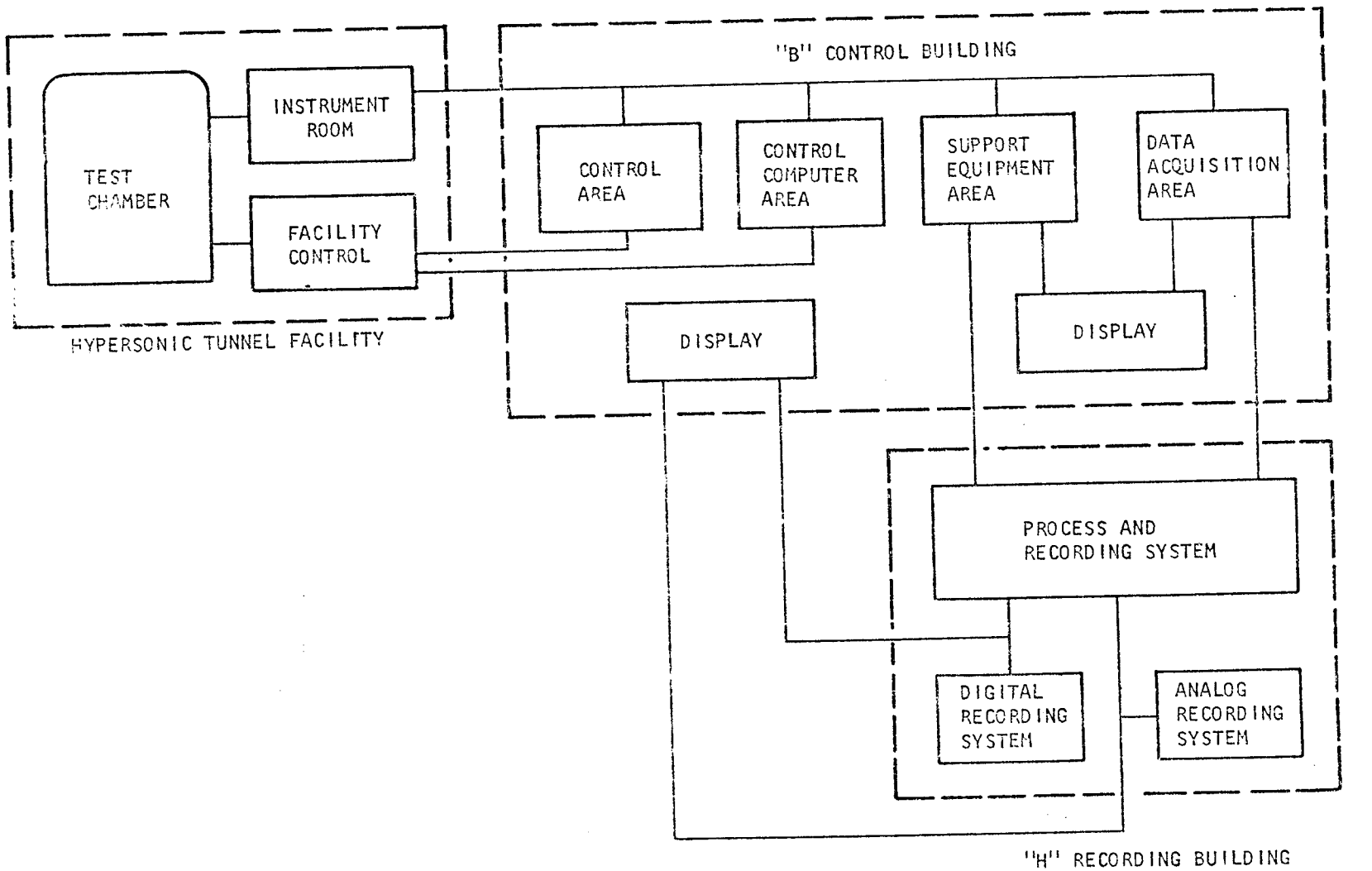

Figure 3-9. Instrumentation Signal System

(c) Two mini-computers with a 180,000-word RDS to interface with graphical printout.

(d) Five cathode ray displays

(e) Plotter

(f) Printer

Equipments available at "H" Building were:

(a) Two central record trains to record prime digital data (with capability of 400 channels)

(b) Two FM recorders for recording 10 KH_2 analog data

(c) Ten strip-chart recorders

(d) Two 36-channel, oscillograph recorders

3.1.9 Facility Control System

The control system for the HTF consisted of (a) normally manual-operated console (b) a Xerox Data System (XDS) 910 digital computer and a hybrid analog computer system used to initiate special sequence of events and to control ramp rates of fuels and alike, and (c) special abort monitor interfacing with the XDS 910 computer.

The abort monitor system consisted of XDS-CF16A minicomputer programmed as the software for the abort system. The digital data from the central recording system was compared against the stored programmed tables of high and low limits. Whenever an abort or out-of-limit condition was detected, the XDS 910 computer was interrupted from continuing to execute the test program, and facility shutdown sequence was initiated. Although this abort system is slower than the normal hardware abort monitor, this system was deemed more flexible and could best handle the complex system.

Additional photos of the Hypersonic Tunnel Facility are shown in Figure 3-10.

F-21406

Figure 3-10. Hypersonic Tunnel Facility

Computer Control Room

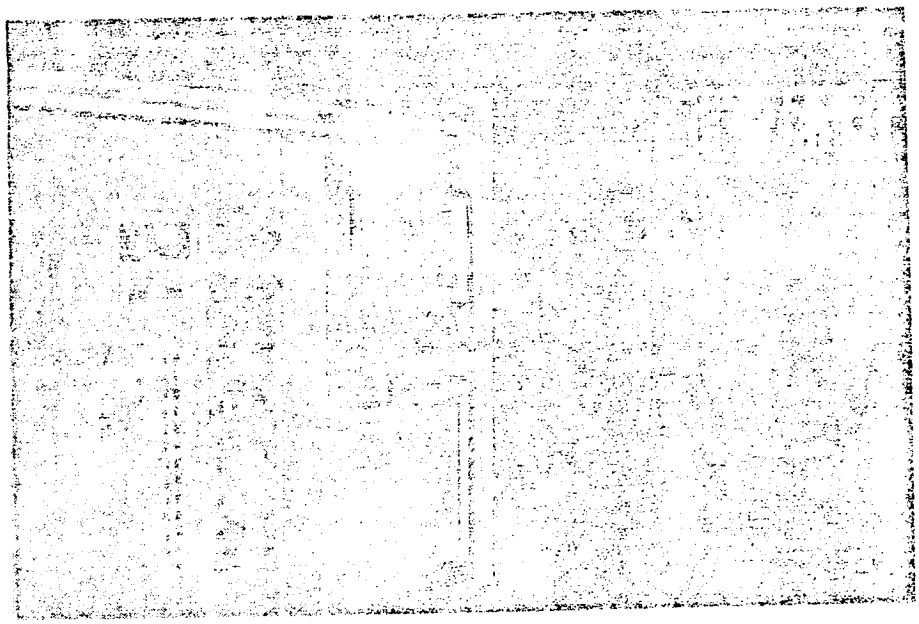

Recording System

F-21405

Figure 3-10. (Continued)

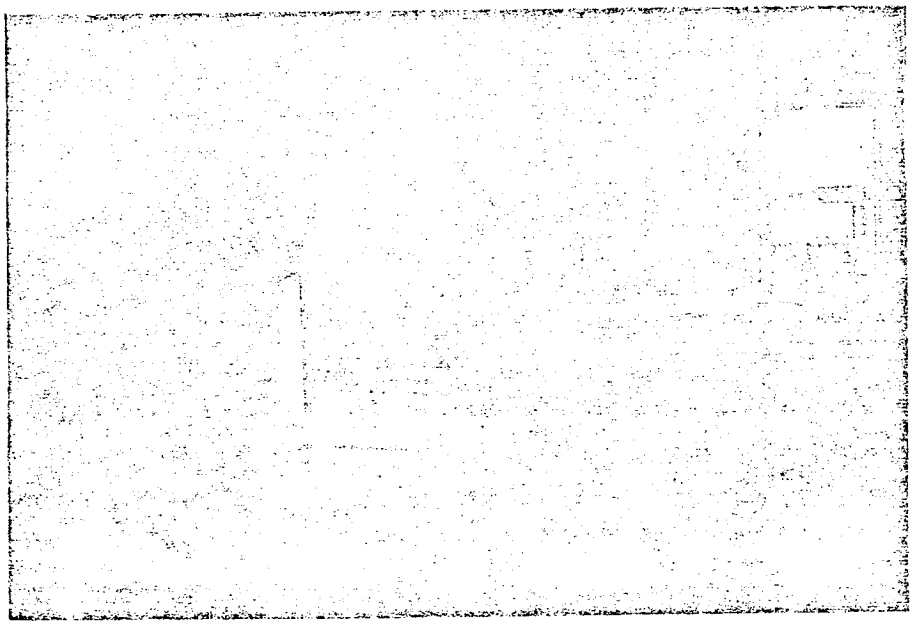

Facility and Fuel Control System

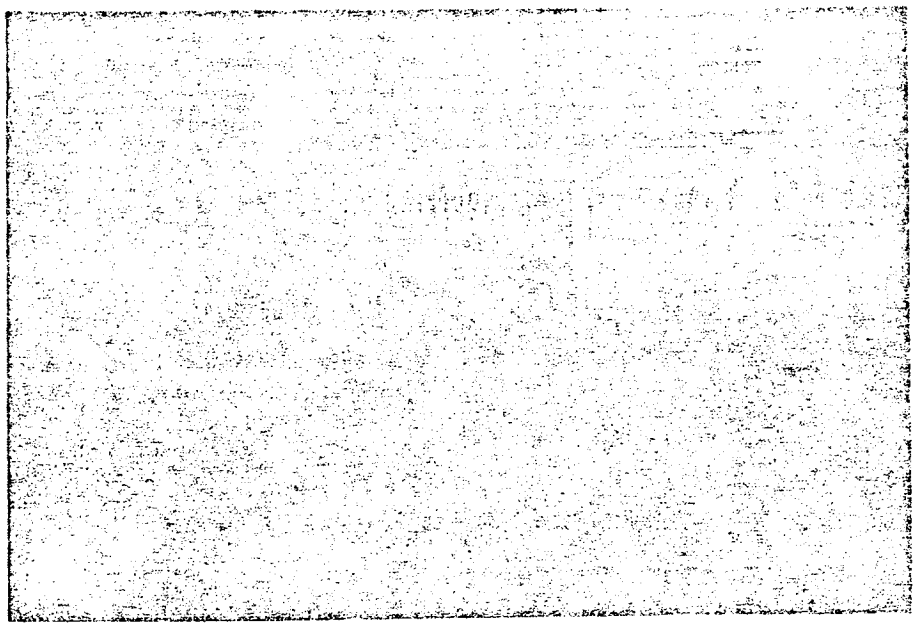

F-21404

Signal Conditioning Equipment

Figure 3-10. (Continued)

4. PROCEDURE

4.1 PRE-TEST/POST-TEST PROCEDURE

Procedure for preparing the facility for test required approximately six hours of checks and final adjustments of various valves and control devices. A step-by-step check list consisting of approximately 700 steps was used to ensure a successful test. Check list for post-test consisting of approximately 300 steps was used to ensure maintaining the facility in an operable condition. Pre-test and post-test check lists were also made for the HRE-AIM. Checks included: (a) correct coolant system valve position and pressure setting, (b) inlet spike position setting, (c) notation of physical conditions, and (d) dimensional check of critical areas.

4.2 TEST PROCEDURE

After the pre-test check list had been completed and system status established as acceptable for test, a summary meeting was held for personnel responsible for various test functions to review and re-establish objectives, go/no-go limits, and alternate plans.

Testing was coordinated between the NASA Facility test director and the Garrett Corporation representative responsible for establishing acceptability of the test condition, initiating and terminating the pre-program fuel schedule, and initiating alternate plans to achieve objectives targeted.

The basic test sequence was as follows:

1. When system readiness was established, coolant system and recording system were initiated.

2. Radiation shutter was opened.

3. Dewar coolant system was actuated.

4. Steam to facility ejector was initiated.

5. A check was made to ensure that the test chamber had reached predetermined pressure limits.

6. Start synthesized air through wind tunnel.

7. Establish the fact that hypersonic airflow around the engines has been obtained by observing Schlieren system.

8. Open the engine inlet spike assembly, and establish the fact that engine start has been obtained.

9. Initiate fuel valve.

10. If facility unstarted or engine unstart was experienced, fuel injection was terminated and inlet spike assembly closed. Re-establish engine start and initiate alternate plan.

11. Test was automatically terminated whenever pre-determined point in the test schedule was reached, or manually terminated when minimum facility limits were reached.

5. DESCRIPTION OF TESTS

5.1 CALIBRATION TESTS

During the process of installing the AIM in the test facility, calibrations were performed on the fuel and thrust measurement systems. The tests are described below:

5.1.1 Fuel System Calibration

5.1.1.1 Pre-Installation Calibration

A preliminary fuel system calibration was performed before the AIM was installed in the wind tunnel. The test was intended to reveal any unforseen problems which could be corrected prior to the installation, thereby preventing later delays.

A typical test setup schematic for one of the eight AIM fuel manifolds is shown below:

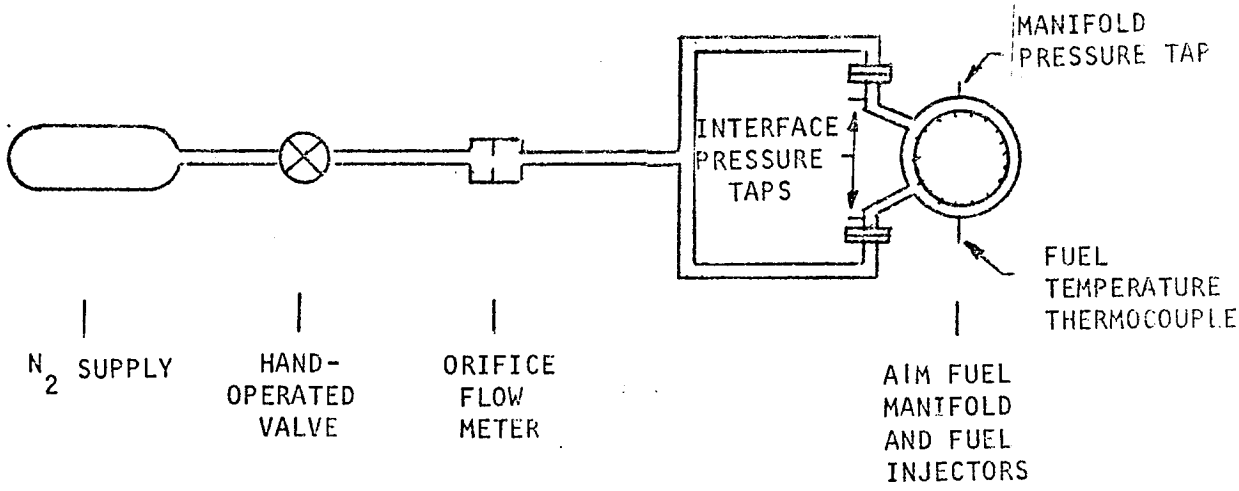

The purpose of the test was as follows:

(a) Determine the pressure drop between the facility interface and the fuel manifold for each fuel system.

(b) Determine the fuel injector discharge coefficients.

These data provide a means of determining the relationship between fuel flow rate and fuel line pressure at the facility interface. Over-pressure of the fuel lines could then be avoided during wind tunnel testing. Also, the data

provided a means of checking fuel flow measured by the venturis used during wind tunnel tests.

5.1.1.1.1 Test Results

Nitrogen was fed to each fuel manifold through the orifice meter. Flow rate and fuel line and manifold pressures and temperatures were measured. Manifold pressures were set at values high enough to choke the injector. The discharge coefficients were calculated as follows:

$$Cd = \frac{W\sqrt{T}}{0.5228\ P\ A}, \text{ where}$$

W = orifice meter flow rate

T = fuel manifold temperature

$$0.5228 = \frac{W\sqrt{T_t}}{PtA} \text{ for nitrogen at sonic velocity, where}$$

P = manifold pressure

A = measured injector area

The interface to manifold pressure drops were calculated as follows:

$$\frac{\Delta P}{P} = \frac{\text{interface pressure - manifold pressure}}{\text{interface pressure}}$$

The results of the tests are presented in the following table:

Fuel System	Interface-to-Manifold Pressure Drop, %	Injector Discharge Coefficient
1A	31	91
1B	9	74
1C	29	85
4	7	89
2a	20	75
2c	28	84
3A	5	77
3B	24	77

The variation in discharge coefficient between the different injectors is due to different manifold and injector configurations used in each case.

5.1.1.2 Post-Installation Calibration

The AIM fuel system was calibrated after the AIM was installed in the test facility. The fuel system, instrumentation, and data acquisition systems were in the configuration to be used for wind tunnel tests. The purpose of this calibration was to

(a) Checkout the fuel system and adjust the fuel control.

(b) Measure the injector discharge coefficients for comparison to the values obtained in the pre-installation calibration.

Nitrogen was fed to each fuel manifold through the facility fuel system. Fuel manifold pressures were set at values high enough to choke the injectors. The results of the calibration are compared to the pre-installation calibration in the following table:

Fuel System	Pre-Installation Discharge Coefficient	Post-Installation Discharge Coefficient
1A	91	91
1B	74	--
1C	85	84.5
4	89	--
2a	75	72
2c	84	84
3A	77	78
3B	77	77

Discharge coefficients were generally in good agreement. Values were not obtained for systems 1C and 4 due to a data acquisition problem.

5.1.2 Thrust Calibration

5.1.2.1 Load Cell Calibration

A schematic of the thrust measurement system is given in Figure 5-1. The system consisted of a conventional thrust bed mounted on flexure plates. The bed was grounded through a 3000 lb load cell capable of measuring thrust or drag. Applied forces on the AIM were transmitted through mounting struts to the thrust bed. The struts were isolated from the tunnel flow by the outer cowl body (OCB) legs.

The system is shown in its calibration configuration. A thrust calibration fixture replaced the AIM exhaust nozzle plug. Another fixture mounting a hydraulic actuator was bolted to the test cell floor. The actuator was used to apply calibration loads up to 3000 lb in the thrust and drag directions. Hydraulic power was supplied by a hand-operated pump. The applied

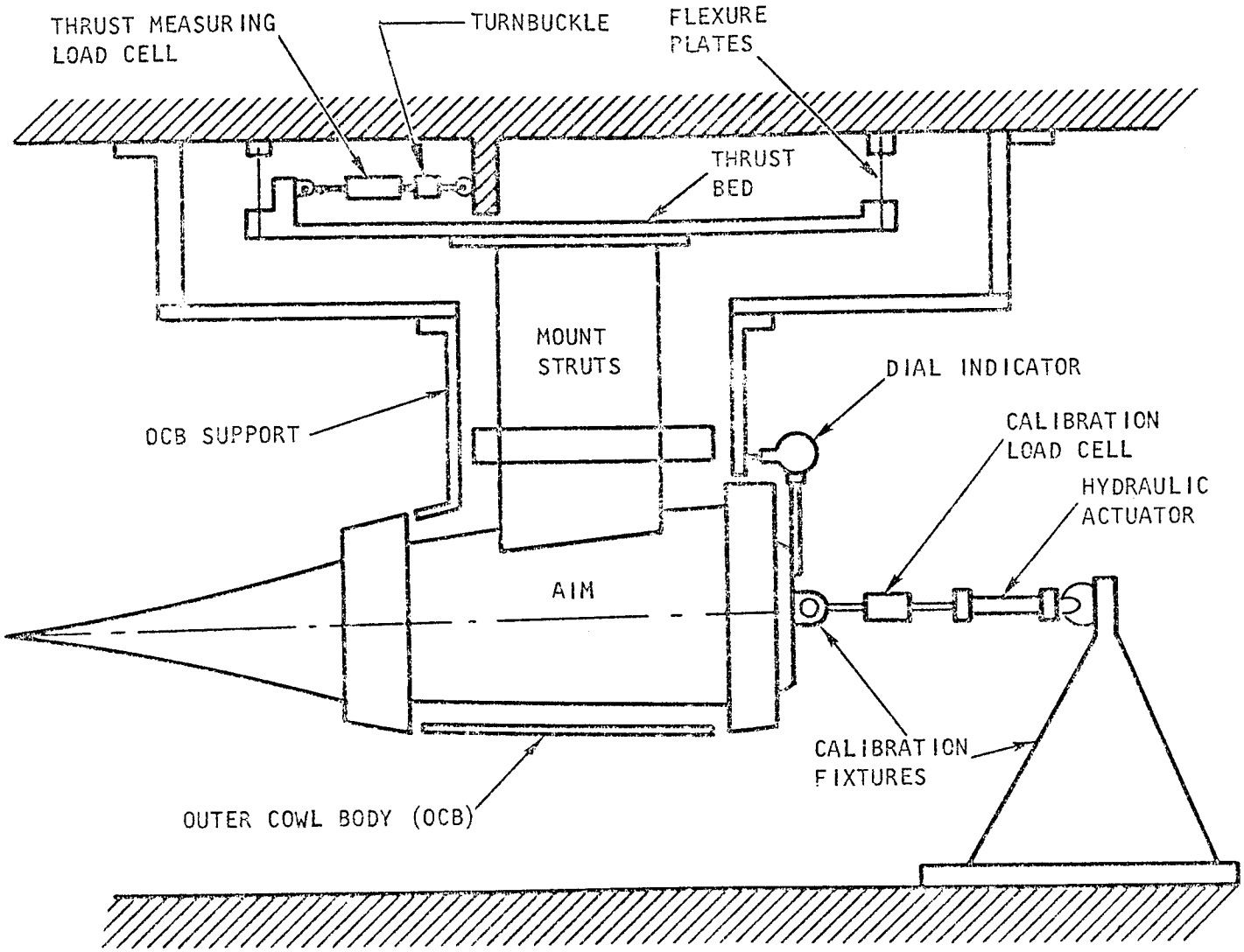

Figure 5-1. Thrust Calibration System Schematic S-93798

force was measured by the calibration load cell. The corresponding facility load cell output was recorded for both upscale and downscale readings. The axial deflection of the AIM due to the applied load was measured by a dial indicator. Deflection measurements were used for diagnostic purposes.

5.1.2.1.1 Test Results

The data for a typical calibration is plotted in Figure 5-2. An equation was fit to the data for each calibration. The equation was programmed in the data reduction computer program to correct the load cell readings taken during wind tunnel testing. Table 5-1 defines the equations applicable to each run.

The facility load cell reading is seen to be considerably less than the applied load in Figure 5-2. This difference is because of the force required to swing the thrust bed on its flexure plates and to deflect the service lines connected to the AIM.

5.1.2.2 Thrust Measurement System Development

Early in the program considerable difficulty was encountered due to the engine contacting the OCB. This introduces a thrust measurement error because an unknown portion of the force applied to the engine is transmitted to the OCB instead of the load cell. The problem was detected by non-linearity or excessive hysterisis in the thrust stand calibration data. The problem was caused by two major factors, (1) A low design clearance (1/8 in. minimum) was held between the OCB and the engine, and contact occurred on parts where close tolerances were not held, such as fuel tubing and insulation; and (2) the outer cowl body was subject to distortion due to heating loads applied to the engine during wind tunnel tests. The distortion was sufficient to cause contact with the engine. Distortion was a factor early in the program when the tunnel was not fully started. (See Section 5.2.) During this period strong shock waves were impinging on the OCB causing an excessive amount of heating. This was evidenced by pressure measurements in the tunnel test section and by abnormal discoloration of the OCB. At the time in the program when the tunnel-starting problems were solved, the OCB was out-of-round by 0.070 in. on a radius. It remained at this condition for the remainder of the program. The contact points were relieved by repositioning or reshaping the required components.

5.1.2.3 Service Line Tare Forces

Several tests were performed to determine the tare forces applied to the thrust measurement system by the cooling and fuel lines. The tests are described below.

5.1.2.3.1 Cooling System

The cooling system tare force was measured by comparing load cell readings with the cooling system shown in Figure 5-3. The nozzle plug was installed and the calibration load was applied through a fixture normally used to install the plug. A 509 lb weight was used to apply the load through a cable and pulley arrangement. The results of this test are given in the following table:

Figure 5-2. Thrust Stand Calibration

TABLE 5-1

LOAD CELL CALIBRATION EQUATION SUMMARY

Readings	Load Cell Reading-LCR Range, lb	Equation
16-38	$-\infty$ to -15	FLCL = 1.102LCR-123.5
	-15 to +30	= 4.09LCR-78.7
	+30 to $+\infty$	= 1.115LCR+10.6
39-55	$-\infty$ to -25	FLCL = 1.124LCR-22.0
	-25 to +35	= 2.25LCR+6.0
	+35 to $+\infty$	= 1.096LCR+47.0
56-95	$-\infty$ to -29	FLCL = 1.1347LCR-17.03
	-29 to +24	= 2.01LCR+8.0
	+24 to $+\infty$	= 1.106LCR+29.45
96-97	$-\infty$ to -130	FLCL = 1.0584LCR-62.4
	-130 to +95	= 1.538LCR+0
	+95 to $+\infty$	= 1.0849LCR+42.9

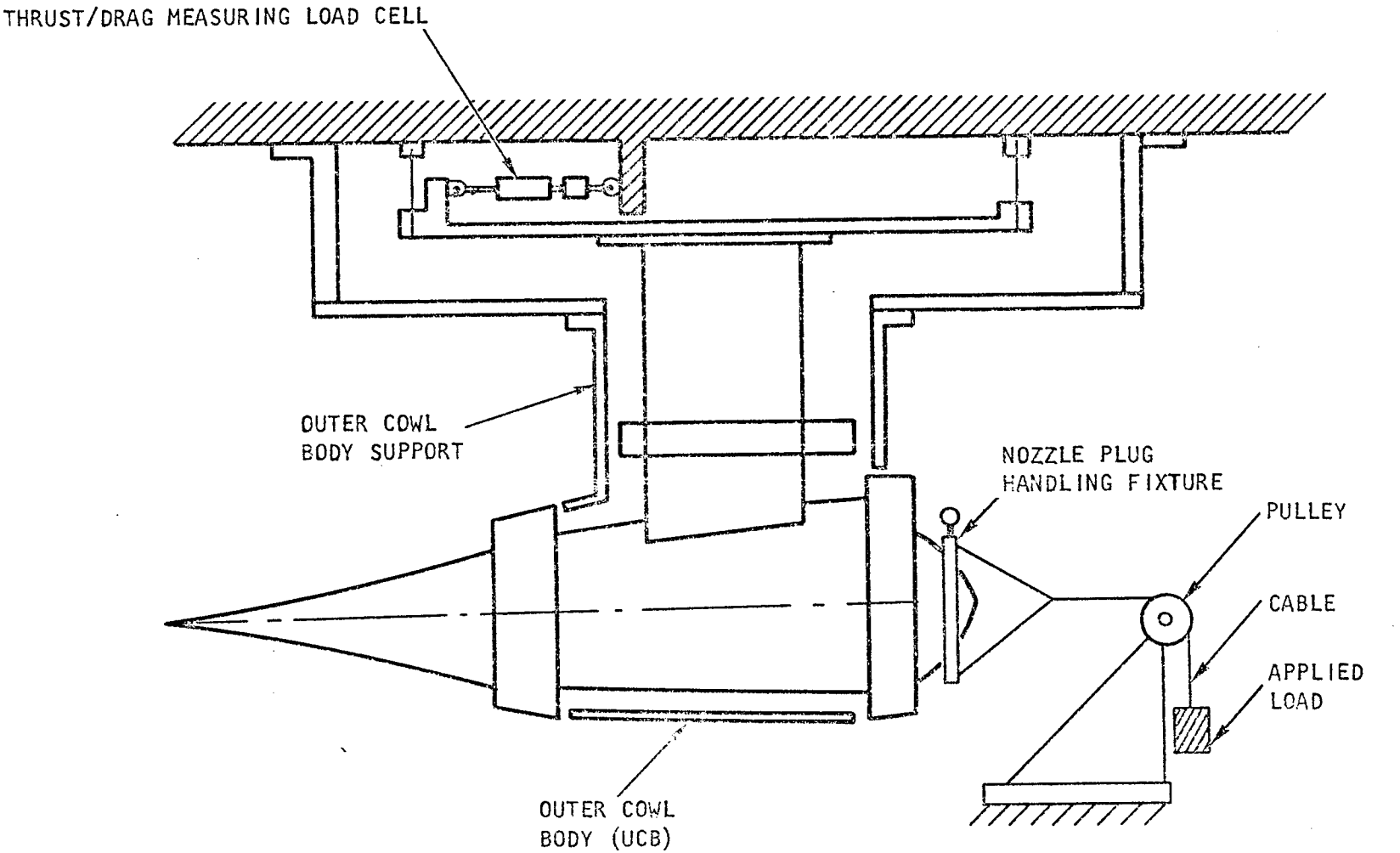

Figure 5-3. Thrust Calibration System Schematic - Modified for Measuring Tare Forces

The results of the test are given in the following table:

CHANGE IN LOAD CELL READING DUE TO COOLING FLOW

Applied Load, lb	*Change in Load Cell Reading, lb
0	+48.5
-509	+50

*Positive indicates thrust direction

These data were used to correct the thrust measurement load cell readings for cooling system tare force. All load cell readings were reduced 49 lb to account for cooling system tare force.

5.1.2.3.2 Fuel System

Tests were performed to check for the presence of tare forces applied by pressure in the fuel lines. Ambient temperature nitrogen was flowed through fuel systems 1A, 1B, 4, 2a, and 2c. The test cell was at ambient pressure with no wind tunnel flow. The change in load cell reading was recorded as the fuel manifold pressure was increased from ambient to 300 psia in each fuel manifold.

A source of error in determining the tare force in this manner is the thrust produced by the discharge of gas from the engine inlet and exhaust nozzle, as shown below. The thrust should not be included in the measured tare force.

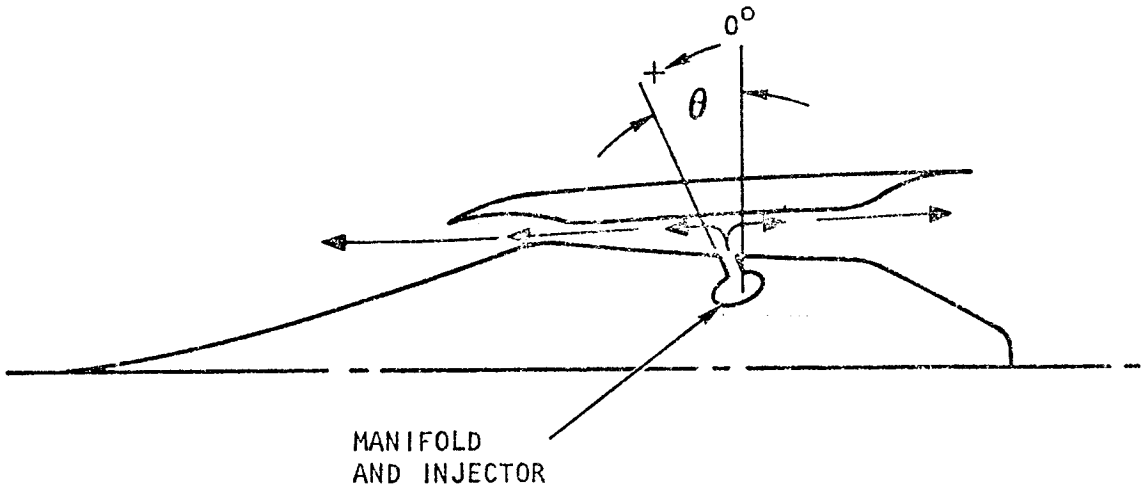

The net thrust force applied to the engine is the difference between the inlet and nozzle thrusts. The inlet spike was set at the open position to provide maximum cancellation between the inlet and nozzle thrusts.

The results of the tests are given below:

CHANGE IN LOAD CELL READING
FROM AMBIENT TO 300 PSIA FUEL MANIFOLD PRESSURE

Injector	*Force Change, lb	Injector Angle, θ, deg from Vertical
1A	+5	90
1B	-4	90
4	-5	90
2a	-22	+23
2c	-32	+30

* Positive indicates thrust direction

The results show the forces to be negligible with the exception of injectors 2a and 2c. These injectors are inclined forward, as shown in the above table and figure.

The forward inclination tends to increase the net force in the drag direction. This is due to the axial component of fuel injector thrust. The higher forces measured for injectors 2a and 2c (see table above) show a trend supporting the above explanation. Due to the low forces measured, no tare correction for fuel line pressure was made to the wind tunnel data.

Tests were also performed to check for the presence of tare forces applied by thermal expansion of the fuel lines. Nitrogen at approximately 1300°R was flowed through each fuel system to heat the fuel lines. When the AIM fuel manifold temperature reached its maximum value, the flow was turned off. Load cell readings and fuel manifold temperature and pressure were taken continuously during the testing of each system. The load cell readings just before and just after the heating period were compared to determine the tare force. These results are given below:

CHANGE IN LOAD CELL READING DUE TO HEATING
FUEL LINES

Fuel Station	Change in Load Cell Reading, lb
1A	+4
1B	-2
4	-4
2a	-3
2c	-10

Due to the low forces measured, no tare force correction was made for wind tunnel tests.

5.1.2.4 Nitrogen Purge Force Calibration

5.1.2.4.1 Purge System Description

A schematic of the AIM cavity purge system is presented in Figure 5-4. The outer cowl body (OCB) is isolated from the AIM so that aerodynamic forces applied to the OCB and its supporting legs will not be applied to the thrust measurement load cell. The cavity between the AIM and the OCB is purged with nitrogen. The purge provides inert gas around the fuel manifolds and prevents the hot wind tunnel flow from entering the cavity through the slots at the leading and trailing edge of the OCB. The purge flow exhausts from the cavities through these slots.

The force exerted on the AIM by the pressure in the cavity is transmitted to the load cell. The purge tare force must be known to make the necessary correction to the load cell reading to determine thrust.

Initial estimates showed the cavity force to be in the order of twice the internal thrust of the AIM. To minimize the purge force, a seal was installed dividing the cavity into two compartments as shown. A separate purge line and control valve supplied each compartment. This permitted the forward and aft cavities to be independently controlled to the minimum pressure required to prevent hot gas entry.

The forward slot is located on a forward-facing external surface. This results in a higher static pressure in the external flow approaching the slot; thus, a higher pressure is required at the forward slot to prevent hot gas entry. Therefore, the seal was positioned as close as possible to the forward slot to minimize the projected area exposed to the higher pressure.

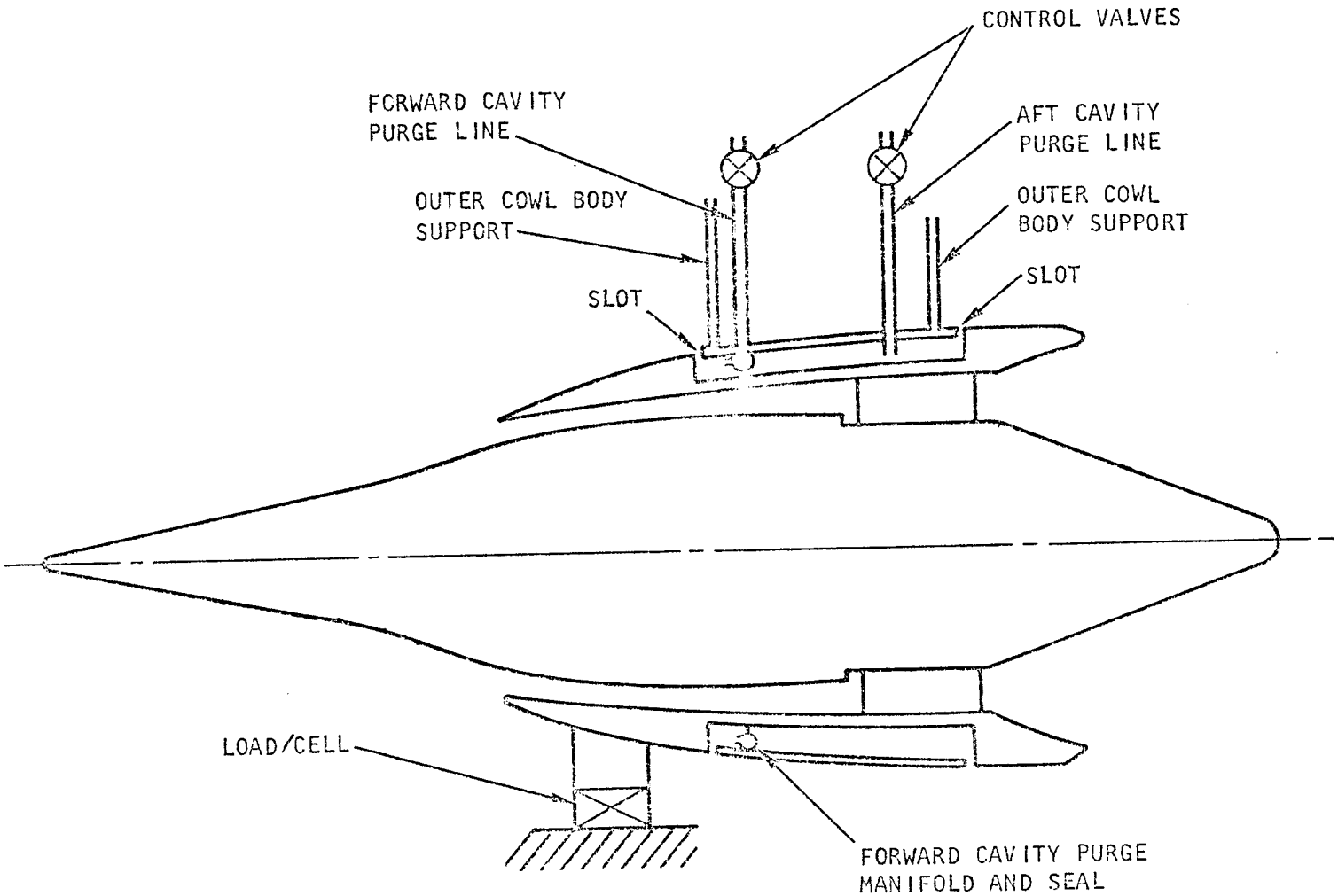

Figure 5-4. Cavity Purge System Schematic

Initial estimates based on simple pressure-times-area calculations showed that the absolute value of the purge force could be reduced by a factor of three, using the seal. It was also estimated that forces on the forward cavity could cancel the aft cavity forces, resulting in a small or negligible net tare force.

The forward cavity purge flow was supplied with a manifold which was integral with the seal as shown in Figure 5-4. The sealing surface was 1/8-in.-thick teflon, seated against the AIM outerbody. The seal was interrupted at several points to clear instrumentation and fuel lines. This resulted in leakage to the aft compartment. The aft cavity purge line supplied the additional flow required to raise the compartment to the required pressure.

5.1.2.4.2 Determination of Purge Tare Force

The plan to determine the purge tare force is described in detail in AIM Test Plan (Document No. AP-71-7877), Appendix B. The plan is summarized below.

The purge tare force was to be determined by pressurizing the cavities and measuring the force using the thrust measuring load cell. The force was to be measured with and without external flow. Preliminary tests would be performed with the test cell at ambient pressure to check out the system and adjust the purge control valves. Preliminary force mreasurements would be taken. The tests would then be repeated with the test cell evacuated using the facility steam ejector. This would provide data over the required range of cavity-to-test-cell pressure ratios. The slots could be choked at this condition.

The tests would then be repeated with external flow over the range of tunnel operating conditions to be used in AIM performance tests. The cavity pressures would be varied over a wide enough range so that the force versus pressure could be extrapolated to zero pressure to determine the absolute change in force on the AIM due to purge. This method is discussed in detail in Appendix B of the AIM Test Plan.

The purge force, as measured by this method, would include the effect of shock wave impingement on the AIM cowl. The shocks are generated by the purge jet leaving the slot between the OCB and the cowl. The strength of the shocks and the area of the cowl surfaces affected by the shock pressure rise were expected to be affected by the purge pressure. The force change due to the pressure rise on the cowl would be incorporated in the measured purge force. Also, any effect of external flow on the cavity wall pressures in the region of the slots would be included in the force measurement.

The wind tunnel would be run at a reduced total temperature of 1500°R for these runs. This would reduce the chance of damage due to hot gas entry. Purge pressures would be reduced until thermocouples in the cavities and in the forward slot showed a temperature rise, indicating incipient hot gas entry. This would establish the low limit for the allowable purge pressure.

The calibration would be spot checked during later performance runs at a higher tunnel total temperature to determine if the calibration shifted with temperature.

5.1.2.4.3 Test Results

Figure 5-5 shows typical purge force calibration data with no wind tunnel flow. The following procedure was used to generate the data:

(1) Evacuate the test cell using the facility steam ejector.

(2) Set the aft cavity purge valve at a fixed position.

(3) Vary the forward cavity valve setting.

(4) Repeat steps 2 and 3 to obtain data at 4 aft cavity valve settings.

The test cell pressure and the four cavity pressures defined in Figure 5-6 were recorded. The tare force was measured by the thrust measurement load cell and corrected using the calibration described in Section 5.1.2.1.

The tare force is plotted versus $PA2-P_{cell}$ for this explanation. It is to be understood that the remaining cavity pressures also affect the tare force. Note that any combination of valve settings causes a force in the drag direction. This is contrary to the prediction based on simple pressure times area calculations that cancellation of the forward and AFT cavity forces could be achieved. Had cancellation been achieved the tare force would have been zero at some conditions tested.

The possible reasons for this anomily are given below:

(1) The projected area subjected to the cavity pressures in the region of the aim-support struts was neglected in the prediction of tare force due to its complicated shape. Also, the seal configuration in this area made it difficult to predict local pressures.

(2) Pressure variations due to aerodynamic forces within the cavities were neglected in the force prediction due to the complicated flow paths and shapes involved.

Aerodynamic effects in the purge flow are apparent in the following table which presents the four cavity pressures for a typical case.

Cavity Pressure, psia				Tare Force, lb
PA1	PA2	PB1	PB2	
19.45	21.28	10.61	7.69	-1518

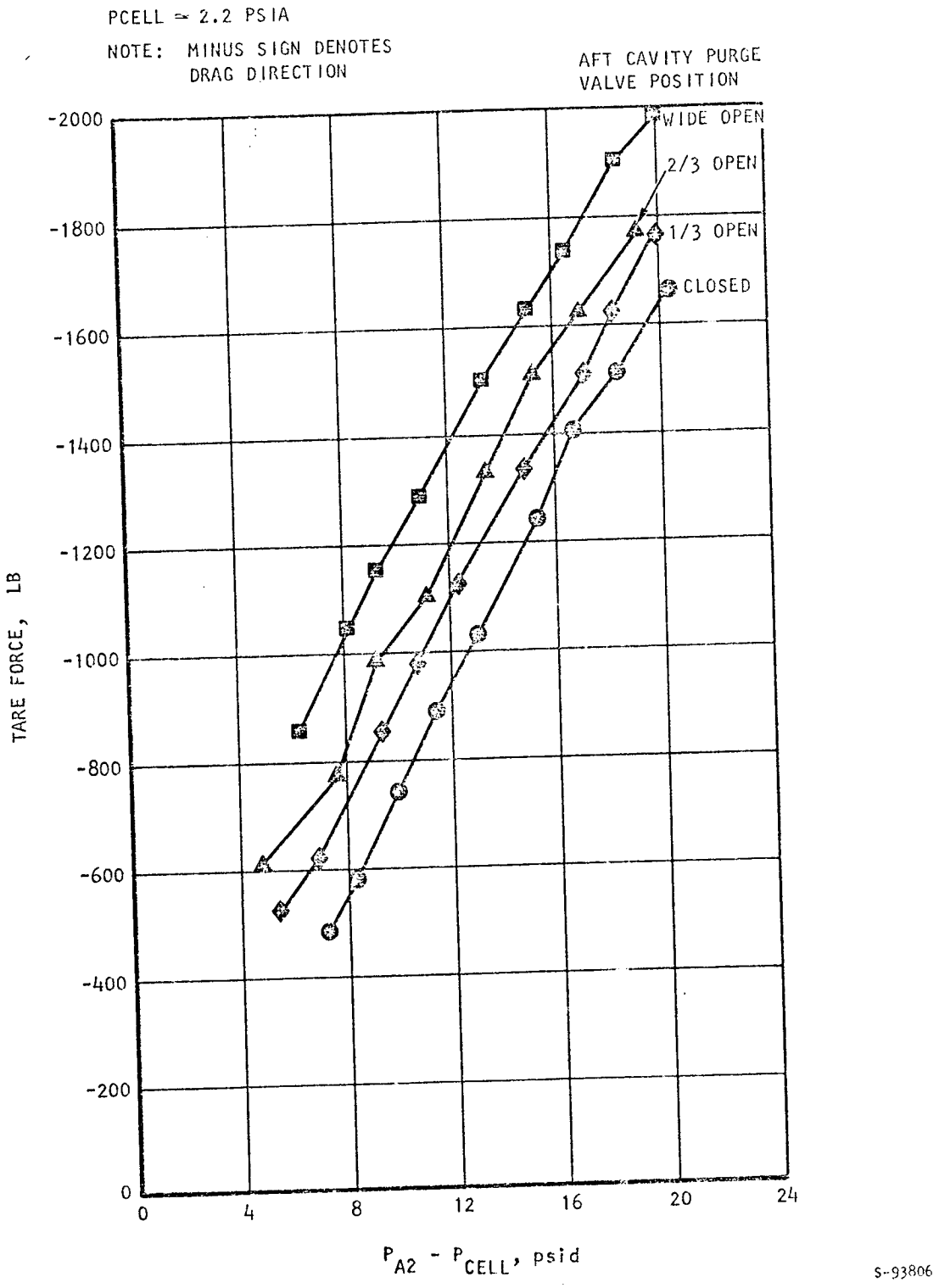

Figure 5-5. Cavity Purge Force Calibration Data

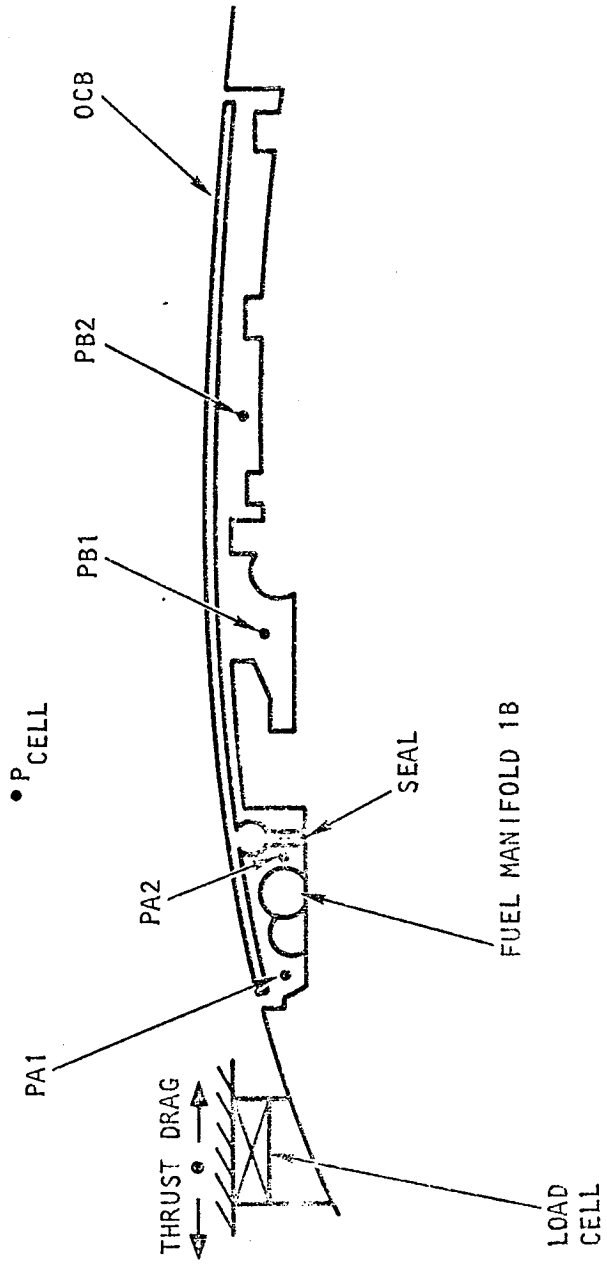

Figure 5-6. Cavity Pressure Tap Locations

s-93797

ORIGINAL PAGE IS
OF POOR QUALITY

Had velocities within the cavity forward of the seal been negligible, PA1 and PA2 would have been equal. The same holds true for PB1 and PB2 which are in the cavity aft of the seal.

Another aerodynamic effect within the cavities was discovered during AIM performance testing. The load cell reading was seen to change significantly while the AIM was operating at a constant fuel equivalence ratio. The reason for the anomaly was traced to purge force change due to pressure variations within the purged cavities. Examination of the data showed that the cavity pressures changed with the fuel temperature in manifold 1B. The suspected reason for this was the thermal expansion of the manifold and its insulation closing the gap between the manifold and the outer cowl body (see Figure 5-6). This restricted the purge flow through the gap causing a higher pressure loss. This was verified to be true in later purge tests described below.

To investigate the effect of the heated fuel manifold on the purge force, a test was performed similar to that described in the above paragraphs. The same test procedure was used except 1300°R nitrogen was flowed through fuel system 1B to heat the fuel manifold. A sample of the data is compared to previous results from tests with a cold manifold in the following table:

1B Manifold Gas Temp	Cavity Pressure, Psia				Tare Force, lb
	PA1	PA2	PB1	PB2	
1300°R	14.04	21.44	8.44	6.36	-1069
Ambient	19.45	21.28	10.61	7.69	-1518

The comparison is made at a fixed value of PA2 with the aft cavity purge valve closed. PA1 is lower when the manifold is hot, indicating a higher pressure drop in the flow across the manifold. Note the large difference in tare force.

Calibration data were also taken with the AIM translated 0.020 in. in the aft direction from its zero load position. It was known that the AIM translated forward about 0.020 in. from an unlit to a maximum-thrust condition. This translation was caused by the deflection of the thrust stand, the AIM support struts, and the load cell. A 0.020-in. translation causes the purge slot widths to change about 22 percent. This, in turn, causes a corresponding change in the purge flow. The resulting changes in velocities could change the pressure distribution within the cavities thereby affecting the tare force.

To translate the AIM, the load cell turn-buckle (see Figure 5-1) was adjusted to close the forward slot from 0.090 to 0.070 in. The load cell was

then re-calibrated, and a purge force calibration performed. Sample data for the two slot widths is compared below. The AFT cavity purge valve is closed in both cases.

Forward Purge Slot Width, in.	PA1	PA2	PB1	PB2	Tare Force, lb
0.090	15.93	17.55	8.67	6.27	-1185
0.070	16.45	17.81	8.74	6.43	-1260

The comparison shows a slight difference between the two conditions.

The following conclusions were drawn regarding the tare force calibrations:

(1) Flow velocities within the cavities are sufficiently high to cause significant aerodynamic effects on the measured cavity pressures.

(2) Independent variation of any one of the four measured pressures could cause a significant variation to the tare force.

(3) Correlation of the data by plotting as originally proposed is impractical because of the large number of variables involved.

(4) Calculations of the tare force using wall pressure integrals are impractical because of instrumentation limitations.

However, analysis of the calibration data showed that the tare force can be accurately correlated at various conditions knowing only the four cavity pressures. The analysis is described in the following section.

5.1.2.4.4 Correlation of Data

Calibration data taken at the following conditions was used for the purpose of correlating the purge tare force with the cavity pressures.

(a) No external flow.

(b) Test cell at ambient pressure, PA1 varied from ambient to 24 psia.

(c) Test cell evacuated to a nominal pressure of 2.2 psia. PA1 varied from 2.2 to 23 psia.

(d) Same as c above with heated fuel manifold.

(e) Same as c above with the forward purge slot width increased 22 percent.

Data were used only for the case where the aft cavity was pressurized by seal leakage from the forward cavity. Data taken with flow through the aft cavity purge line were not used. Wind tunnel tests showed that seal leakage alone was sufficient to prevent hot gas entry into the aft cavity. Thus, the aft cavity purge system was not used for subsequent tunnel tests.

Data at the above conditions was input into a curvilinear regression computer program. The program was used to determine an equation which would yield the minimum deviation between the measured tare force and the force calculated as a function of the four measured cavity pressures. The following equation was found to give the best results:

$$F_{TARE} = A_1(P_{A1} - P_{amb}) + A_2(P_{A2} - P_{amb}) + A_3(P_{B1} - P_{amb}) \qquad (5\text{-}1)$$
$$+ A_4(P_{B2} - P_{amb}) + A_5(P_{A2} - P_{amb})\frac{P_{A2}}{P_{A1}}$$
$$+ A_6(P_{A2} - P_{amb})\frac{P_{A2}}{P_{B1}} + A_7(P_{A1} - P_{amb})\left(\frac{P_{A1}}{P_{amb}}\right)$$
$$+ A_8(P_{B2} - P_{amb})\left(\frac{P_{B2}}{P_{amb}}\right) + A_9(P_{B1} - P_{amb})\left(\frac{P_{B1}}{P_{B2}}\right) + A_{10}$$

The coefficients calculated by the program are as follows:

$A_1 = 142.5$ $A_2 = 94.02$ $A_3 = 122.5$ $A_4 = -29.12$

$A_5 = 68.74$ $A_6 = 21.33$ $A_7 = 2.409$ $A_8 = -12.08$

$A_9 = 105.1$ $A_{10} = -4.7$

The program calculated the standard error as follows:

$$\text{Standard Error} = \sum_{1}^{N} (F_{calculated} - F_{measured})$$

The error as defined above was 21 lb over the entire range of conditions defined above. The constant, A_{10}, represents an assumed extraneous force as a check on the validity of the data. The low value of -4.7 lb verifies the absence of a constant offset in the data due to an extraneous force.

A comparison of the tare forces calculated from Equation (5-1) and the measured forces is given in Figure 5-7. The measured and calculated forces show good agreement.

The cavity pressure (psia) for a typical wind tunnel test at Mach 6, at a tunnel total pressure of 750 psia, are given below.

PA1 = 15.06; PA2 = 18.7; PB1 = 7.81; PB2 = 7.26

The absolute purge tare force calculated from Equation (5-1) using the above pressure is -1400 lb.

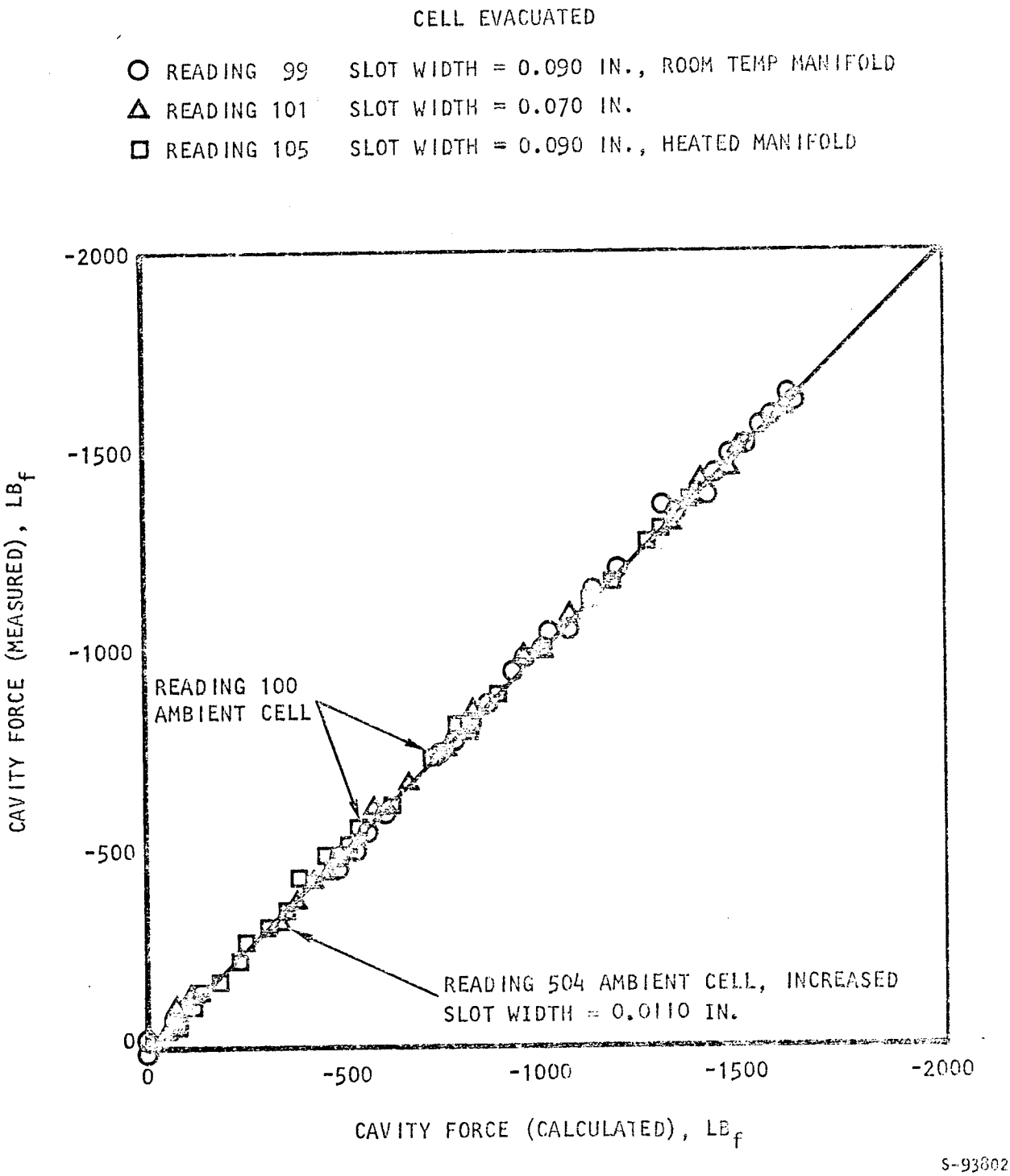

Figure 5-7. Correlation of Cavity Forces

5.2 TUNNEL DEVELOPMENT

Initial wind tunnel tests showed the test section flow field to be unacceptable due to the aerodynamic blockage of the AIM. Modification of the tunnel test section and 29 development tests investigating tunnel starting and other operational problems were required to achieve acceptable tunnel operation at Mach 6. Additional modifications and eleven tests were required for the Mach 7 test condition. Also, tunnel unstarts were encountered when fuel was admitted to the AIM. This work is discussed in the following section.

5.2.1 Tunnel Test Section Configuration

The test section configuration used at the start of wind tunnel testing is given in Figure 5-8. The shrouded free-jet configuration consisted of a water-cooled shroud and contraction cone. These exhausted through a 45-in.-dia constant-area heat sink cooled diffuser to a spray chamber and steam ejector. An annular Mach 4 nozzle (referred to as the "wedge nozzle") was circumferentially located around the tunnel exit. The wedge nozzle was designed to flow 40 pounds per second of ambient temperature nitrogen at 115 psia. The purpose of the wedge nozzle was to aspirate the tunnel boundary layer, thereby reducing the tunnel total pressure required to start and maintain hypersonic flow. Additional details of the test facility are presented in Section 3.

The tunnel blockage due to the maximum cross-section of the AIM and its support struts was 50 percent of the wind tunnel exit area. The blockage level was high, relative to existing experience. This prompted scale model wind tunnel starting tests to be performed at the NASA Langley Research Center. This work is reported in References 5-1 and 5-2. The tests showed that the tunnel could be started with models simulating the full-scale installations at Mach 5 and 7. The tunnel configuration shown in Figure 5-8 is similar to the configurations successfully operated in the model tests. Dissimilarities between the model test configurations and that of Figure 5-8 are noted in the following sections.

5.2.2 Test Procedure

The procedure for starting the tunnel and the AIM inlet (simplified here for the sake of this explanation) was as follows at the start of the test program:

(a) Set the AIM inlet spike at the inlet closed position.

(b) Start the steam ejector and allow the test cell to approach its minimum pressure of about 1 psia.

(c) Set the wedge nozzle inlet pressure at the desired value.

(d) Start the wind tunnel flow. The tunnel total pressure was linearly raised to its operating value in 33 sec. (Typical value for $M_o = 6.0$, $P_{to} = 750$ psia.)

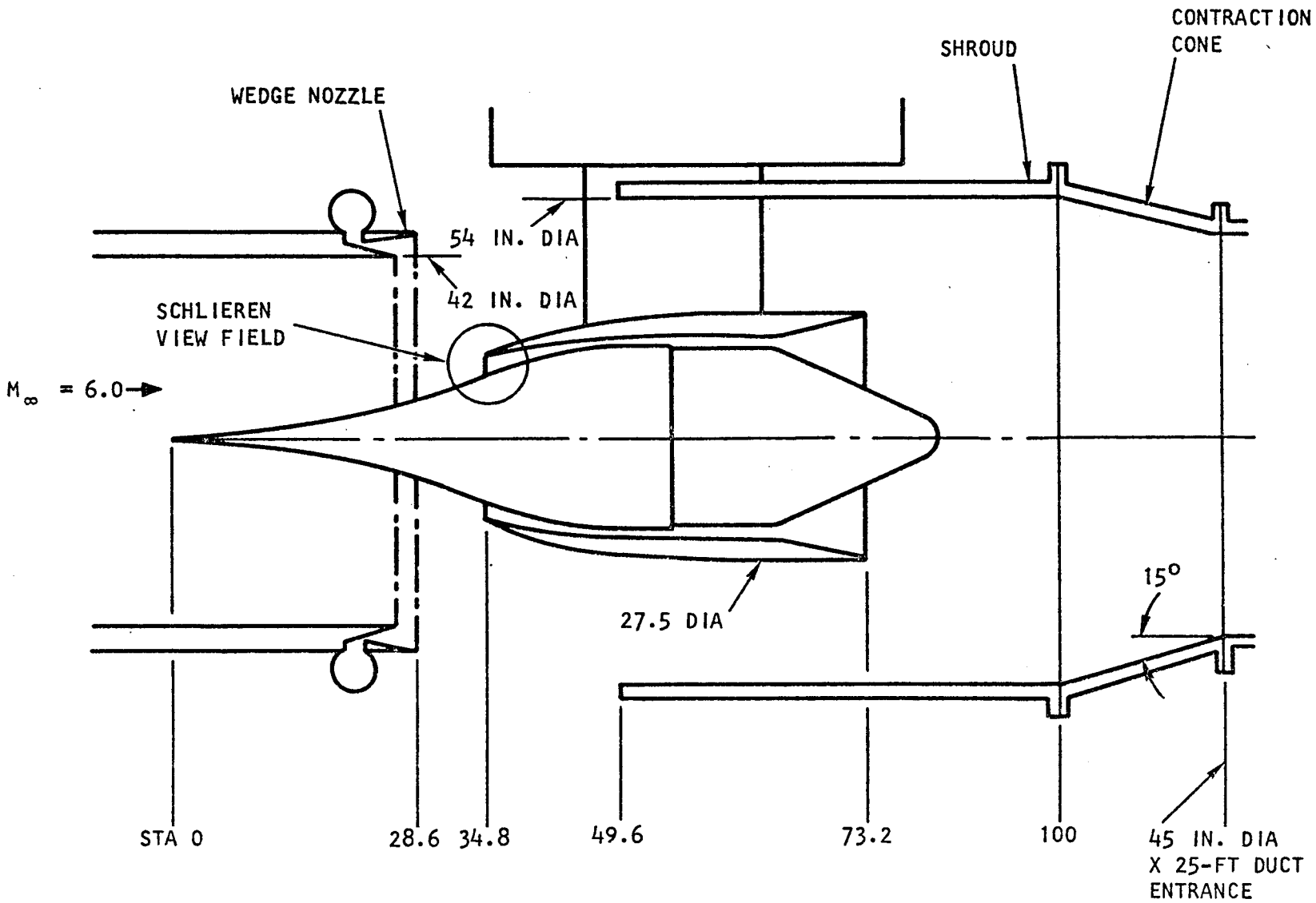

Figure 5-8. Initial Test Section Configuration Schematic

S-93796

(e) The inlet spike was translated to the open position by the automatic control system in nine seconds after the tunnel pressure reached its operating value.

5.2.3 Development Tests

The various modifications to the wind tunnel which led to successfully starting the tunnel are shown in chronological order in Figure 5-9. The test results for each of these configurations are discussed below. The tests are also summarized in Table 5-2.

Configuration A - Configuration A in Figure 5-9 was the first to be tested and is shown in more detail in Figure 5-8. The tunnel conditions for the first runs were as follows:

$$M_o = 6.0$$

$$P_{to} = 466 \text{ psia}$$

$$T_{to} = 1650^{\circ}R$$

In the first attempts to start the tunnel in readings 6 and 7, the Schlieren image showed the facility nozzle had started and that hypersonic flow had been established at the AIM inlet (see Figure 6-1 and 6-2). The spike was translated to the design position and the inlet started. The test section wall pressure distribution with the inlet started is given in Figure 5-10. Note that the wall pressures on the facility shroud and the AIM exhaust nozzle are on the order of 10- to 18-times higher than the freestream static pressure. The high pressures indicated that strong shock waves existed in the test section, caused by the pressures adjustment required to raise the static pressure in the tunnel flow by a factor of 8.2 to match the cell pressure.

This condition was unacceptable because of the backpressure on the AIM exhaust nozzle and pressure distortion on the outer surfaces of the AIM.

Work was then initiated to modify the test section to configurations B and C described below.

Configuration B

Test results in Reference 1 showed that an improvement in the performance of the tunnel could be achieved with a "washer" installed at the shroud inlet, as shown in Figure 5-9.

The purpose of the washer was to prevent the relatively high-pressure flow inside the shroud from recirculating back into the test cell. This increases the cell pressure and the strength of the shocks required to equalize the wind tunnel static pressure and the cell pressure.

The model test results also suggested that the tunnel exit to shroud inlet gap must be short enough to prevent the flow from impinging on the washer and spilling air into the cell.

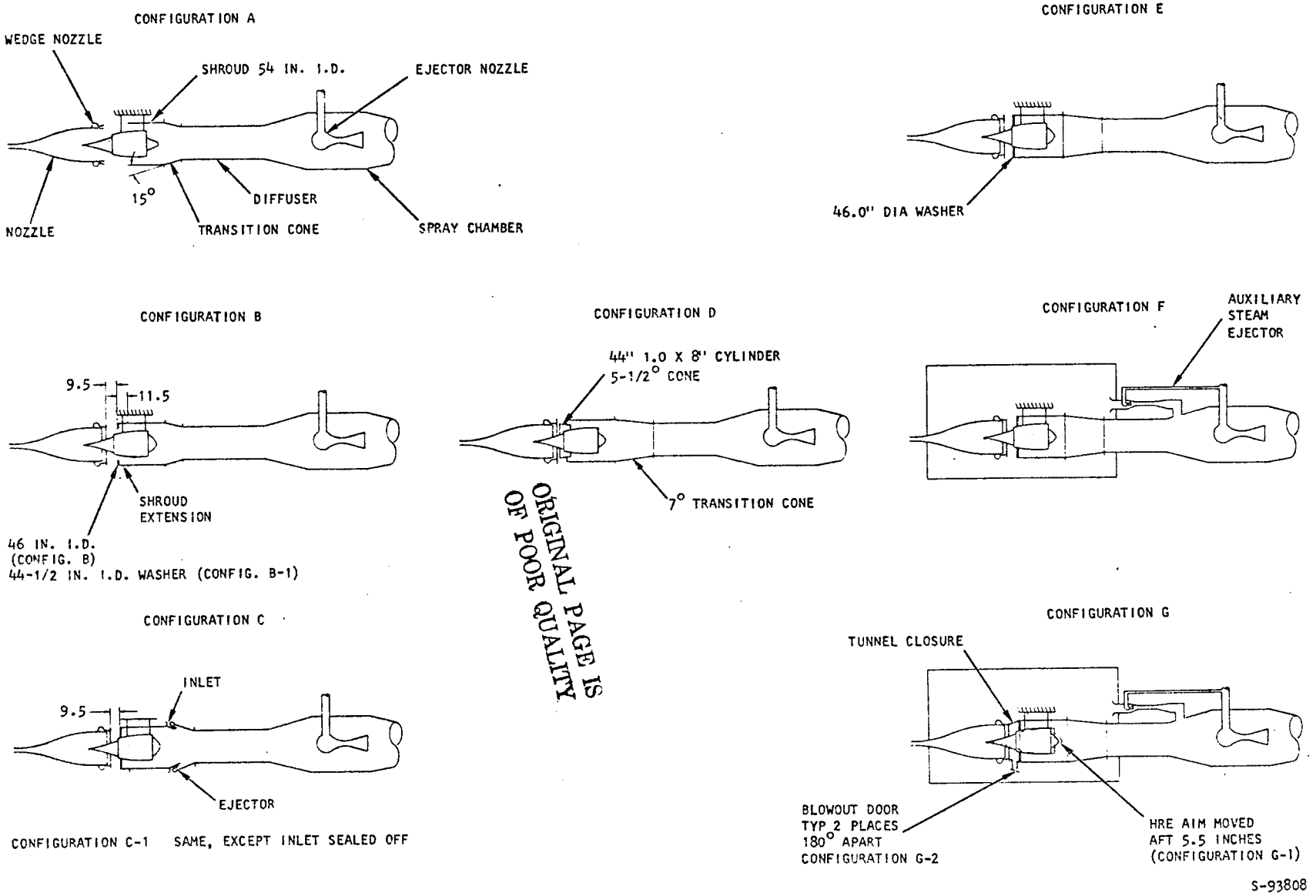

Figure 5-9. Test Section Configurations

TABLE 5-2

TEST RUN SUMMARY

Run No.	Reading No.	Date	Inlet Condition			Inlet Spike Position, In.	Fuel Injectors Used	Tunnel Config.	Time				Objective of Test	Comments
			Mach No.	P_{TO}, Psia	T_{TO}, °R				Run Min	Run Sec	Useful Min	Useful Sec		
1	1 through 5	9/14/72	-	-	-	-	-	A	-	-	-	-	Pre-run reference No-airflow engine Purge system calibration	Data not valid due to mechanical interference between AIM and outer cowl body
2	6	10/31/72	6	466	1500/2100	4.266	-	A	-	40	-	-	Facility and engine checkout	Test terminated due to cooling system overpressure abort system failure.
3	7	11/1	6	466	1500	4.266	-	A	2	26	-	-	Same as run 2	Tunnel nozzle started. Inlet started. Strong shocks in test section. Cell pressure ≈ 2.0 psia.
4	8	11/2	6	466	1500	4.266	-	A	-	5	-	1	Establish facility operational procedure	Test aborted due to facility problem (TAFP).
5	9	11/16	6	466	1500	4.266	-	B1	-	-	-	-	Same as run 4	Facility shroud extended and washer added to assist tunnel start (TAFP).
	10	11/16	6	466	1500	4.266	-		-	-	-	-	Same as run 4	TAFP
	11	11/16	6	466	1500	4.266	-		2	39	-	99	Same as run 4	Nozzle start and inlet start obtained Cell pressure ≈ 1.2 psia. Wedge nozzle pressure changed from 50 to 60 psia. No improvement in cell pressure.
6	12	11/21	6	466	2250	3.962	-	B1	-	-	-	-	Same as run 4	TAFP
	13	11/21	6	466	2250	3.962	-		1	07	-	-	Same as run 4	Wedge nozzle pressure 55 to 90 psig. No tunnel nozzle start. Nozzle started when inlet closed for shutdown.
7	14	11/21	6	466	2950	3.962	-	B1	-	34	-	-	Same as run 4	TAFP
8	15	12/8/72	6	466	2950	4.266	-		-	16	-	-	Same as run 4	TAFP
9	16	1/18/73	6	466	2800	4.266	1C, 4	B1	-	35	-	-	Same as run 4	First combustion attempt. TAFP
	17	"	"	"	"	"	1C, 4		1	06	-	-	Same as run 4	Nozzle start not obtained. TAFP.
	18	"	"	"	"	"	1C, 4		1	00	-	-	Same as run 4	Nozzle start obtained by cycling inlet spike open and closed. Inlet start obtained. Fuel ramped to equivalence ratio = .25 prior to tunnel unstart and TAFP.
10	19	2/2	6	466	2950	0.99/ 4.00	-	B1	-	13	-	-	Same as run 4	Nozzle start with inlet partially open. ($\Delta x = 0.99$). TAFP. No fuel injected.
11	20	2/2	6	466	2950	0.99/ 4.00	1C, 4	B1	1	02	-	-	Same as run 4	No start at $\Delta X = 0.99$. Nozzle started by cycling inlet spike. Combustor lit causing tunnel unstart.
12	21	2/15/73	6	750	3000	0.99/ 4.00	-	C1	-	-	-	-	Establish facility operational procedure	Jet pump installed. Test aborted due to freezing of coolant supply system.
13	22	2/21	6	750	3000	0.99/ 4.00	-	C1	-	22	-	-	Same as run 12 above	Jet pump used for this test. Nozzle start obtained. Unstart experienced when inlet was opened. Test aborted manually. Nozzle restart noted during shutdown.
14	23	2/21	6	750	3000	0.99/ 4.00	-	C1	-	58	-	-	Same as run 12 above	Jet pump and wedge nozzle inlet pressure varied. Nozzle start was not obtained. Use of jet pump did not affect test chamber pressure. Seals between AIM support struts and facility shroud blown out.
15	24	2/23	6	750	3000	0.99/ 4.00	-	C2	-	-	-	-	Same as run 12 above	Jet pump inactivated. TAFP
	25	2/23	6	750	3000	0.99/ 4.00	-	C2	-	-	-	-	Same as run 12 above	TAFP
	26	2/23	6	750	3000	0.99/ 4.00	1A, 1B	C2	-	49	-	-	Same as run 12 above	Nozzle start and engine start obtained. Fuel injected for 4 seconds prior to nozzle unstart. Unstart attributed to excessive fuel injected caused by facility valve malfunction.
16	27	3/1	6	930	3100	0.99/ 4.00	-	C2	1	42	-	-	Same as run 12 above	Nozzle start and inlet start obtained. Jet pump inactivated. Fuel was injected, engine inlet unstart experienced 12 seconds later. Inlet start reestablished and fuel again injected. Inlet unstart experienced 9 seconds later. Test was manually aborted. Cowl leading edge assembly separated from the outer body. Cause of the separation was attributed to failure of the screw heads. The failure was caused by overheating of the screw heads resulting from ingesting the hot tunnel environment into this area. Ingestion of tunnel ambient was the result of a shock standing on the AIM cowl. Additional diagnostic instrumentation was installed in the facility shroud and diffuser.
17	28	3/16	6	930	3100	0.99/ 4.00	1A, 1B	B2	1	11	-	-	Establish facility operational procedure to obtain hypersonic airflow.	Tunnel configuration same as config. 8 except washer inside diameter changed to 44.5 inches. Tunnel unstart observed 19 seconds after fuel introduced. Start reestablished. Test manually aborted 3 seconds later when excessive heating of HPE-AIM cowl leading edge assembly mount flange was noted. Excessive heating of the external skin of the AIM was noted.

TABLE 5-2 (Continued)

Run No.	Reading No.	Date	Inlet Condition			Inlet Spike Position, in.	Fuel Injector Used	Tunnel Config.	Time				Objective of Test	Comments
			Mach No.	P_{TO}, Psia	T_{TO}, °R				Run		Useful			
									Min	Sec	Min	Sec		
18	29	3/22	6	930	3100	0.99/ 4.00	1A, 1B	C1	-	36	-	-	Same as run 17 above	Re-run of reading 23 with seal repaired. Jet pump did not improve tunnel start.
19	30	4/27	6	750	2000	0.99/ 4.00	Fuel injec. not planned	D	1	16	-	-	Same as run 17 above	Shroud inlet washer replaced with cone-cylinder and 15° conical diffuser inlet contraction replaced with 7° cone; tunnel nozzle did not start.
20	31	4/30	6	750	2000	0.99/ 4.00	Fuel injec. not planned	E	-	51	-	-	Establish operational procedure	First run with fully started tunnel. Shroud inlet cone cylinder replaced with original 46 in. diameter washer. Tunnel start obtained when inlet spike was cycled twice; supersonic flow in diffuser. Test terminated when target conditions achieved due to limited supply of nitrogen. Test cell pressure was 1.2 psia.
21	32	4/30	6	750	2000	0.99/ 4.00	Fuel injec. not planned	E	1	42	-	-	Determine effect of varying wedge nozzle flow	Tunnel config. identical to run 20. Tunnel start obtained when inlet spike cycled twice. Test cell pressure of 1.0 psia obtained. Wedge nozzle has negligible effect on cell pressure.
22	33	5/4	6	750		0.99/ 4.00	1B, 2B	E	1	25	-	-	Investigate inlet unstart limit with first stage combustion	First successful supersonic combustion run. Intentional inlet unstart when first stage equivalence ratio reached 0.34. No second stage fuel added. O-ring between the outerbody and the cowl leading edge extruded.
23	34	5/15/73	6	750/ 930	3000	0.99/ 4.00	1A,1B,2A, 3A	E	2	08	-	-	Checkout AIM and facility. Fuel rich at P_{TO} = 750 psia ϕ= 1.0 at P_{TO} = 930 psia	Tunnel start and inlet start obtained. ϕ of 1.35 set at P_{TO} = 150 psia and ϕ of 1.00 set at P_{TO} = 930 psia. Facility fuel control value for injector 1B oscillated. Run proved AIM and tunnel can operate at $\phi > 1.0$. Erosion of zirconium oxide coating on outer cowl body crossover manifold noted. Erosion caused by carbon dust in tunnel flow.
24	35	5/16/73	6	750	3000	0.99/ 4.00	1A,1B,2A,2C	E	-	25	-	-	Checkout AIM and facility. Design injector locations	Test was aborted when engine inlet unstart was observed three seconds after initiation of fuel injection. The engine unstart was result of injecting excessive fuel, caused by malfunction of facility control valve. Inspection of the unit revealed that the coolant leak on the spike assembly had progressed, and repair was necessary.
25	36	5/24	6	750	3000	0.99/ 4.00	1A,1B,2A,2C	E	2	19	1	38	Demonstrate operation with design injector location and determine auto ignition limit	First good run with design injector locations. Auto ignition obtained at ϕ = 0.55; first stage did not light until second stage fuel added. Overall ϕ ramped to 1.0 with first stage ϕ held at 0.24.
26	37	5/30/73	6	750	3000	0.99/ 4.00	-	E	-	-	-	-	Determine effect of first stage ϕ on combustor performance	Test aborted due to malfunction of the steam ejector system
	38	5/30	6	750	3000	0.99/ 4.00	1A,1B,2A,2C	E	-	47	-	26	Determine effect of first stage ϕ on combustor performance	Test aborted when inlet unstarted. Malfunction of the facility fuel control valve resulted in injecting excessive fuel into injector 2C. 3 small cracks in spike skin in region of ignitors found in post run inspection. Cracks repaired to prevent water leak into combustor.
	39 thru 48	-	-	-	-	-	-	E	-	-	-	-	Purge system calibration test	
27	49	10/4/73	6	750	3000	-	-	E	-	-	-	-	Combustor optimization	TAFP
	50	10/5/73	6	750	3000	-	-						Combustor optimization	TAFP
	51	10/5/73	6	750	3000	0.99/ 4.00	1A,1B,2A,2C	E	2	39	2	09	Combustor optimization	Fuel control problems encountered.
28	52	10/10/73	6	750	3000	0.99/ 4.00	1A,1B,2C,4	E	1	21	-	50	Combustor optimization	Investigating performance improvement due to injecting fuel closer to inlet. Inlet unstarted at overall ϕ of .83.
	53	10/10	-	-	-	-	-	E	-	-	-	-	Purge system calibration test. Evacuated test cell.	
29	54	10/11/73	6	750	3000	0.99/ 4.00	1A,1B,2A,2C	E	3	04	2	13	Combustor optimization	Attempt to determine effect of first stage ϕ and thrust on performance. Auto ignition obtained at ϕ = .54. Data taken with ignitors on and off to determine effect on performance. Inspection of unit revealed excessive coolant leak at spike/ ignitor body interface. Repair necessary. Tunnel operating procedure modified to reduce water ingestion into AIM wall pressure taps.
	55	10/17/74	-	-	-	-	-	E	-	-	-	-	Purge system calibration evacuated test cell	
30	56	11/2/73	6	750	3000	-	-	E	-	-	-	-	Combustor optimization	Effect of fuel split between 1st and second stage injectors at overall ϕ = 1.0 investigated. Also all second stage fuel added from innerbody side (system 2C). Fuel system purges turned off to determine effect on combustor wall pressure distribution. Found thrust measurement affected by thermal expansion of fuel manifold 1B. Inlet unstarted at overall ϕ of 1.0 with first stage ϕ = 0.36. Cavity pressure tap PA2 repaired for this run. Encountered fuel control problems.

TABLE 5-2 (Continued)

Run No.	Reading No.	Date	Inlet Condition			Inlet Spike Position, in.	Fuel Injectors Used	Tunnel Config.	Time				Objective of Test	Comments
			Mach No.	P_{T0}, Psia	T_{T0}, °R				Run Min	Run Sec	Useful Min	Useful Sec		
	57	11/2/73	6	750	3000	0.99/ 4.00	1A,1B,2A 2C	E	-	-	-	-		
	58	11/7/74	-	-	-	-	-	E	-	-	-	-	Purge system calibration	Determine effect of thermal expansion of fuel manifold 1B.
31	59	11/8/73	6	750	3000	-	-		-	-	-	-	Combustor optimization	TAFP
	60	11/8/73	6	750	3000	0.99/ 4.00	1A,1B,2A. 2C	E	2	34	2	04	Combustor optimization	Overall ϕ held constant while amount of fuel from innerbody and outerbody injectors varied. Fuel temperature compensation added to fuel control
32	61	11/13/73	6	750	3000	0.99/ 1.72/ 2.52	1A,1B,2A, 2C	E	2	50	2	21	Determine effect of spike position on engine performance	Inlet massflow ratios of 0.81 and 0.58 ran by varying the inlet spike position. AIM wall pressure distribution measured with fuel line purge flow shut off. Reworked section of the innerbody assembly burned and damaged during combustion; damaged section was removed. Operational procedure modified to prevent further damage.
33	62	11/20/73	6	930/ 466	3000			E					Performance test	TAFP
	63	11/21/73	6	930/ 466	3000	0.99/ 4.00	1A,1B,2A, 2C		2	59	1	52	Performance test	Tunnel total pressure varied to determine effect of altitude on performance.
34	64	11/28/73	6	750	3000	0.99/ 4.00	1B,2A,2C, 3A,3B	E	3	38	2	35	Subsonic-supersonic combustor mode transition	Transition from subsonic to supersonic combustion mode demonstrated. Inspection of unit revealed coolant was flowing into the 1B fuel manifold and a nickel plated section of the innerbody had blistered. Separation at the spike skirt-spike body has progressed to approximately 1.0 inches. Forward facing step at the interface of the cowl leading edge assembly and the outerbody had progressed to approximately .065 inches. Larger fuel metering venturi installed in fuel system E.
35	65	12/11/73	6	750	3000	4.00	1A,1B,2A, 2C	E	2	52	1	44	Supersonic combustion with instrumentation rig	Instrumentation rake installed. Rake caused tunnel to unstart at $\phi \approx 1.05$. Exhaust gas sampling data taken.
	66	12/14	-	-	-	-	-	E	-	-	-	-	Purge system calibration	TAFP
	67	12/14	-	-	-	-	-		-	-	-	-	Purge system calibration	N_2 purge force calibration with cell evacuated.
36	68	12/14/73	6	750	3000	-	-		-	-	-	-		Time of steady state fuel flow increased to 20 seconds to allow gas sampling data to stabilize.
	69	12/14/73	6	750	3000	4.00	1A,1B,2A, 2C	E	3	20	2	17	Supersonic combustion	One tunnel unstart experienced near end of run. Several tunnel unstarts prevented by shutting off fuel. Incipient unstart detected by monitoring luminescent normal shock position in T.V. view of tunnel.
37	70	12/19/73	6	750	3000	-	-	E	-	-	-	-	Determine effects of angle of attack	Test terminated prematurely due to frozen vent valve.
	71	12/19/73	6	750	3000	4.00	1A,1B,2A, 2C		3	56	2	29		Cowl leading edge assembly removed after this run to remove facing step noted after reading 64.
	72												Purge system calibration	Calibration with 1B fuel injector manifold heated test cell evacuated.
47	73,74,75	1/22/74	7	1000	3200	-	-	F	-	-	-	-	Mach 7 facility check-out	Test aborted due to facility problems (TAFP)
	76	1/23/74	7	1000	3200	-	-	F	-	-	-	-	Mach 7 facility check-out	TAFP
	77	1/23/74	7	1000	3200	2.57	-	F	2	-	-	-	Mach 7 facility check-out	Attempt to start tunnel at Mach 7 unsuccessful. Secondary steam ejector used; wedge nozzle pressure varied; inlet spike assembly translated.
48	78	1/25/74	7	1000	3500	2.57	-	G	2	-	-	-	Mach 7 facility check-out	Test aborted while attempting tunnel start. TAFP. Unusual amount of carbon dust deposited on AIM.
49	79	2/15/74	7	1000	3100	-	-	G1	-	-	-	-	Facility check-out	AIM moved aft 5.5 inches.
	80	2/15/74	7	1000	3100	2.57	-	G1	-	-	-	-	Facility check-out	TAFP (dewar water system frozen).
	81	2/20/74	7	1000	3300	2.57	2A, 2C	G2	2	38	-	-	Facility check-out	Blowout doors installed in tunnel closure. Tunnel started when wedge nozzle pressure reduced. Tunnel unstarted when combustor lit. Restart not obtained due to change in wedge nozzle inlet pressure.
50	82	2/22/74	7	1000	3300	-	-	G2					Facility check-out	TAFP. Seal around outer cowl body support damaged.
	83	2/22/74	7	1000	3300	2.57	-	G2	2	05	-	-	Facility check-out	Tunnel start not obtained.
51	84,85,86	2/28/74	7	1000	3300	-	-	G2	-	-	-	-	Facility check-out	TAFP
	87	2/28/74	7	1000	3300	2.57	1A,1B,2A, 2C		2	46	1	30	Facility check-out	Tunnel nozzle started. Unstarted at $\phi = 0.8$

TABLE 5-2 (Continued)

Run No.	Reading No.	Date	Inlet Condition			Inlet Spike Position, in.	Fuel Injectors Used	Tunnel Config.	Time				Objective of Test	Comments
									Run		Useful			
			Mach No.	P_{T0}, Psia	T_{T0}, °R				Min	Sec	Min	Sec		
52	88	2/28	7	1000	3100	2.57	1A,1B,2A, 2C	F	2	45	1	31	Combustion evaluation	First successful Mach 7 run. Tunnel closure removed. Diffuser seal repaired. Effect of fuel injection location investigated. Row 2 ignitors on. Outer cowl body support damaged by carbon particles in tunnel flow due to failure of carbon part in facility heater. Shroud inlet pressure rake hit and damaged. Repaired outer cowl body support and water cooled protective wedge installed. Coolant leak at the interface of spike skirt and spike body noted at angular location 270° in addition to leak at 180 degrees noted in Rdg 64. Leak at 180° progressed to approximately 1.25 inches. Cowl leading edge tip radius and spike tip damaged by particles. Damaged areas reworked.
53	89	3/15/74	7	1000	3000	2.57	1A,1B,2A, 2C,4	F	3	-	2	02	Combustor optimization	Performance measured with various fuel injection schemes. T_{T0} varied during run. Ignitors on. Test terminated prematurely due to failure of transducer in fuel control causing fuel control valve to fully open. Abnormal amount of carbon dust observed in tunnel flow. Cowl leading edge tip radius and spike tip again damaged. Tip section repaired.
54	90	3/8/75	7	1000	3000	2.57	1A,1B,1C, 4	F	3	09	1	16	Combustor optimization	Second stage fuel injection closer to inlet (injectors 1C, 4). Inlet unstarts encountered.
55	91	3/12/74	7	1000	3000	2.57	1A,1B,2C, 4	F	2	52	1	32	Effect of angle of attack	Tunnel start improved at angle of attack. Tunnel started at P_{T0} = 850 psia. 3 inlet unstarts encountered due to excessive 1st stage fuel. Total coolant leak into combustor estimated to be 5.0 gpm.
56	92	3/18/74	7	1000	2900	2.57	1A,1B,2C, 4	F	3	50	2	30	Combustor performance with instrumentation rake installed.	Instrumentation rake blockage had adverse effect on tunnel start. Inlet spike stroked twice to start tunnel. Oxygen content of tunnel flow varied while AIM exhaust gas sampling data taken.
57	93	3/27/74	5	415	2210	4.0	1A,1B,2A, 3A,3B	F	0	85	-	-	Facility check-out	First Mach 5 run. Subsonic combustion data obtained. Run terminated prematurely (TAFP).
58	94	3/28/74	5	(a) 415 (b) 300 (c) 206	2210 3000 2210	4.00 4.00 4.00	1A,1B,2A, 3A,3B 1A,1B,2A, 3A,3B 1A,1B,2A, 3A,3B	F	2	25	2	01	Combustor optimization	Subsonic and supersonic combustion and transition demonstrated. Four unstarts experienced, three unstarts attributed to high cell pressure, one to injecting excessive fuel intentionally into the AIM. More carbon in tunnel flow. Cowl leading edge and spike tip damaged. Both reworked.
59	95	3/29/74	5	415 300 206	2210 3000 2210	4.00 4.00 4.00	1A,1B,2A, 2C 1A,1B,2A, 2C 1A,1B,2A, 2C	F	3	41	3	20	Combustor optimization	All comments made for Rdg 94 applicable for this run, except combustion was limited to supersonic combustion mode. Four engine unstarts experienced. Three unstarts were attributed to facility conditions and the other to programmed to determine inlet unstart limit.
60	96	4/15	5	415 300 206	2210 3000 2210	4.00 4.00 4.00	1A,1B,2A, 3A,3B	F					Evaluate effects of angle of attack	Subsonic and supersonic combustion and transition demonstrated at angle of attack. Intentional engine unstart obtained when excessive fuel was injected in supersonic combustion mode.
61	97	4/22	5	206/ 415	2210	4.00	2A, 3A, 3B	F					Combustor performance with instrumentation rake installed	Combustor exit flow conditions surveyed. Gas sampling data taken. Blockage of instrumentation rake had adverse effect on tunnel operation.

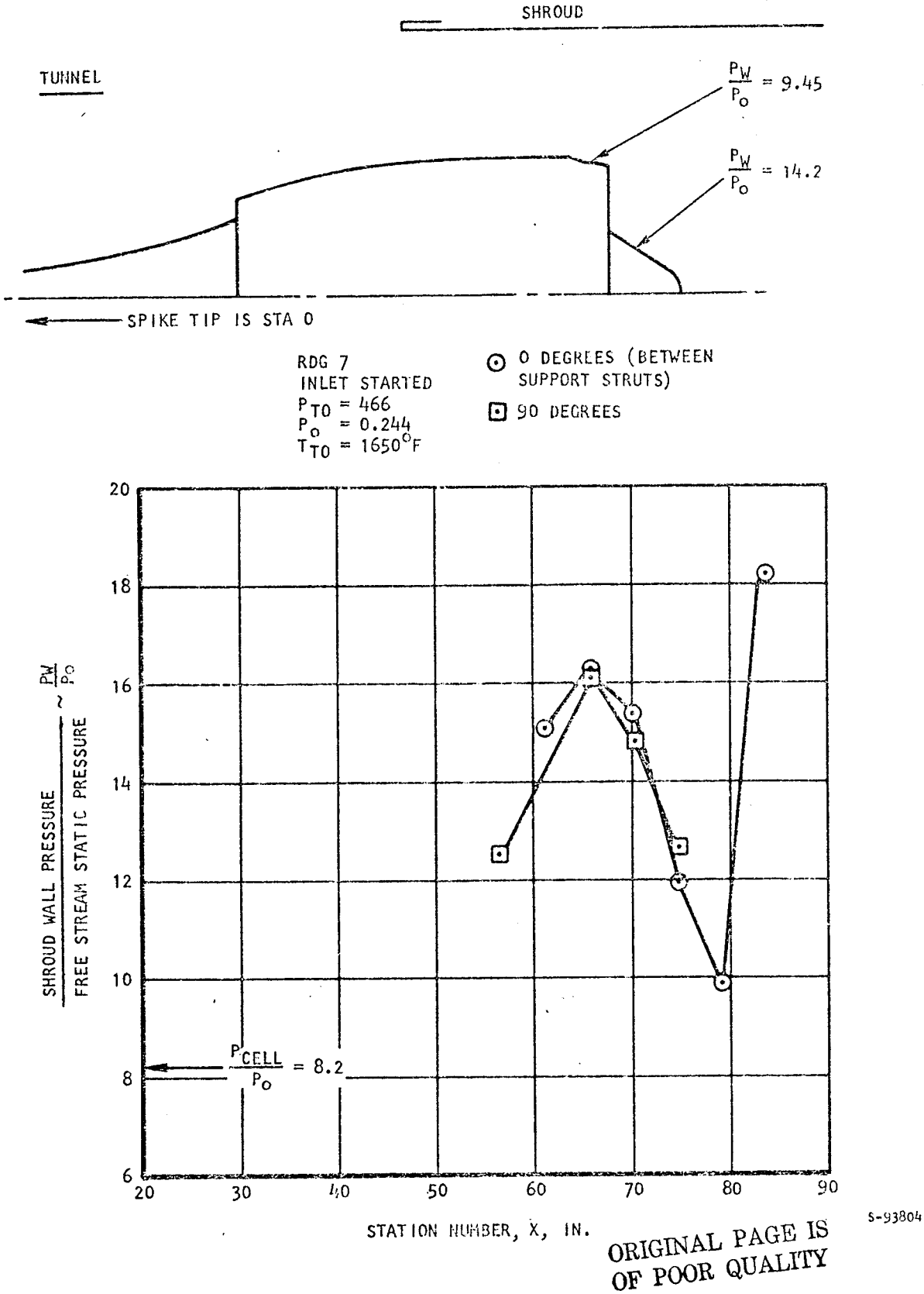

ORIGINAL PAGE IS OF POOR QUALITY

Figure 5-10. Facility Shroud Pressure, Configuration A

Thus, the shroud was extended 11-1/2 in. and a 46-in. inside dia washer was added to configuration A to form configuration B. Water cooling was not provided for these parts because of their near proximity to the cool wedge nozzle flow.

Test data taken in readings 11 to 13 with configuration B showed a 40 percent improvement in test cell pressure over configuration A. Pressures on the AIM exhaust nozzle, although improved, were still 4.5- to 5-times higher than the tunnel exit static pressure. It was still apparent that strong shocks remained in the test section. No significant improvement in this condition was seen when the wedge nozzle pressure was varied from 10 to 90 psia.

Although high pressures prevailed in the test section, the AIM inlet could be started and supersonic flow established in the combustor. The preceeding runs had shown the AIM cooling system and the facility systems to be functioning properly. Thus, it appeared feasible to attempt a run with combustion; then any problems that arose with combustion runs could be solved concurrently with the tunnel starting problems.

To light the combustor it was necessary to raise the tunnel total temperature to the Mach 6 condition of 2950°R. This was done in the two cooling system checkout runs in readings 13 and 14. It was found in these runs that the tunnel starting problems became more severe at higher tunnel total temperature. The reasons for this were never resolved. Possible reasons are as follows:

(a) The specific heat ratio change with temperature in the tunnel causes a reduction in tunnel Mach number. This changes shock positions which effect the entire test section flow field.

(b) The higher temperature increases the velocity in the tunnel boundary layer relative to that of the ambient temperature wedge nozzle flow. This reduces the pumping effectiveness of the wedge nozzle.

In reading 13, the tunnel nozzle did not start until the tunnel had just entered its shutdown process. When shutdown was initiated, the inlet spike received a command to close and the tunnel immediately started. It was then apparent that this inlet spike stroking sequence could be used to start the tunnel nozzle for the next run.

The inlet spike position control mode was changed from automatic to manual from the control room. This spike stroking sequence was used in reading 18 and is shown in Figure 5-11. The inlet was opened followed by an immediate drop in the wind tunnel nozzle exit static pressure. The inlet was then closed and a tunnel nozzle start was observed on the Schlieren screen. The inlet was reopened and started.

The ignitors were lit and fuel was introduced to the combustor through first-stage injectors 1c and 4. The combustor lit as fuel was ramped from an equivalence ratio of 0.15 to 0.25.

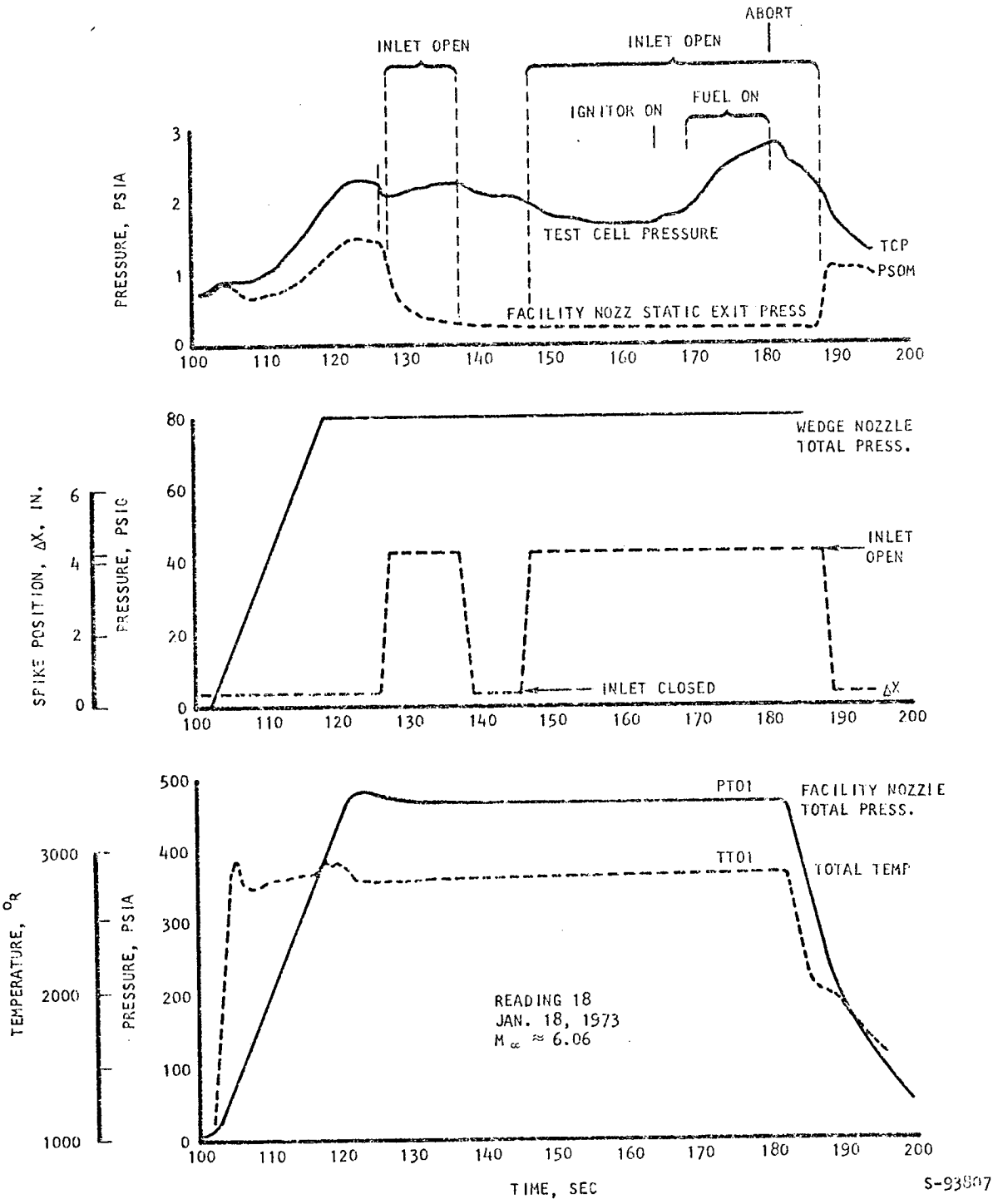

Figure 5-11. Reading 18 Test Conditions

It was immediately apparent that lighting the combustor had a significant effect on the tunnel flow. A thickening of the cowl boundary layer was observed on the Schlieren as fuel flow increased. The tunnel unstarted at the top of the fuel flow ramp. Note the rise in cell pressure with fuel flow in Figure 5-11.

Review of the test data led to the following conclusions:

1. AIM combustor wall pressures and temperatures showed increases when fuel was injected, indicating a lit condition.

2. Test cell pressure, facility shroud pressures, and external wall pressures on the AIM showed a marked increase at the time of ignition.

3. Pressure increases in the tunnel test section associated with combustion in the AIM caused the tunnel nozzle to unstart.

4. Wall pressures on the AIM outer cowl surfaces had nearly doubled at an equivalence ratio of 0.25. This indicated shock waves had migrated upstream onto the cowl surface when fuel was increased.

5. Most of the AIM exhaust nozzle wall pressures were on the order of 12-times higher than tunnel exit static pressure, indicating separated flow in the nozzle.

6. No meaningful determination of thrust could be made under the above conditions.

7. Additional instrumentation was needed in the facility to investigate this problem.

Readings 19 and 20 were made to investigate the tunnel unstarting due to fuel injection. In these runs it was learned that the tunnel would start without restroking the inlet previously described if the inlet were set at a partially open position. An inlet ΔX of 0.99-in. was chosen because this was the spike position where the inlet contraction ratio was just low enough to allow the inlet to self-start.

The open inlet allowed a portion of the tunnel flow to bypass the annulus between the facility shroud and the AIM. This apparently reduced the pressure loss in this area enough to allow the tunnel to start. Although restroking the inlet was occasionally required, the tunnel was started with the inlet at $\Delta X = 0.99$ in. for all subsequent runs.

Configuration C

Significant improvements in the tunnel starting and operating pressure ratios were obtained in the scale model starting tests of Reference 1 by a diffuser inlet ejector as shown in Figure 5-9, configuration C. The ejector was designed to pump air from the test cell into the exhaust diffuser, thereby reducing the cell pressure. Configuration B was converted to configuration C

by sliding the diffuser aft and installing the ejector between the shroud and the contraction cone entrance. The ejector was designed to flow 10.2 lb per sec of ambient temperature nitrogen at a pressure of 93 psia.

Readings 21, 22, 23, and 29 were made with configuration C-1. The tunnel total pressure was increased for these runs from 466 to 750 psia. This was done in attempt to start the tunnel by improving the overall pressure ratio.

In contrast to the model tests, the ejector showed no improvement in the tunnel operating characteristics. The test cell pressure was about 8-times higher than tunnel exit static compared to the values around 6.5 for configuration B. Excursions were made with the ejector primary and wedge nozzle pressures with no significant effect on the test cell pressure.

Consequently, the ejector inlet was sealed off to form configuration C-1. This configuration was tested in readings 24 to 27 to determine if the increased tunnel total pressure would improve tunnel starting. Reading 26 showed no significant improvement and the tunnel total pressure was raised to the Mach 6 design value of 930 psia in readings 27 and 28.

The higher pressure and heat transfer in conjunction with tunnel unstarts due to fuel addition caused structural damage to the AIM. Shockwaves impinging on the AIM caused noticable discoloration to the skin on the cowl and the outer cowl body. About half of the bolts retaining the cowls to the outer body failed in tension and the flanges parted about 0.060 in. (See para 6.3.1) Also, the outer cowl body was distorted about 0.070-in. out-of-round, causing additional binding problems in the thrust measurement system (see para 5.1.2.2).

As a consequence, further running with the tunnel unstarted at 930 psia was avoided. Any Mach 6 tests where inlet unstarts could be encountered were run at a tunnel pressure no higher than 750 psia. Later in the program, tunnel unstart problems were solved and satisfactory combinations of injectors and equivalence ratios were selected. Tests were then performed at 930 psia without incident.

For reading 27, additional instrumentation was installed in the test section and diffuser. This made a significant contribution to the solution of the unstarting problems. Figure 5-12 presents wall pressure measurements in the facility diffuser. The following analysis of the diffuser flow conditions was made using this data:

(a) The mass averaged diffuser exit total temperature, T_T, was calculated as a function of equivalence ratio knowing the initial temperatures and flow rates of the wind tunnel, wedge nozzle, and the AIM fuel flow. Complete combustion was assumed.

(b) Theoretical values of ESP2 as a function of equivalence ratio were then calculated using $\frac{W\sqrt{T_T}}{ESP2\ A} = f(M) = 0.960$. The value of 0.960 corresponds to sonic conditions.

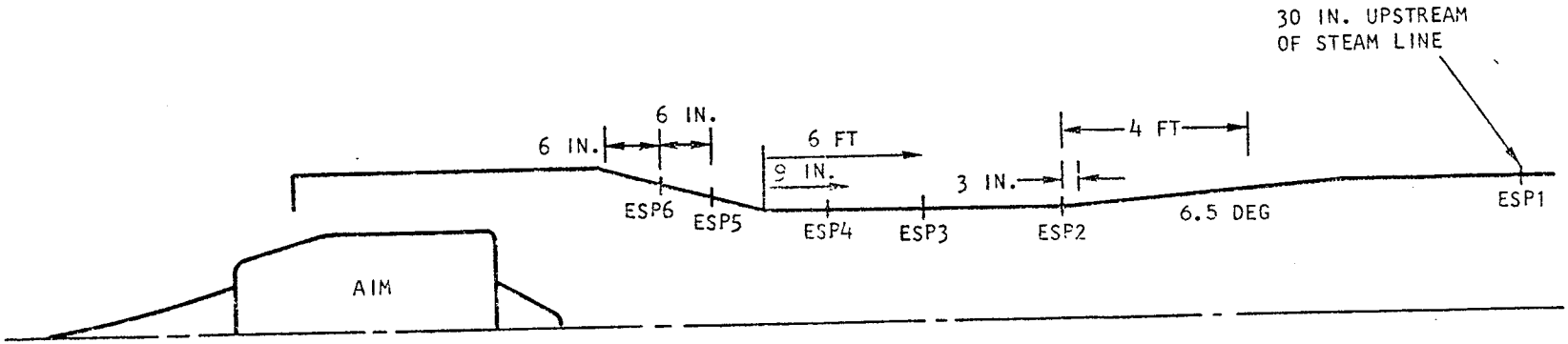

TIME, SEC	DIFFUSER PRESSURE, PSIA ESP 6	ESP 5	ESP 4	ESP 3	ESP 2	ESP 1	EQUIVALENCE RATIO
115.28	3.7625	8.6250	9.2375	7.3650	6.0900	5.7300	0
133.28	4.0750	9.3250	9.9250	7.6050	6.2700	5.8050	0.175

READING 28

P_{TO} = 930 PSIA

T_{TO} = 3000°R

S-93805

Figure 5-12. Measured Diffuser Pressures

The measured values of ESP2 are compared in close agreement to the theoretical values in Figure 5-13. This shows the diffuser exit is effectively choked. Note the pressure drop in Figure 5-12, between the diffuser inlet and exit. The above characteristics indicate subsonic diffuser flow with the exit choking due to duct losses. Had the core of the flow been supersonic, the pressure would have increased toward the exit.

The facility was designed with the intent of supersonic flow in the diffuser with the terminal shock in the spray chamber downstream of the diffuser. With subsonic diffuser flow, the terminal shocks stand on or near the AIM. The position of the shocks is determined by the pressure required to drive the flow through the choked diffuser. As the diffuser exit temperature increases due to combustion, the pressure must also increase to meet continuity. Thus, as fuel is added, the terminal shocks must move toward the shroud inlet to adjust to a position of lower pressure loss. Also, the static pressures downstream of the shocks must rise in accordance with the increasing diffuser static pressures. With sufficient fuel addition, the shocks eventually move upstream far enough to impinge on or near the AIM spike tip shock which unstarts the AIM inlet. Schlieren movies show that this immediately unstarts the wind tunnel.

Configuration B-1

For reading 28, the 46-in.-dia shroud inlet washer was replaced by 44.5-in.- dia washer (configuration B-1) in an attempt to reduce recirculation of the tunnel flow into the test cell. A total pressure rake was installed to survey the pressure at the washer inlet. The pressures are compared in Figure 5-14 for the two washer sizes tested. The probe pressures away from the tunnel centerline show only slight increases above the tunnel static pressure. Only the innermost probe shows a marked pressure rise. This indicates the flow has turned toward the tunnel centerline and the jet boundary is somewhere near the innermost probe 3-1/4 in. from the washer lip. Higher cell pressure and further turning toward the centerline are evident when the combustor is lit. No significant improvements were observed with the smaller washer.

At this time in the program, the starting problem was reviewed by NASA and AiResearch in conjunction with Fluidyne Engineering Corporation who were called in as consultants to AiResearch. Figure 5-15 presents the flow conditions in the tunnel as estimated by Fluidyne for reading 28. Measured wall pressures referenced to the tunnel total pressure are noted on the figure. Fluidyne made the following comments regarding their analysis:

1. With no fuel addition, the facility nozzle is started and the engine inlet is started.

2. The test chamber pressure with no fuel addition is about seven times the nozzle exit static pressure, so the M=6 nozzle flow contracts after leaving the nozzle and shockwaves impinge on the engine cowl.

3. The resulting flow produces unrealistically high-pressures and separated flow around the engine nozzle and large total pressure losses occur.

$M_o = 6.0$

$P_{TO} = 930$ PSIA

$T_{TO} = 3100°R$

⊙ MEASURED IN READING 28

——— CALCULATED ASSUMING SONIC FLOW

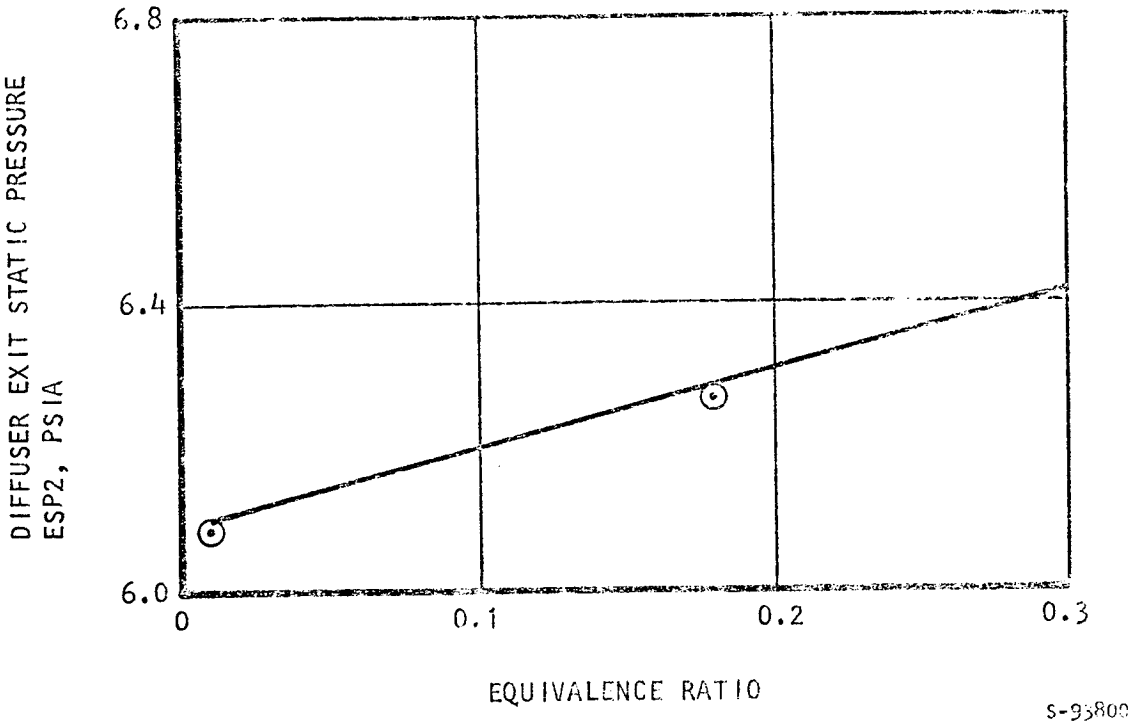

Figure 5-13. Effect of AIM Combustion on Facility Diffuser Exit Pressure

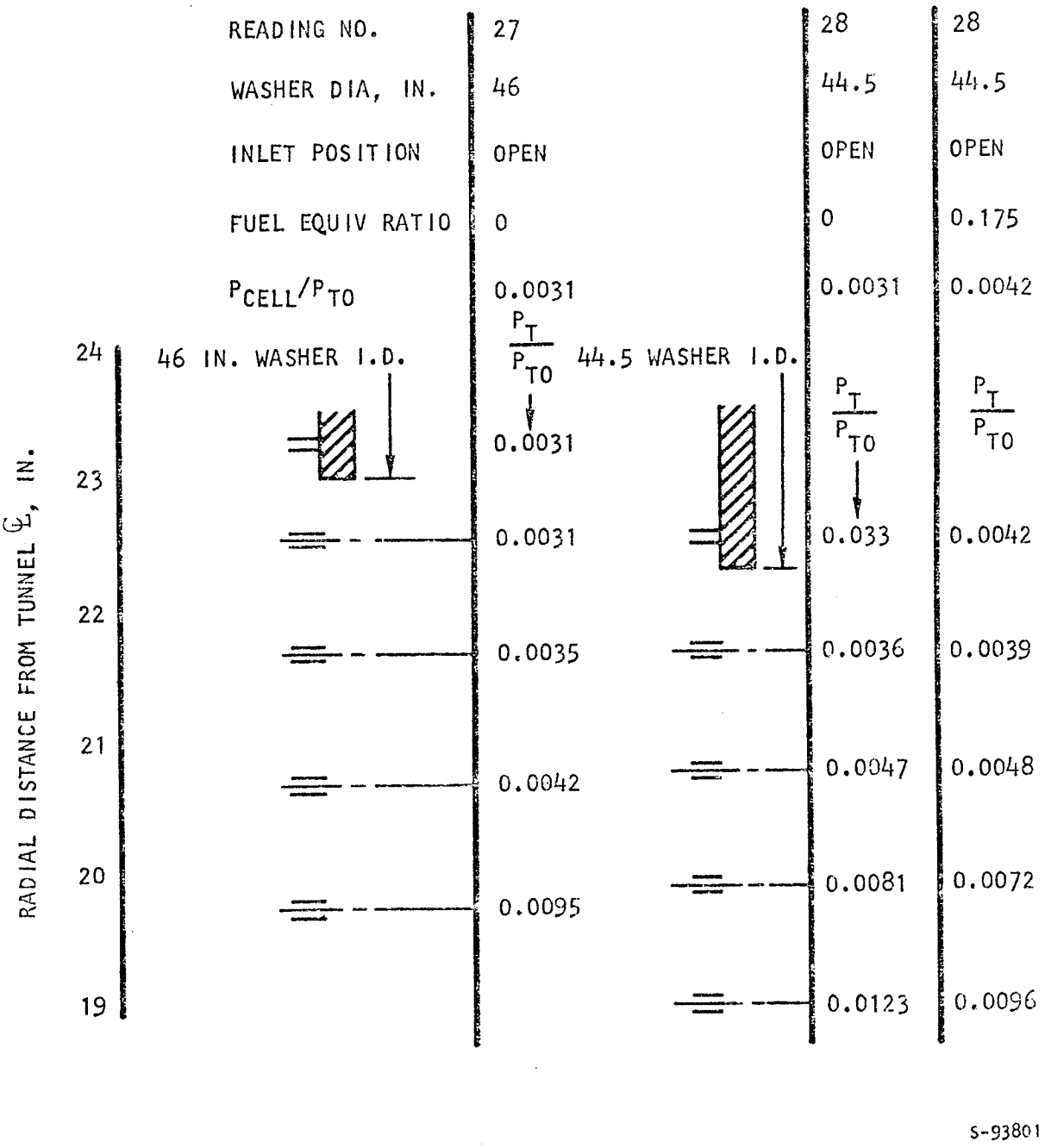

Figure 5-14. Shroud Inlet Pressure Survey

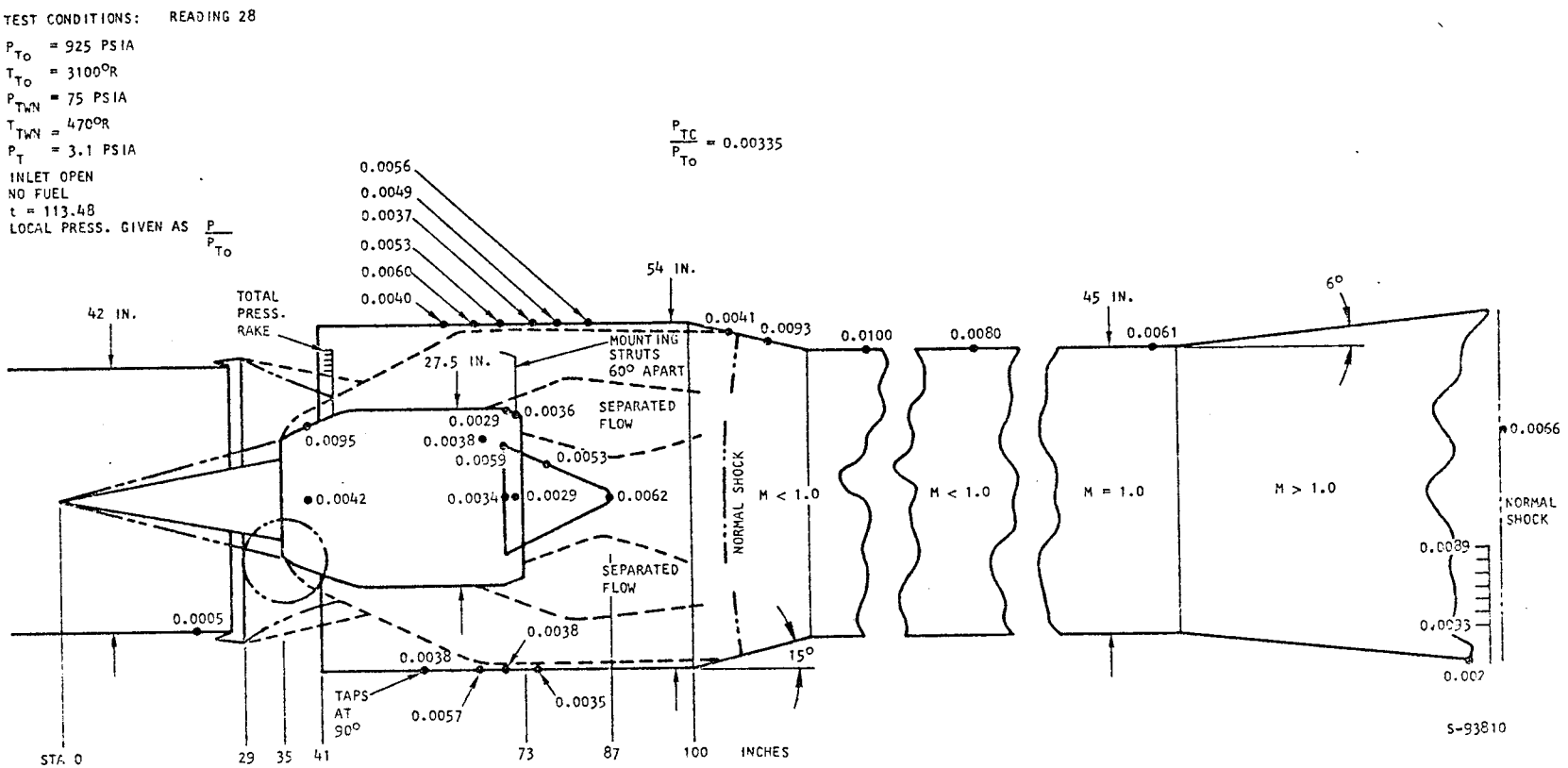

(a) Fuel Off

Figure 5-15. Wind Tunnel Flow Conditions

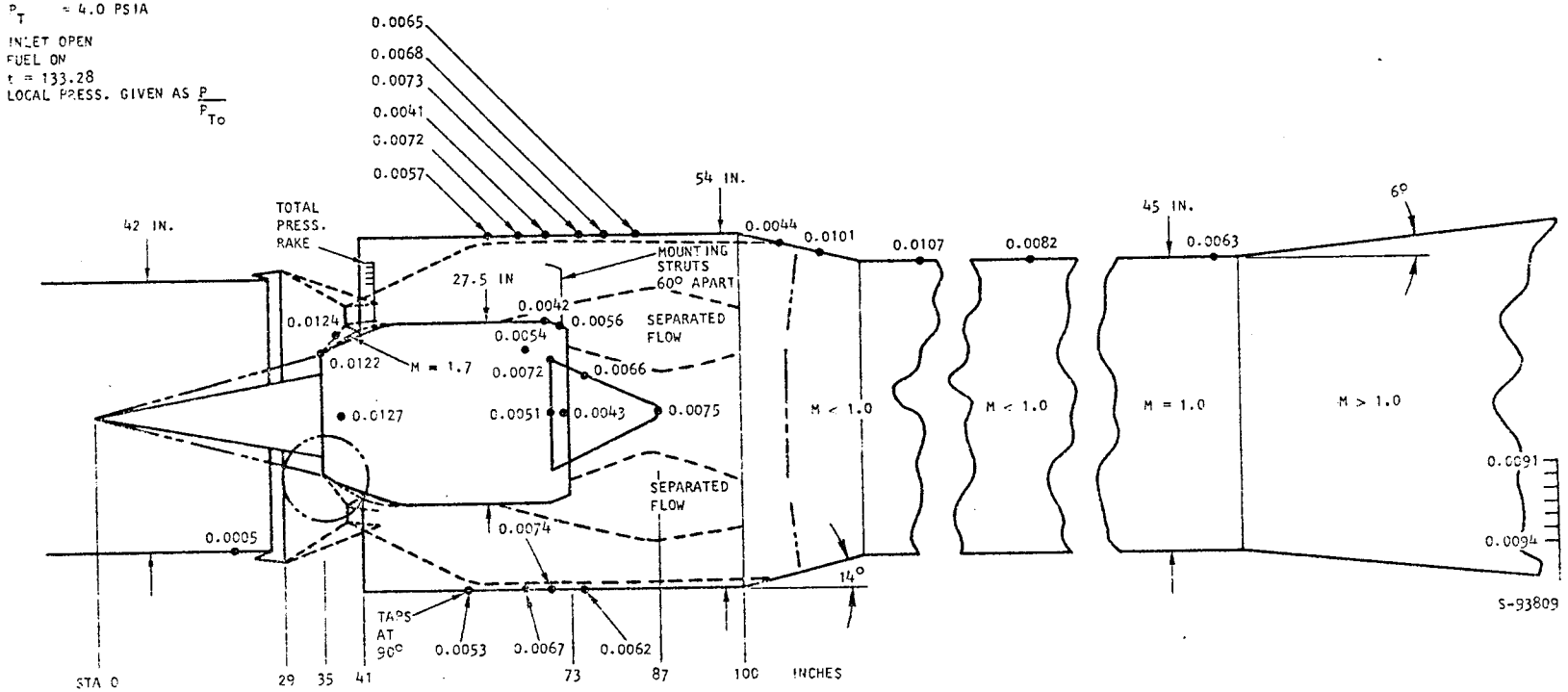

(b) Fuel On

Figure 5-15. Wind Tunnel Flow Conditions (Continued)

4. Because of the high static pressure level and large total pressure losses in the flow around the engine, valid engine thrust data is unobtainable and the external flow Mach number is so low it can't negotiate the 15 deg turn at the diffuser contraction, so a normal shock occurs in the contraction.

5. Subsonic flow exists in the constant area diffuser throat up to the exit where choking occurs.

6. The downstream steam ejector performance is more than adequate, so the flow re-expands in the subsonic diffuser and shocks down again, probably near the rake station.

In the review a number of fixes were suggested and discussed. The most promising of these considering lead time and probability of success were voted to be configurations D and E.

Configuration D

The following changes were made to configuration C to form configuration D.

1. The diffuser inlet ejector and 15-deg contraction cone were replaced with a 7 deg cone. This was done to allow the flow to negotiate the contraction supersonically.

2. A 44.5-in.-dia cylinder with a 5-1/2-deg conical inlet was added to the shroud inlet washer.

This configuration was tested in reading 30. The tunnel nozzle did not start.

Configuration E

The cone-cylinder inlet was removed and replaced by the existing 46-in.-dia washer to form configuration E. This configuration was first tested in reading 31.

The test section and diffuser wall pressure distribution for configurations E and B-1 are compared in Figure 5-16. The data shows that the tunnel had fully started with configuration E. The diffuser exit Mach number, calculated from continuity using the measured static pressure, is 1.42. The total pressure recovery was about 0.59-times the normal shock pressure recovery. The cell pressure was 1.2 psia or 3.15-times the freestream static pressure. Pressures on the AIM nozzle outer shroud improved from a value of 5-times the freestream static for configuration B-1 to a value of 0.4 for configuration E. Configuration E was used for the remainder of the Mach 6 tests.

Configurations F and G

Starting problems were expected to be more severe at Mach 7. The tunnel nozzle exit static pressure is 1/3 of the Mach 6 value for a given total pressure. Thus, a lower cell pressure is required to start the tunnel. The procurement of the auxiliary ejector, shown as configuration E in Figure 5-9, was initiated during the Mach 6 testing. The ejector design conditions were

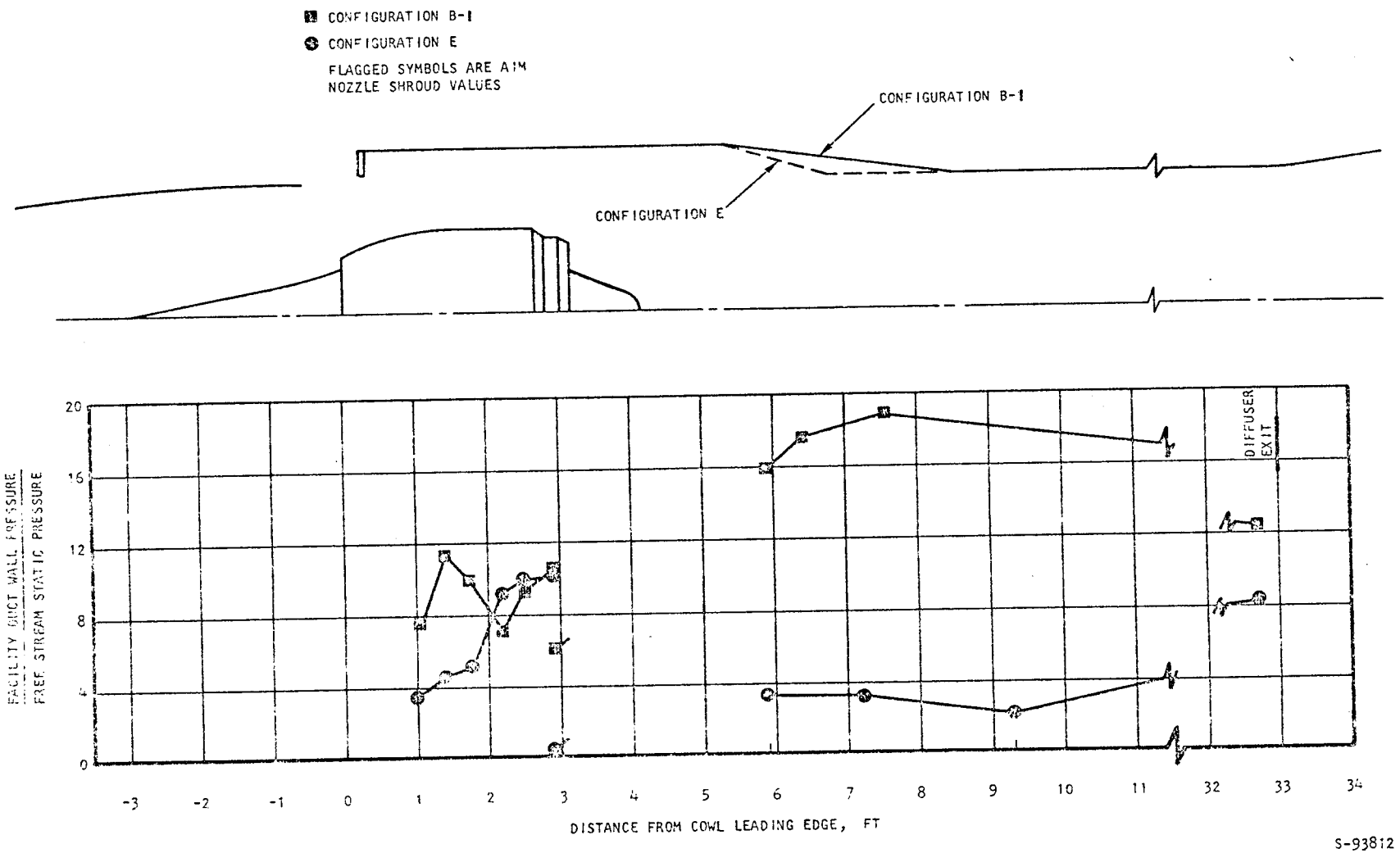

Figure 5-16. Duct Wall Pressure Distribution, $M_o = 6.03$

as follows:

Primary nozzle steam pressure	=	140 psia
Primary nozzle steam flow rate	=	10.6 lb/sec
Secondary flow inlet pressure	=	1 psia
Secondary flow rate	=	5 lb/sec

The ejector was intended to reduce the cell pressure by pumping air from the cell into the spray chamber. However, the tunnel did not start in the first attempts. Variations in wedge nozzle pressure and inlet spike position proved ineffective.

Configuration F was then abandoned for configuration G. A closure cone was installed between the wedge nozzle and the existing shroud to form this configuration. Configuration G was unsuccessful. High-pressures on the AIM inlet spike indicated that the tunnel terminal shock was standing about 6 inches upstream of the AIM cowl leading edge. The contraction in the flow path in this region formed by the tunnel exit lip and the AIM inlet spike and cowl, was apparently contributing to this problem. Therefore, the AIM was moved 5.5 in. aft to reduce the contraction (configuration G-1). The tunnel did not start.

An attempt was then made to relieve the contraction by bleeding air out of the tunnel. Two 6-in.-dia blowout doors were installed in the closure cone on opposite sides of the tunnel to form configuration G-2. The doors were spring loaded closed. Thus, when high-pressures were imposed by the terminal shock, the doors would be driven open and air exhausted into the test cell. This would bleed air out near the contraction throat and permit the shock to proceed downstream into the diverging area.

The tunnel was started with this configuration in reading 81. However, it unstarted immediately when fuel was introduced to the AIM.

A circumferential seal around the 45-in.-dia diffuser was then found to be leaking air from the diffuser to the test cell. The calculated leak rate was 8 lb per sec. This was sufficient to have a significant effect on the cell pressure. The seal was repaired and the tunnel restored to configuration F.

When the attempt was made to start the tunnel with configuration F, reading 88, the total pressure was ramped to 1000 psia without success. The inlet was opened in an attempt to achieve a start. When this failed, the inlet was closed and re-opened in a second attempt. Both the tunnel and the inlet started. Fuel equivalence ratio was then ramped up to 0.94 without unstarting the tunnel. Apparently the tunnel starting process was marginal. In subsequent runs the tunnel sometimes self-started and other times required the inlet to be opened to start.

Review of the data showed the diffuser flow to be supersonic. The calculated duct exit Mach number was 1.4 and the total pressure recovery was 0.835-times the normal shock value.

5.2.4 Tunnel Unstarts Due to Combustion

Combustion in the AIM caused the tunnel to unstart by two different processes.

(a) Thermal choking in the tunnel diffuser exit.

(b) Excessive first-stage injector fuel flow in the AIM.

The process of thermal choking is described in Figure 5-17. A map of calculated one-dimensional diffuser exit flow conditions is shown; also, measured diffuser exit static pressures are plotted versus (ϕ) for readings 36 and 65. As equivalence ratio is increased, the measured exit pressures are seen to move toward the calculated values for sonic flow. This process takes place at a nearly constant diffuser exit total pressure, as apparently the heat addition pressure loss in AIM is partially compensated by the upstream movement of shockwaves in the external flow. This improves the pressure recovery for that portion. When sonic conditions are first reached at the diffuser exit, the diffuser inlet flow remains supersonic. Further addition of fuel causes shocks to move upstream through the diffuser and into the test section accompanied by subsonic diffuser flow. When the shocks reach the AIM cowl on or near the inlet spike tip shock, the inlet unstarts, causing a tunnel unstart.

An unstart occurred in this manner in reading 65 with the instrumentation rake (see Section 3.2) installed. The instrumentation rake was found to adversely affect tunnel unstarts. The unstart point is plotted in Figure 5-17 at a ϕ of 1.05. The tunnel unstarted 5 sec after ϕ was set and held at this value. During this time, the cell pressure increased from 6.3 to 7.6 times the freestream static pressure. Also, the diffuser inlet pressure increased, indicating a transition from supersonic to subsonic flow. Unstart occurred immediately after the transition.

An oncoming tunnel unstart due to thermal choking was always apparent on the Schlieren screen. As the terminal shocks moved toward the AIM cowl, a thickening and unsteadiness was seen in the cowl boundary layer. Another warning was also apparent in the television screen monitoring the AIM inlet through the slot between the tunnel exit and the test section shroud. A normal shock which appeared as a luminescent ring around the cowl could be clearly seen moving slowly toward the AIM inlet as shown in Figure 5-18. When the ring appeared to be several inches from the inlet, the tunnel unstarted. At unstart, the AIM was obscured by luminescent gas as strong shocks moved upstream of the inlet.

The cause of this shock was the intersection of the tunnel exit shock and the shock generated by the AIM cowl as previously described in the Fluidyne Analysis in Figure 5-15b. When the cell pressure became excessively high, the flow could not negotiate the required turning angles through oblique shocks and a normal shock was generated.

The position of the luminescent ring was monitored on the television screen during reading 68 to prevent unstarting the tunnel. The ring position

NOTE

MEASURED EXIT PRESSURES

● RDG 36 INSTRUMENTATION RAKE REMOVED

▣ RDG 65 INSTRUMENTATION RAKE INSTALLED

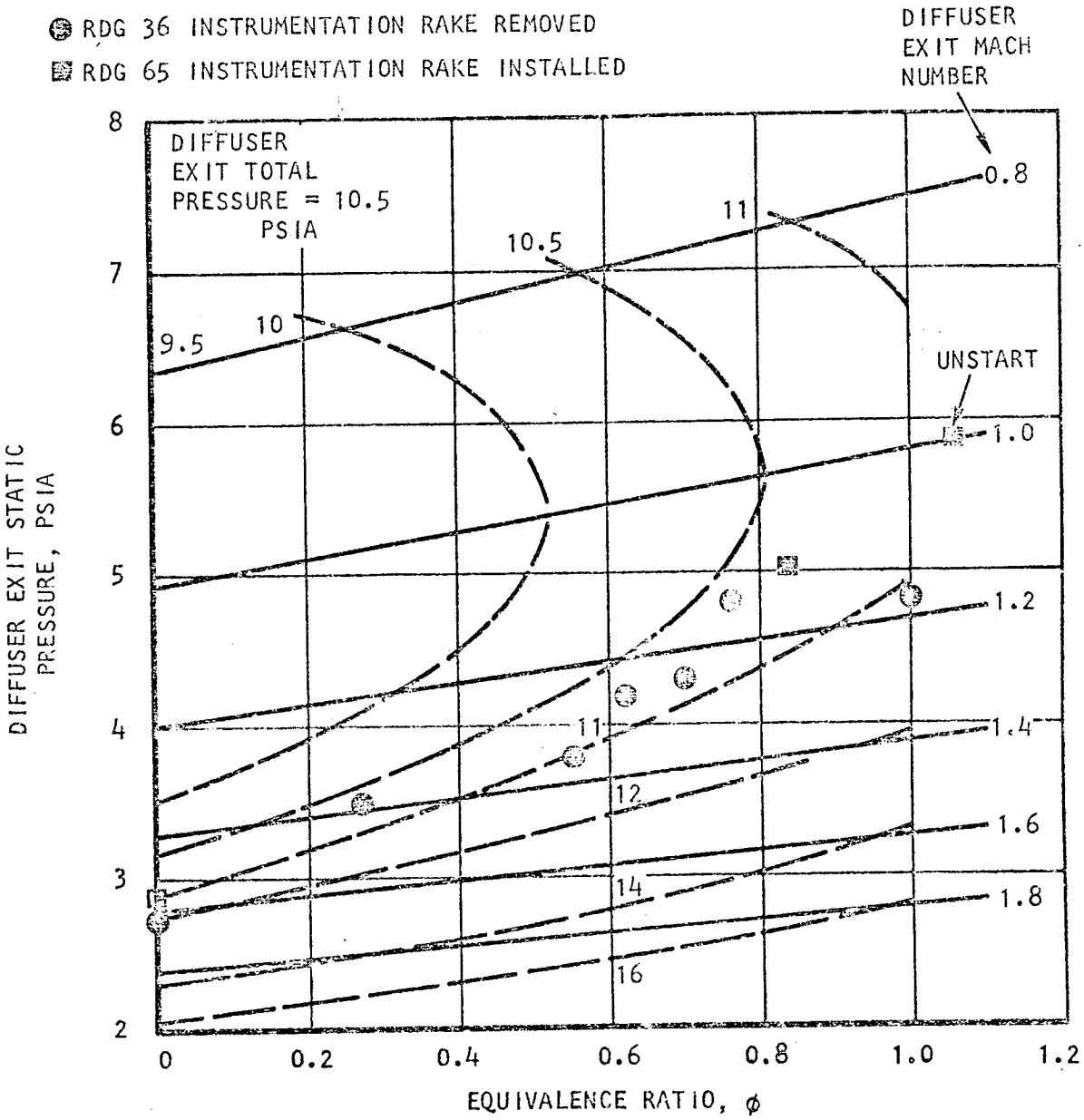

P_{TO} = 750 PSIA

T_{TO} = 3000°R

MACH 6.0 TUNNEL

WEDGE NOZZLE PRESSURE = 75 PSIA

S-93956

Figure 5-17. Diffuser Exit Conditions

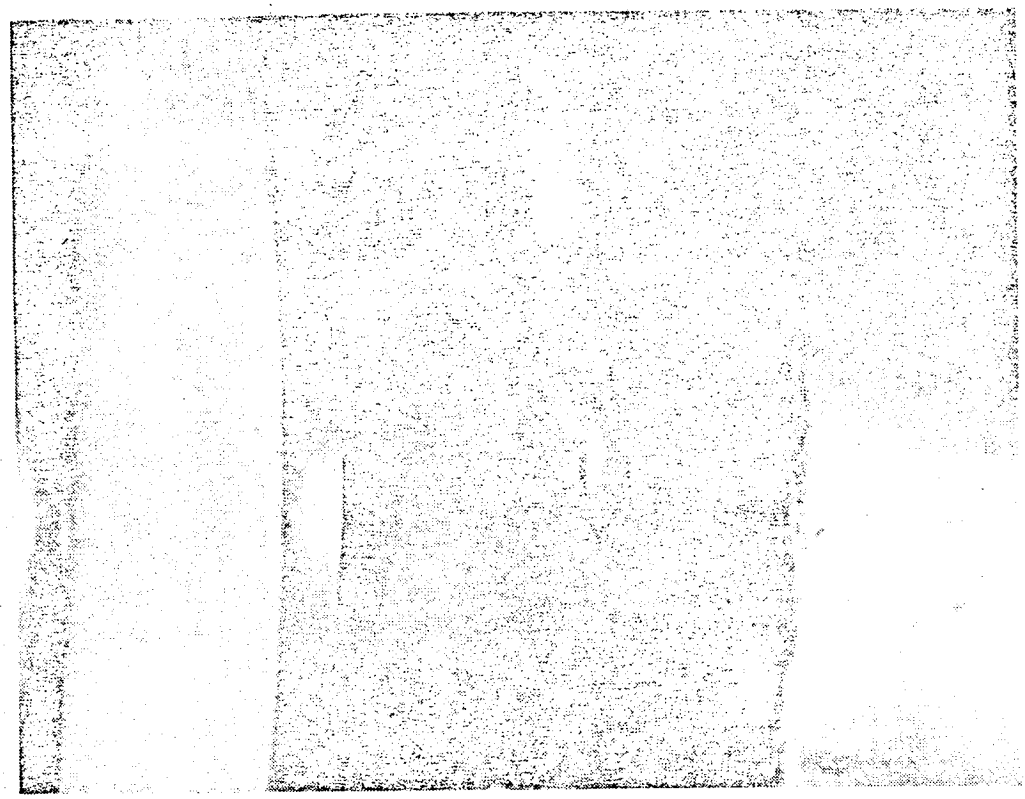

(a) VIEW OF COWL BEFORE UNSTART

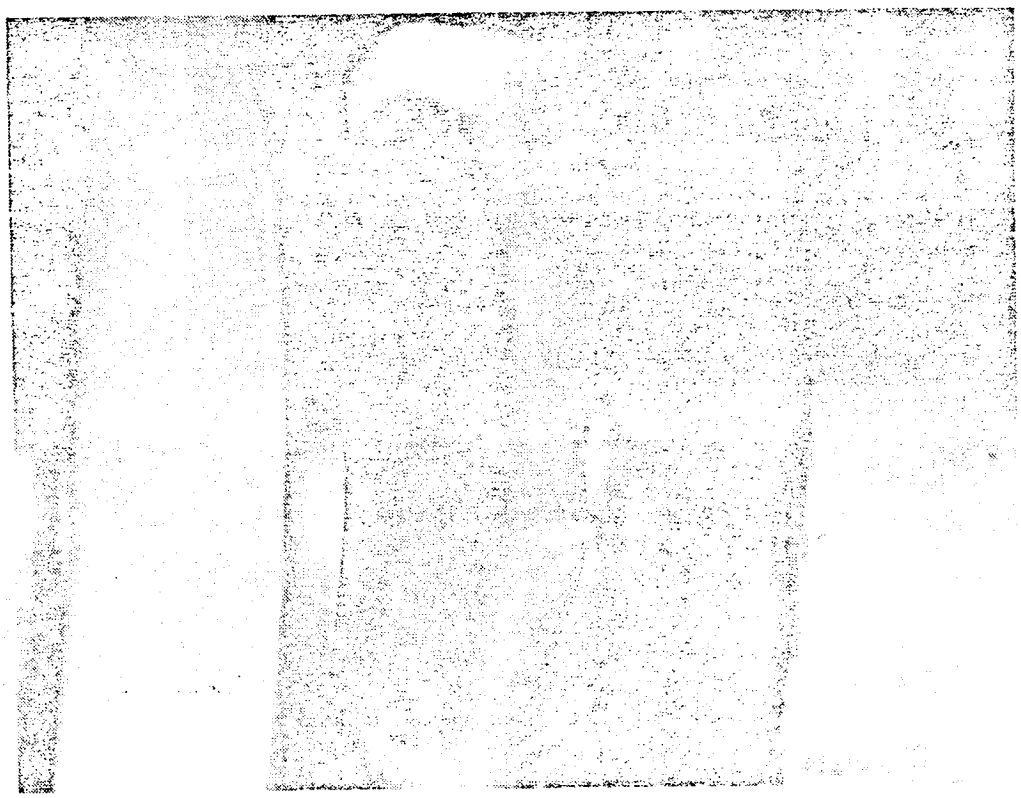

(b) LUMINESCENT RING APPROACHING INLET S-93975

Figure 5-18. Tunnel Unstart Due to Thermal Choking

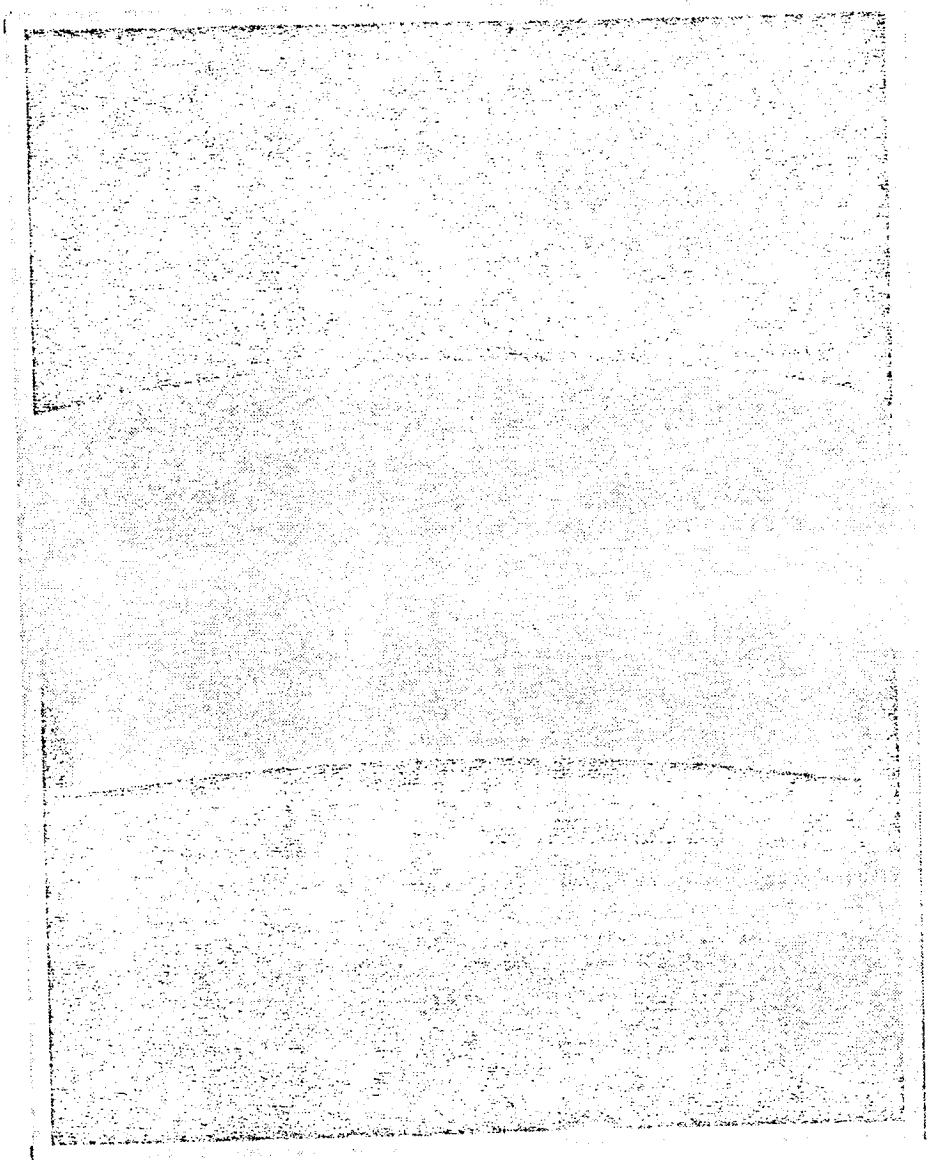

(c) TUNNEL UNSTARTED

S-93976

Figure 5-18. (Continued)

at tunnel unstart was marked on the television screen. The unstart point was established from video tape playbacks of reading 65. When the ring approached the mark in reading 68, fuel flow was terminated. The ring was then observed to retreat downstream and the unstart prevented.

These measures were necessary only with the instrumentation rake installed. A ϕ of 1.35 was successfully run without the rake in reading 64. At this condition, the diffuser exit had choked from the supersonic side; that is, the flow upstream was supersonic with the exit driven to sonic conditions by duct losses. The tunnel was apparently on the verge of unstarting at this condition.

The tunnel could also be unstarted by excessive first-stage fuel injection in the AIM. This was encountered in reading 33. The AIM inlet was to be intentionally unstarted in this run to determine the maximum first-stage equivalence ratio with the second stage inoperative. Fuel flow was linearly ramped toward a (ϕ) 0.4 and the inlet unstarted at a value of 0.34. This immediately unstarted the tunnel. The unstart was caused by pressure losses due to strong shocks ahead of the AIM inlet.

5.3 COMBUSTION TESTS

A summary of the initial wind tunnel tests is presented in Table 5-3. The plan was based on the rationale given below.

The Mach 6 tests were to be run first for the following reasons:

> Mach 6 is the design transition Mach number from the subsonic- to supersonic-combustion mode. Data could be accumulated in both modes and intermode transition demonstrated.
>
> Mach 6 is the most critical condition, considering both inlet unstart and ignition delay. These would be evaluated early in the program.
>
> A large amount of useful data could be obtained before subjecting the AIM and the facility to the higher-risk Mach 7 conditions.

At each Mach number, a purge force calibration test (see paragraph 5.1.2.4) would be run first. This would determine a thrust correction due to cavity purge. The purge prevented hot tunnel flow entry into the cavity containing fuel mainfolds between the engine and the outer cowl body. The tests were to be performed at 1500°R, as this low temperature would prevent damage to the AIM if hot gas should enter. Also, the test would provide a system checkout at low temperature before the engine was run at more severe conditions. At each Mach number, tests would be performed to determine the captured inlet weightflow at various spike positions. The tests would be made with a flow meter replacing the engine exhaust nozzle.

TABLE 5-3

SUMMARY OF AIM WIND TUNNEL TESTS

RUN	M_0	PTO, PSIA	TTO, °R	α	FUEL SYSTEMS	FUEL SCHED.	INLET ΔX, IN.	COMBUSTION MODE	RUN TYPE AND PURPOSE
1	6	466	1500	0	-	-	4.23	-	Purge force, nominal case
2	6	466	1500	0	-	-	1.90	-	Purge force, effect of spike position
3	6	466	1500	3	-	-	4.23	-	Purge force, effect of angle of attack
4	6	466	2000	0	-	-	4.23	-	Operation checkout, effect of higher TTO
5	6	466	3000	0	-	-	0, 1.71, 2.52 4.23, aft stop	-	Airflow calibration, effect of altitude
6	6	930	2946	0	-	-	0, 1.71, 2.52 4.23, aft stop	-	Airflow calibration, nominal case
7	6	930	2946	3	-	-	0, 1.71, 2.52 4.23, aft stop	-	Airflow calibration, effect of angle of attack
8	6	930	2946	0	1a, 1b	1	4.23	Supersonic	Inlet-combustor performance, ignition and inlet unstart limits
9	6	930	2946	0	1a, 1b, 2a, 2c	2	4.23	Supersonic	Inlet-combustor performance, injector optimization
10	6	930	2946	0	1c, 4, 2a, 2c	2	4.23	Supersonic	Inlet-combustor performance, injector optimization
11	6	930	2946	0	1a, 1b, 1c, 4	3	4.23	Supersonic	Inlet-combustor performance, injector optimization
12	6	930	2946	0	TBD	TBD	4.23	Supersonic	Inlet-combustor performance, injector optimization
13	6	466	3000	0	1a, 1b, 2a, 2c	2	4.23	Supersonic	Inlet-combustor performance, effect of altitude
14	6	700	3000	0	1a, 1b, 2a, 2c	2	4.23	Supersonic	Inlet-combustor performance, effect of altitude
15	6	930	2946	0	1a, 1b, 2a, 2c	2	Aft stop	Supersonic	Inlet-combustor performance, effect of spike position
16	6	930	2946	0	1a, 1b, 2a, 2c	2	2.52	Supersonic	Inlet-combustor performance, effect of spike position
17	6	930	2946	0	1a, 1b, 2a, 2c	2	1.71	Supersonic	Inlet-combustor performance, effect of spike position
18	6	930	2946	0	3a, 3b	4	4.23	Subsonic	Inlet-combustor performance, subsonic combustion
19	6	930	2946	0	3a, 3b	5	4.23	Subsonic & transition	Engine performance, subsonic combustion and transition
20	6	930	2946	0	1a, 1b, 2a, 2c	2	4.23	Supersonic	Engine performance, nominal case
21	6	466	2946	0	1a, 1b, 2a, 2c	2	4.23	Supersonic	Engine performance, effect of altitude
22	6	930	2946	3	1a, 1b, 2a, 2c	2	4.23	Supersonic	Engine performance, effect of angle of attack
23	7	520	1500	0	-	-	2.88	-	Purge force
24	7	520	3965	0	-	-	2.34, 2.88 3.24	-	Airflow calibration, effect of altitude
25	7	1000	3840	0	-	-	1.98, 2.88 3.24	-	Airflow calibration, nominal case
26	7	1000	3840	3	-	-	2.34, 2.88 3.24	-	Airflow calibration, effect of angle of attack
27	7	520 & 1000	3965 3840	0	1a, 1b	6	2.88	Supersonic	Inlet-combustor performance, ignition and inlet unstart limits
28	7	1000	3840	0	1a, 1b, 2a, 2c	7	2.88	Supersonic	Inlet-combustor performance, injector optimization
29	7	1000	3840	0	1c, 4, 2a, 2c	7	2.88	Supersonic	Inlet-combustor performance, injector optimization
30	7	1000	3840	0	1a, 1b, 1c, 4	8	2.88	Supersonic	Inlet-combustor performance, injector optimization
31	7	1000	3840	0	TBD	TBD	2.88	Supersonic	Inlet-combustor performance, injector optimization
32	7	522	3965	0	1a, 1b, 2a, 2c	7	2.88	Supersonic	Inlet-combustor performance, effect of altitude
33	7	700	3965	0	1a, 1b, 2a, 2c	7	2.88	Supersonic	Inlet-combustor performance, effect of altitude
34	7	1000	3840	0	1a, 1b, 2a, 2c	7	3.24	Supersonic	Inlet-combustor performance, effect of spike position
35	7	1000	3840	0	1a, 1b, 2a, 2c	7	2.34	Supersonic	Inlet-combustor performance, effect of spike position
36	7	1000	3840	0	1a, 1b, 2a, 2c	7	1.98	Supersonic	Inlet-combustor performance, effect of spike position
37	7	1000	3840	0	1a, 1b, 2a, 2c	7	2.88	Supersonic	Engine performance, nominal case
38	7	522	3965	0	1a, 1b, 2a, 2c	7	2.88	Supersonic	Engine performance, effect of altitude
39	7	1000	3840	3	1a, 1b, 2a, 2c	7	2.88	Supersonic	Engine performance, effect of angle of attack
40	5	445	1500	0	1a, 1b, 2a, 2c	-	4.23	-	Purge force
41	5	206	2210	0	1a, 1b, 2a, 2c	-	4.23	-	Airflow calibration
42	5	415	2210	0	1a, 1b, 2a, 2c	9	4.23	Supersonic	Inlet-combustor performance, nominal case effect of altitude
43	5	415	2210	0	1a, 1b, 2a, 2c	TBD	4.23	Supersonic	Inlet-combustor performance, and ignitor flow rate
44	5	415	2210	0	1a, 1b, 2a, 2c	9	4.23	Supersonic	Engine performance, supersonic combustion
45	5	415	2210	0	3a, 3b	10	4.23	Subsonic	Engine performance, subsonic combustion
46	5	415	2210	3	1a, 1b, 2a, 2c	11	4.23	Subsonic & Supersonic	Engine performance, effect of angle of attack

The inlet-combustor performance tests would then be run at various fuel injector combinations and equivalence ratios. Inlet-combustor performance, unstart limits, and ignition limits would be determined. These tests would be performed with the combustor exit instrumentation rig installed (see paragraph 2.10.1). The instrumentation rig would survey combustor exit total pressure, temperature, Mach number, and flow direction at the duct centerline. Also, gas samples would be taken to determine the local fuel-air ratio and gas composition.

The inlet-combustor performance data would be used to select the best combination of fuel injector locations. This combination would then be used for engine performance tests. The combustor exit rake would be removed for these tests because it was anticipated that the thrust measurement data would be affected by impingement of the probe shocks on the exhaust nozzle walls.

Performance would be measured at various conditions. Tunnel pressure would be varied to determine the effect of altitude, and spike position would be varied to determine the effect of combustor inlet Mach number. Performance would be measured at a 3-deg angle of attack. Subsonic combustion performance would be measured at Mach 5 and 6; also, transition between subsonic and supersonic combustion would be demonstrated.

In general, the above plan was followed with the following exceptions:

The purge force calibration tests were not completed until the end of the program, since initial tests had indicated that techniques must be developed to properly account for all factors involved. A detailed description of these factors appears in a later section.

The airflow calibration tests were deleted due to schedule limitations. In lieu of these inlet flow calibrations, the captured inlet weightflow was determined from the cowl area and tunnel flow conditions. The 2/3-scale inlet test data was used to determine the inlet mass flow ratio at off-design conditions.

The number of injector combinations evaluated in the injector optimization tests was reduced because of schedule limitations.

The injector optimization tests were performed at a tunnel total pressure of 750 psia, instead of the planned 930 psia, to avoid subjecting the AIM to tunnel unstarts at high pressure. The AIM had been previously damaged under this condition (see paragraph 5.2.3 under "Configuration C"). Intentional inlet unstarts were planned for the combustor optimization tests and these were known to unstart the tunnel.

A-2

5.3.1 Fuel System Operation

Fuel flow to the AIM was computer controlled by the system described in paragraph 3.1.5. The AIM fuel manifold pressures required to deliver the scheduled full-flow were calculated prior to a run and programmed on magnetic tape. During the run, the pressures were controlled to match the values on tape by a closed-loop control system.

Typical fuel schedules are given in Figures 5-19a to 5-38a. These show the planned equivalence ratios as a function of time for selected runs.

Some schedules were divided into segments, as shown in Figure 5-29a. If an inlet or tunnel unstart occurred, the fuel flow could be terminated and the fuel schedule skipped to the next segment. Operation of the system is described below.

At the start of a test, the fuel control computer entered a "hold" condition just after the tunnel total pressure reached its operating value. In the "hold" condition, the fuel system was armed so that actuation of a switch would clear the hold and start the fuel schedule. Thus, the tunnel flow conditions could be verified and the inlet starting procedure executed at the discretion of the test conductor before admitting fuel. Tunnel and inlet starts were verified by observing the Schlieren television monitor.

In the event of a tunnel or inlet unstart during the run, a "skip" switch was actuated. The skip signal closed the fuel control valves, advanced the tape to the next segment, and re-established a "hold" condition while the tunnel and inlet were re-started. The tunnel was re-started by commanding the inlet to a partially closed position ($\Delta X = 0.99$). The inlet was then returned to its operating position. The hold was then cleared to continue the fuel schedule from the start of the next segment. Examples of this procedure are discussed in the following section.

5.3.2 Discussion of Tests

The testing aspects of selected combustion test runs are discussed in chronological order in this section. The planned fuel schedules and the measured fuel equivalence ratio (ϕ) plots are given in Figures 5-19 through 5-38.* The corresponding thrust measurement load cell readings and measured cavity purge pressure (PA2) are also presented. A complete listing of all runs was given in the Test Run Summary, Table 5-2. Fuel injector locations used in the discussion are defined in Section 2.3.

The runs prior to reading 53 were not used for performance calculations due to difficulties encountered in recording AIM wall pressure measurements. The pressure taps injested water from the spray chamber and condensed steam from the facility ejector. This occurred during the periods of unsteady ejector operation during tunnel startup and shutdown. Continual experimentation with facility operating procedures was required to minimize this problem.

*NOTE: All figures for this discussion appear at the end of Section 5.3.

Thrust measurements were not valid before reading 57. It was found that a damaged purged cavity pressure line in the AIM was affecting the purge force calibrations (see Section 5.1.2.4). Also, binding between the outer cowl body and the AIM affected true thrust-drag measurement (see paragraph 5.1.2.2). The readings prior to 57 are included in the discussion, since useful information concerning the operation of the AIM and the facility was obtained.

Readings prior to 33 were devoted to the solution of wind tunnel starting problems and are discussed in Section 5.2. Reading 33 was the first run with combustion in a fully started wind tunnel.

Reading 33

The purpose of this run was to determine the inlet unstart limit for the first-stage fuel injectors. The first-stage ϕ would be ramped from 0.04 to 0.4 in injectors 1a and 1b as shown in Figure 5-19a. Ignitor rows 1 and 2 would be lit for the entire run. A ten-second flat would occur at $\phi = 0.175$ as a check on the stabilization of instrumentation and the AIM wall temperatures. The 1a, 1b injectors were selected because they are closest to the combustor inlet, and thus, provide a check on the combination giving the best theoretical performance. These are also the most critical with respect to inlet unstart.

Figures 5-19b and c reveal that the inlet unstarted at $\phi = 0.34$. This value was used as a guide in selecting the first-stage ϕ for future runs using both stages.

Examination of the data in the flat portion of the fuel ramp revealed that the ramp rate was slow enough to give stable wall temperature and pressure measurements. In other words, the measurements followed the trend of the fuel flow with no significant lag.

Reading 34

The purpose of this run was to determine if the tunnel would remain started at the most adverse conditions. Also, operation at the design Mach 6 P_{T0} of 930 psia would be demonstrated. The run was intended to expose problem areas so that the required remedial action could be initiated at the earliest date.

The worst case considering tunnel unstart was expected to occur with incomplete combustion in the AIM. The unburned fuel could ignite at low-pressure in the constant-area diffuser downstream of the AIM exhaust nozzle. The resulting high-heat-addition pressure loss would affect the tunnel operation in an unfavorable manner.

The 2a and 3a second-stage injectors were selected for the run on the basis of their yielding the lowest potential combustion efficiency. Also, the combustor would be operated fuel rich. This could cause the excess fuel to burn in the diffuser as it mixed with the external flow.

The fuel schedule is given in Figure 5-20a. ϕ was to be ramped to a value of 1.34 at PT0 = 750 psia. If the tunnel did not unstart at these conditions, P_{T0} would be ramped to 930 psia at constant-fuel flow as shown in Figure 5-20d. This would result in a reduction in ϕ as PT0 increased, so that an unstart at high pressure would be avoided. Ignitor rows 1 and 2 would be lit for the entire run.

The run was completed without unstarting the tunnel.

Reading 36

This run was made to demonstrate the operation of the AIM and the facility using the Mach 6 design injector (fuel systems 1a, 1b, 2a, 2c). Autoignition was to be attempted. First-stage fuel was to be introduced at ϕ = 0.24, as seen in Figure 5-21a, and held for 5 sec to obtain stable operation. Second-stage fuel would then be ramped to a ϕ of 1.0 in 94 sec so that the autoignition point could be determined. If ignition did not occur when ϕ had reached a value of 0.6, the ignitors were to be lit.

Autoignition occurred after the second-stage fuel was initiated at an overall ϕ of 0.53 at 128 sec, as seen in Figures 5-21b and c. The data showed that the first stage had not lighted prior to second-stage injection. Ignition of both stages occurred after the second-stage fuel had been introduced.

Reading 52

Second-stage fuel was injected in more upstream locations for both the first and second stages (injectors 1a, 1b, 4, 2c) in this run as shown in Figure 5-22a. In theory, this yields better performance, but is more conducive to unstarting the inlet.

The effect of first-stage ϕ on performance would also be evaluated in this run. Second-stage ϕ would be increased, while holding the first stage constant. This would be done at each of several first-stage values. The range selected for the first-stage ϕ's was felt to be a reasonable spread between the first-stage lean ignition limit and the inlet unstart limit. Row 1 and 2 ignitors would be lit to insure that combustion data could be obtained at the low ϕ conditions. Ignitors would be turned off in segment 4 to determine their effect on performance.

Figures 5-22b and c show that full thrust was not obtained because of an inlet unstart encountered at an overall ϕ of 0.83, with the first stage at ϕ = 0.22. The run was manually terminated at this point. The cavity purge pressure, PA2, is seen to oscillate in Figure 5-22c because of excessive gain in the pressure control system.

Reading 54

The effect of first stage and overall ϕ on performance with injectors 1a, 1b, 2a, 2c was to be evaluated in this run as shown in Figure 5-23a. Forty seconds of ϕ = 1.0 operation was planned at the end of the run, while cavity

purge pressure was to be varied to determine the effect on tare force. Also, ignitors were to be operated the same as planned for reading 52.

The entire fuel schedule was performed in the run as seen in Figures 5-23b and c. Good wall pressure measurements were determined in this run and the data was the first to be used for a complete combustor performance analysis.

Variations from the planned first-stage fuel schedule were encountered, as seen in Figure 5-23b. The first stage ϕ is seen to decrease with time, instead of holding a constant value as planned. The cause of this was a gradual increase in the AIM fuel manifold hydrogen temperature during the run (see Section 5.3.2). ϕ was scheduled to be set at 0.24, 0.27 and 0.3, resulting in a 25-percent overall variation. An 8-percent variation was obtained in the run.

Because of the above consideration and also because random variations in the fuel temperature were encountered from run to run, a fuel manifold temperature compensation feature was planned for the fuel control.

Reading 57

An improved approach was taken in this run to measure the effect of first stage ϕ on performance. Overall ϕ was to be held constant at a value of one, while the first- to second-stage fuel split was varied as seen in Figure 5-24a. This method has the advantage of covering a wider ϕ range than the method of reading 54. The first-stage ignition limit and the inlet unstart limit can be covered in a single fuel ramp. Ignitors were lit for the entire run. Comparison of the thrust and ϕ plots of Figure 5-24b and c show that the combustor lit immediately at a first-stage ϕ of 0.2, and the inlet unstarted at 0.37 about 235 sec into the run.

In the second segment of the fuel schedule, all second-stage fuel was added from the innerbody injector, 2c, to determine the effect on performance.

Note the 80-pound change in load cell reading in Table 5-2 between 198 and 235 sec. The cause of this change is not the variation in combustor fuel distribution as the data shown here might suggest. Analysis reveals that the change to be caused by variation in purged cavity tare force due to thermal expansion of the 1B fuel manifold. This effect is described in paragraph 5.1.2.4.3.

Reading 60

Various combinations of innerbody and outerbody fuel injection were investigated in this run, while the nominal overall ϕ was held at unity as shown in Figure 5-25a. An inlet unstart was encountered at 286 sec when a high second-stage ϕ was injected on the outerbody wall.

Reading 60 was the last run investigating the effect of fuel injection schemes. Fuel temperature compensation was added to the fuel control.

Reading 61 (Figure 5-26)

The effect of inlet spike position on performance was investigated in reading 61. The selected spike positions resulted in inlet mass flow ratios of 0.58 and 0.81. The 2/3-scale inlet test mass flow ratio data was used to select the spike position settings. Ignitors were on for the entire run. The fuel line purge nitrogen flow was turned off and on to investigate the effect of the purge jets on the combustor wall pressure distribution at each spike position.

Reading 63

This run was made to investigate the effect of altitude on performance. The tunnel total pressure was run at 466 and 930 psia corresponding to altitudes of 91,000 and 76,000 feet respectively.

The first portion of the fuel schedule was devoted to the high pressure condition as shown in Figure 5-27d. Since the AIM was previously damaged by a tunnel unstart at this condition, the maximum ϕ was limited to a value of 1.0. A maximum ϕ of 1.3 was to be run at PT0 = 466 psia.

The ϕ = 0 interval between the two pressure ramps was devoted to the adjustment of PT0.

Reading 64

Combustion mode transition was demonstrated and subsonic combustion performance was measured in this run. Subsonic combustion was obtained using injectors 3A and 3B. Supersonic combustion was obtained with all of the first stage fuel injected from outerbody injector 1B. Fuel line limitations within the AIM innerbody prevented the use of an additional innerbody injector with the subsonic combustion injectors in operation.

The row 3 ignitors, intended for subsonic combustion, were not used in this run. Schedule limitations prevented the allocation of the time required to make the necessary plumbing changes within the AIM innerbody; consequently, the run was planned so that supersonic combustion always preceded subsonic combustion, then the supersonic stages were used to light the subsonic stage in lieu of the ignitors, thereby insuring a successful run.

The conditions planned in the fuel schedule of Figure 5-28a are listed below.

Time, sec	Condition
0-7	Lightoff with supersonic combustion
7-29	Supersonic to subsonic transition
29-37	Subsonic combustion, ϕ = 1.0
41-49	Subsonic combustion, ϕ = 1.24
49-69	Subsonic combustion, performance at reduced ϕ

Time, sec	Condition
73-80	Lightoff with supersonic combustion
80-109	Transition to subsonic combustion
109-114	Subsonic combustion
114-140	Transition to supersonic combustion

Transition was successfully demonstrated in the run.

Reading 65

Combustor exit flow conditions were surveyed with the instrumentation rig (see paragraph 2.10.2) in this run. The instrumentation rig consisted of 10 probes located at the combustor exit station on the flow path outerline. Five probes were designed to extract gas samples and measure the combustor exit total temperature, and the remaining five were cone probes with a pitot and 4 cone static-pressure taps. These were intended to measure total pressure and temperature, Mach number, and flow direction.

The fuel schedule was planned with 10-sec steady-state portions at various operating conditions. Ten seconds was felt to be adequate for the stabilization of the gas sampling data.

It was found in the run that the instrumentation rig affected the operation of the wind tunnel. The tunnel unstarted at $\phi = 1.05$ and fuel flow was terminated while the inlet spike was cycled to restart the tunnel and the AIM inlet. A total of three such unstarts was encountered in the run, as seen in Figures 5-29b and c.

Reading 69 (Figure 5-30)

The results from reading 65 indicated that the ten seconds allowed for stabilization of the gas sampling data was inadequate. Reading 69 was a rerun of reading 65, with the stabilization time increased to 20 sec. Also, ϕ was reduced in an attempt to avoid tunnel unstarts.

The closed circuit television monitoring the AIM cowl was to be used to detect incipient tunnel unstart. This would provide a means of detecting a normal shock approaching the aim inlet so that fuel flow could be terminated to avoid unstarting the tunnel (see para 5.2.4).

Fuel was prematurely terminated for most of the conditions planned, due to incipient tunnel unstart in spite of the reduction in ϕ. However, an adequate amount of gas sampling data was obtained. No further attempts were made due to a limited time remaining in the program.

The T.V. monitor proved to be a reasonably effective method of anticipating an unstart. Three unstarts were avoided in this manner by terminating the fuel flow. In the fourth attempt, the tunnel unstarted when the shock was permitted to come too close to the AIM inlet.

Reading 71

The AIM was run at a 3-deg angle of attack with supersonic combustion in reading 71. Fuel flow was terminated in segment 1 of the fuel schedule (see Figure 5-31a) when the AIM inlet unstarted at a ϕ of 1.27. This unstarted the wind tunnel. A ϕ of 1.4 was reached with the second stage only in segment 2, without unstarting the inlet. The run was prematurely shutdown in segment 2 due to a facility problem.

Reading 72 through 87

Reading 72 was a cavity purge force calibration run. Readings 73 through 87 were devoted to tunnel development for the Mach 7 tests. These runs are discussed in para 5.2.3.

Reading 88

Reading 88 was the first valid run at Mach 7 with combustion. However, the true Mach 7 total temperature of 3840°F was not obtained due to a problem with the facility nitrogen heater. Insufficient time remained in the program to make the necessary repairs; therefore, the Mach 7 tests were performed at a nominal temperature of 3000° to 3200°R.

The fuel schedule given in Figure 5-32a was planned to investigate various fuel injection schemes consistent with those used in the Mach 6 tests. Segments 1 and 2 were skipped in the run because a significant portion of the run time was absorbed in achieving a tunnel start. Segment 3 was intended to determine the inlet unstart limit with the first stage only. The lean ignition limit with row 1 and 2 ignitors lit would also be investigated. The change in load cell reading in Figure 5-32c at 264 seconds indicates a lightoff. The corresponding ϕ in Figure 5-32b is 0.41. ϕ was increased to 0.58 without unstarting the inlet.

The effects of increasing first stage ϕ on performance was investigated in segment 4. Comparison of Figures 5-32b and c show that the combustor lit at a ϕ of 0.34 at 290 sec. A first stage ϕ of 0.5 was reached without unstarting the inlet.

The AIM sustained foreign object damage in this run. Pieces of carbon were dislodged from the lining of a duct leading from the facility nitrogen heater to the wind tunnel. Carbon fragments as large as one inch long were found that had passed through the tunnel. The damage and repair are discussed in Section 6.3.4.

Reading 89

Investigation of the effect of fuel injection schemes on performance was continued in reading 89. In segment 1 of the fuel schedule, ϕ was stepped to determine performance as a function of ϕ with injector locations 1a, 1b, 2a and 2c. However, the load cell reading plot of Figure 5-33c shows that the combustor did not light. Ignitors were lit for the entire run. Conditions

for ignition were apparently marginal with the reduced total temperature at Mach 7. The combustor had lit in the previous run at similar conditions.

In segment 2, the tunnel total temperature was to be varied while ϕ was held at a value of one. Figure 5-33d shows that the nominal values obtained were 2800°R and 2400°R. Figure 5-33c shows the combustor lit at 308 sec just before the total temperature ramp toward 2800°R was initiated. Lightoff occurred when first stage fuel was introduced.

Performance as a function of ϕ was to be measured in segment 3 using injectors 2c and 4. The combustor lit with this combination but the run was prematurely terminated due to a fuel control problem.

Reading 90

Further investigation of performance was made using injectors 1a and 1b as the first stage and the further-upstream injectors 1c and 4 as the second stage. It was found that this combination resulted in inlet unstarts, as in the case of the Mach 6 tests.

Reading 91

The AIM was tested at a 3-deg angle of attack in this run. Several combinations of injectors were attempted in the initial portion of the run which unstarted the inlet. In fuel schedule segment 4 using injectors 1b, 2c, and 4, the combustor was successfully lit. Lightoff is seen to occur at 209 sec in Figure 5-34c.

Reading 92

Combustor performance was determined in this run with injectors 1a, 1b, 4, and 2c with the instrumentation rake installed. In fuel schedule segments 1 through 4, the effect of ϕ and the use of injector 1b only for the first stage was investigated.

In segments 5 and 6, the weight flow of oxygen supplied to the tunnel flow was varied. This was done to investigate the extent of fuel-air mixing. The run was terminated near the end of segment 6.

This concluded the Mach 7 testing.

Readings 93 and 94 (Figure 5-36)

Reading 93 was the first run at Mach 5. No tunnel starting problems were anticipated and combustion was attempted in the first run. Segment 1 was planned to investigate subsonic conbustion at 2 altitude conditions. First P_{T0} would be set at 415 psia and T_{T0} at 2210°R. The combustor would be lit in the supersonic combustion mode using injector 2A and the row 2 ignitors. Fuel would then be introduced in injectors 3a and 3b to obtain subsonic combustion performance.

At 48 seconds into the schedule, PT0 was ramped to 206 psia to obtain the low-altitude condition.

Comparison of Figures 5-36b and c shows that the combustor lit with a ϕ of 0.5 in 2a injectors. Subsonic combustion performance was then obtained when fuel was introduced in the 3a and 3b injectors and terminated in 2a. The low-altitude case was not encountered due to a premature shutdown of the facility.

The same fuel schedule was used again in reading 94. Several tunnel unstarts were encountered.

Reading 95

Performance was to be obtained with a Mach 6 total temperature of 3000°R and a total pressure of 300 psia in this run. The effects of ϕ on supersonic combustion performance would be obtained in segment 1 using injectors 1a, 1b, 2a, and 2c. Good data was obtained up to an overall ϕ of 1.1 when a tunnel unstart occurred.

The schedule was skipped to segment 2 where performance was obtained with injectors 2a and 2c only. The inlet unstarted when fuel was introduced in injector 1a and 1b in the second half of segment 3. The tunnel total temperature was to be ramped to 415 psia at this point. Figure 5-37d shows that control problems were encountered as indicated by the excursions in the tunnel pressure and temperature. Inlet unstarts were encountered in segments 4 and 5.

Reading 97 (Figure 5-38)

Subsonic combustion performance was measured with the combustor exit instrumentation rig installed in this run. Segment 1 was run at P_{T0} = 206 psia and T_{T0} at 2210°R. The combustor ignition was obtained using injector 2a with the row 2 ignitors. Fuel was then introduced in injectors 3a and 3b and terminated in 2a. ϕ was increased to a nominal value of 1.0 and then terminated, while PT0 was set at 415 psia. The procedure followed in segment 1 was then repeated in segment 2. ϕ reached a value of 1.2 when a tunnel unstart occurred due to the blockage of the combustor exit rake.

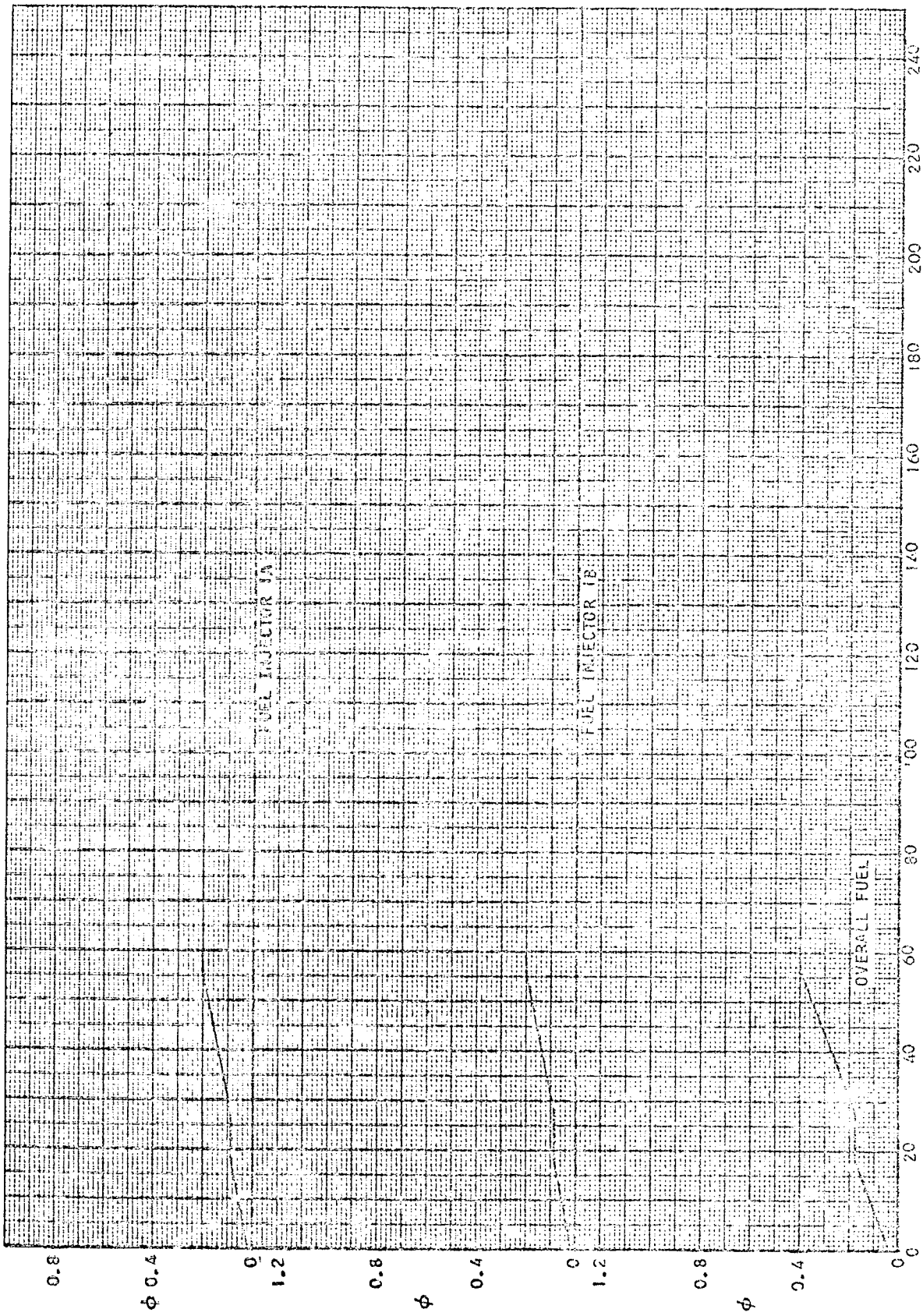

Figure 5-19a. Reading 33 - Fuel Schedule

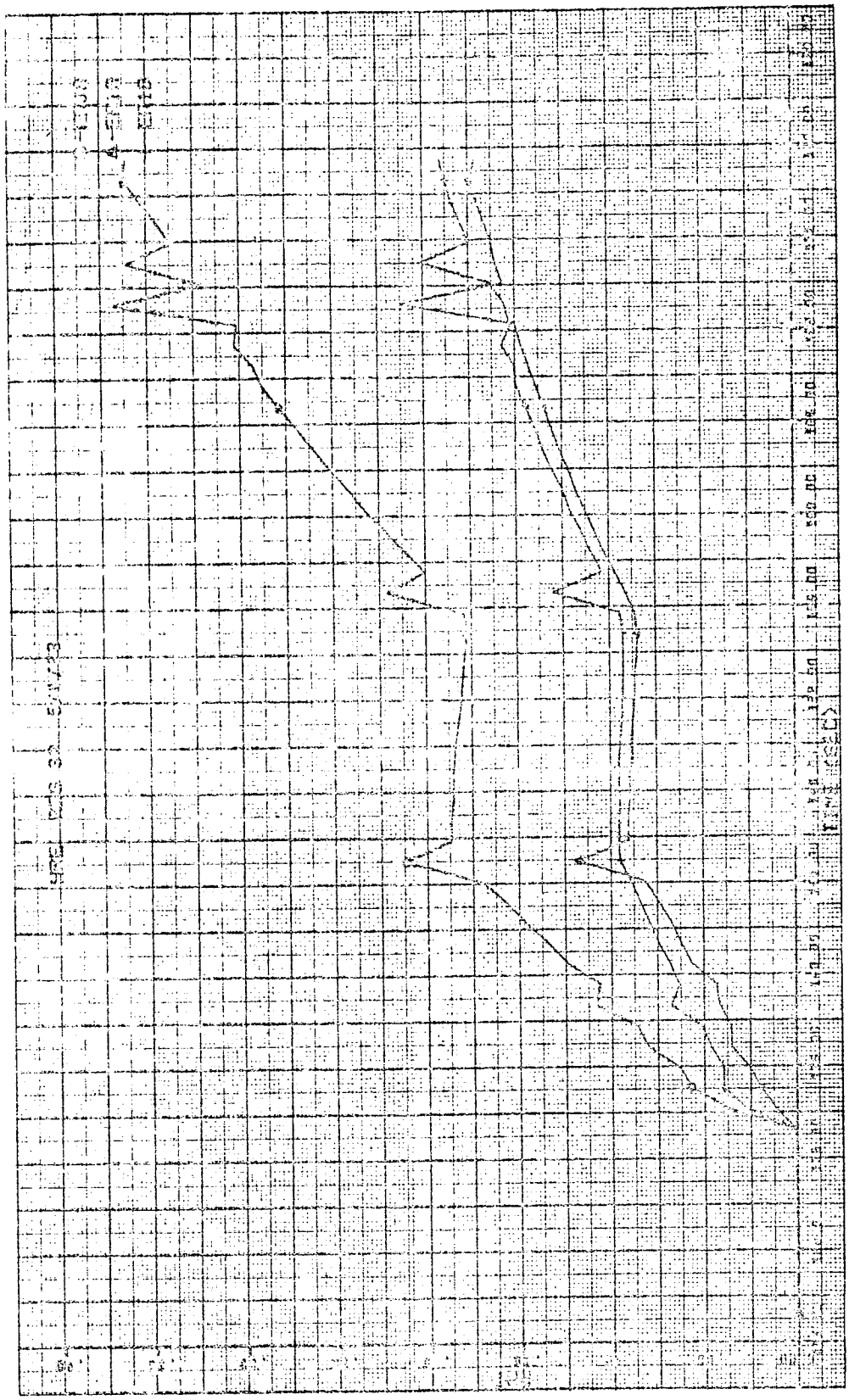

Figure 5-19b. Reading 33 - Measured Equivalence Ratio, ϕ

ORIGINAL PAGE IS
OF POOR QUALITY

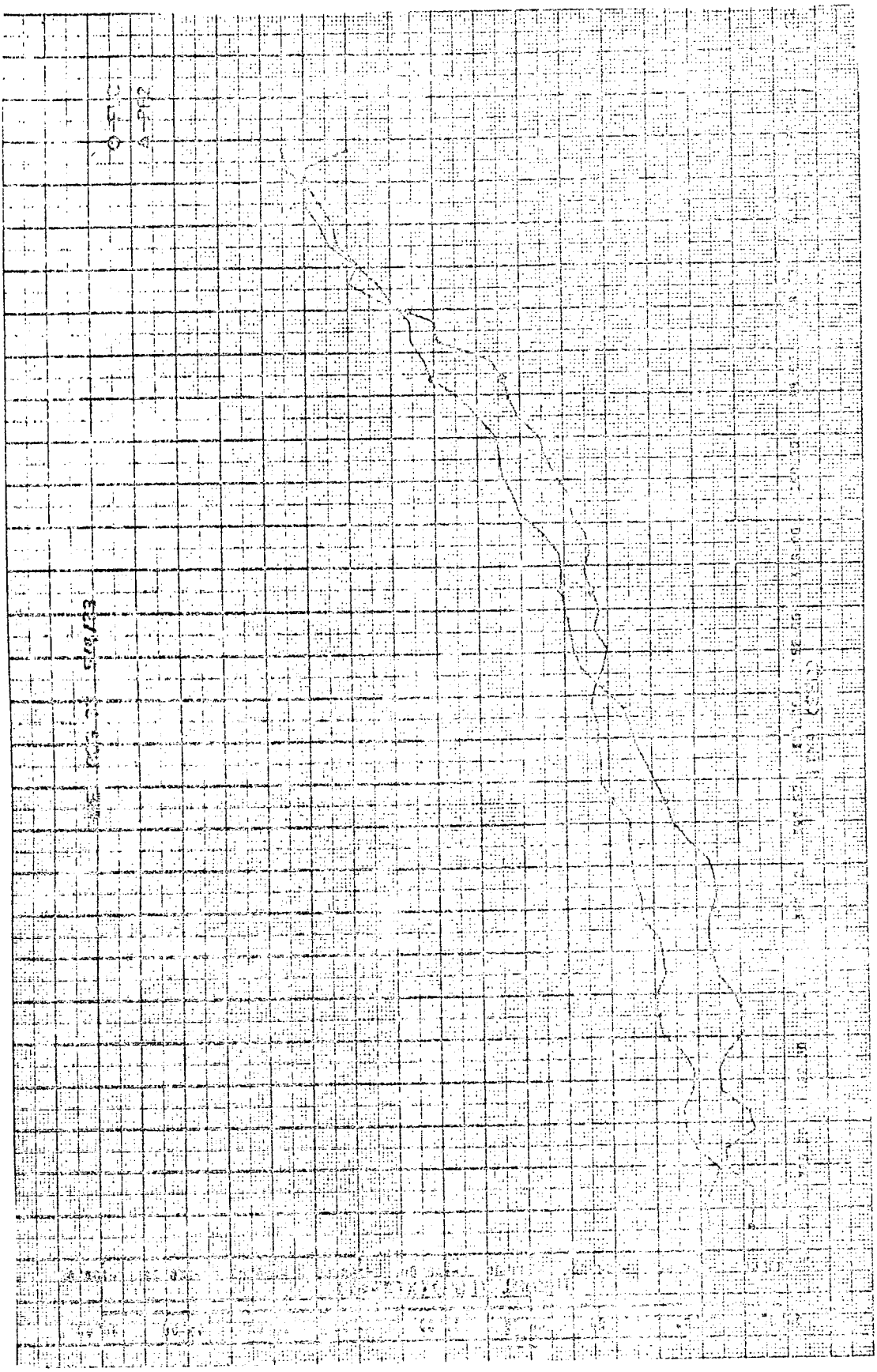

Figure 5-19c. Reading 33 - Purge Pressure and Load Cell Reading

Figure 5-20a. Reading 24 - Fuel Schedule

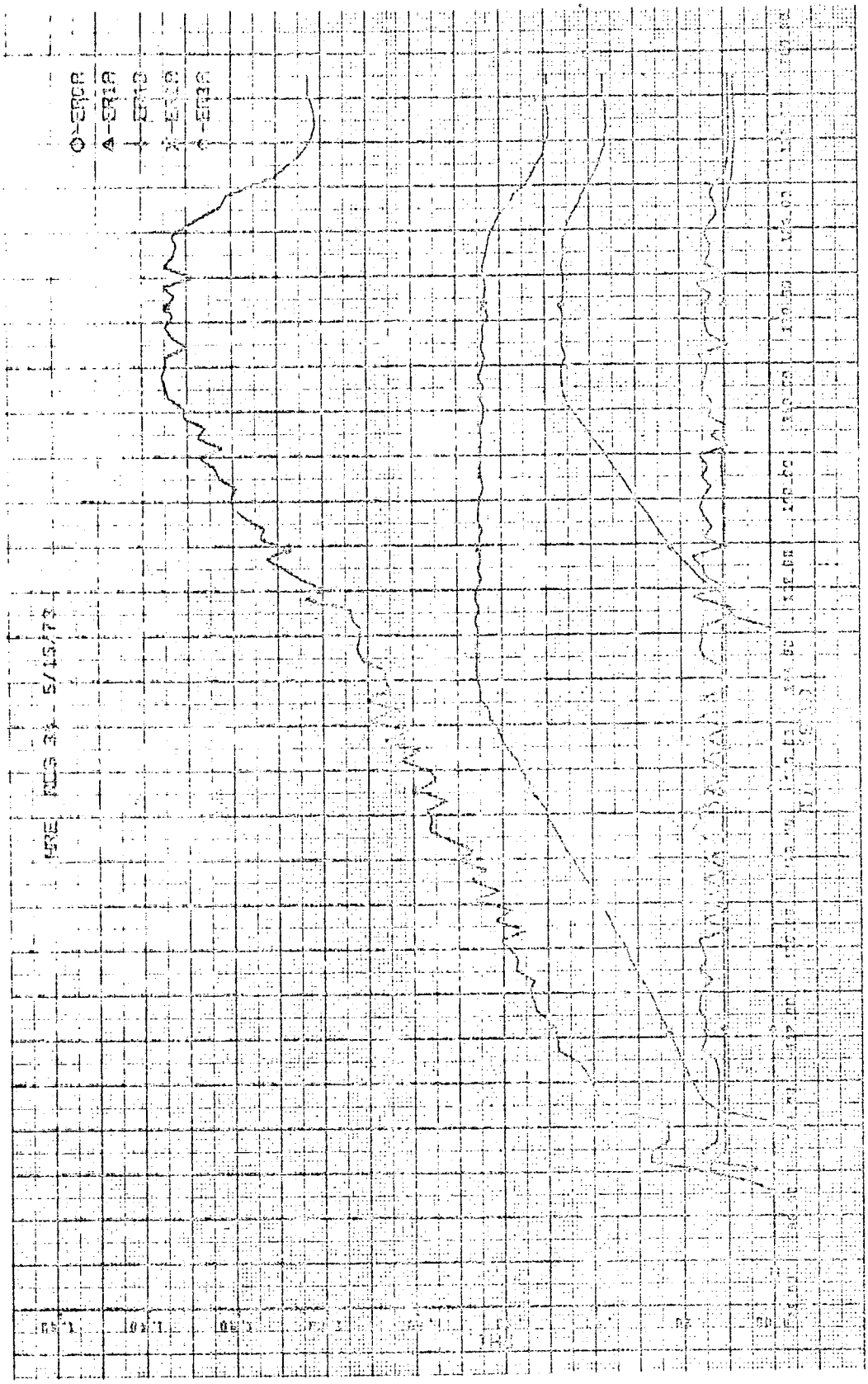

Figure 5-20b. Reading 34 - Measured Equivalence Ratio, ϕ

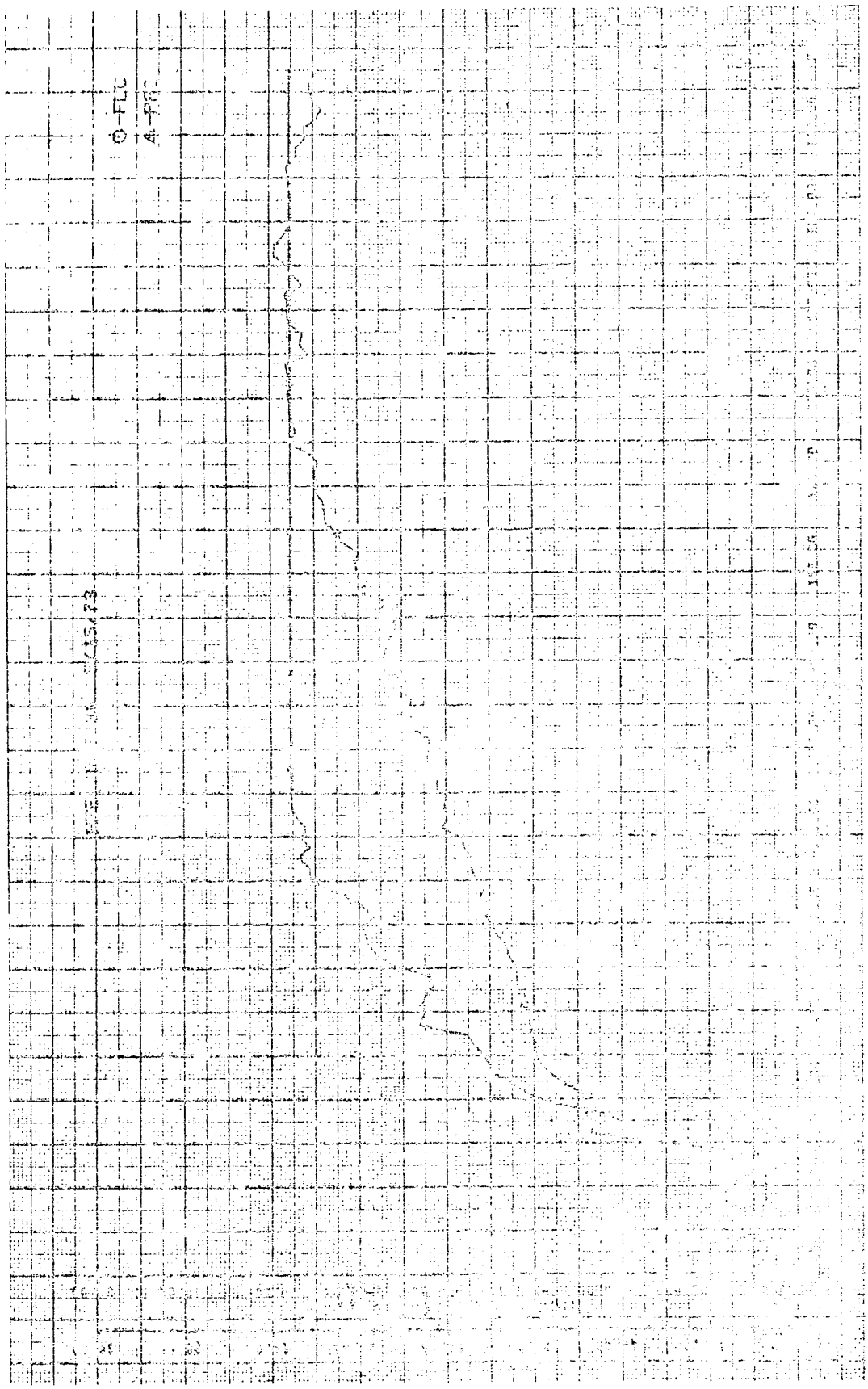

Figure 5-20c. Reading 34 - Purge Pressure and Load Cell Reading

ORIGINAL PAGE IS
OF POOR QUALITY

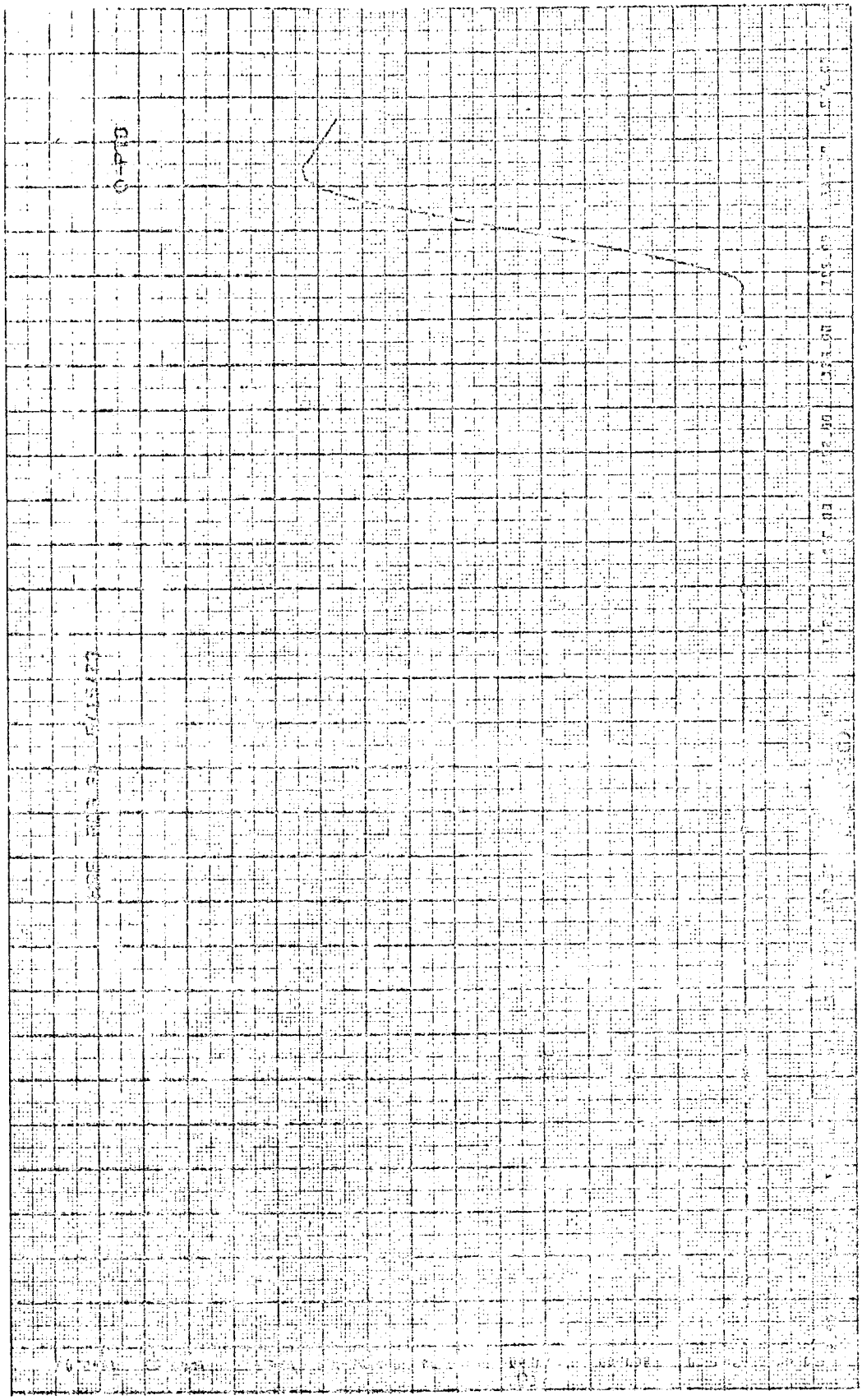

Figure 5-20d. Reading 34 - Tunnel Total Pressure

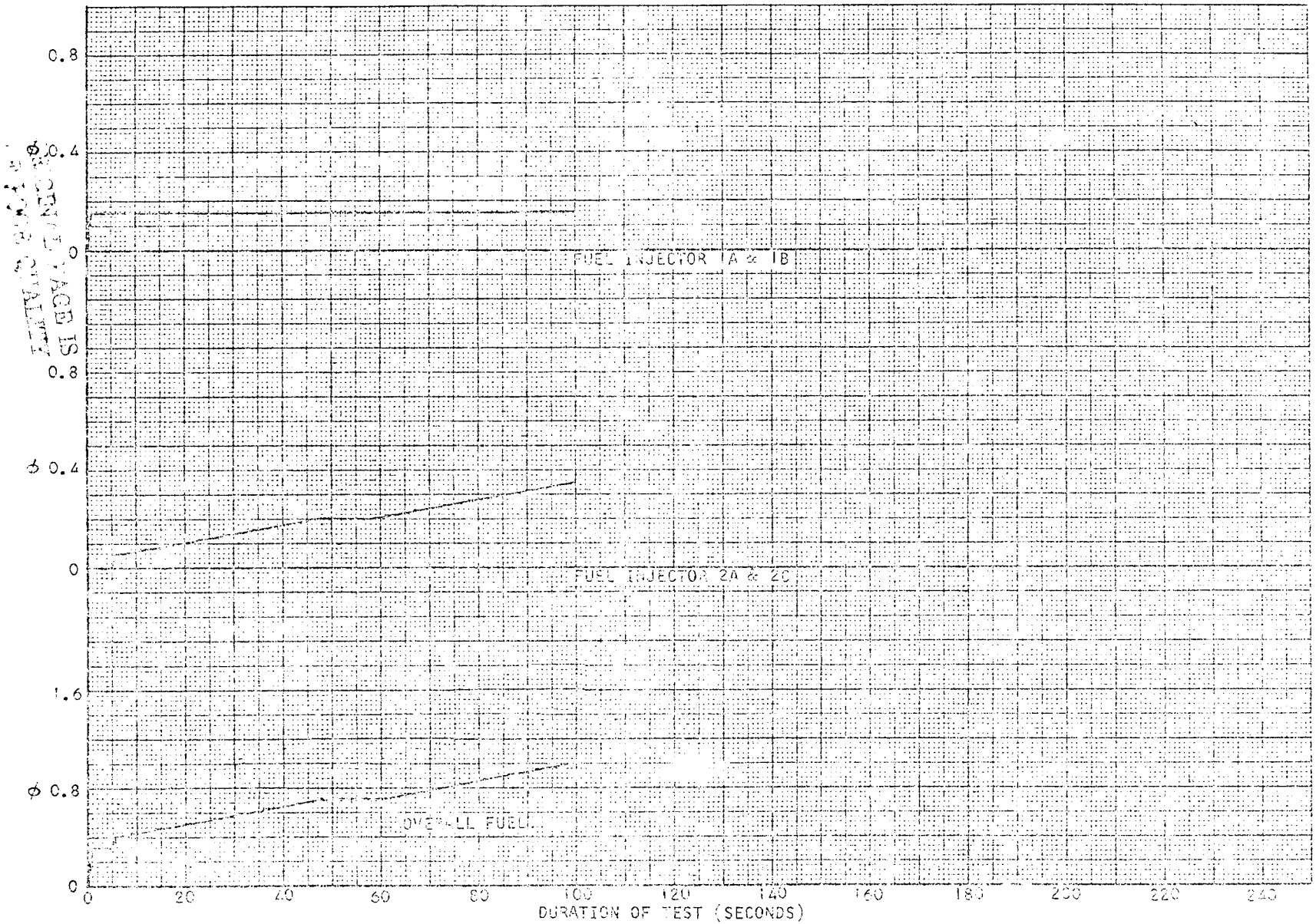

Figure 5-21a. Reading 36 - Fuel Schedule

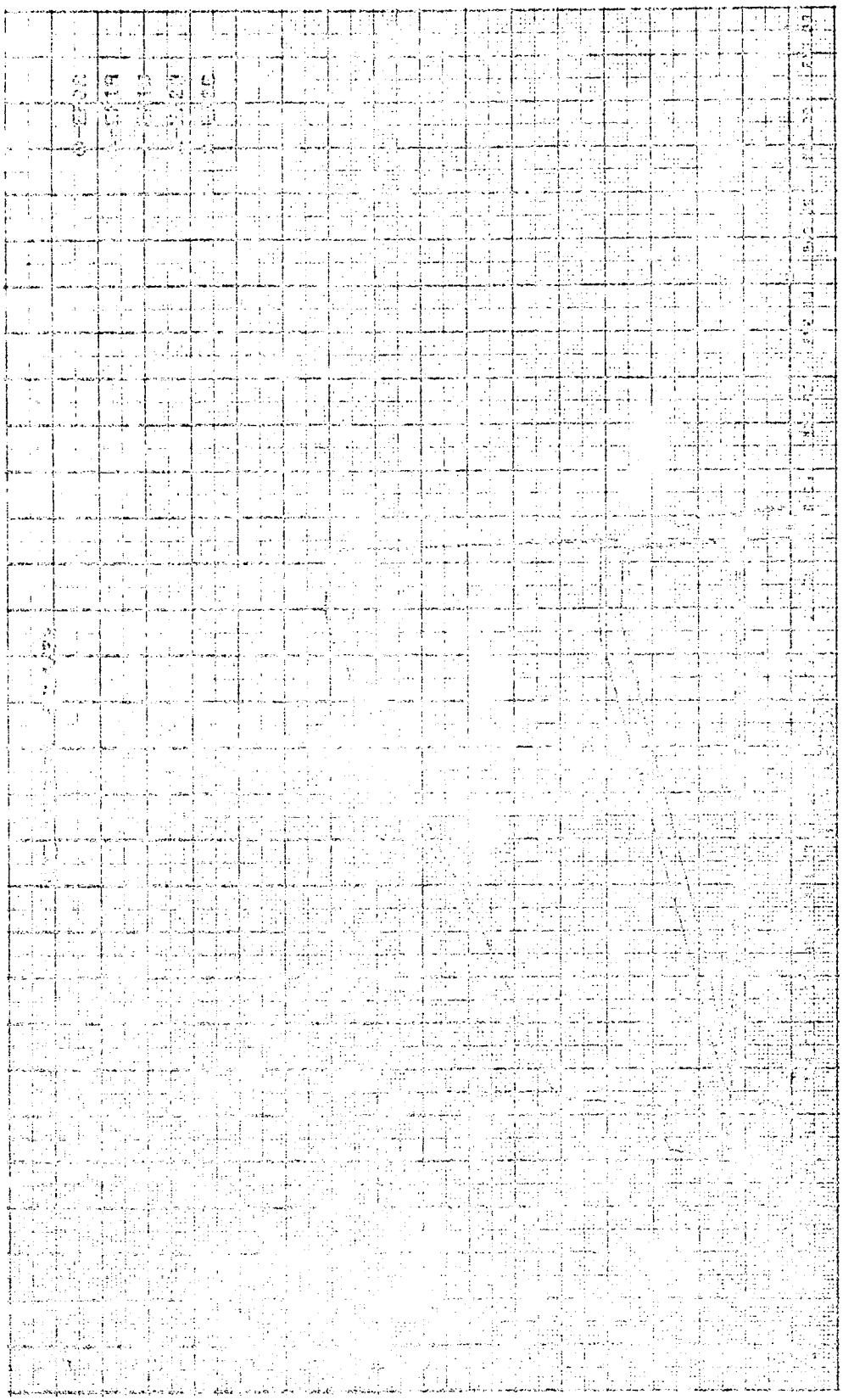

Figure 5-21b. Reading 36 - Measured Equivalence Ratio, ϕ

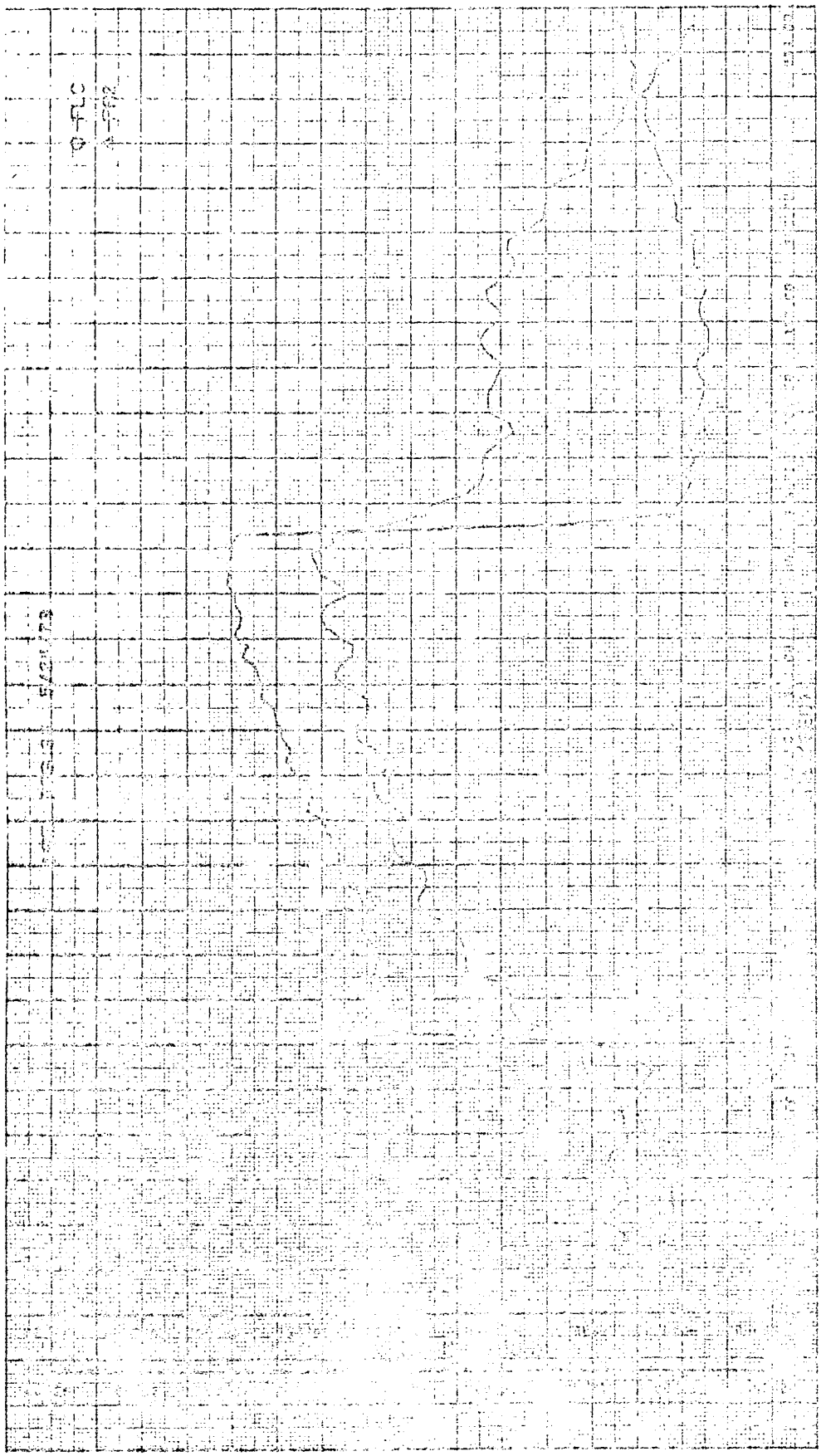

Figure 5-21c. Reading 26 - Purge Pressure and Load Cell Reading

Figure 5-22a. Reading 52 - Fuel Schedule

Figure 5-22b. Reading 52 - Measured Equivalence Ratio, ϕ

Figure 5-22c. Reading 52 - Purge Pressure and Load Cell Reading

Figure 5-23b. Reading 54 - Measured Equivalence Ratio.

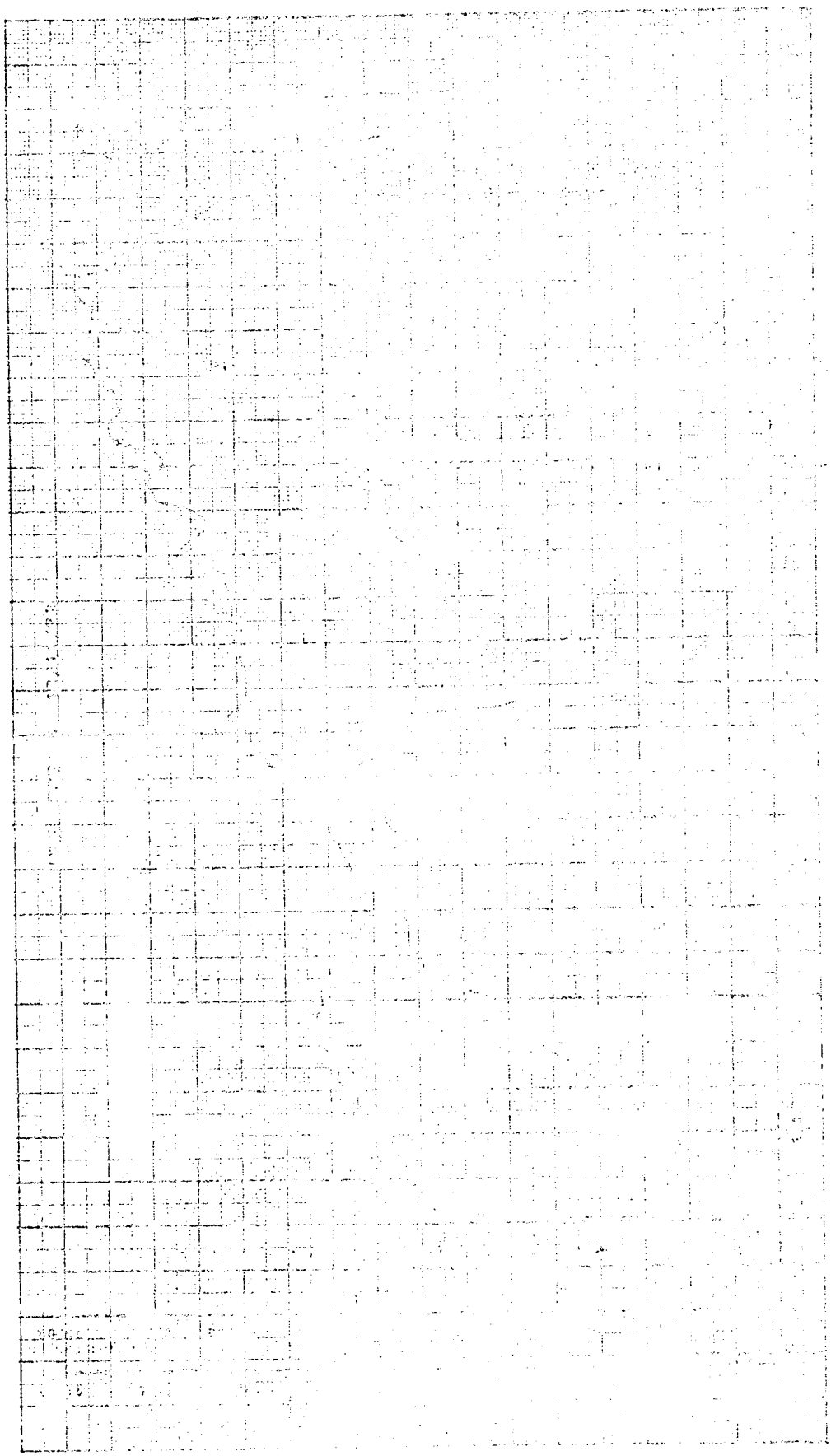

Figure E-55. Reading 31 - Pump Pressure and Load Cell Output

Figure 3-2(a). Reading 97 - Fuel Schedule

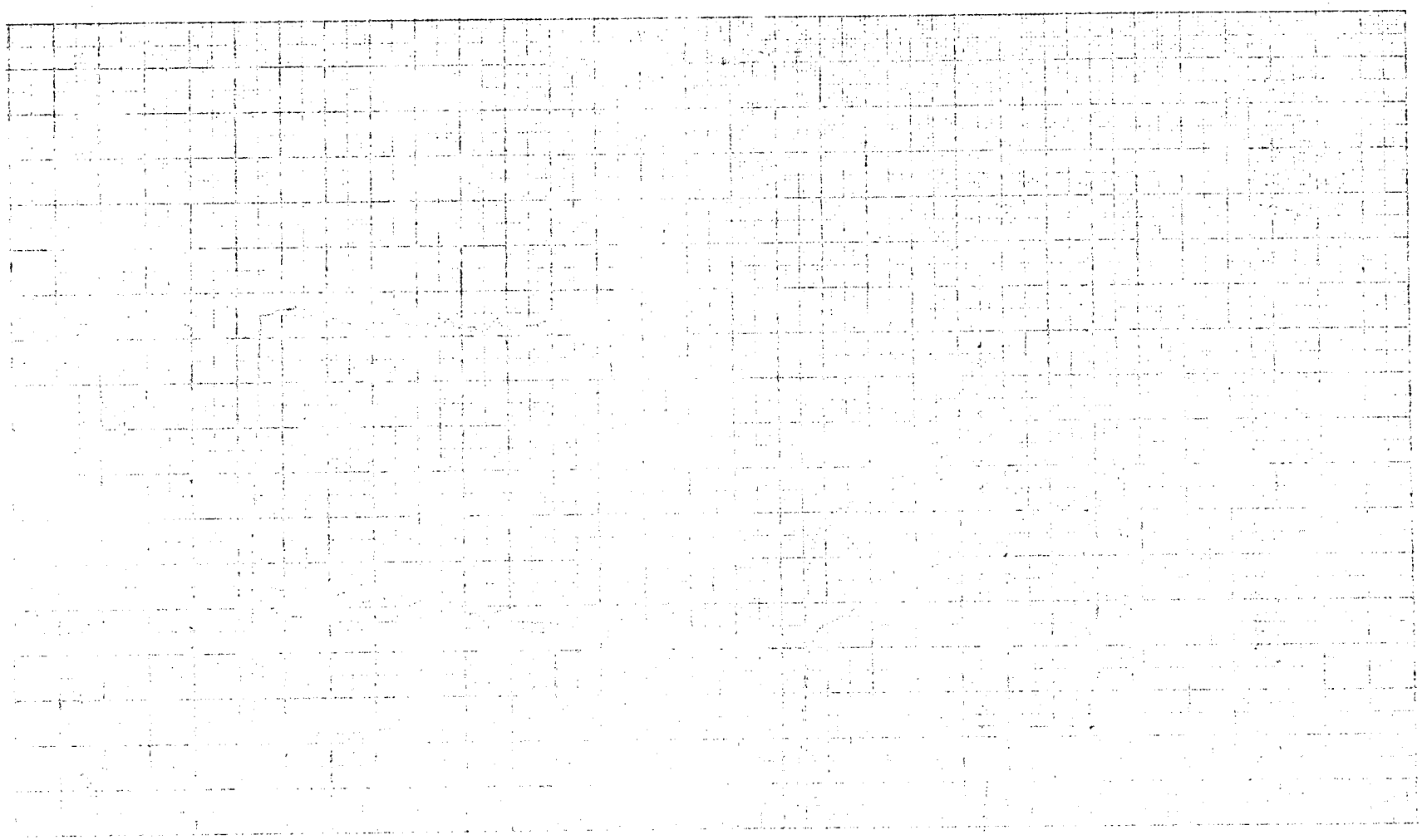

Figure 5-21a. Roadline 27 - Measured Equivalence Ratio

Figure 5-24c. Reading 57 - Purge Pressure and Load Cell Reading

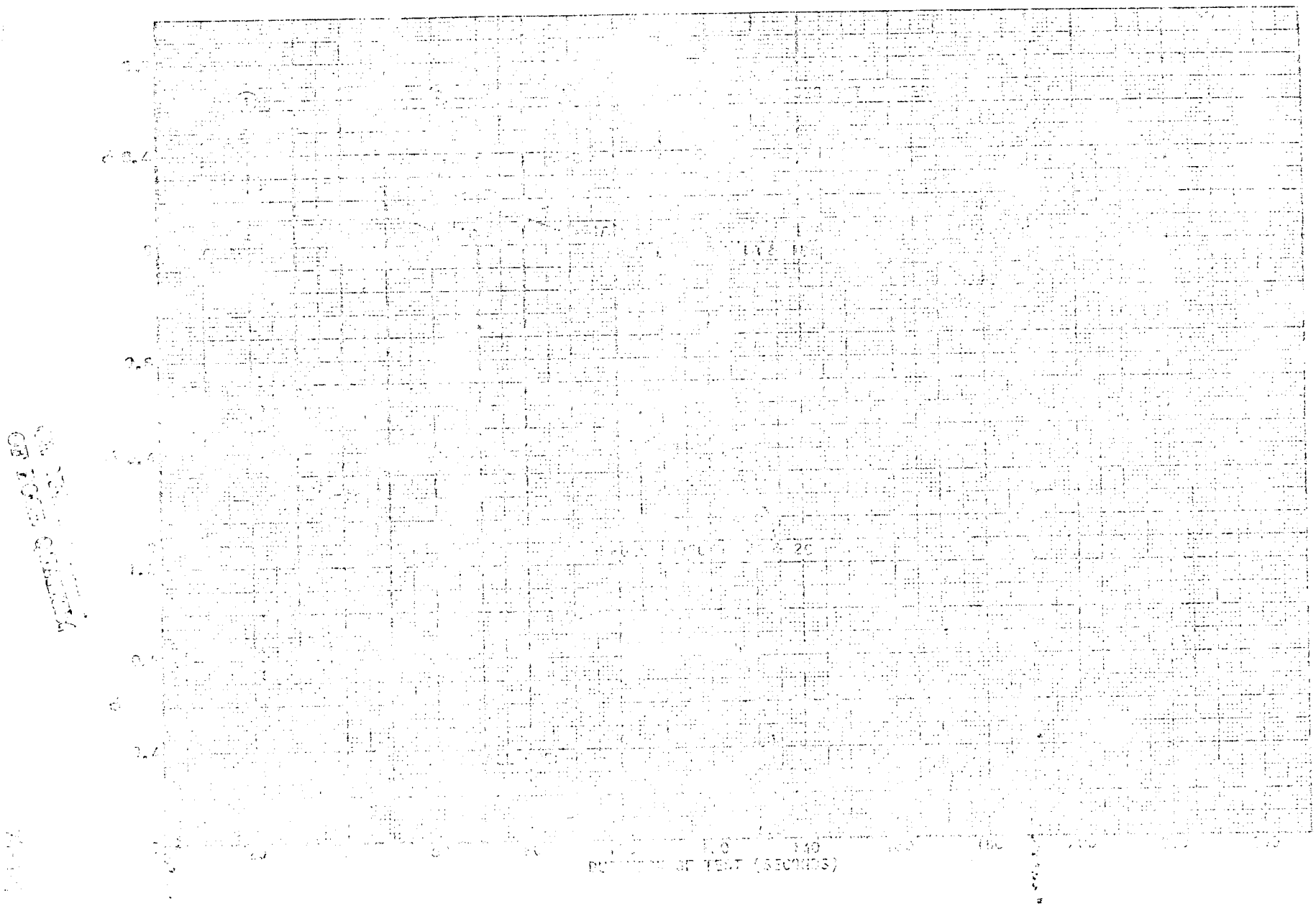

Figure 5-2[illegible] Reading 03 - Fuel Schedule

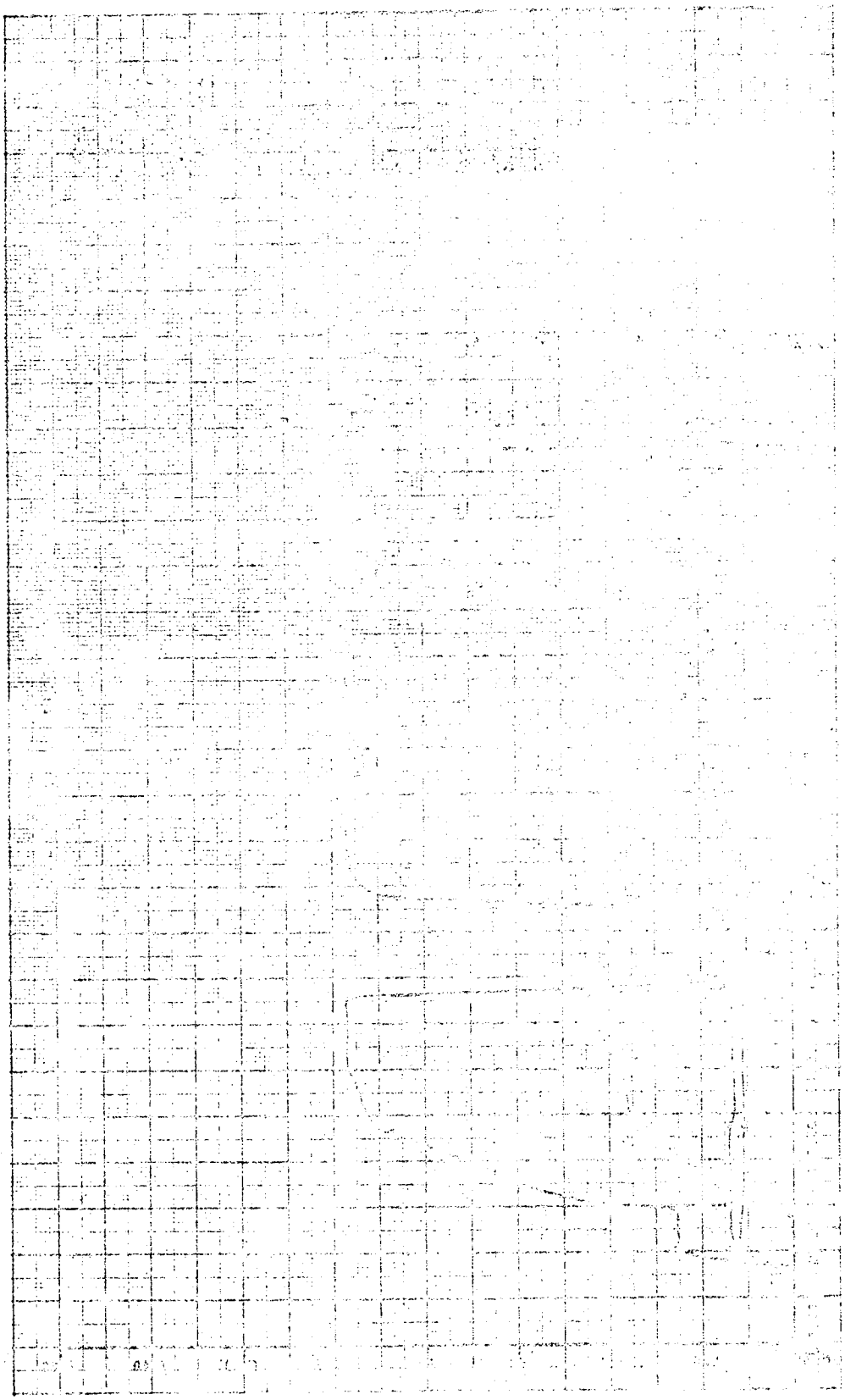

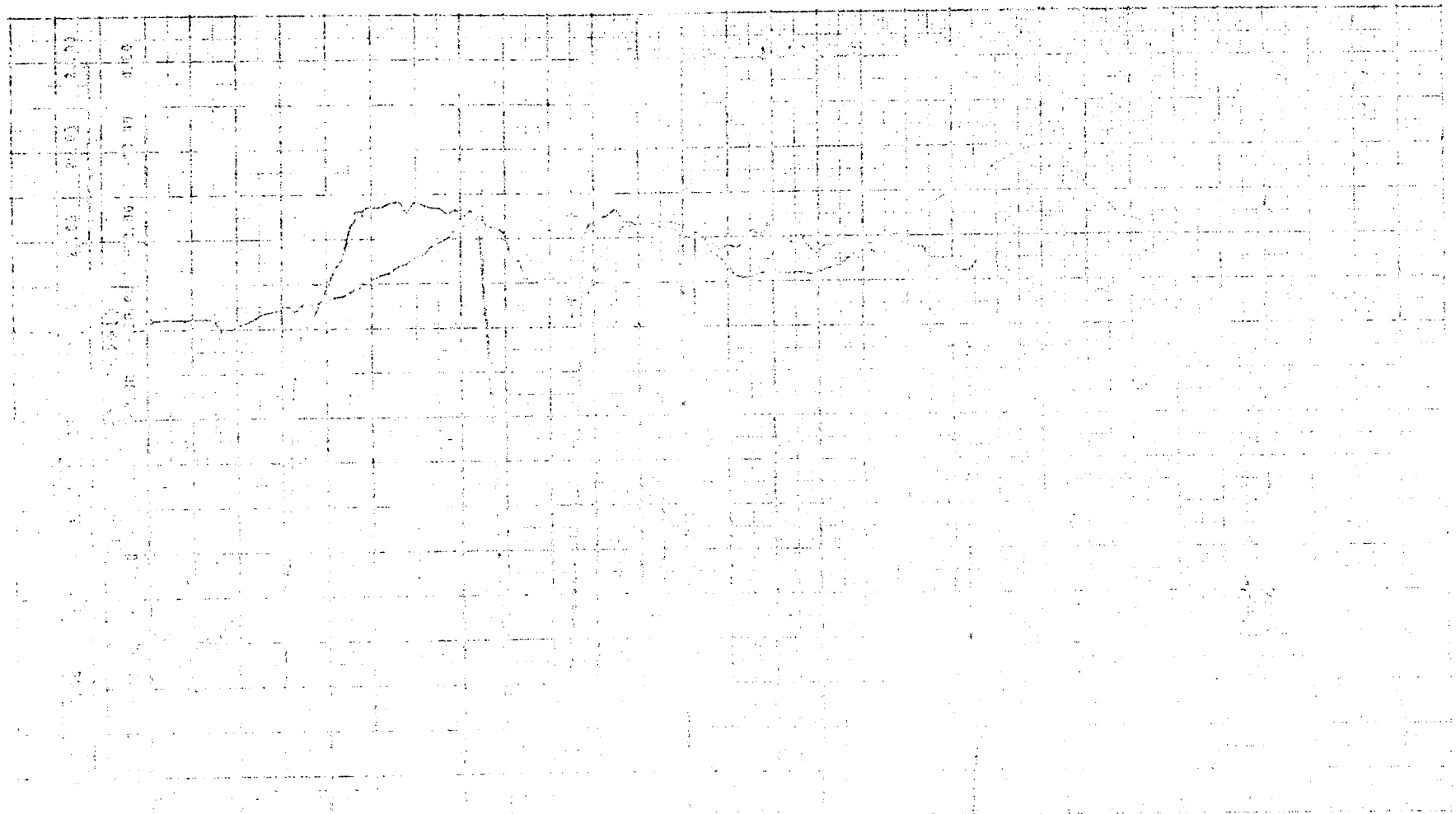

Figure C-26 . Flooding G1 - Fuel Schedule

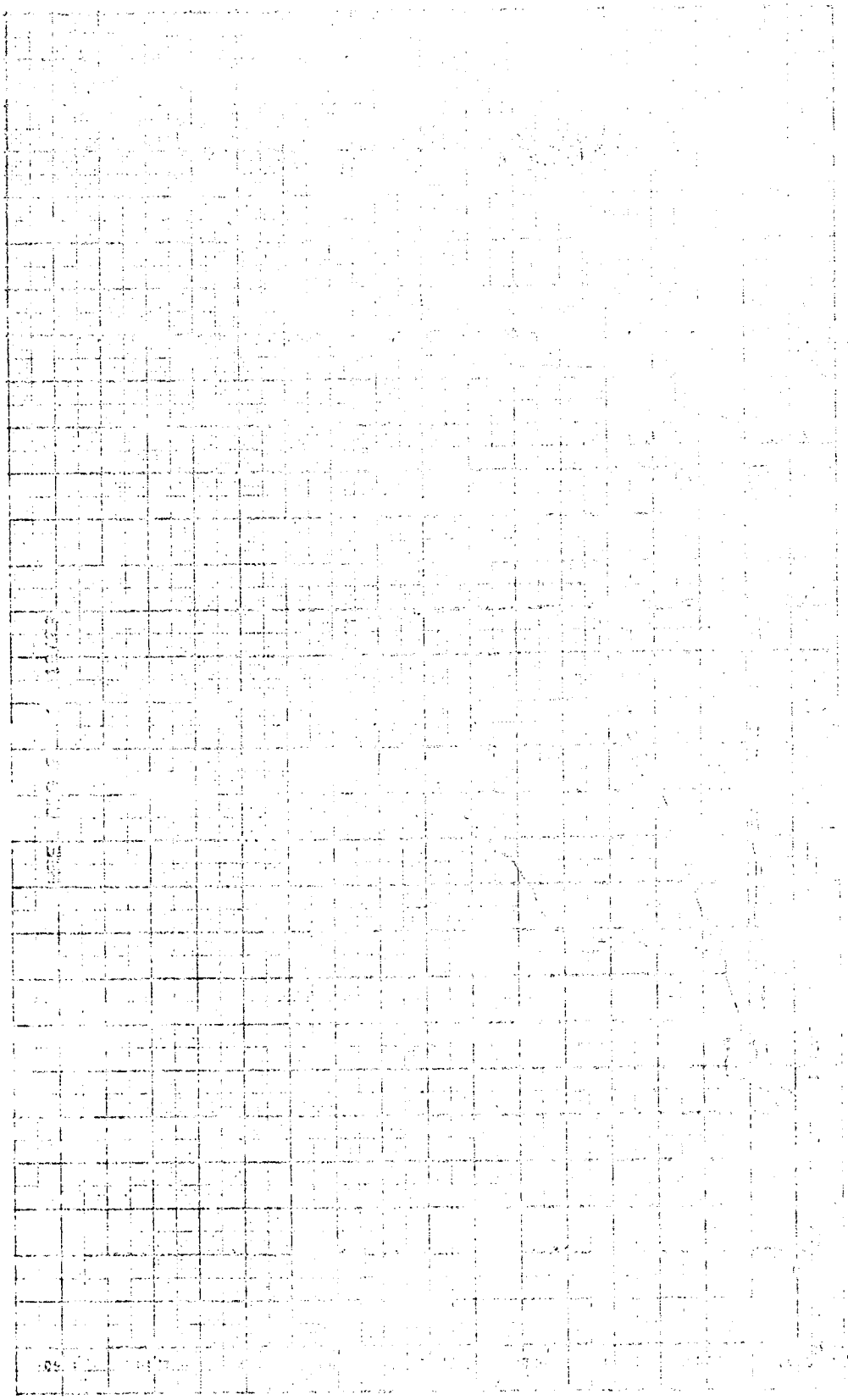

Figure [illegible] Reading [illegible] - Surge Pressure and Load [illegible] Reading

Figure 5-26b. Reading 61 - Lined Solid Reflection

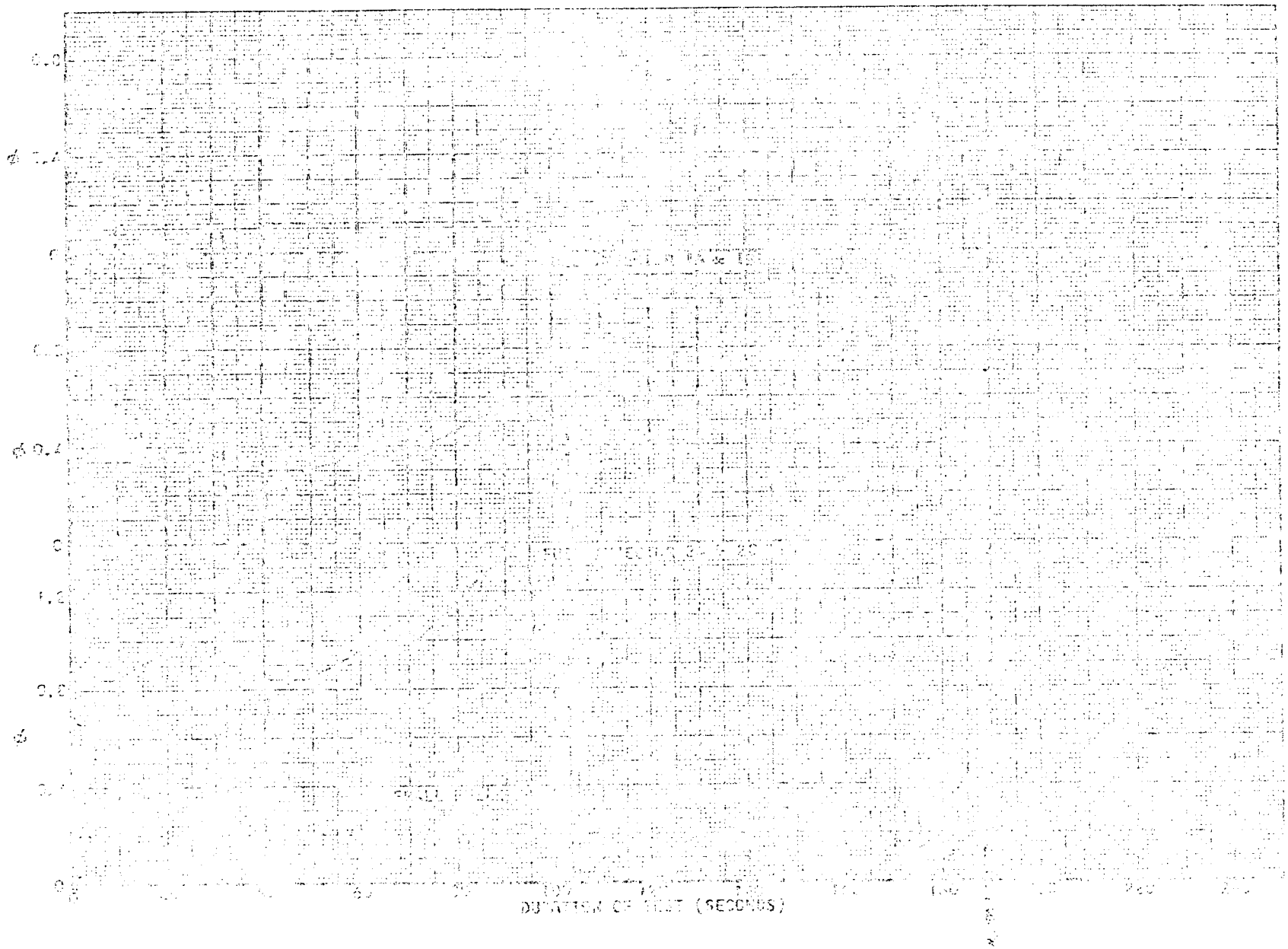

Figure 5-27a. [illegible] 63 - Fuel Schedule

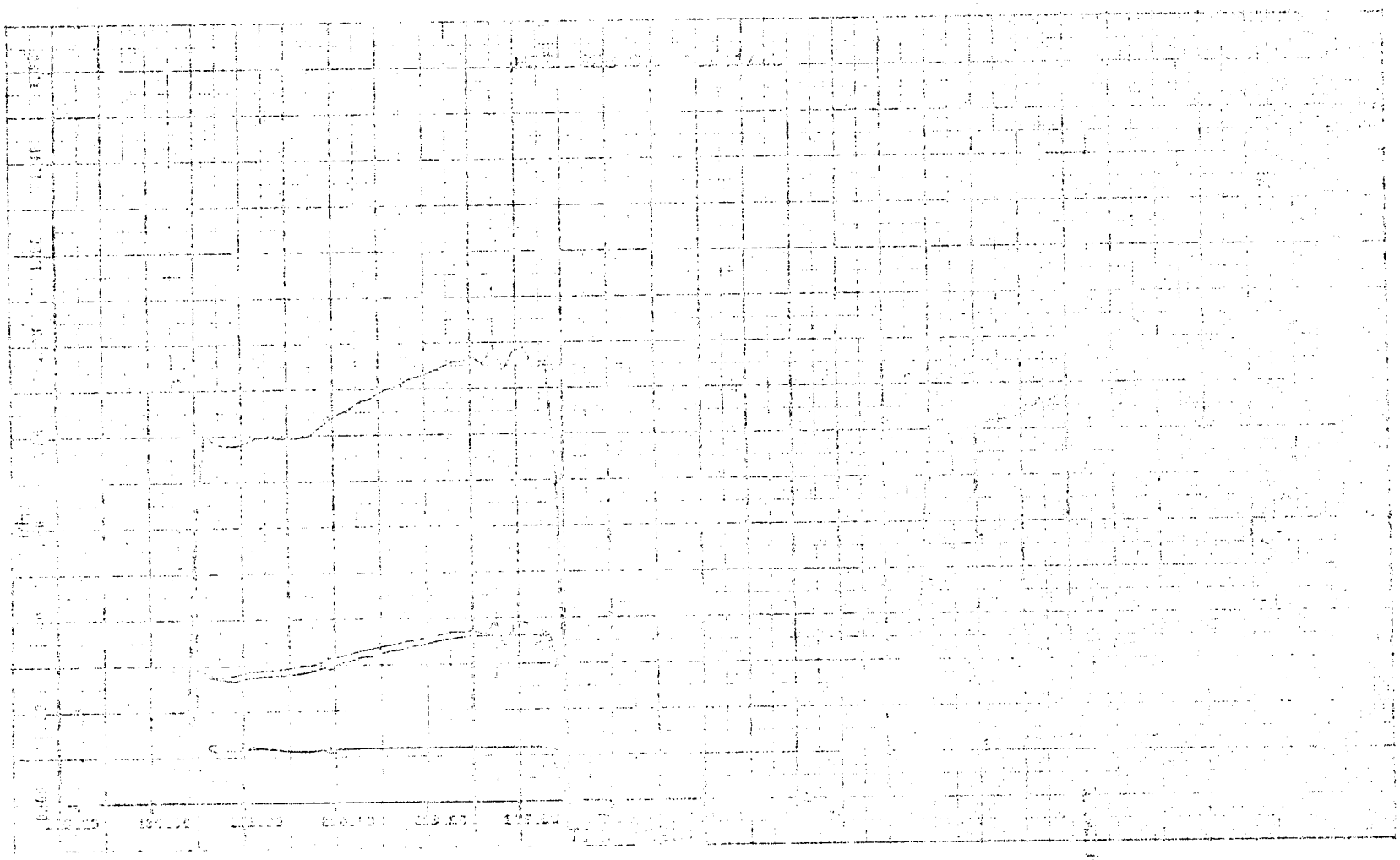

Figure 5-270. Reading 63 - Measured Equivalence Ratio, ϕ

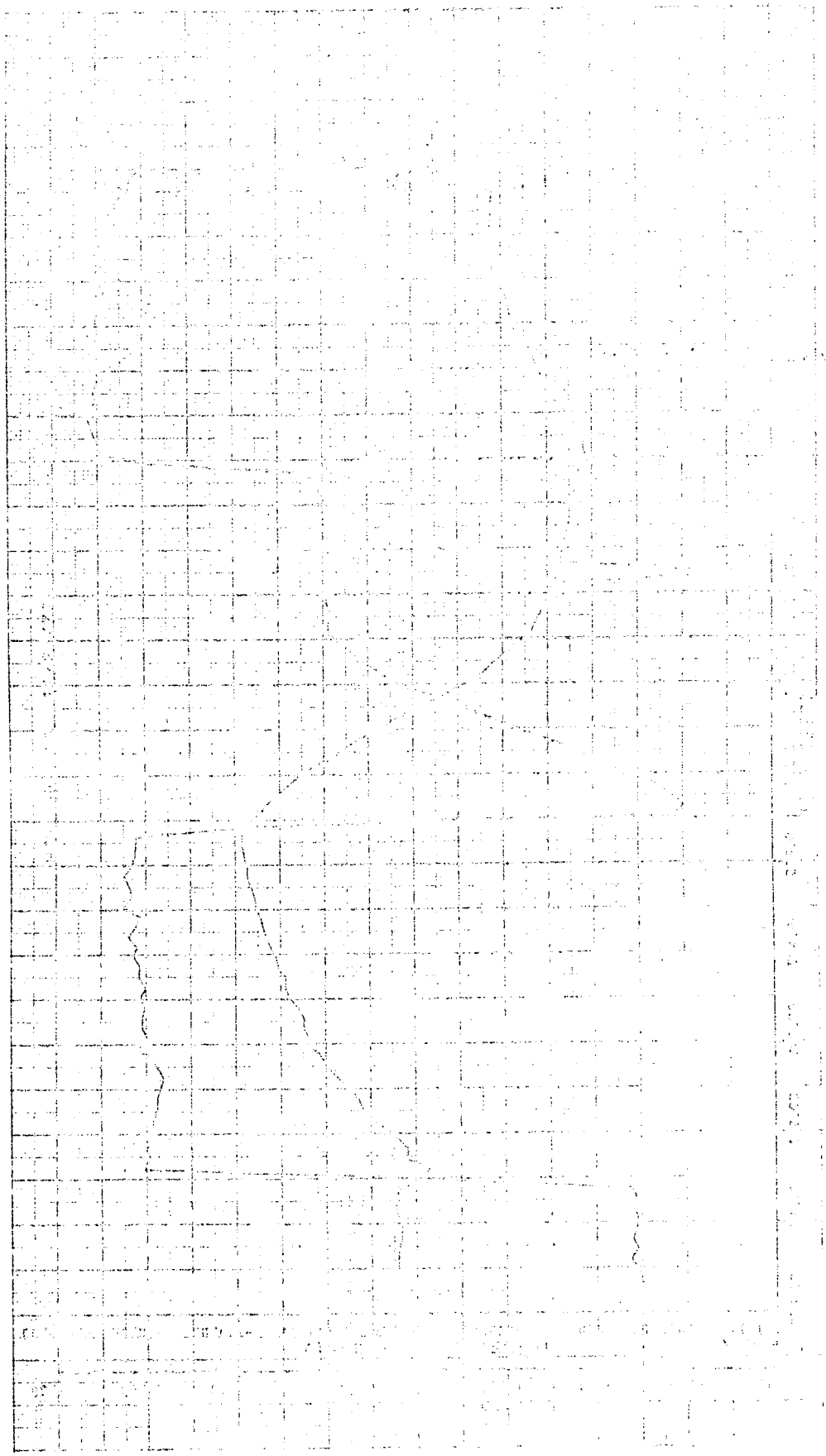

ORIGINAL PAGE IS
OF POOR QUALITY

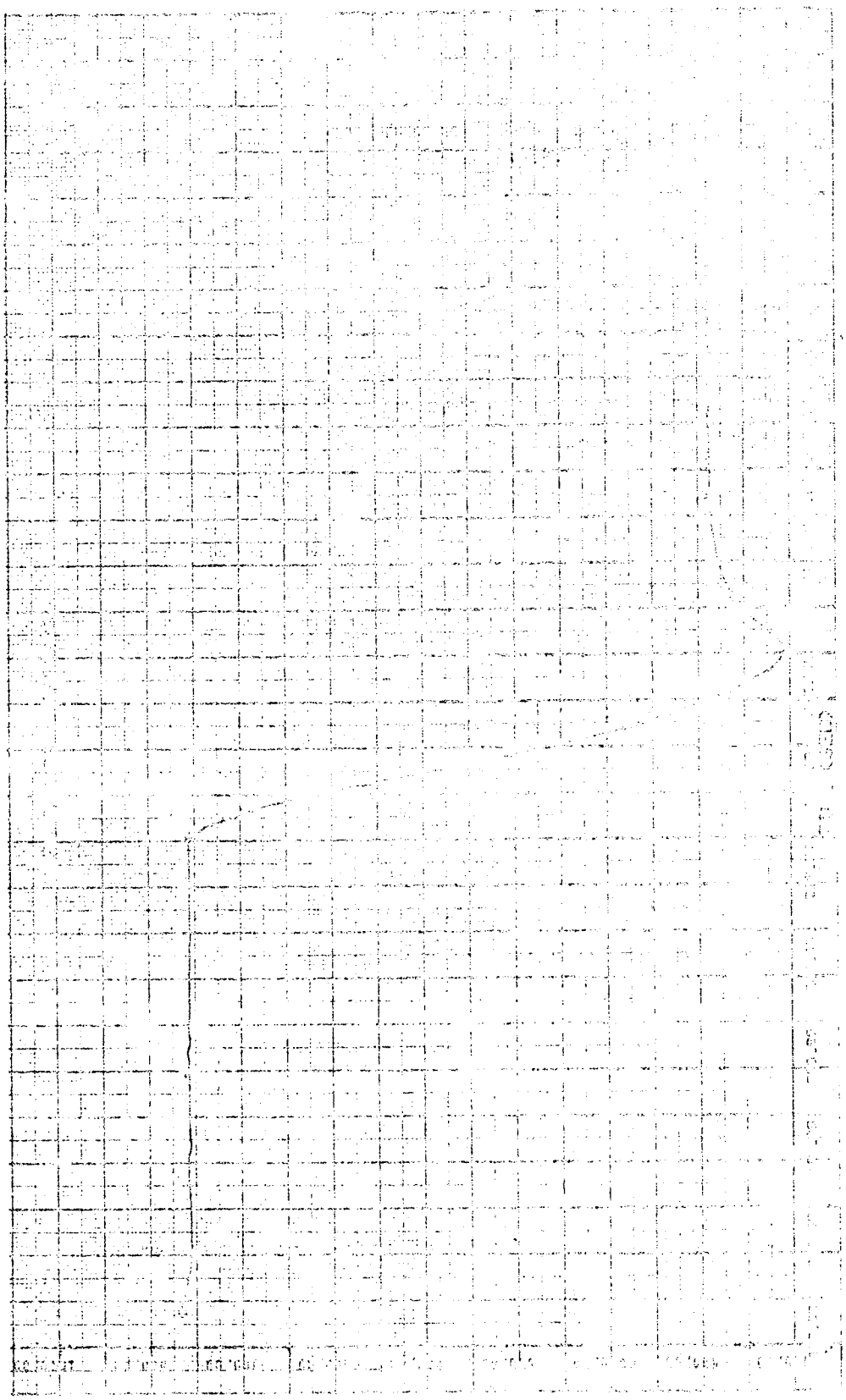

Figure 5-27d. Config 63 - Tunnel Test Program

Figure 5-26b. Reading 64 - Measured Equivalence Ratio, ϕ

Figure 5-29c. Reading 65 - Purge Pressure and Load Cell Reading

Figure 5-30a. Reading 69 - Fuel Schedule

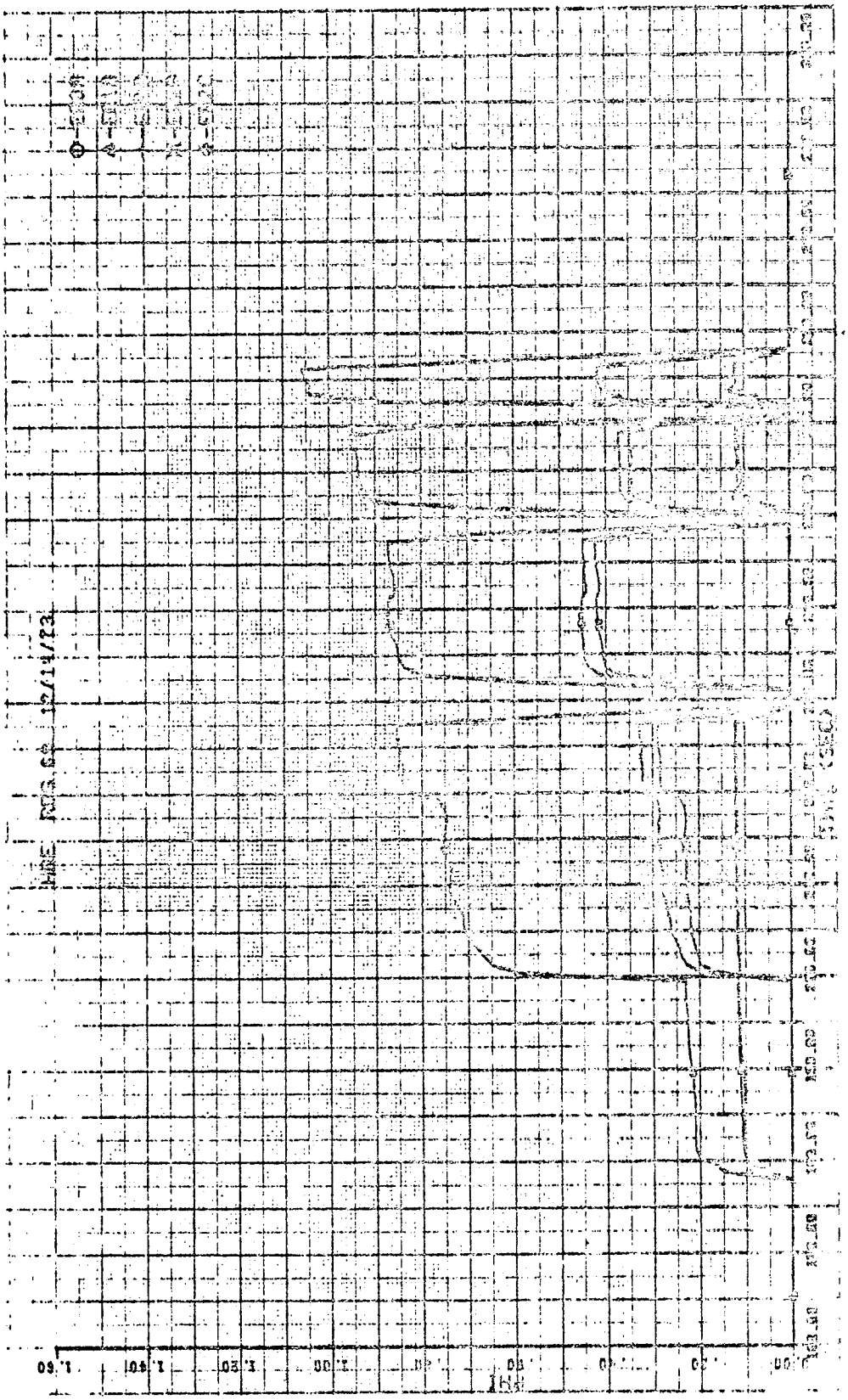

Figure 5-30b. Reading 69 - Measured Equivalence Ratio, Φ

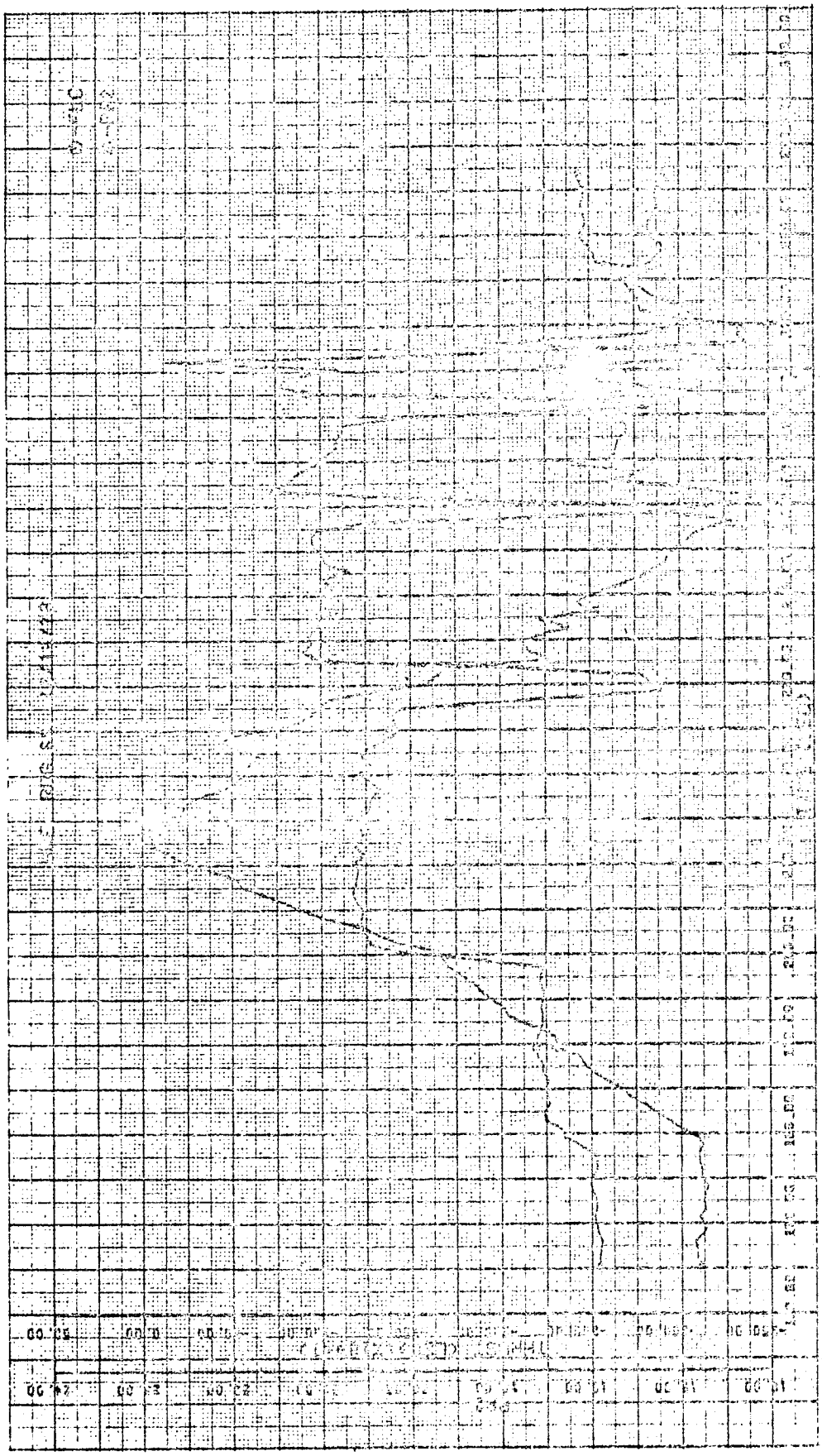

Figure 5-30c. Reading 69 - Purge Pressure and Load Cell Reading

Figure 5-31a. Reading 71 - Fuel Schedule

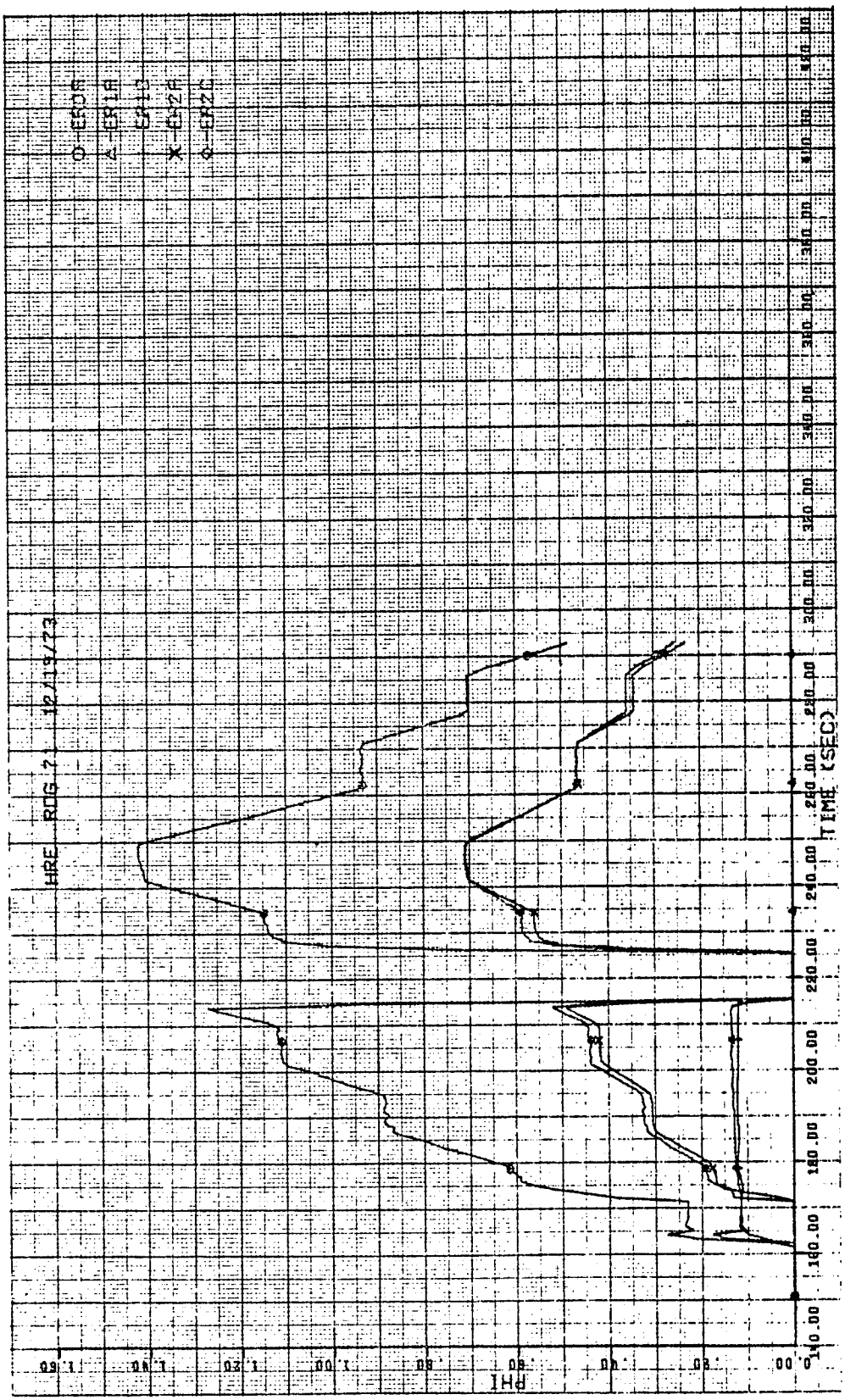

Figure 5-31b. Reading 71 - Measured Equivalence Ratio, ϕ

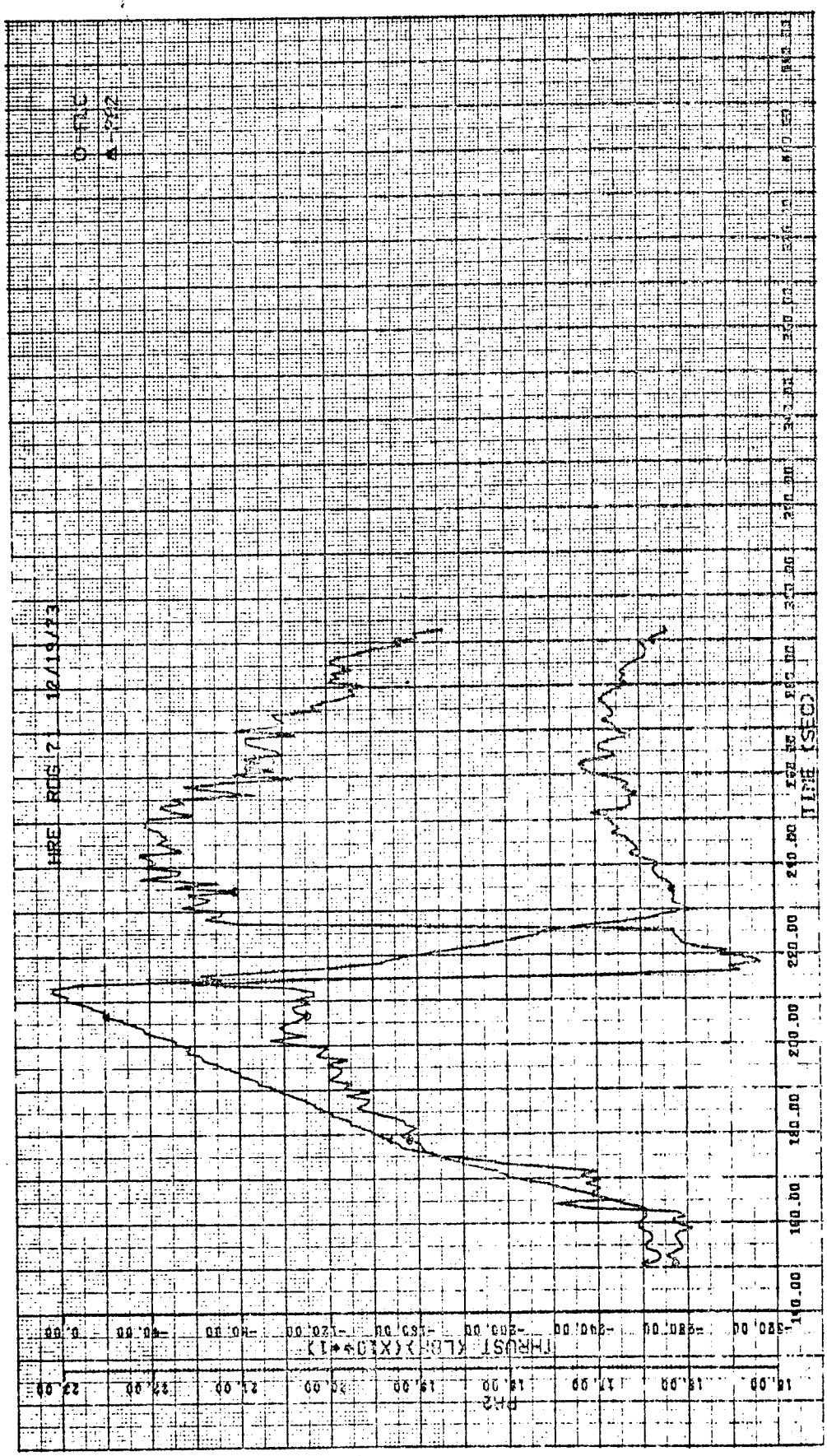

Figure 5-31c. Reading 71 - Purge Pressure and Load Cell Reading

Figure 5-32a. Reading 88 - Fuel Schedule

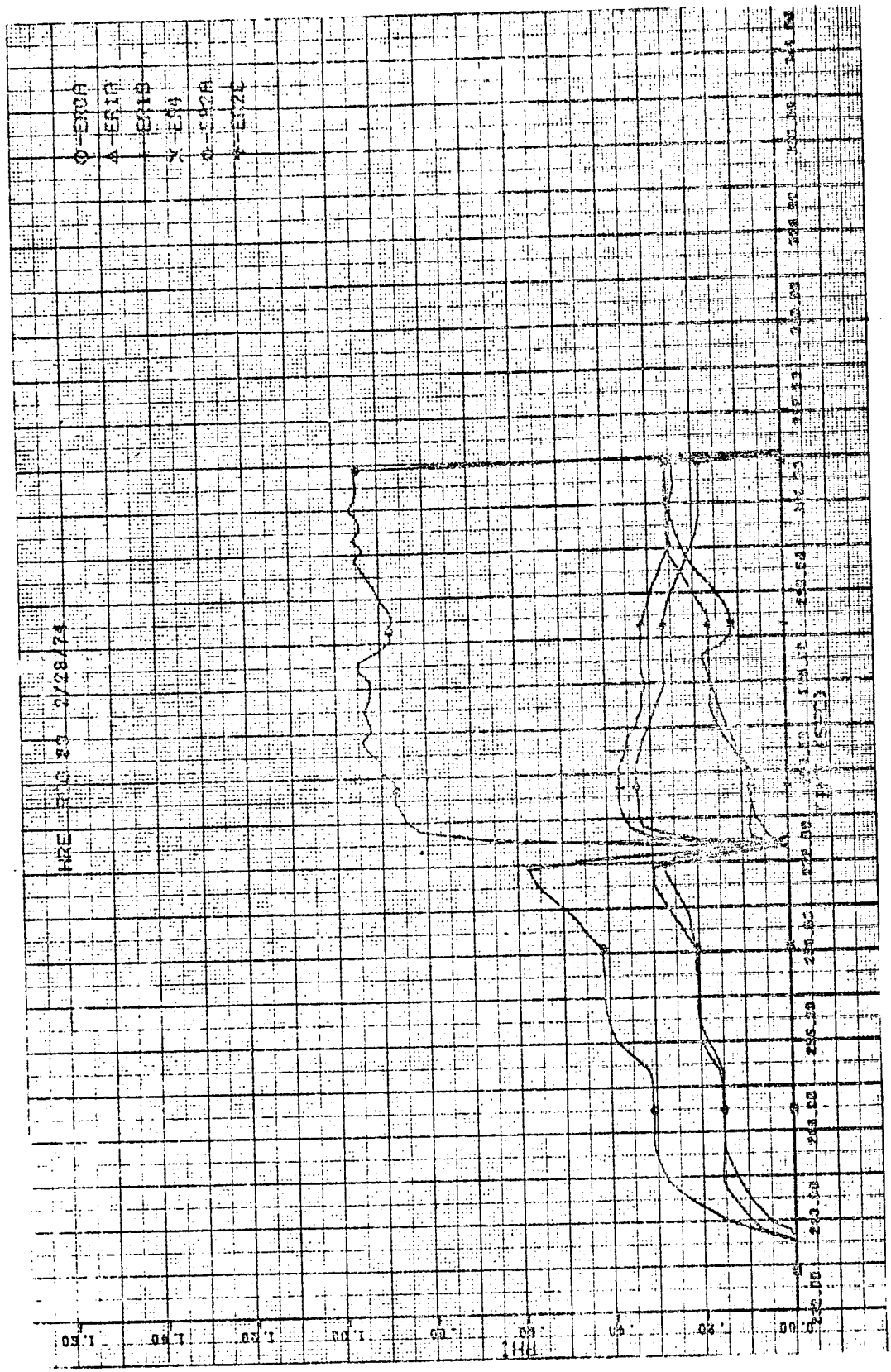

Figure 5-32b. Reading 88 - Measured Equivalence Ratio, ϕ

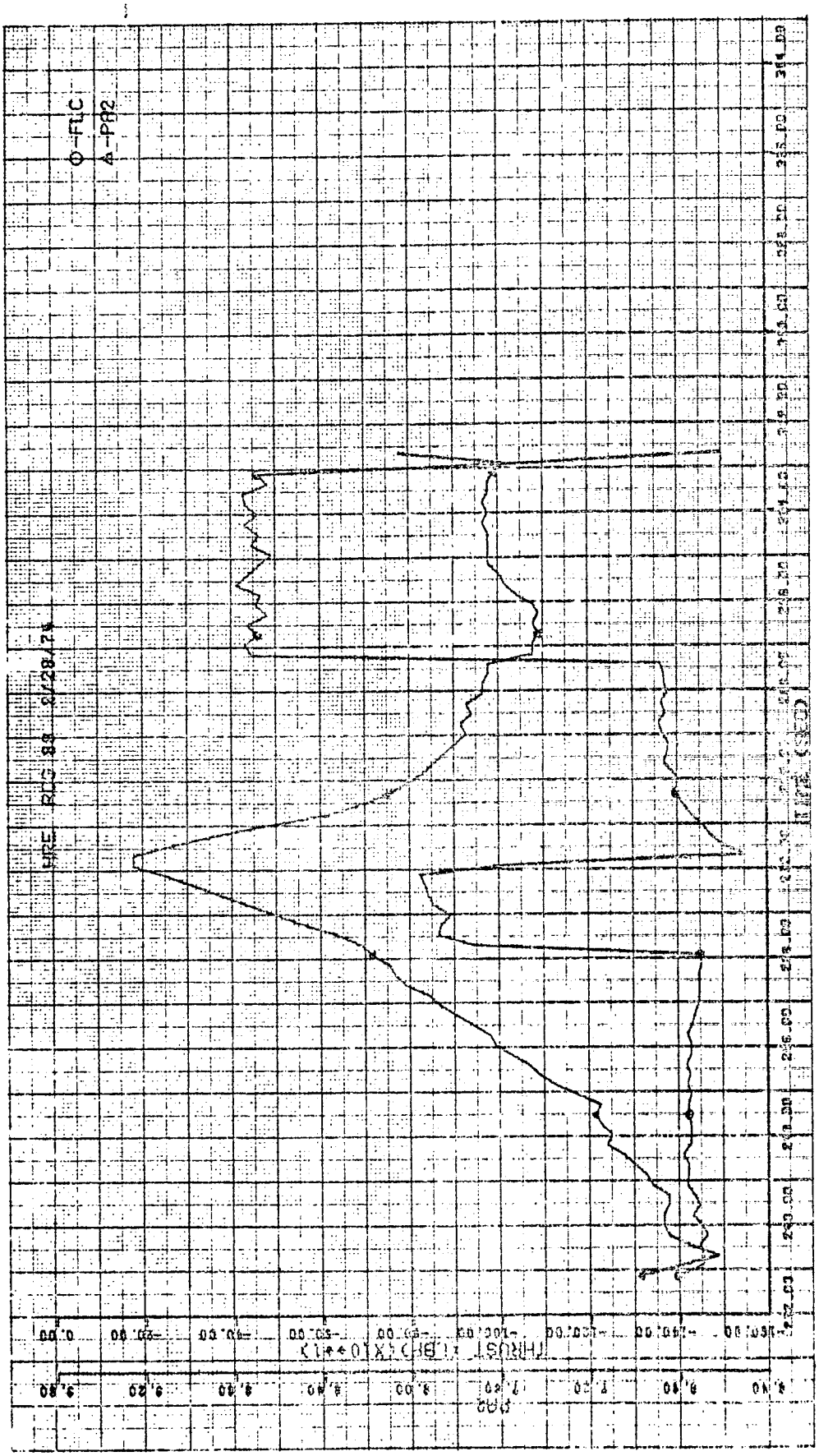

Figure 5-32c. Reading 88 - Purge Pressure and Load Cell Reading

Figure 5-33a. Reading 89 - Fuel Schedule

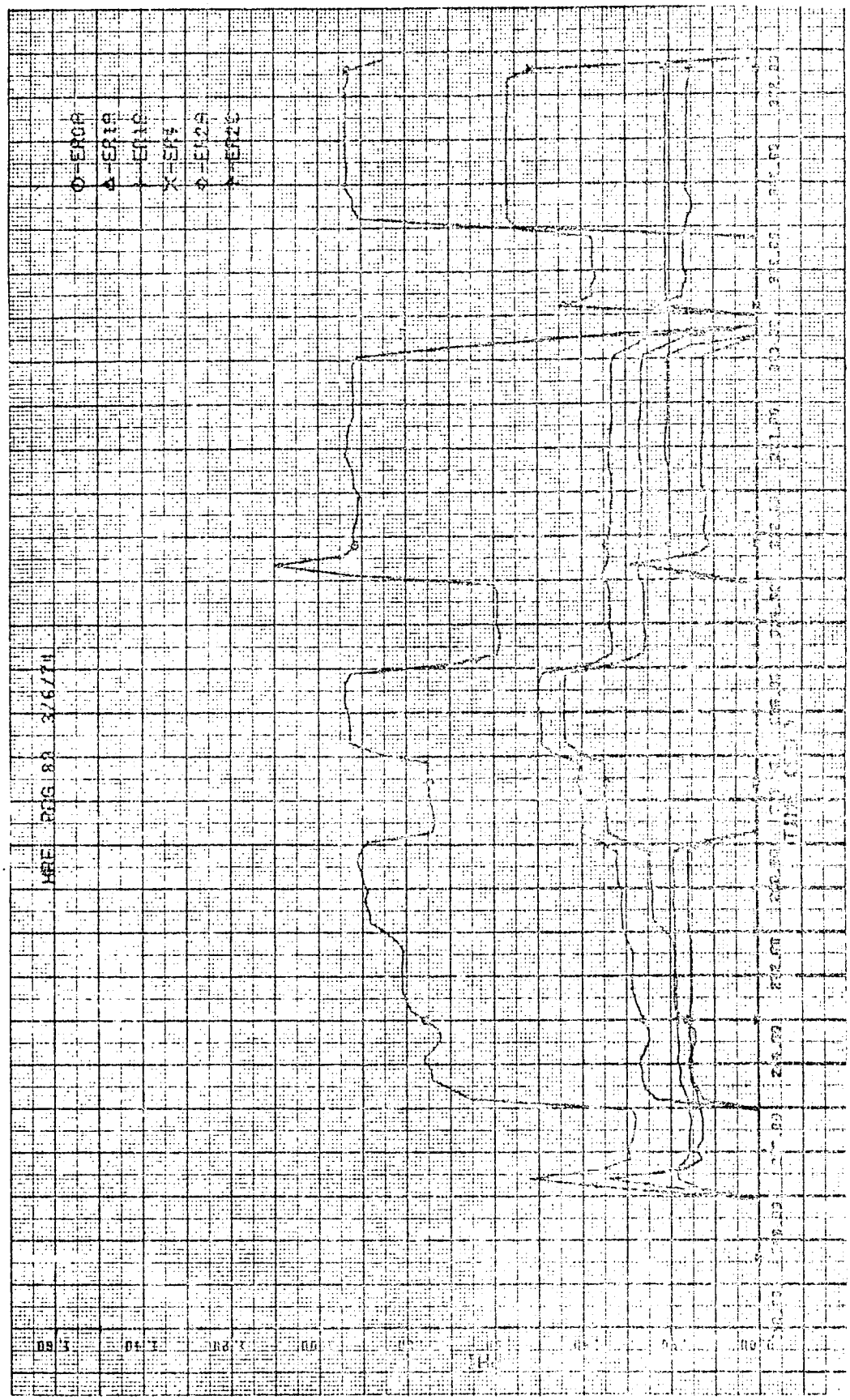

Figure 5-33b. Reading 89 - Measured Equivalence Ratio, Φ

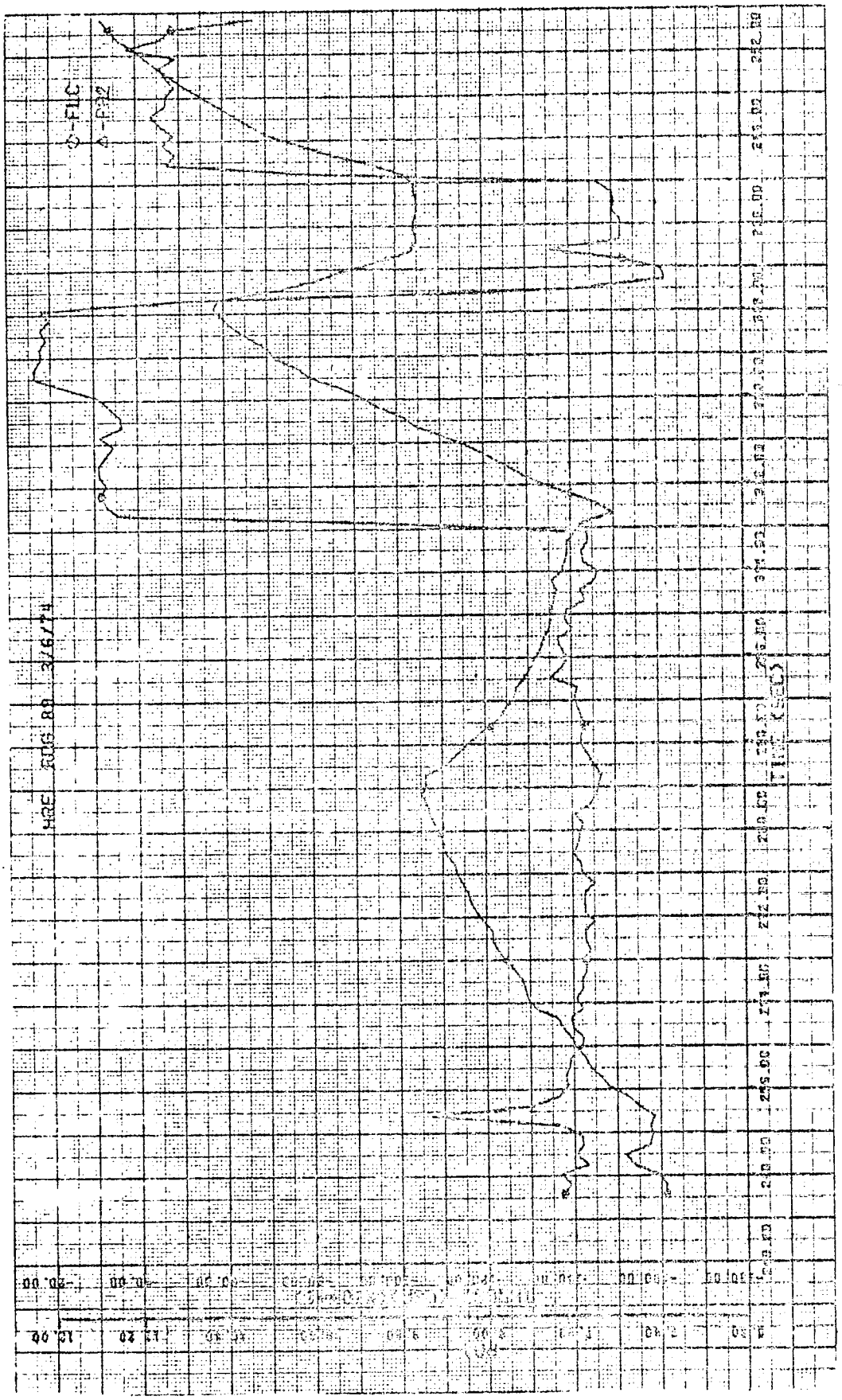

Figure 5-33c. Reading 89 - Purge Pressure and Load Cell Reading

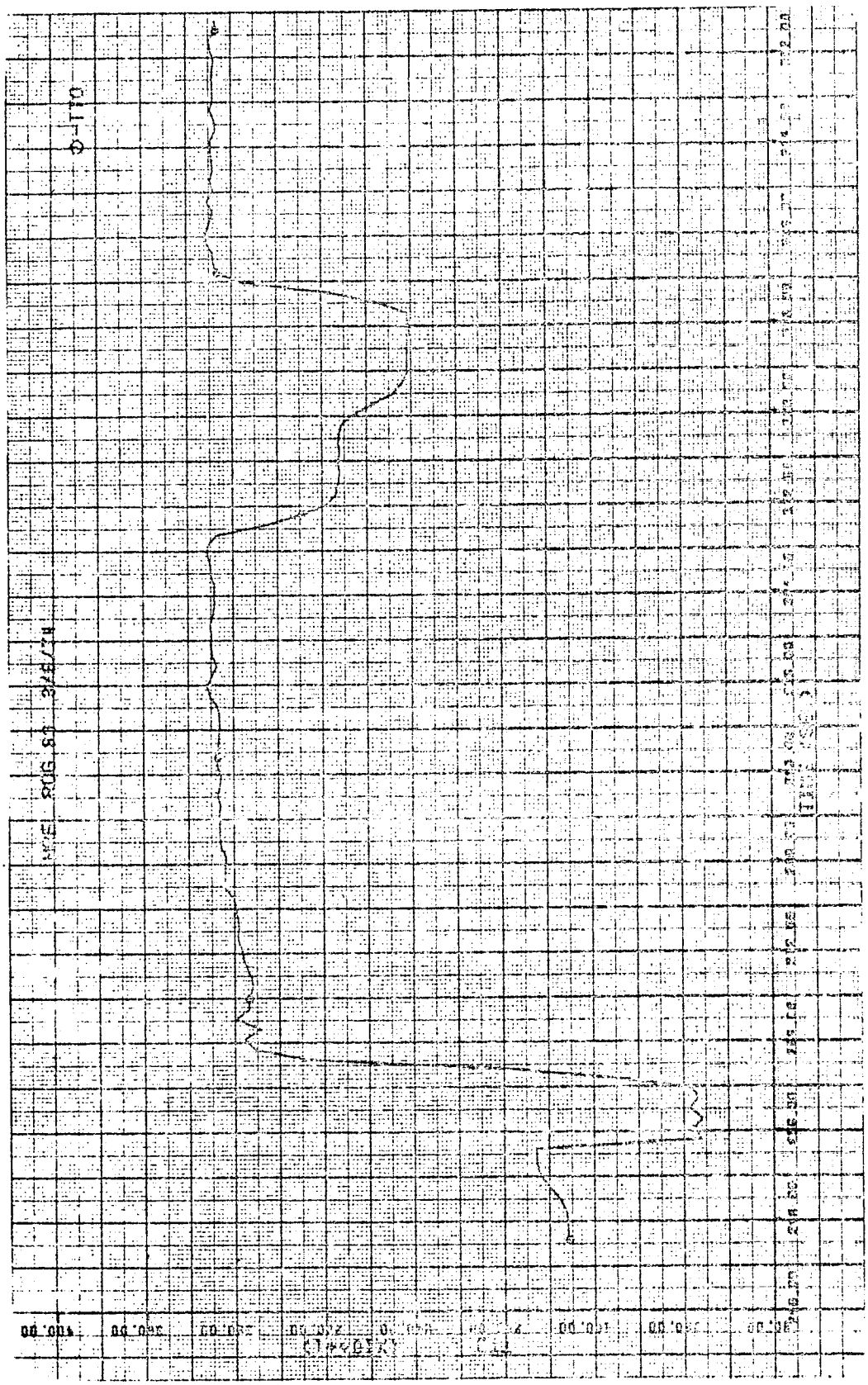

Figure 5-33d. Reading 89 - Tunnel Total Temperature

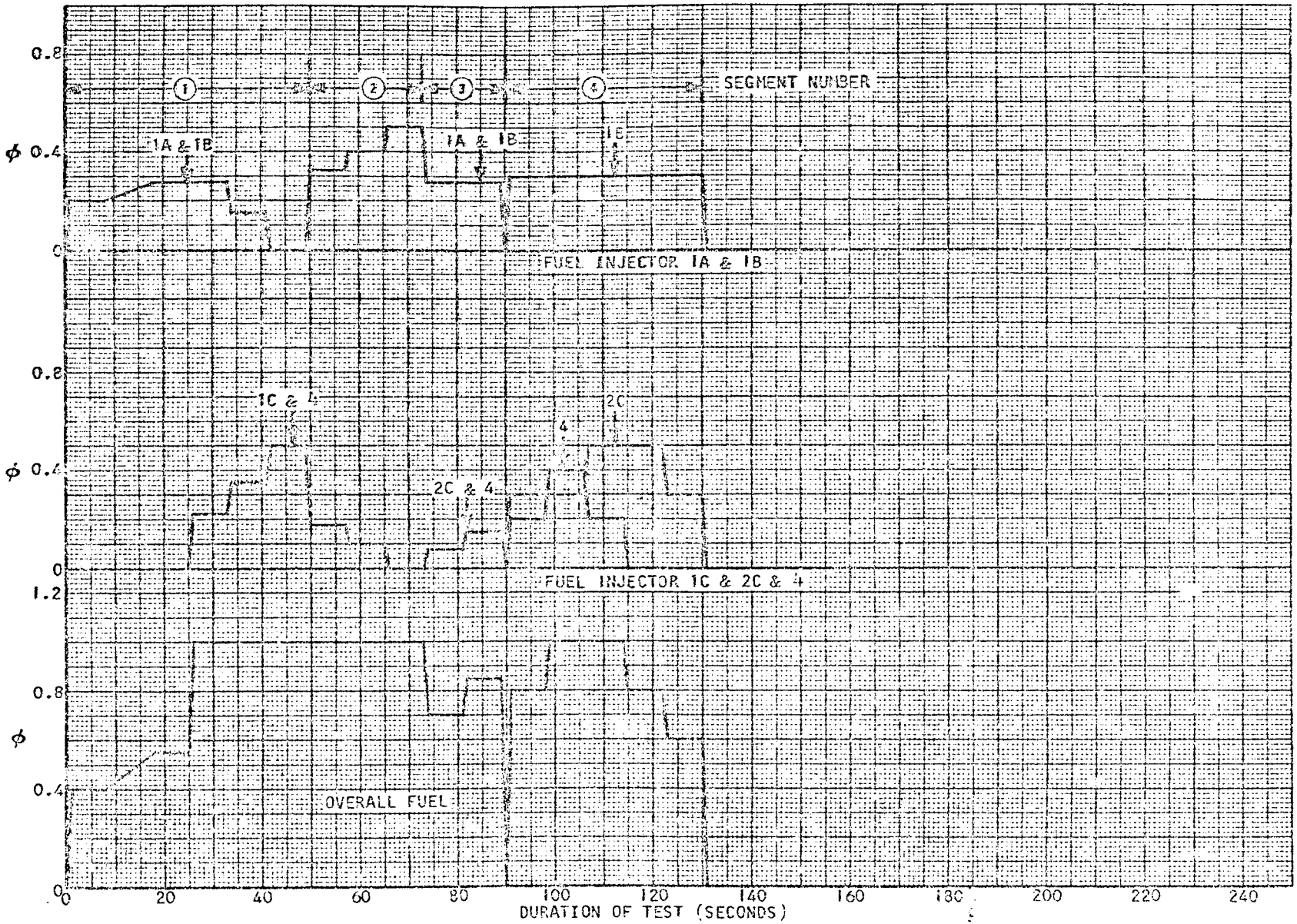

Figure 5-34a. Reading 91 - Fuel Schedule

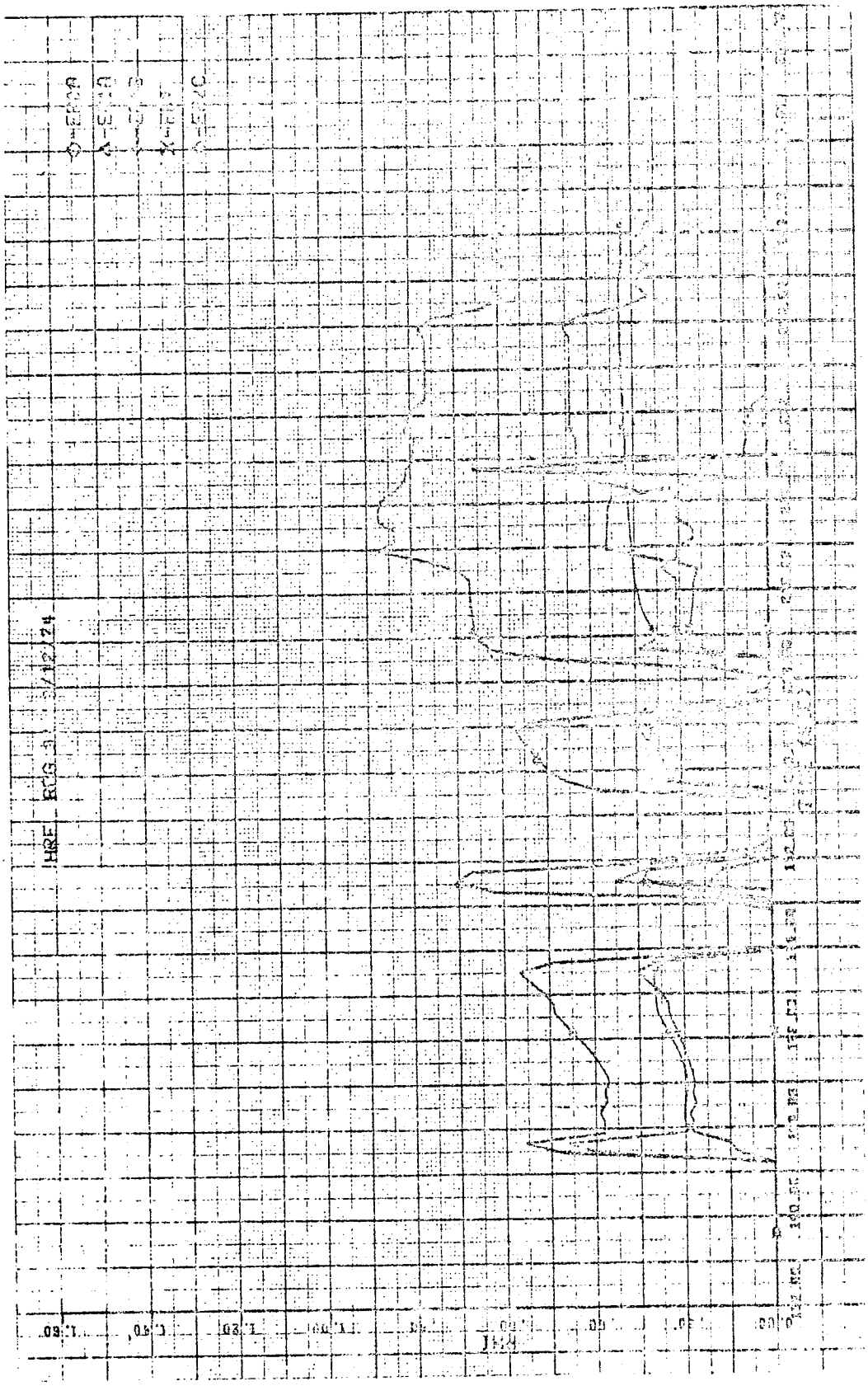

Figure 5-34b. Reading 31 - Measured Equivalence Ratio, Φ

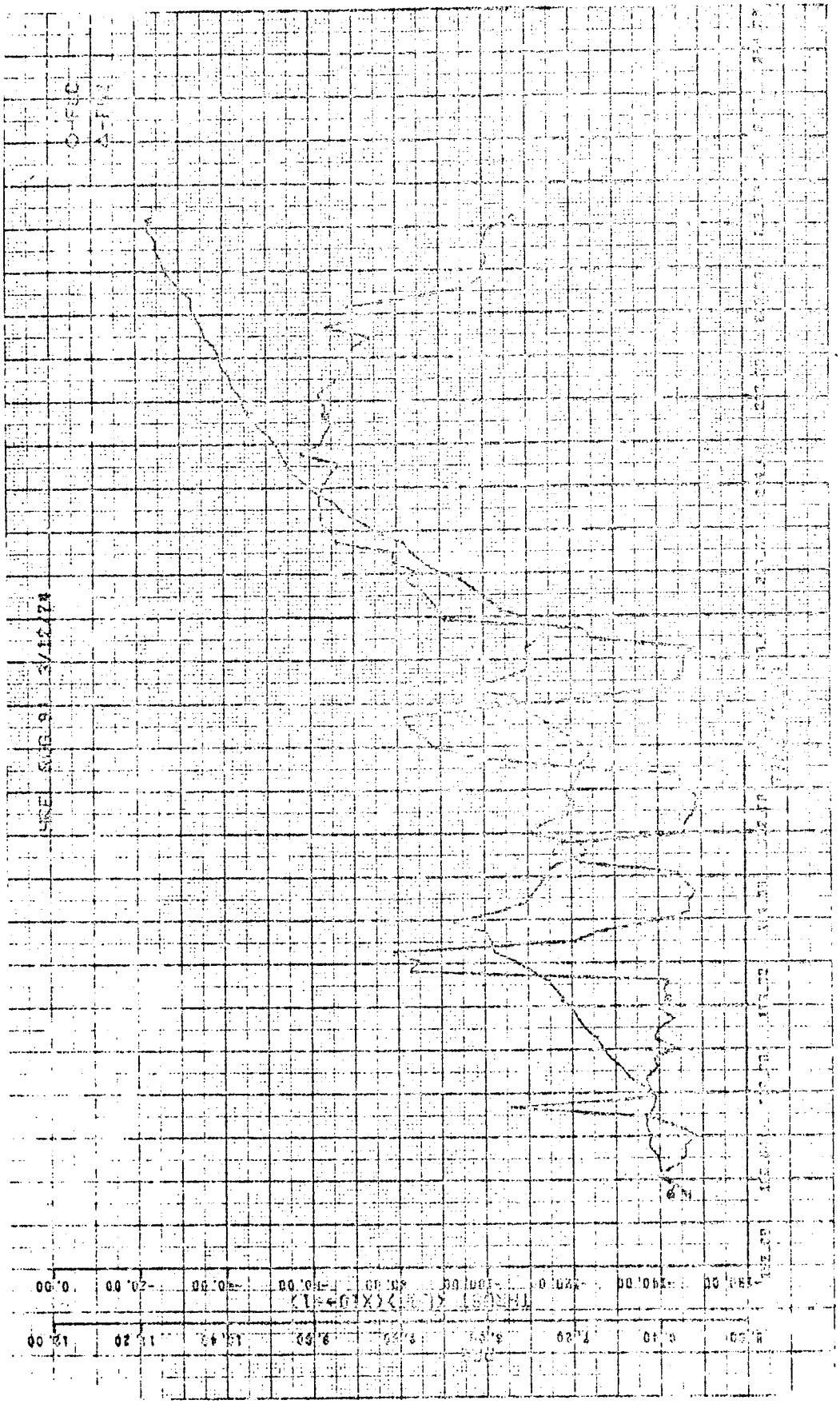

Figure 5-34c. Reading 93 - Purge Pressure and Load Cell Reading

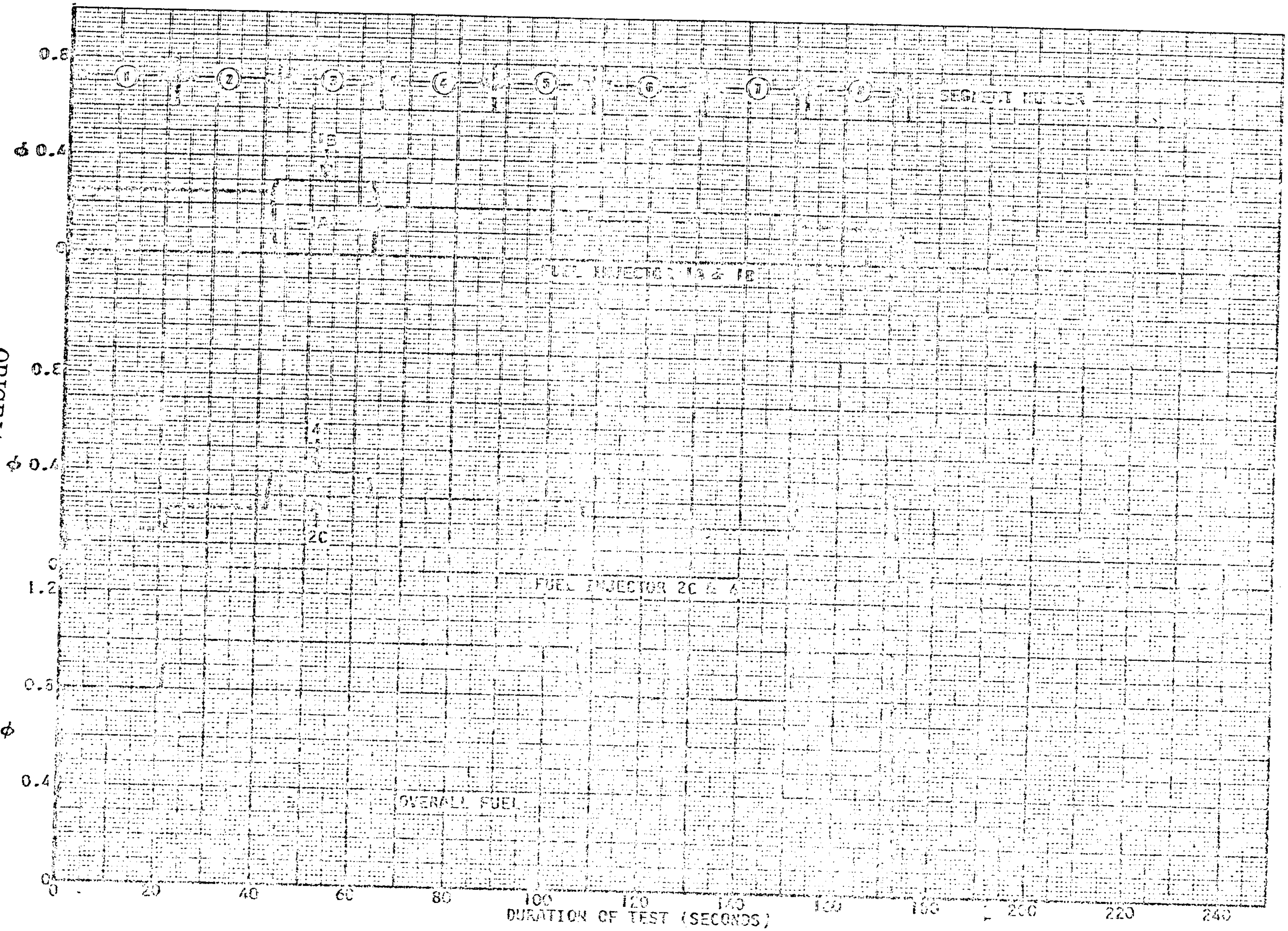

Figure 5-35a. Reading 92 - Fuel Schedule

ORIGINAL PAGE IS
OF POOR QUALITY

Figure 5-35b. Reading 92 - Measured Equivalence Ratio, Φ

Figure 5-35c. Reading 92 - Purge Pressure and Load Cell Reading

Figure 5-36r. Reading 93 - Fuel Schedule

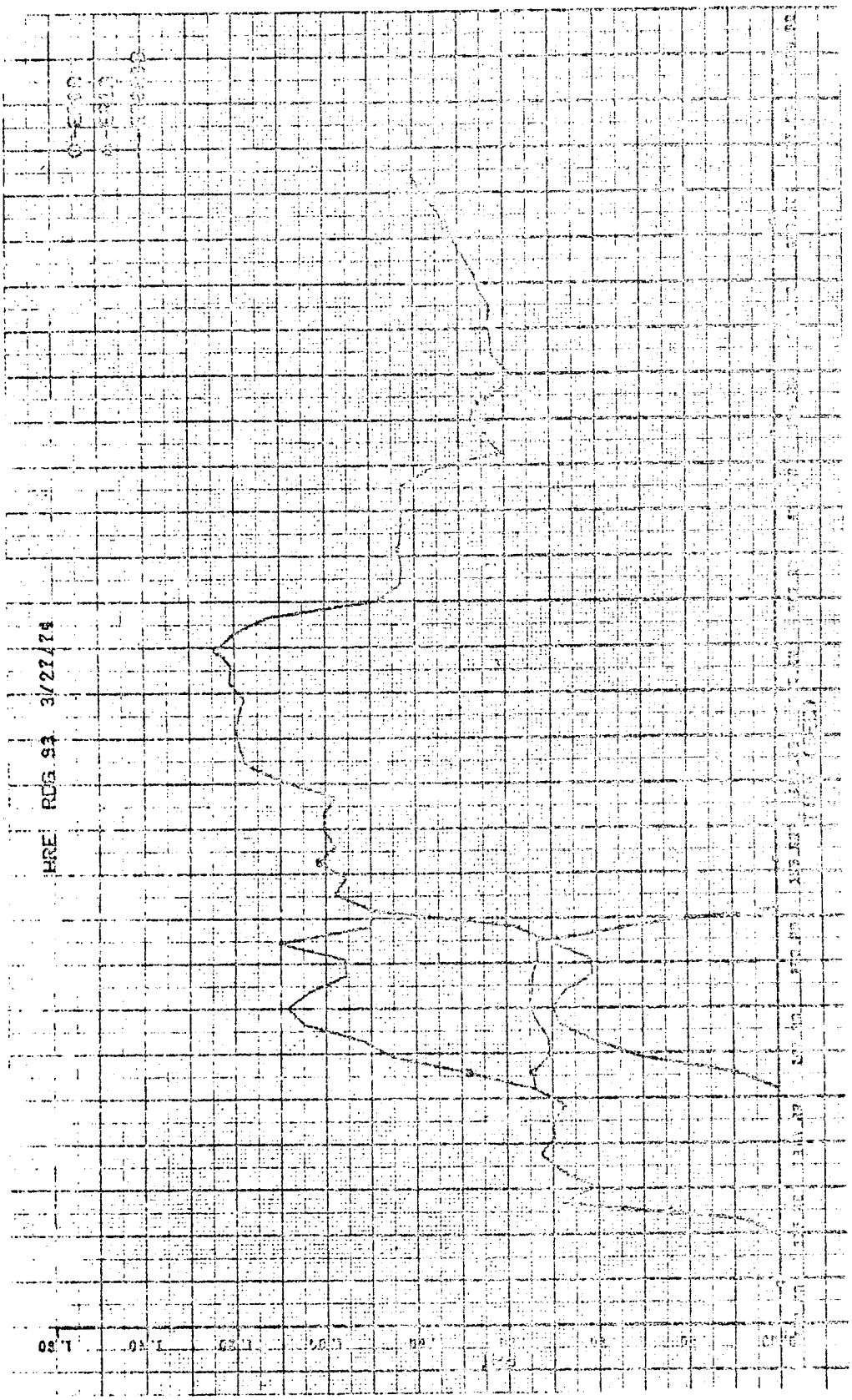

Figure 5-36b. Reading 93 - Measured Equivalence Ratio, Φ

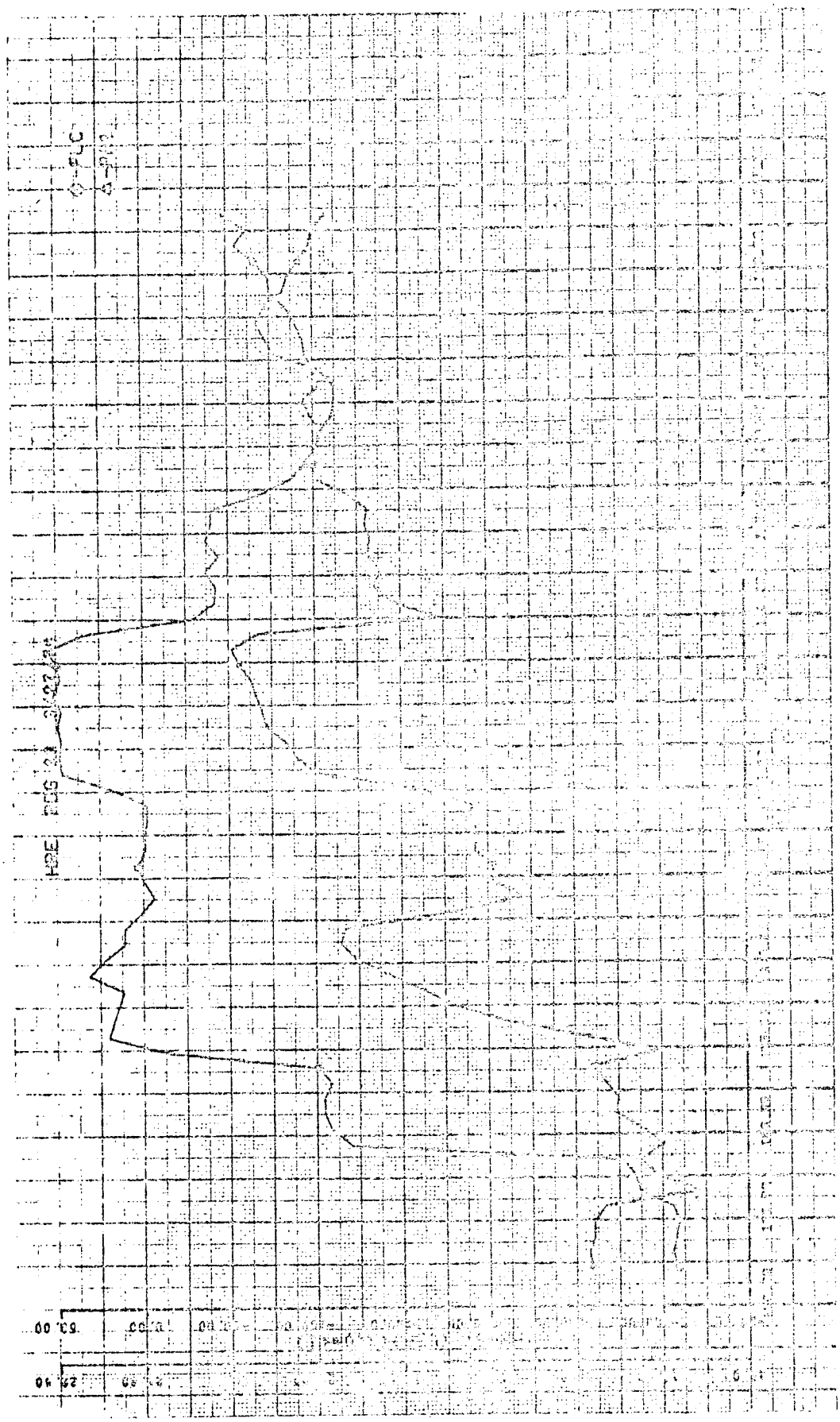

Figure 5-36c. Reading 52 - Purge Pressure and Load Cell Reading

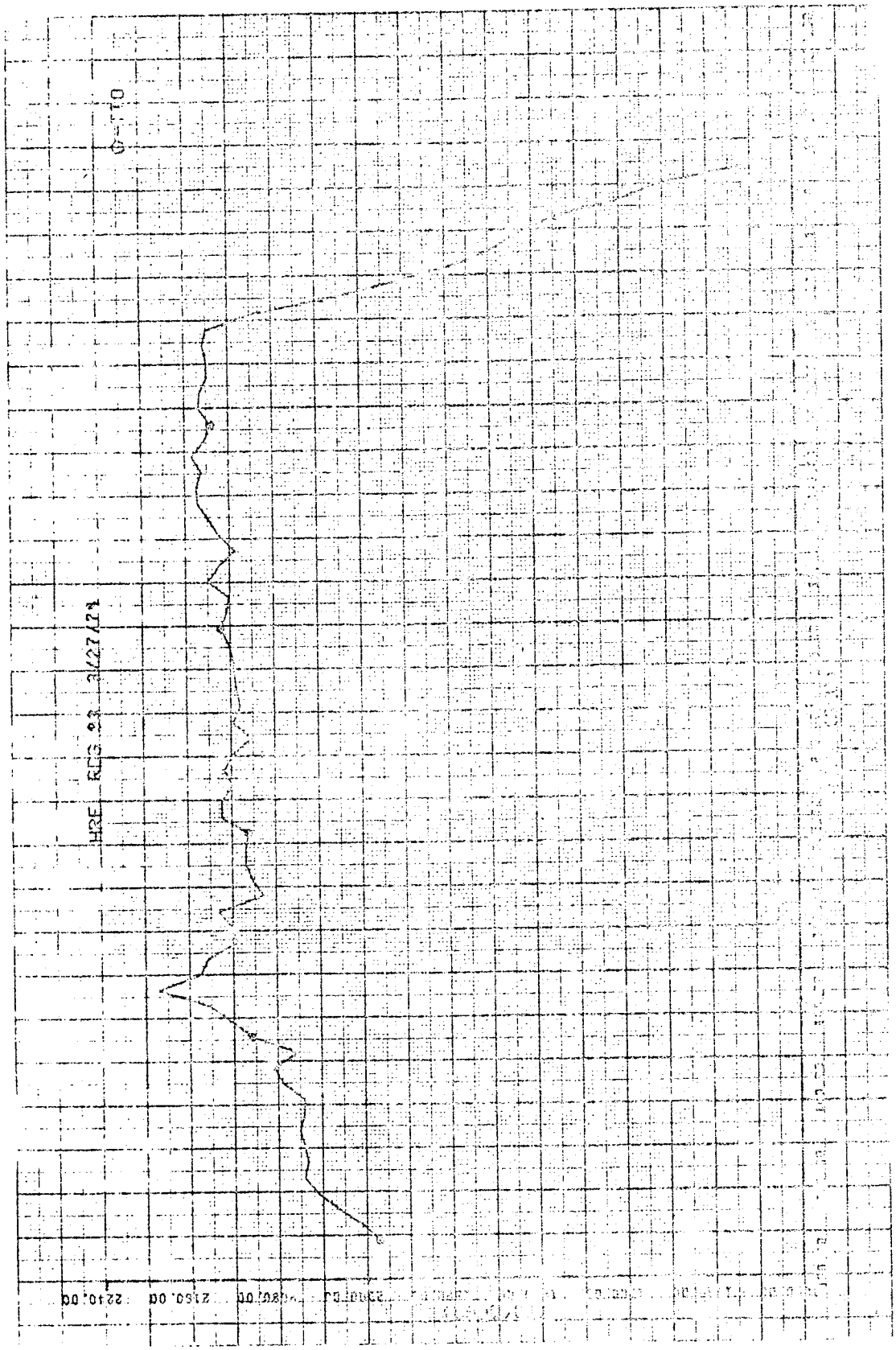

Figure 5-36d. Reading 93 - Tunnel Total Temperature

Figure 5-37a. Reading 95 - Fuel Schedule

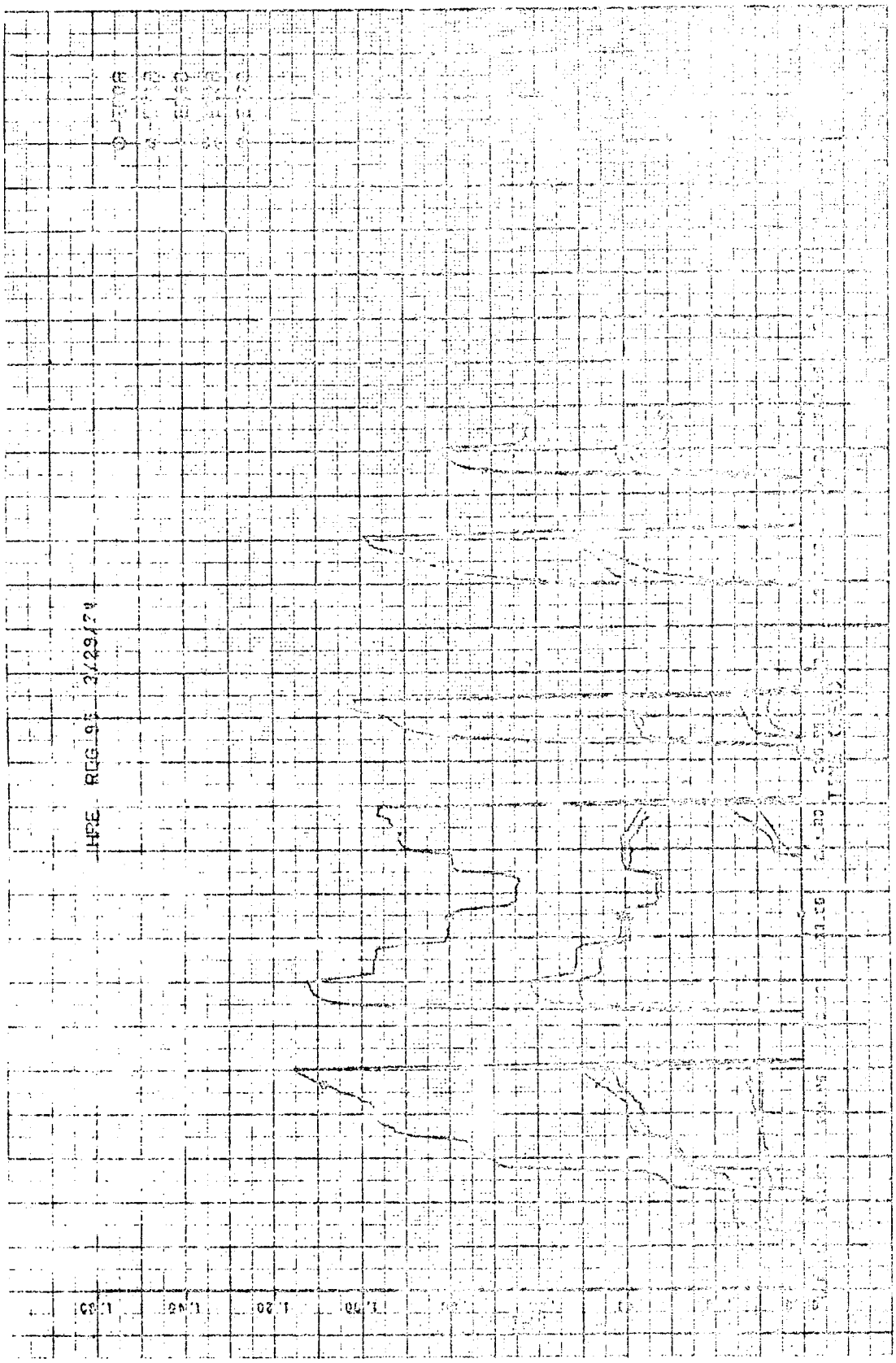

Figure 5-375. Reading 95 - Measured Equivalence Ratio, Φ

ORIGINAL PAGE IS
OF POOR QUALITY

Figure 5-31c. Reading 95 - Purge Pressure and Load Cell

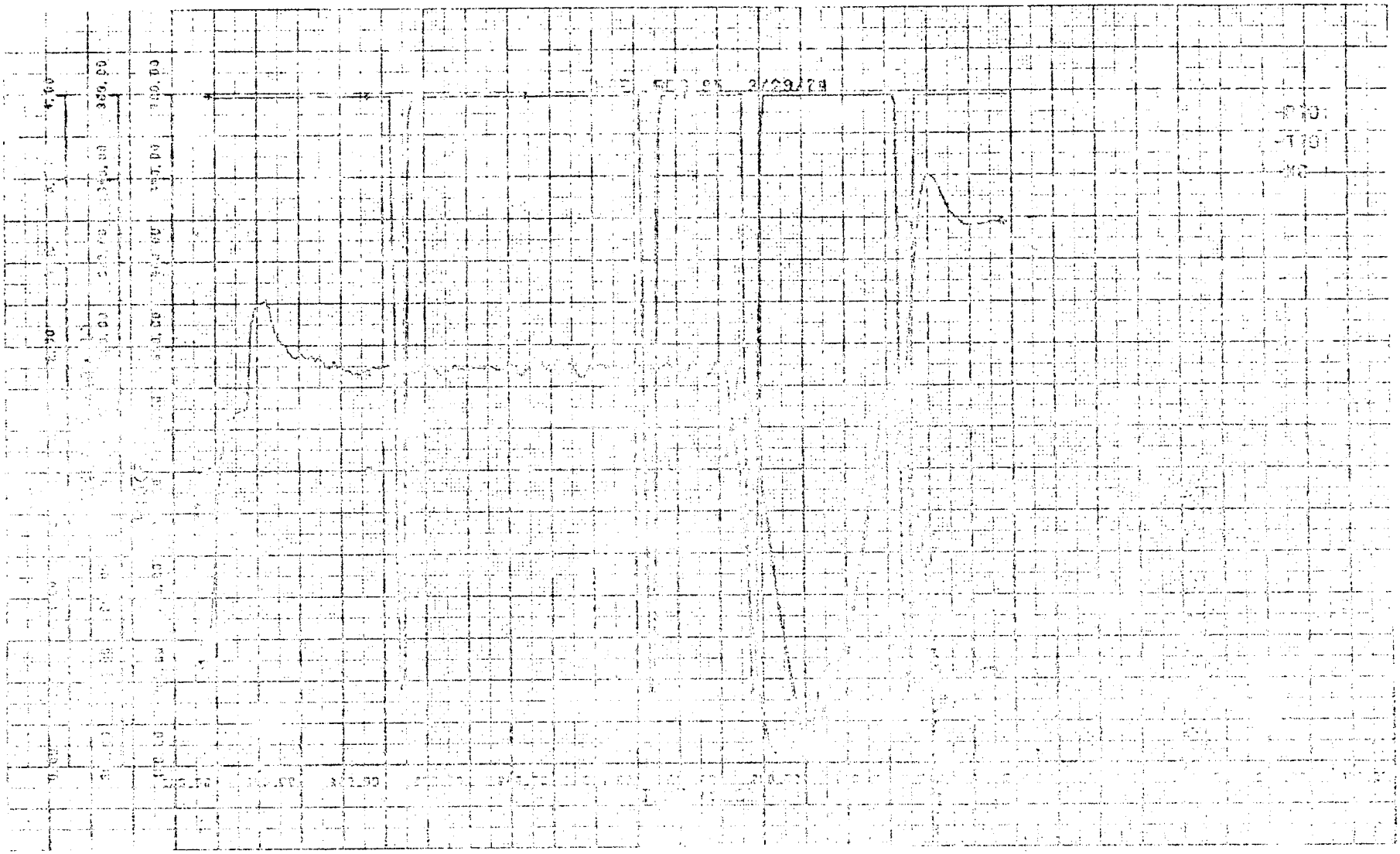

Figure 5-37d. Reading 95 - Tunnel Total Pressure, Temperature, and AIM Inlet Spike Position

Figure 5-36e. Reading 97 - Fuel Schedule

Figure 5-23b. Reading 97 - Measured Equivalence Ratio, ϕ

Figure 5-33c. Reading 17 - Tube Pressure and Leaf Cell Reading

5.4 MEASURED DATA

All instrumentation provided on the NRE/AIM was not recorded due to limited provision at the hypersonic tunnel facility. Table 5-4 tabulates instrumentation provided and recorded.

The code for the instrumentation listed in the "Identification" column is as follows: Sample, S-P-14.492-0°11'-90-3 (A-B-C-D-E-F).

"A" designates the component on which the instrumentation is located:

S = inlet spike assembly

I = innerbody assembly

NP = nozzle plug assembly

CO = cowl leading edge assembly (outside)

C = cowl leading edge assembly (combustor side)

O = outerbody

N = nozzle shroud (combustor side)

NO = nozzle shroud (outside)

CE = combustor exit

EF = engine airflow-metering duct

F = fluids

"B" designates type of instrumentation

P = pressure

T = temperature

"C" designates the location of the instrumentation in terms of station, with the inlet spike assembly positioned for testing at Mach 6 condition.

"D" designates the angular location in degrees and minutes.

"E" designates position of the pressure pickup with respect to airflow in degrees, or, if the instrument is a temperature sensor, it designates the thermocouple:

C/A = chromel alumel

CuC = copper constantan

P/rh = platinum-platinum/rhodium

"F" designates the leg through which the leads are brought out.

An "X" anywhere in the Identification Code indicates that the parameter was not applicable.

xxx/yy in the "Reading No." column indicates the Channel No. (xxx) on which the parameter was recorded, and the rated capacity (yy) of the transducer used.

The "N/U" Code in the "Reading No." Column indicates channels that were not used.

"LeRC Sys" - recorded on separate system, therefore no channel number.

TABLE 5-4

HRE-AIM INSTRUMENTATION LIST

Measurement Number	Identification	READING NUMBER 31	33	34	36	37	38	51	57	61	63	64	65	69	70	73	78	84	88	89	91	97	98	99
1-S	S-P - 0.595 - 0 - 0-3	121/25	→	*																				
2-S	S-P - 14.492 - [illegible] - 90-3	N/U	→	*																				
3-S	S-P - 14.483 - 2[illegible] - 90-3	123/10	→			123/10																		
4-S	S-P - 14.473 - 180°51' - 90-3	N/U	→	*																				
5-S	S-P - 14.4 - 90 - 90	Not Routed																						
6-S	S-P - 20.695 - 359°36' - 90-3	125/10																						
[illegible]	S-P - 35.685 - 359°34' - 90-3	126/10																						
[illegible]	S-P - 35.071 - 269°25' - 90-3	127/10																						
9-S	S-P - 35.071 - 179°28' - 90-3	239/25																						
10-S	S-P - 35.079 - 89°33' - 90-3	260/10		*																				
11-S	S-P - 35.180 - 359°32' - 90-3	261/10																						
12-S	S-P - 26.077 - 359°24' - 90-3	262/10																						
13-S	S-P - 56.487 - 359°30' - 90-3	263/10																						
14-S	S-P - 35.476 - 269°31' - 90-3	264/10																						
15-S	S-P - 36.476 - 179°27' - 90-3	265/25																						
[illegible]	S-P - 36.482 - 89°23' - 90-3	266/15	→													266/10								
[illegible]	S-P - 35.384 - 359°32' - 90-3	268/10	→																				128/15	→
18-S	S-P - 37.5 - 0 - 90-3	Not Routed																						
[illegible]	S-P - 35.0 - 0 - 90-3	Not Routed																						
[illegible]	S-P - 35.072 - 269°27' - 90-3	122/10	→																				122/15	→
[illegible]	S-P - 38.00 - 179°23' - 90	Not Routed																						
[illegible]	S-P - 35.00 - 270 - 90	Not Routed																						
[illegible]	S-P - 38.5 - 0 - 90	Not Routed																						
[illegible]	S-P - 35.024 - 359°25' - 90-4	129/20	→																				129/25	→
[illegible]	S-P - 35.071 - 269°27' - 90-4	N/U	→	*																				
[illegible]	S-P - 35.076 - 179°23' - 90-4	N/U	→	*																				
[illegible]	S-P - 38.0 - 270 - 90	Not Routed																						
[illegible]	S-P - [illegible] - 359°24' - 90-4	130/25	→													130/15	→						130/20	→
[illegible]	S-P - 35.021 - 359°26' - 90-4	131/25	→	*																				
[illegible]	S-P - 35.073 - 269°25' - 90-4	132/25	→	*																				
[illegible]	S-P - 35.075 - 179°25' - 90-4	267/25	→									267/50	→			267/25	→							
[illegible]	S-P - 35.073 - 89°23' - 90-4	133/25	→	*																				
[illegible]	S-P - 34.480 - 359°30' - 90-4	134/25	→													134/25	→				134/50	→	134/75	→
[illegible]	S-P - 35.078 - 359°28' - 90-4	135/25	→													135/50	→						135/75	→
[illegible]	S-P - 35.7 - 0 - 90	Not Routed																						
[illegible]	S-P - 43.5 - 90 - 90	Not Routed																						
[illegible]	S-P - 35.7 - 180 - 90	Not Routed																						
[illegible]	S-P - 43.5 - 270 - 90	Not Routed																						
[illegible]	S-P - [illegible] - 359°28' - 90-4	135/75	→													136/50	→				136/75	→		
[illegible]	S-P - 35.0 - 0 - 90	Not Routed																						
34-S	S-P - 35.075 - 359°30' - 90-4	268/75	→									268/100	→			268/50	→						268/75	→
[illegible]	S-T - [illegible] - 269°22' - 90-4	137/75	→													137/50	→						137/75	→
[illegible]	S-T - [illegible] - 179°25' - 90-4	138/75	→													138/50	→						138/75	→
[illegible]	S-T - 35.079 - 89°20' - 90-4	139/75	→													139/50	→						139/75	→
[illegible]	S-T - 34.484 - 359°28' - 90-4	269/75	→									269/100	→			269/50	→						269/75	→
[illegible]	S-T - 24.0 - 359°37'	Not Routed																						
37-S	S-T - 37.479 - 359°30' - CA-3	303/50mv	→	*																				
40-S	S-T - 38.017 - 359°35' - CA-3	N/U																						
50-S	S-T - [illegible] - 359°30' - CA-4	305/50mv	→	*																				
50-S	S-T - [illegible] - 359°30' - CA-4	306/50mv	→	*																				
51-S	S-T - [illegible] - 359°27' - CA-4	307/50mv	→	*																				
52-S	H.P.T. (Spike Position)	120/10mv = 4.372 inches → *																						
77-T	Load Cell	127/30[illegible] lb = 20mv → *																						

*Continuous to end

TABLE 5-4 (Continued)

Measurement Number	Identification	READING NUMBER 31	33	34	36	37	38	51	57	61	63	64	65	69	70	73	78	84	88	89	91	92	93	96	97
1-P	P-P - 54.519 - 359°49' - 90-3	143/20	→								143/25	143/50	→									→	143/100	→	
2-P	P-P - 54.520 - 269°49' - 90-3	N/U	→	N/U	186/50	→										141/50						→	186/100	→	
3-P	P-P - 54.512 - 179°41' - 90-3	141/75	→																			→	141/75	→	
4-P	P-P - 54.514 - 99° 0' - 90-4	N/U	→	N/U	191/50	→										271/50						→	191/100	→	
5-P	P-P - 56.004 - 0°48' - 90-4	271/75	→																			→	271/100	→	
6-P	P-P - 56.0 - 32°30' - 90	Not Routed																							
7-P	P-P - 56.0 - 170°30' - 90	Not Routed																							
8-P	P-P - 56.0 - 262°30' - 90	Not Routed														270/20						→	270/50	→	
9-P	P-P - 64.739 - 359°45 - 90-4	270/75	→																						
10-T	T-T - 54.0 - 0	Not Routed																							
11-T	T-T - 55.25 - 0	Not Routed																							
12-T	T-T - 70.0 - 0	Not Routed																							
13-T	T-T - 59.979 - 240° 0' - CA-2	308/50 mv	→																						
14-T	T-T - 60.019 - 120° 0' - CA-4	290/50 mv	→	*																					
15-T	T-T - 64.799 - 354°56' - CA-4	350/50 mv	→																						

*Continuous to end

S-88486

Measurement Number	Identification	READING NUMBER 31	33	34	36	37	38	51	57	61	63	64	65	69	70	73	78	84	88	89	91	92	93	96	97
1-NP	NP-P - 66.640 - 59°54' - 90-4	144/20	→													144/10	→					→	144/25	→	
2-NP	NP-P - 68.090 - 119°38' - 90-4	145/10	→																			→	145/25	→	
3-NP	NP-P - 69.405 - 180° 8' - 90-4	146/10	→																						
4-NP	NP-P - 70.790 - 240°12' - 90-4	147/10	→																						
5-NP	NP-P - 73.855 - 300°13' - 90-4	148/10	→																						
6-NP	NP-P - 74.550 - 0°10' - 90-4	150/10	→	*																					
7-NP	NP-P - 77.100 - 60° 0' - 90-4	150/10	→																						
8-NP	NP-P - 81.235 - 120° 3' - 90-4	151/10	→																						
9-NP	NP-P - 84.105 - 180° 5' - 90-4	152/10	→																						
10-NP	NP-P - 88.367 - [illegible] - X-4	153/10	→																						
11-NP	NP-T - 63.026 - 120°15' - CA-3	311/50 mv	→	*																					
12-NP	NP-T - 70.730 - 245°12' - CA-3	311/50 mv	→	*																					
13-NP	NP-T - 84.165 - [illegible]	Not Routed																							
14-NP	NP-T - 84.200 - 125° 8' - CA-3	311/50 mv	→	*																					

*Continuous to end

S-88487

TABLE 5-4 (Continued)

Measurement Number	Identification	READING NUMBER 31	33	34	36	37	38	51	57	61	63	64	65	69	70	73	78	84	88	89	91	92	93	96	97
1-CO	CO-P - 35.525 - 83° 2' - 90-4	N/U →	*									→	N/U	155/25	155/15							N/U	155/15	125/20	N/U
2-CO	CO-P - 35.514 - 172°58' - 90-4	155/25 →										→	↑	156/15								↑	155/15	156/20	↑
3-CO	CO-P - 35.544 - 262°56' - 90-3	N/U →		N/U	156/15							→	↑	157/25 →		N/U	N/U	N/U	N/U	157/25	→	↑	157/15 →	↑	↑
4-CO	CO-P - 35.519 - 352°59' - 90-3	157/25 →										→	↑	158/10 →						158/10	→	↑	158/10 →	↑	↑
5-CO	CO-P - 37.040 - 83° 4' - 90-4	N/U →		N/U	158/10							→	↑	159/15 →							→	↑	159/15 →	↑	↑
6-CO	CO-P - 37.044 - 173° 5' - 90-4	159/15 →										→	↑	160/10 →		N/U	N/U	N/U	N/U	160/10	→	↑	160/10 →	↑	↑
7-CO	CO-P - 37.047 - 263° 5' - 90-3	N/U →		N/U	160/10							→	↑	161/15 →			161/10			161/10	→	↑	161/10 →	↑	↑
8-CO	CO-P - 37.044 - 353° 2' - 90-3	161/15 →										→	↑	162/10 →		N/U	N/U	N/U	N/U	162/10	→	↑	162/10 →	↑	↑
9-CO	CO-P - 39.003 - 83° 7' - 90-4	N/U →		N/U	162/10							→	↑	163/15 →							→	↑	163/15 →	↑	↑
10-CO	CO-P - 39.004 - 173° 7' - 90-4	163/15 →										→	↑	164/10 →							→	↑	164/10 →	↑	↑
11-CO	CO-P - 39.004 - 263° 7' - 90-3	N/U →		N/U	164/10							→	↑	165/15 →		165/10					→	↑	165/10 →	↑	↑
12-CO	CO-P - 39.000 - 353° 6' - 90-3	165/15 →										→	↑	166/15 →		N/U	N/U	N/U	N/U	166/15	→	↑	166/15 →	↑	↑
13-CO	CO-P - 40.503 - 83° 6' - 90-4	N/U →		N/U	165/10						166/15	→	↑	167/15 →		167/10					→	↑	167/10 →	↑	N/U
14-CO	CO-P - 40.507 - 173° 6' - 90-4	167/15 →										→	↑	↑		↑	↑	↑	↑	↑	→	N/U	↑	↑	↑
15-CO	CO-P - 40.504 - 263° 4' - 90-3	Not Routed										→	↑	169/15 →		N/U	N/U	N/U	N/U	169/15	→	N/U	169/15 →	169/20	N/U
16-CO	CC-P - 40.500 - 353° 5' - 90-3	169/15 →										→	↑	170/15 →		↑	↑	↑	↑	170/15	→	↑	170/15 →	↑	↑
17-CO	CC-P - 40.004 - 210° 2' - 90-3	170/15 →										→	↑	171/10 →		↓	↓	↓	↓	171/10	→	↓	171/10 →	↓	↓
18-CO	CC-P - 40.260 - 210° 7' - 75-3	N/U →		N/U	171/10							→	↑	172/10 →						172/10	→		172/10 →		
19-CO	CO-P - 40.500 - 210° 3' - 110-3	N/U →		N/U	172/10							→	↑	173/15 →						173/15	→		173/15 →		
20-CO	CO-P - 40.240 - 330° 1' - 135-3	173/15 →										→	↑	174/10 →		N/U	N/U	N/U	N/U	174/10	→	N/U	174/10 →	N/U	
21-CO	CO-P - 40.[illegible] - 330° 0' - 110-3	N/U →		N/U	174/10							→	↑	↑		↑	↑	↑	↑	↑	→	↑	↑	↑	
22-CO	CO-P - 40.[illegible] - 0° 5' - 110-4	N/U →		N/U	175/25							→	↑	↑		↑	↑	↑	↑	↑	→	↑	↑	↑	
23-CO	CO-P - 40.354 - 359°57' - 75-3	N/U →		N/U	176/10							→	↑	177/15 →		N/U	N/U	N/U	N/U	176/10	→		176/15 →		
24-CO	CO-P - 40.055 - 0° 3' - 110-3	177/15 →										→	↑	178/20 →		N/U	N/U	N/U	N/U	177/15	→	N/U	177/15 →	N/U	
25-CO	CO-P - 40.200 - 180°10' - 135-4	178/15 →									178/20	→	N/U	179/25 →		N/U	N/U	N/U	N/U	178/20	→	N/U	178/20 →	N/U	
26-CO	CO-P - 40.656 - 180° 5' - 110-4	175/15 →			178/25							→	N/U	↑		↑	↑	↑	↑	179/25	→	N/U	179/25 →	↑	
27-CO	CO-P - 35.514 - 359°58' - 90-3	180/50 →										→	↑	↑		↑	180/25 →			↑	→	↑	180/50 →	↑	
28-CO	CO-P - 37.0 - 0 - 90	181/50 →										→	↑	↑		↑	181/25 →			↑	→	↑	181/50 →	↑	
29-CO	CO-P - 36.695 - 0° 8' - 90-4	182/50 →										→	↑	↑		↑	182/25 →			↑	→	↑	182/50 →	↑	
30-CO	CO-P - 36.694 - 180°10' - 90-3	183/50 →										→	↑	↑		↑	183/25 →			↑	→	↑	183/50 →	↑	
31-CO	CO-P - 37.[illegible] - 0° 9' - 90-4	184/50 →										→	↑	↑		↑	184/25 →			↑	→	↑	184/50 →	↑	
32-CO	CO-P - 37.044 - 180°10' - 90-4	185/50 →										→	↑	↑		↑	185/25 →			↑	→	↑	185/50 →	↑	
33-CO	CO-P - 37.049 - 180° 7' - 90-3	N/U →	*																						
34-CO	CO-P - 37.034 - 270° 7' - 90	Damaged																							
35-CO	CO-P - 37.[illegible] - 0°10' - 90-4	187/50 →										→	↑	↑		↑	187/25 →			↑	→	↑	187/50 →	↑	
36-CO	CO-P - 37.[illegible] - 0°10' - 90-4	188/50 →										→	↑	↑		↑	188/25 →			↑	→	↑	188/50 →	↑	
37-CO	CO-P - 37.[illegible] - 90°10' - 90-4	189/50 →										→	↑	↑		↑	189/25 →			↑	→	↑	189/50 →	↑	
38-CO	CO-P - 37.[illegible] - 180° 7' - 90-4	190/50 →										→	↑	↑		↑	190/25 →			↑	→	↑	190/50 →	↑	
39-CO	CO-P - 39.041 - 270° 7' - 90-3	N/U →	*																						
40-CO	CO-P - 38.[illegible] - 0° 5' - 90-4	192/50 →										→	↑	↑		↑	192/25 →			↑	→	↑	192/50 →	↑	
41-CO	CO-P - 38.[illegible] - 0° 5' - 90-4	193/50 →										→	↑	↑		↑	193/25 →			↑	→	↑	193/50 →	↑	
42-CO	CO-P - 39.034 - 90° 7' - 90-4	194/50 →										→	↑	↑		↑	194/25 →			↑	194/50				
43-CO	CO-P - 39.0[illegible] - 180° 4' - 90-	Damaged																							
44-CO	CO-P - 39.01[illegible] - 270° 0' - 90-3	195/50 →										→	↑	↑		↑	195/25 →			↑	→	↑	195/50 →	↑	
45-CO	CO-P - 39.0[illegible] - 359° 4' - 90-3	196/50 →										→	↑	↑		↑	196/25 →			↑	→	↑	196/50 →	↑	
46-CO	CO-P - 39.035 - 0° 6' - 90-4	197/50 →										→	↑	↑		↑	197/25 →			↑	→	↑	197/50 →	↑	
47-CO	CO-P - 40.[illegible] - 90° 7' - 90-4	N/U →	*																						
48-CO	CO-P - 39.994 - 180° 7' - 90-3	199/50 →										→	↑	↑		↑	199/25 →			↑	→	↑	199/50 →	↑	
49-CO	CO-P - 40.[illegible] - 270° 5' - 90	Damaged																							
50-CO	CA-T - 37.[illegible] - 7° 9' - CA-4	314/50 mv →	*																						
51-CO	CA-T - 38.[illegible] - 7° 9' - CA-4	315/50 mv →	*																						
52-CO	CA-T - 38.[illegible] - 7° 8' - CA-4	315/50 mv →	*																						
53-CO	CA-T - 40.0 - 90° - CA	Not Routed																							
54-CO	CA-T - 40.004 - 180° 7' - CA-3	N/U →	*																						N/U
55-CO	CA-T - 39.[illegible] - 270° 4' - CA-3	202/50 mv →							N/U																
56-CO	CO-T - 35.[illegible] - 359° 2' - CA-3	213/50 mv →	*																						
57-CO	CO-T - 38.504 - 0 - CA	Not Routed																							

*Continuous to end

TABLE 5-4 (Continued)

Measurement Point Number	Identification	READING NUMBER																							
		31	33	34	35	37	38	51	57	61	62	66	65	69	70	73	75	34	83	89	91	95	93	5	97
	0-P - 41.0[illegible] - 0°0' - 110-4	201/75	→														201/50								
	0-P - 41.06 - 180°0' - 110-4	272/75	→														272/50						272/75		
	0-P - 41.06 - 210°0' - 110-3	N/U	→	N/U	228/75	→											226/50								
	0-P - 41.06 - 330°0' - 110-3	N/U	→				N/U	200/75	→								200/50								
	0-P - 43.786 - 180° - 90-4	202/75	→								202/100	→					202/50						202/75		
	0-P - 43.786 - 90°0' - 90-4	N/U	→				N/U	203/75	→		203/100	→					203/50						203/75		
	0-P - 43.731 - 180°0' - 90-3	204/75	→														204/50						204/75		
	0-P - 43.786 - 270°0' - 90-3	N/U	→				N/U	205/75	→								205/50						205/75		
	0-P - 43.829 - 180° - 90-4	206/75	→														206/50						206/75		
	0-P - 43.016 - 180° - 90-4	273/75	→								273/100	→					273/50						273/75		
	0-P - 46.005 - 180° - 90-4	207/75	→														207/50						207/75		
	0-P - 46.020 - 90°0' - 90-4	N/U	→				N/U	219/50	→														219/75		
	0-P - 46.003 - 180°0' - 90-4	N/U	→																						
	0-P - 46.305 - 270°0' - 90-3	N/U	→				N/U	198/50	→		198/75	198/75					198/50						198/75		
	0-P - 46.506 - 0° - 90-3	N/U	→																						
	0-P - 39.405 - 0° - 90-4	208/75	→														208/50						208/75		
	0-P - 50.411 - 90° - 90-4	N/U	→				N/U	221/50	→			221/75					221/50						221/75		
	0-P - 50.411 - 180° - 90-4	N/U	→																						
	0-P - 50.411 - 270° - 90-3	N/U	→																						
	0-P - 50.355 - 0° - 90-4	N/U	→																						
	0-P - 52.063 - 0° - 90-3	209/75	→														209/50						209/100		
	0-P - 52.008 - 0° - 90-4	210/75	→														210/50						210/100		
	0-P - 52.005 - 90° - 90-4	N/U	→				N/U	211/75	→		211/100	→					211/50						211/100		
	0-P - 52.005 - 180° - 90-4	212/75	N/U	→																					
	0-P - 52.008 - 270° - 90-3	N/U	→				N/U	212/75	→		212/100	→					212/50						212/100		
	0-P - 50.410 - 0° - 90-3	213/75	→														213/50						213/100		
	0-P - 50.[illegible] - 0° - 90-4	215/75	→														215/50						215/100		
	0-P - [illegible] - [illegible] - 90-2	N/U	→				N/U	213/75	→		213/100	→					213/50						213/100		
	0-P - 50.479 - 0° - 90-4	216/75	→														216/50						216/100		
	0-P - 50.474 - 0° - 90-3	N/U	→																						
	0-P - 50.476 - 0° - 90-4	217/50	→								217/75	→					217/50						217/75		
	0-P - 41.540 - 90° - 90-3	218/50	→								218/75	→					218/50						218/75		
	0-P - 41.081 - 110° - 90-4	N/U	→																						
	0-P - 41.881 - 180° - 90-3	220/75	→														220/50						220/75		
	0-P - 41.874 - 270° - 90-3	N/U	→																						
	0-P - 50.476 - 0° - 90-4	N/U	→																						
	0-P - 50.[illegible] - 0° - 90-4	N/U	→																						
	0-P - 44.475 - 0° - 90-4	222/20	→		222/50	→											222/75						222/75		
	0-T - 41.[illegible] - 0° - 0A-3	317/50mv	→																						
	0-T - 41.[illegible] - 90° - 0A-3	318/50mv	→																						
	0-T - 41.[illegible] - 180° - 0A-4	319/50mv	→																						
	0-T - 41.838 - 180° - 0A-	320/50mv	→																						
	0-T - 46.[illegible] - 0° - 0A-3	321/50mv	→																						
	0-T - 46.[illegible] - 90° - 0A-4	322/50mv	→																						
	0-T - 46.629 - 180° - 0A-3	324/50mv	→																						
	0-T - 46.[illegible] - 270° - 0A-3	325/50mv	→																						
	0-T - 47.016 - 180° - 0A-3	327/50mv	→																						
	0-T - 50.[illegible] - 0° - 0A-	Not Routed																							
	0-T - 49.005 - 3196 - 0A-3	322/50mv	→																						
	0-T - 50.005 - 0° - 0A-3	323/50mv	→																						
	0-T - 50.014 - 90° - 0A-	Not Routed																							
	0-T - 50.014 - 180° - 0A-4	326/50mv	→																						

*Continuous to end

TABLE 5-4 (Continued)

Measurement Number	Identification	READING NUMBER 31	33	34	36	37	38	51	57	61	63	64	65	69	70	73	78	84	88	89	91	92	93	96	97
52-0	0-T - 50.010 - 2700 - CA-	Not Routed																							
56-0	0-T - 51.503 - 3590 - CA-3	324/50mv		*																					
54-0	0-T - 52.010 - 00 - CA-4	325/50mv																							
55-0	0-T - 52.996 - 3590 - CA-3	326/50mv																							
57-0	0-T - 54.0 - 00 - CA-	Not Routed																							
58-0	0-T - 56.0 - 00 - CA-	Not Routed																							
59-0	0-T - 56.00 - 00 - CA-3	327/50mv																							
60-0	0-T - 56.00 - 1200 - CA-3	297/50mv																							
61-0	0-T - 56.00 - 2400 - CA-4	298/50mv																							
62-0	0-T - 57.010 - 00 - CA-3	328/50mv																							
63-0	0-T - 57.270 - 00 - CA-3	329/50mv																							
64-0	0-T - 58.949 - 00 - CA-3	330/50mv																							
65-0	0-T - 59.955 - 00 - CA-4	331/50mv																							
67-0	0-T - 60.974 - 00 - CA-4	332/50mv		*																					
68-0	0-T - 62.474 - 00 - CA-4	333/50mv																							
69-0	0-T - 62.474 - 1200 - CA-3	299/50mv																							
70-0	0-T - 62.474 - 2400 - CA-4	300/50mv																							
71-0	0-T - 63.950 - 00 - CA-3	334/50mv																							
72-0	0-T - 66.475 - 00 - CA-4	335/50mv																							
73-0	0-T - 66.2[illegible] - 3590 - CA-3	336/50mv																							
75-0	0-T - 66.0 - 00 - CA-	Not Routed																							

*Continuous to end

Measurement Number	Identification	READING NUMBER 31	33	34	36	37	38	51	57	61	63	64	65	69	70	73	78	84	88	89	91	92	93	96	97
1-N	N-P - 66.635 - 2[illegible] - 90-3	223/20															223/10						223/25		
2-N	N-P - 67.387 - 240[illegible] - 90-3	224/15		*																					
3-N	N-P - 68.[illegible] - 120[illegible]	Not Routed																							
4-N	N-P - 68.880 - 1[illegible] - 90-3	225/10		*																					
5-N	N-P - 69.[illegible] - 59[illegible] - 90-3	N/U	N/U	N/U	226/10																				
6-N	N-P - 70.360 - 359[illegible] - 90-3	227/10																							
7-N	N-P - 71.225 - 2[illegible] - 90-3	N/U		*																					
8-N	N-P - 72.330 - 23[illegible] - 90-3	228/10																							
9-N	N-P - 73.030 - 17[illegible] - 92.5-4	230/10			230/25												230/15								
10-N	N-P - 73.274 - 0[illegible] - 120-4	N/U																							
11-N	N-P - 73.224 - 1[illegible] - 180-3	232/10																							
12-N	N-P - 69.330 - 23[illegible] - CA-4	301/50mv		*																					
13-N	N-P - 68.865 - 11[illegible] - CA-4	302/50 mv																							
14-N	N-P - 70.350 - 359[illegible] - CA-4	337/50mv																							
15-N	N-P - 72.3[illegible] - 24[illegible] - CA-4	338/50mv																							

*Continuous to end

Measurement Number	Identification	READING NUMBER 31	33	34	36	37	38	51	57	61	63	64	65	69	70	73	78	84	88	89	91	92	93	96	97
16-N	N-P - 70.401 - 180[illegible] - 90-4	233/10											N/U	233/10								N/U	233/10		N/U
17-N	N-P - 70.[illegible] - 1[illegible] - 90-3	234/10											N/U	234/10								N/U	234/10		N/U
18-N	N-P - 71.[illegible] - 1[illegible] - 90-4	235/10											N/U	235/10								N/U	235/10		N/U
19-N	N-P - 71.004 - 1[illegible] - 90-4	N/U																	N/U	134/15					
20-N	N-P - 71.053 - 1[illegible] - 90-4	237/10											N/U	237/10								N/U	237/10		N/U
21-N	N-P - 71.978 - [illegible] - 90-4	238/10											N/U	238/10								N/U	238/10		N/U
22-N	N-P - 71.946 - 1[illegible] - 90-4	239/10											N/U	239/10								N/U	239/10		N/U
23-N	N-P - 71.955 - 1[illegible] - 90-3	N/U																	N/U	159/15					
24-N	N-P - 71.[illegible] - 1[illegible] - 90-3	N/U		*																					
25-N	N-P - 71.[illegible] - 2[illegible] - 90-3	240/10											N/U	240/10								N/U	240/10		N/U
26-N	N-P - 71.[illegible] - 6[illegible] - 90-3	N/U																							
27-N	N-P - 71.[illegible] - 1[illegible] - 90-3	243/10		N/U	243/10								N/U	243/10								N/U	243/10		N/U
28-N	N-P - 71.[illegible] - 2[illegible] - 90-3	N/U		*																					
29-N	N-P - 71.[illegible] - 2[illegible] - 90-3	245/10												245/10									245/10		
30-N	N-P - 71.957 - 1[illegible] - 90-3	246/10												246/10									246/10		
31-N	N-P - 71.971 - 2[illegible] - 90-4	247/10												247/10									247/10		
32-N	N-P - 71.970 - 1[illegible] - 90-4	N/U		*																					
33-N	N-P - 71.979 - 3[illegible] - 90-4	249/10												249/10									249/10		
34-N	N-P - 72.43[illegible] - 1[illegible] - 90-4	250/10												250/10									250/10		

*Continuous to end

TABLE 5-4 (Continued)

Measurement Number	Identification	READING NUMBER 31	33	34	36	37	38	51	57	61	63	64	65	69	70	73	78	82	89	59	91	92	93	96	97
35-00	003 - P - 65.34 - X - 180-X	251/10	→	*																					
1-F	S-P - 1A - 172 - X-3	N/U																							
2-F	S-P - 1A - 25 - X-3	244/200						73/300																	
3-F	S-P - 1C - 175 - X-3	N/U					N/U	74/300																	
4-F	S-P - 1C - 25 - X-3	N/U		*																					
5-F	S-P - 2C - 175 - X-4	N/U	123/500	→	123/500	231/500	231/500	75/500																	
6-F	S-P - 2C - 25 - X-4	N/U	124/500	→	124/500																				
7-F	1-P - 3B - 95 - X-4	N/U					N/U	76/300																	
8-F	1-P - 3B - 275 - X-4	N/U		*																					
9-F	0-P - 1B - 30 - X-4	240/200						77/300																	
10-F	0-P - 1B - 270 - X-3	241/200		*																					
11-F	0-P - 4 - 90 - X-4	N/U					N/U	78/300																	
12-F	0-P - 4 - 270 - X-4	Not Routed																							
13-F	0-P - 2A - 90 - X-4	Not Routed																							
14-F	0-P - 2A - 270 - X-3	N/U					N/U	79/500																	
15-F	0-P - 3A - 90 - X-4	N/U	→	N/U	123/500	→		80/300																	
16-F	0-P - 3A - 270 - X-3	N/U	→	N/U	124/500																				
17-F	S-T - 1A - 188 - CA-3	53/50																							
18-F	S-T - 1A - 30 - CA-3	54/50																							
19-F	S-T - 1C - 180 - CA-4	55/50																							
20-F	S-T - 1C - 30 - CA-4	56/50																							
21-F	S-T - 2C - 180 - CA-3	57/50																							
22-F	S-T - 2C - 30 - CA-3	58/50																							
23-F	S-T - 3C - 90 - CA-4	59/50																							
24-F	S-T - 3C - 270 - CA-4	60/50																							
25-F	S-T - 4C - 90 - CA-4	61/50		→	*																				
26-F	S-T - 4C - 270 - CA-3	62/50																							
27-F	S-T - 2A - 90 - CA-4	63/50																							
28-F	S-T - 2A - 270 - CA-3	64/50																							
29-F	S-T - 4 - 90 - CA-4	65/50																							
30-F	S-T - 4 - 270 - CA-3	66/50																							
31-F	S-T - 3A - 90 - CA-4	67/50																							
32-F	S-T - 3A - 270 - CA-3	68/50																							
33-F	S-P - 1GN O_2 - Y - X-3	248/200																							
34-F	S-P - 1GN O_2	Not Routed																						239/500	→
35-F	S-P - 1GN O_2 - X - X-4	236/300	→																						
36-F	S-P - 1GN O_2	Not Routed																						250/500	→
37-F	S-P - 1GN N_2 - X - X-4	252/300	→																						
38-F	S-P - 1GN N_2	Not Routed																						253/500	→
39-F	S-P - 1GN N_2 - X - X-4	253/300	→																						
40-F	S-P - 1GN N_2	Not Routed																							
41-F	S-P - H_2O IN (TIP) - X - X-4																								
42-F	S-P - H_2O IN (TIP) - Y - Y-4																								
43-F	S-P - H_2O IN (LE) - X - X-4	Visually Monitored																							
44-F	S-P - H_2O IN (TIP) - X - X-4																								
45-F	S-P - H_2O IN - Y - X-3																								

*Continuous to end

TABLE 5-4 (Continued)

Measurement Number	Identification	READING NUMBER																							
		31	33	34	36	37	38	51	57	61	63	64	65	69	70	73	78	84	88	89	91	92	93	96	97
46-F	OC-P - H_2O IN (A) - X - X-4	Visually Monitored																							
47-F	OC-P - H_2O IN (B) - X - X-4																								
48-F	OC-P - H_2O IN (C) - X - X-4																								
49-F	OC-P - H_2O IN (D) - X - X-4																								
50-F	S-P - H_2O OUT (TIP) - X - X-4																								
51-F	1-P - H_2O OUT - X - X-3																								
52-F	ST-P - H_2O OUT (LE) - X - X-3																								
53-F	ST-P - H_2O OUT (SIDE) -X-X-3																								
54-F	C-P - H_2O OUT -X-X-3																								
55-F	OC-P - H_2O OUT (A) - X - X-3																								
56-F	OC-P - H_2O OUT (B) - X - X-3																								
57-F	OC-P - H_2O OUT (C) - X - X-3																								
58-F	OC-P - H_2O OUT (D) - X - X-3																								
59-F	S-ΔT - H_2O OUT - X - CuC-4	370/Δ5mv												386/5mv											
60-F	S-ΔT - H_2O IN - X- CuC-4													387/5mv											
61-F	1-ΔT - H_2O OUT - X - CuC-3	371/ΔT5mv												370/5mv											
62-F	1-ΔT - H_2O IN - X - CuC-4													371/5mv											
63-F	ST-ΔT - H_2O OUT LE - X - CuC-3	372/ΔT5mv												366/5mv											
64-F	ST-ΔT - H_2O IN LE - X - CuC-3													367/5mv											
65-F	ST-ΔT - H_2O OUT (SIDE) -X-CuC-3	373/ΔT5mv												368/5mv											
66-F	ST-ΔT - H_2O IN (SIDE) -X-CuC-4													369/5mv											
67-F	0-ΔT - H_2O OUT - X - CuC-3	374/ΔT5mv												372/5mv											
68-F	0-ΔT - H_2O IN - X - CuC-3													373/5mv											
69-F	HYD-P - IN - X - X-X	Visually Monitored																							
70-F	HYD-P - OUT - X - X-X																								
71-F	ΔT1B - 60.6 - 3 - CuC-4	375/ΔT5mv												374/5mv											
72-F	ΔT1A - 35.75 - 356 - CuC-3													375/5mv											
73-F	ΔT1B - 60.6 - 181 - CuC-4	376/ΔT5mv												376/5mv											
74-F	ΔT1A - 35.75 - 176 - CuC-3													377/5mv											
75-F	ΔT2D - 55.6 - 357 - CuC-3	377/ΔT5mv												352/5mv											
76-F	ΔT2C - 60.5 - 5 - CuC-4													353/5mv											
77-F	ΔT2E - 55.6 - 177 - CuC-4	378/ΔT5mv												383/5mv											
78-F	ΔT2C - 60.5 - 178 - CuC-4													384/5mv											
79-F	ΔT3E - 66.2 - 356 - CuC-3	379/ΔT5mv												359/5mv											
80-F	ΔT3C - 55.6 - 355 - CuC-3													360/5mv											
81-F	ΔT3E - 66.19 - 176 - CuC-4	380/ΔT5mv												361/5mv											
82-F	ΔT3E - 55.6 - 175 - CuC-4													362/5mv											
83-F	ΔT4A - 72.26 - 356 - CuC-4	381/ΔT5mv												378/5mv											
84-F	ΔT4B - 66.38 - 356 - CuC-4													379/5mv											
85-F	ΔT4A - 72.26 - 176 - CuC-4	382/ΔT5mv												380/5mv											
86-F	ΔT4B - 66.38 - 176 - CuC-4													381/5mv											

TABLE 5-4 (Continued)

Measurement Number	Identification	READING NUMBER 31	33	34	36	37	38	51	57	61	63	64	65	69	70	73	78	84	88	89	91	92	93	96	97
73-F	ΔT5J - 40.0 - 4 - CuC-3	383/ΔT5mv	→	→	→	→	→	→	→	→	→	→	→	→	361/5mv	→	→	→	→	→	→	→	→	→	→
74-F	ΔT5K - 47.84 - 357 - CuC-3		→	→	→	→	→	→	→	→	→	→	→	→	363/5mv	→	→	→	→	→	→	→	→	→	→
75-F	ΔT5J - 40.0 - 184 - CuC-4	384/ΔT5mv	→	→	→	→	→	→	→	→	→	→	→	→	354/5mv	→	→	→	→	→	→	→	→	→	→
76-F	ΔT5K - 47.84 - 181 - CuC-4		→	→	→	→	→	→	→	→	→	→	→	→	355/5mv	→	→	→	→	→	→	→	→	→	→
77-F	ΔT5M - 50.8 - 358 - CuC-3	385/ΔT5mv	→	→	→	→	→	→	→	→	→	→	→	→	364/5mv	→	→	→	→	→	→	→	→	→	→
78-F	ΔT5L - 48.58 - 357 - CuC-3		→	→	→	→	→	→	→	→	→	→	→	→	356/5mv	→	→	→	→	→	→	→	→	→	→
79-F	ΔT5K - 56.3 - 180 - CuC-4	386/ΔT5mv	→	→	→	→	→	→	→	→	→	→	→	→	357/5mv	→	→	→	→	→	→	→	→	→	→
80-F	ΔT5L - 48.58 - 181 - CuC-4		→	→	→	→	→	→	→	→	→	→	→	383/5mv	→	→	→	→	→	→	→	→	→	→	→
81-F	ΔT5P - 60.10 - 356 - CuC-3	387/ΔT5mv	→	→	→	→	→	→	→	→	→	→	→	383/5mv	→	→	→	→	→	→	→	→	→	→	→
82-F	ΔT5N - 52.8 - 354 - CuC-3		→	→	→	→	→	→	→	→	→	→	→	382/5mv	→	→	→	→	→	→	→	→	→	→	→
83-F	ΔT5P - 60.10 - 176 - CuC-4	388/ΔT5mv	→	→	→	→	→	→	→	→	→	→	→	383/5mv	→	→	→	→	→	→	→	→	→	→	→
84-F	ΔT5N - 52.8 - 174 - CuC-4		→	→	→	→	→	→	→	→	→	→	→	360/5mv	→	→	→	→	→	→	→	→	→	→	→
85-F	ΔT - H_2O OUT - X - X-3	389/ΔT5mv	→	→	→	→	→	→	→	→	→	→	→	362/5mv	→	→	→	→	→	→	→	→	→	→	→
86-F	ΔT - H_2O IN - X - X-4		→	→	→	→	→	→	→	→	→	→	→	→	→	→	→	→	→	→	→	→	→	→	→
87-F	T - H_2O OUT - X - X-3	Visually Monitored																							
88-F	T - H_2O IN - X - X-4																								
89-F	T - H_2O - 52.8 - 27 - CA-3	390/5mv	→	*																					
90-F	T - H_2O - 57.8 - 30 - CA-4	391/5mv	→	→	→	→	→	→	→	→	→	→	→	→	391/5mv	→	→	→	→	→	→	→	→	→	→
91-F	PURGE CAVITY PA-1-X - X - X-3	254/50	→	→	→	→	→	254/50	→	→	→	→	→	→	→	→	→	→	→	→	→	→	→	→	→
92-F	PURGE CAVITY PA-2-X - X - X-3	255/25	→	→	255/50	→	→	→	→	→	→	→	→	→	→	→	→	→	→	→	→	→	→	→	→
93-F	PURGE CAVITY PB-1-X - X - X-3	256/25																							
94-F	PURGE CAVITY PB-2-X - X - X-3	257/25																							
95-F	INNER BODY CAV PRES - X - X-4	258/50																							
96-F	INNER BODY CAV TEMP - Y-X-CA-	59/5																							
97-F	PURGE CAVITY TA1 - X - X - CA-	260/5mv		*																					
98-F	PURGE CAVITY TA2 - X - X - CA-	305/5mv																							
99-F	PURGE CAVITY TB1 - X - X - CA-	306/5mv																							
100-F	PURGE CAVITY TB2 - X - X - CA-	307/5mv																							
101-F		N/U																							
102-F		N/U																							
103-F		N/U																							
104-F		N/U																							
105-F		N/U																							
106-F	PURGE CAVITY	70/50																							
107-F	PURGE CAVITY	71/50		*																					
108-F	PURGE CAVITY	72/50																							

*Continuous to end

TABLE 5-4 (Continued)

Measurement Number	Identification	READING NUMBER 65	92	97
ICE	CE-PT - 66.74 - 0 - 00 - X	155/75	155/50	155/75
2	CE-PS - 67.04 - 0 - 13 - X	156/50	156/15	155/50
3	CE-PS - 67.04 - 0 - 109 - X	157/50	157/15	156/50
4	CE-PS - 67.04 - 0 - 193 - X	158/50	158/15	157/50
5	CE-PS - 67.04 - 0 - 283 - X	159/50	159/15	158/50
6	CE-PT - 66.74 - 110 - 00 - X	160/75	160/50	159/75
7	CE-PS - 67.04 - 110 - 18 - X	161/50	161/15	160/50
8	CE-PS - 67.04 - 110 - 108 - X	162/50	162/15	161/50
9	CE-PS - 67.04 - 110 - 198 - X	163/50	163/15	162/50
10	CE-PS - 67.04 - 110 - 288 - X	164/50	164/15	163/50
11	CE-PT - 66.74 - 180 - 00 - X	165/75	165/50	164/75
12	CE-PS - 67.04 - 180 - 1 - X	166/50	166/15	165/50
13	CE-PS - 67.04 - 180 - 91 - X	167/50	167/15	166/50
14	CE-PS - 67.04 - 180 - 181 - X	169/50	168/15	167/50
15	CE-PS - 67.04 - 180 - 271 - X	170/50	170/15	169/50
16	CE-PT - 66.74 - 280 - 00 - X	171/75	171/50	170/75
17	CE-PS - 67.04 - 280 - 355 - X	172/50	172/15	171/50
18	CE-PS - 67.04 - 280 - 95 - X	173/50	173/15	172/50
19	CE-PS - 67.04 - 280 - 175 - X	174/50	174/15	173/50
20	CE-PS - 67.04 - 280 - 265 - X	177/50	177/15	177/50
21	CE-PT - 66.74 - 330 - 00 - X	178/75	178/50	178/75
22	CE-PS - 67.04 - 330 - 3 - X	179/50	179/15	179/50
23	CE-PS - 67.04 - 330 - 93 - X	233/50	233/15	233/50
24	CE-PS - 67.04 - 330 - 183 - X	234/50	234/15	234/50
25	CE-PS - 67.04 - 330 - 273 - X	235/50	235/15	235/50
26	CE-G-GS - 30 - X - X	LeRC sys	LeRC	LeRC
27	CE-G-TT - 30 - P/R - X	LeRC sys	124/20	124/20
28	CE-G-RT - 30 - C/A - X	LeRC sys	142/20	142/20
29	CE-G-PT - 30 - X - X	237/75	237/50	237/75
30	CE-G-PS - 30 - X - X	238/60	238/30	238/60
31	CE-G-GS - 70 - X - X	LeRC sys	LeRC	LeRC
32	CE-G-TT - 70 - P/R - X	LeRC sys	81/20	81/20
33	CE-G-RT - 70 - CA - X	LeRC sys	231/20	231/20
34	CE-G-PT - 70 - X - X	239/75	239/50	239/75
35	CE-G-PS - 70 - X - X	242/60	242/30	242/60
36	CE-G-GS - 170 - X - X	LeRC sys	LeRC	LeRC
37	CE-G-TT - 170 - X - X	LeRC sys	82/20	82/20
38	CE-G-RT - 170 - X - X	LeRC sys	244/20	244/20
39	CE-G-PT - 170 - X - X	243/75	243/50	243/75
40	CE-G-PS - 170 - X - X	245/60	245/30	245/60
41	CE-G-GS - 260 - X - X	LeRC sys	LeRC	LeRC
42	CE-G-TT - 260 - X - X	LeRC sys	345/20	LeRC
43	CE-G-RT - 260 - X - X	LeRC sys	LeRC	LeRC
44	CE-G-PT - 260 - X - X	246/75	246/50	246/75
45	CE-G-PS - 260 - X - X	247/60	247/30	247/60
46	CE-G-GS - 350 - X - X	LeRC sys	LeRC	LeRC
47	CE-G-TT - 350 - X - X	LeRC sys	346/20	LeRC
48	CE-G-RT - 350 - X - X	LeRC sys	140/20	140/20
49	CE-G-PT - 350 - X - X	249/75	249/50	249/75
50	CE-G-PS - 350 - X - X	250/60	250/30	250/60

6. OBSERVED DATA

6.1 SCHLIEREN SYSTEM

A Schlieren system was installed to record the airflow pattern around the inlet section of the HRE-AIM. This system was recorded by photographic means and on a video tape. The Schlieren system was an invaluable guide for ascertaining that tunnel start and HRE-AIM inlet start had been attained. Also, after gaining experience, the probable point where HRE-AIM inlet unstart or tunnel unstart could be predicted (from the position and shape of the shock wave pattern). Figure 6-1 presents a Schlieren view of a started tunnel and started engine inlet. Figure 6-2 shows a Schlieren photograph of an unstarted tunnel.

6.2 VISUAL RECORDING

A television camera and a motion picture camera were installed in the test cell. Although the view was quite limited, this visual aid assisted in making decisions during test. In addition, video tape recording permitted instant replay of the test run, where special conditions or a sequence could be observed, thereby assisting in interpretation of data or in sequencing or observing events for follow-on tests.

6.3 PHYSICAL CONDITION

The general structural integrity and dimensional stability of the HRE/AIM was excellent. Areas where problems were experienced, their probable cause, and method of repair are described below.

6.3.1 Cowl Leading Edge Assembly Mount Screw Failure

The cowl leading edge assembly became separated from the outerbody and its mounting interface during test reference reading No. 27. The separation extended over 30 percent of the circumference with a maximum separation of approximately 0.050 in. in the axial direction at approximately 5:30 o'clock. (See Figure 6-3).

All three sections of the outer cowl body were removed and inspection revealed that a considerable amount of the hot tunnel ambient had entered the cavity between the outer cowl body and the outerbody of the AIM through the opening between the assemblies. (See Figure 6-3). The cavity was pressurized to 16 psia and was deemed sufficient to prevent inflow of the hot tunnel ambient for test conditions anticipated. Inspection revealed an excessively heated zone near the opening, indicating that a shock was located in this area, resulting in a pressure profile greater than anticipated

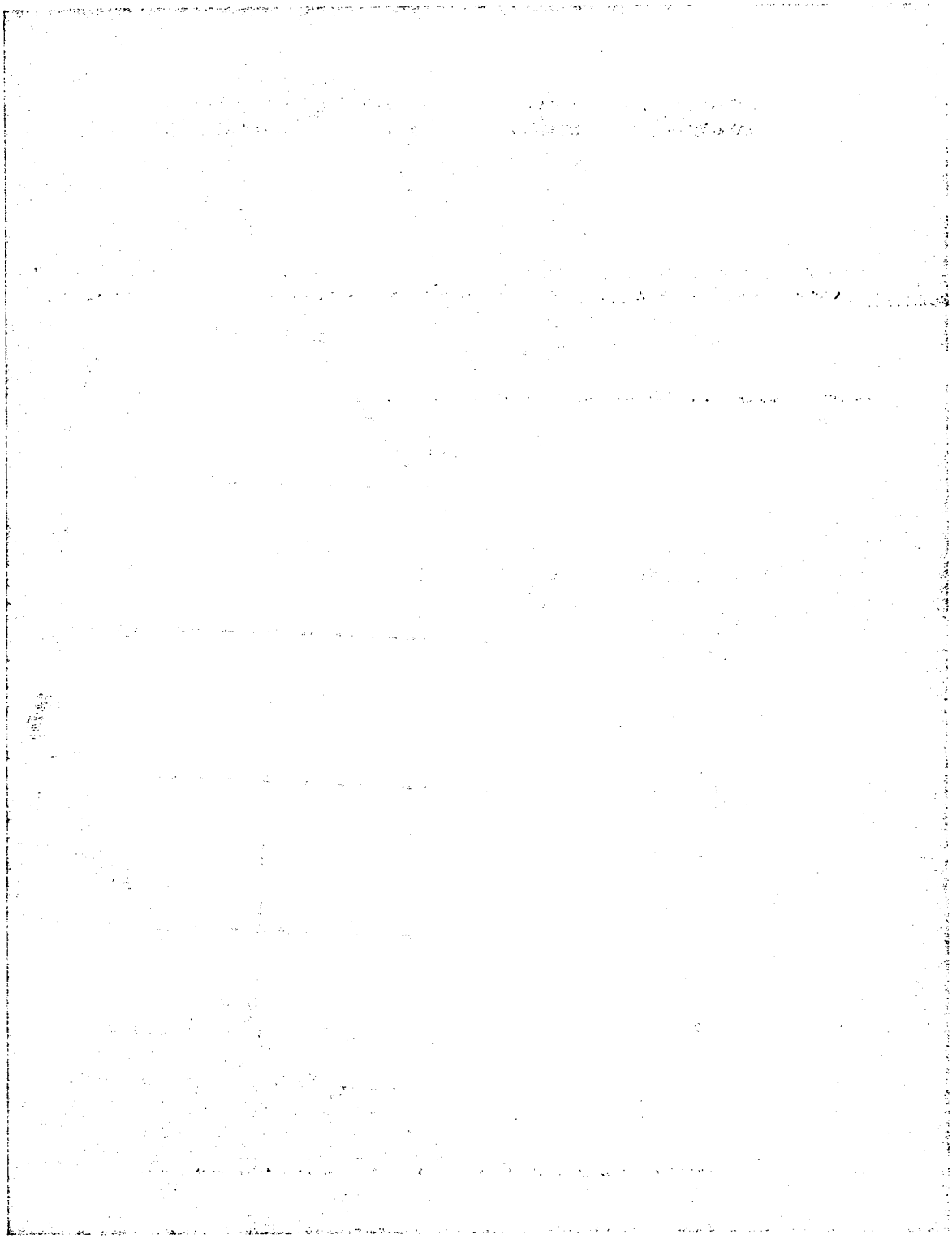

Figure 6-1. Schlieren View, Started Tunnel and HRE Inlet

ORIGINAL PAGE IS
OF POOR QUALITY

Figure C-2. Sector Gear Vibration Instrumentation

for a started tunnel condition. The flange which supports and restrains the cowl leading edge assembly was discolored to a dark-grey color over 20 percent of the circumference at the top center (11:00 o'clock to 1:00 o'clock) and approximately 30 percent of the circumference at the bottom center (4:00 o'clock to 8:00 o'clock). The remaining portion of the flange ranged in color from straw to dark-straw color.

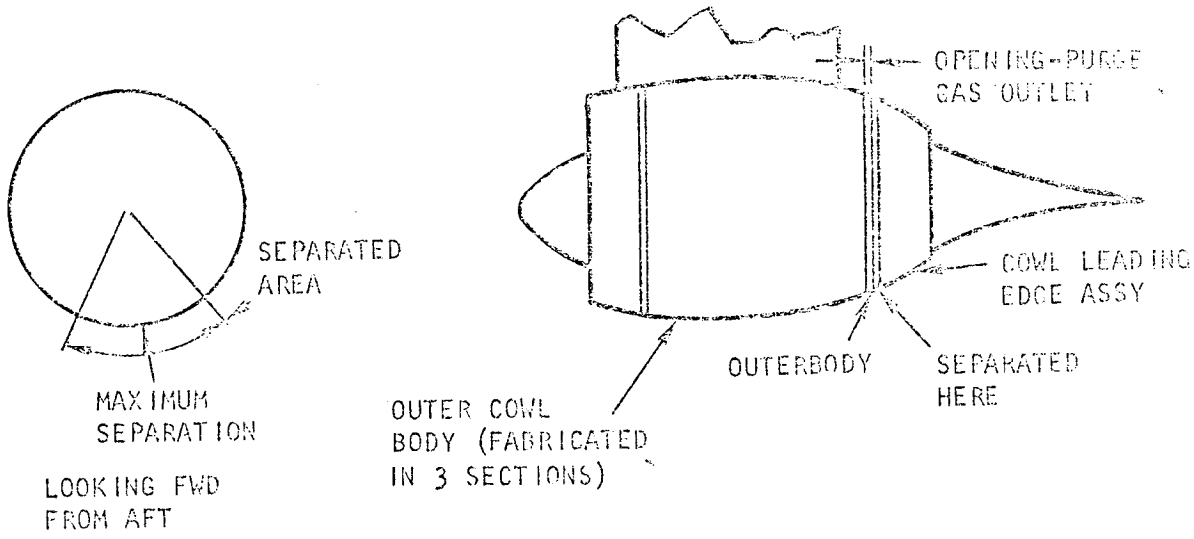

Figure 6-3. Cowl Leading Edge Separation Area

Fifty percent of the screws restraining the cowl leading edge assembly failed at the junction of the screw head and the threaded section. All screws in the grey area of the flange had failed, and the remaining failed screws were randomly distributed over the straw/dark-straw-colored area.

Metallurgical analysis of the failed screws (MS 24698) revealed that the ingested hot tunnel ambient had heated the cadmium plated screws to a point where the cadmium diffused into the high strength steel, alloying in such a manner as to reduce the strength of the material, which then led to the failure of the screws.

These screws were replaced with modified 12-point screws fabricated from A-286 material.

6.3.2 Coolant Leak on the Spike Assembly

Coolant was noted to be leaking from the brazed joint between the ignitor boss and the hot wall of the spike assembly in two places as shown in Figure 6-4a following test reference reading No. 33. Then, after test reference reading No. 35, four additional leaks were noted and the two leaks previously observed had further progressed (see Figure 6-4b).

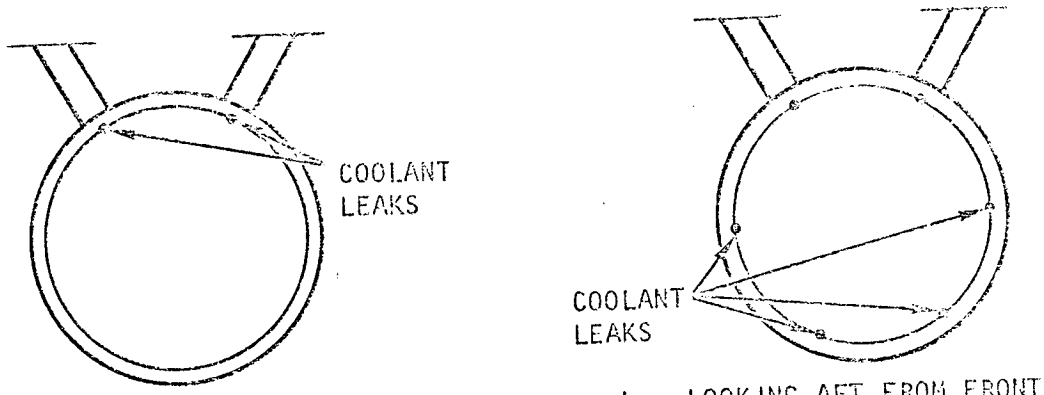

a. LOOKING AFT FROM FRONT

b. LOOKING AFT FROM FRONT

Figure 6-4. Spike Coolant Leakage Areas

Inspection revealed areas of dark-grey discoloration around the failed area, indicating excessive heating. Braze material (Bag 8A) had melted, and erosion of nickel material adjacent to the braze joint was noted (see Figure 6-5a).

The repair operation consisted of grinding the joint (see Figure 6-5b for details) and brazing the joint with braze material having a higher melting temperature and better mechanical properties (NIORO).

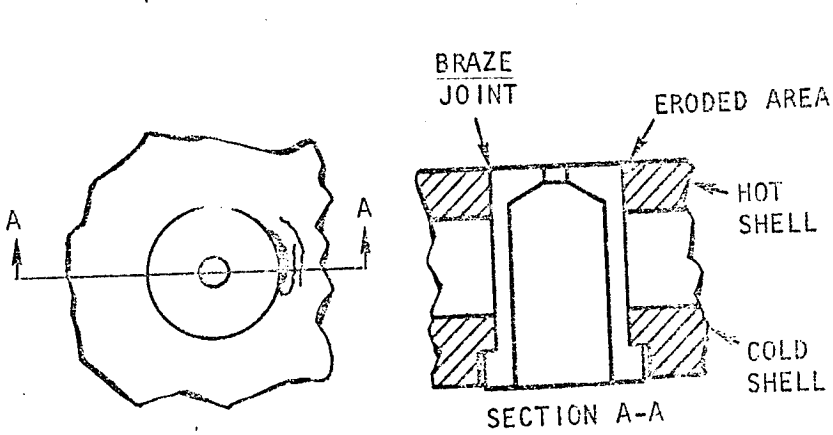

a.

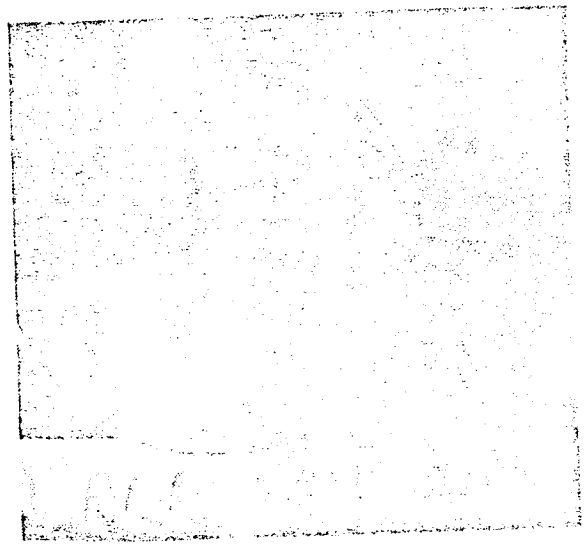

F-20118

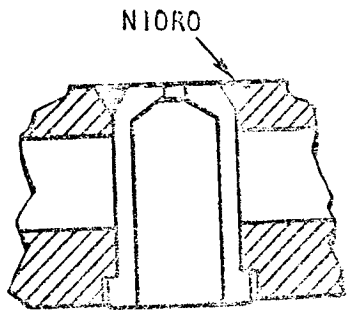

b.

Figure 6-5. Spike Ignitor Boss Braze Joint Failure and Repair

Coolant was again noted to be leaking from this area following test reference reading No. 54. Inspection revealed that the braze joint had failed in shear. Also noted at this time was the visible distortion of the hot wall of the spike assembly adjacent to the ignitor boss (see Figure 6-6). It

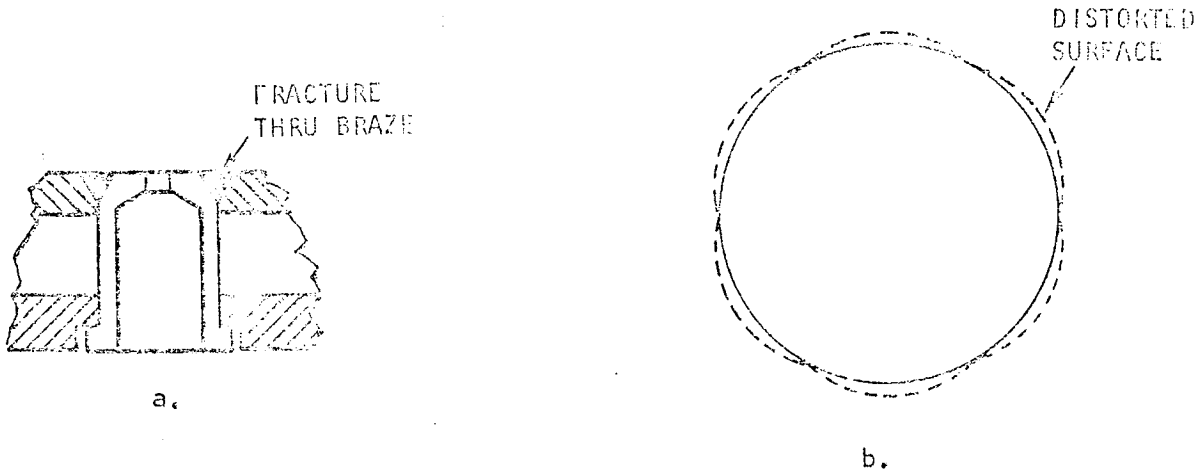

Figure 6-6. Spike Ignitor Boss Braze Joint Second Failure

appeared that the burning of the hydrogen fuel from fuel injector 1A was stratified and that the area approximately 0.5 in. wide by 6 in. long immediately aft of the fuel injector 1A was being heated excessively, resulting in yielding of the hot wall. The repair operation consisted of increasing the depth of the braze joint to the maximum permissible and installing 18 pins approximately 1 in. aft of the ignitor bosses. Also, a decision was made to weld the ignitor outlet shut and purge the ignitor boss with cold gaseous nitrogen to assist the hot nickel shell to maintain its structural integrity (see Figure 6-7).

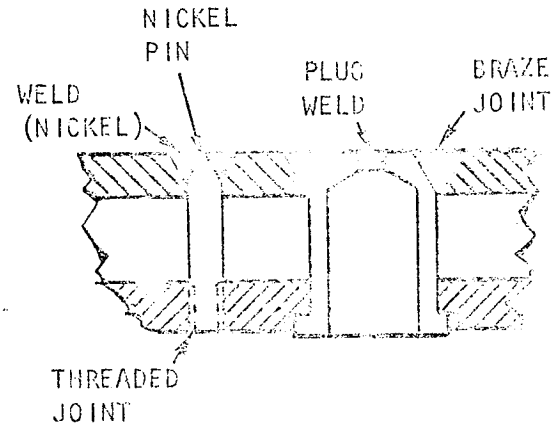

Figure 6-7. Ignitor Boss Repair Operation

No further leaks or problems were observed in this area for the remainder of the test program.

Further aft at Station 48.29 of the spike assembly, a small leak was observed following test reference reading No. 63. Initially, this leak began as a pinhole leak at the interface of the spike skirt assembly and the heavy-walled section of the spike assembly. By the end of the test program, it had progressed to approximately 3/4 in. long by a few thousandths wide. (See Figure 6-8 for details). A similar leak was noted approximately 90 deg away at the same axial station following test reference reading No. 81.

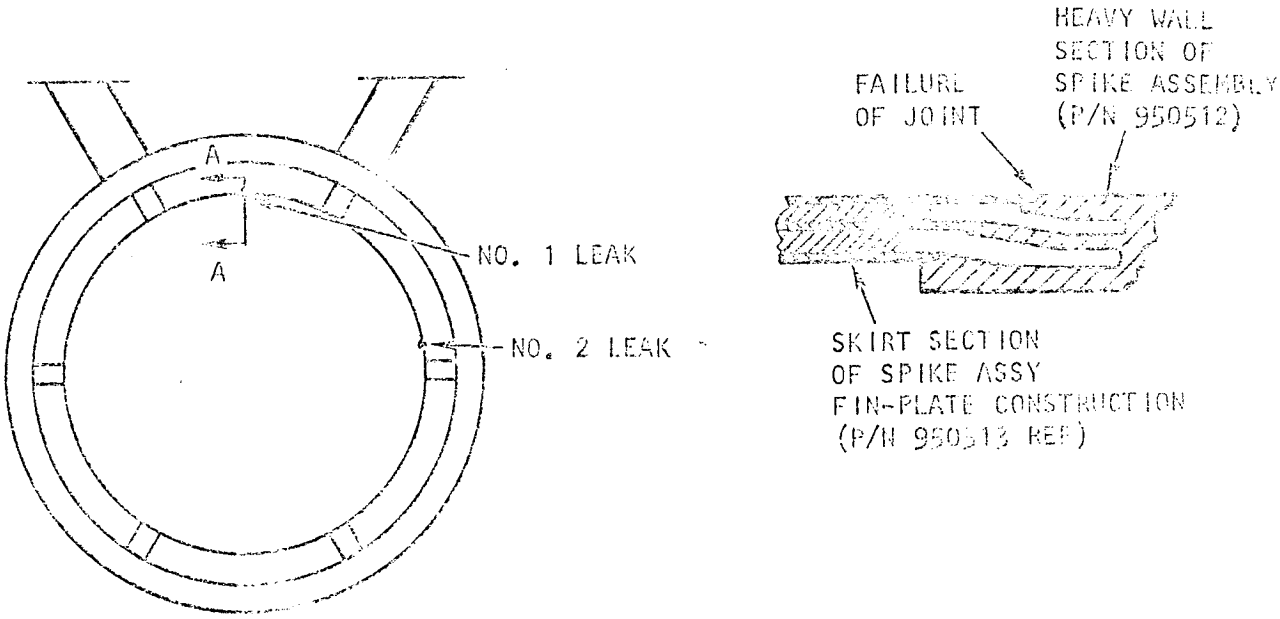

Figure 6-8. Pinhole Leaks in Spike Assembly

Total coolant leakage from these leaks was estimated to be in the order of 1/8 gpm at the end of the test program.

6.3.3 Distortion of the Outerbody Contour

A slightly forward-facing step at the interface of the cowl leading edge assembly and the outerbody was observed following test reference reading No. 61 (see Figure 6-9). The forward-facing step progressed with each test and was noted to be approximately 0.060 in. (per side) following test reference reading No. 64. Also, coolant was noted to be flowing from the fuel injector (see Figure for location). This indicated that the transfer tube connecting the fuel injectors to the fuel manifold had failed and/or the braze joint sealing the fuel injector from the coolant system had failed. Repair of the transfer line could not be achieved without complete disassembly of the unit; hence, no attempt was made to repair this failure. A special

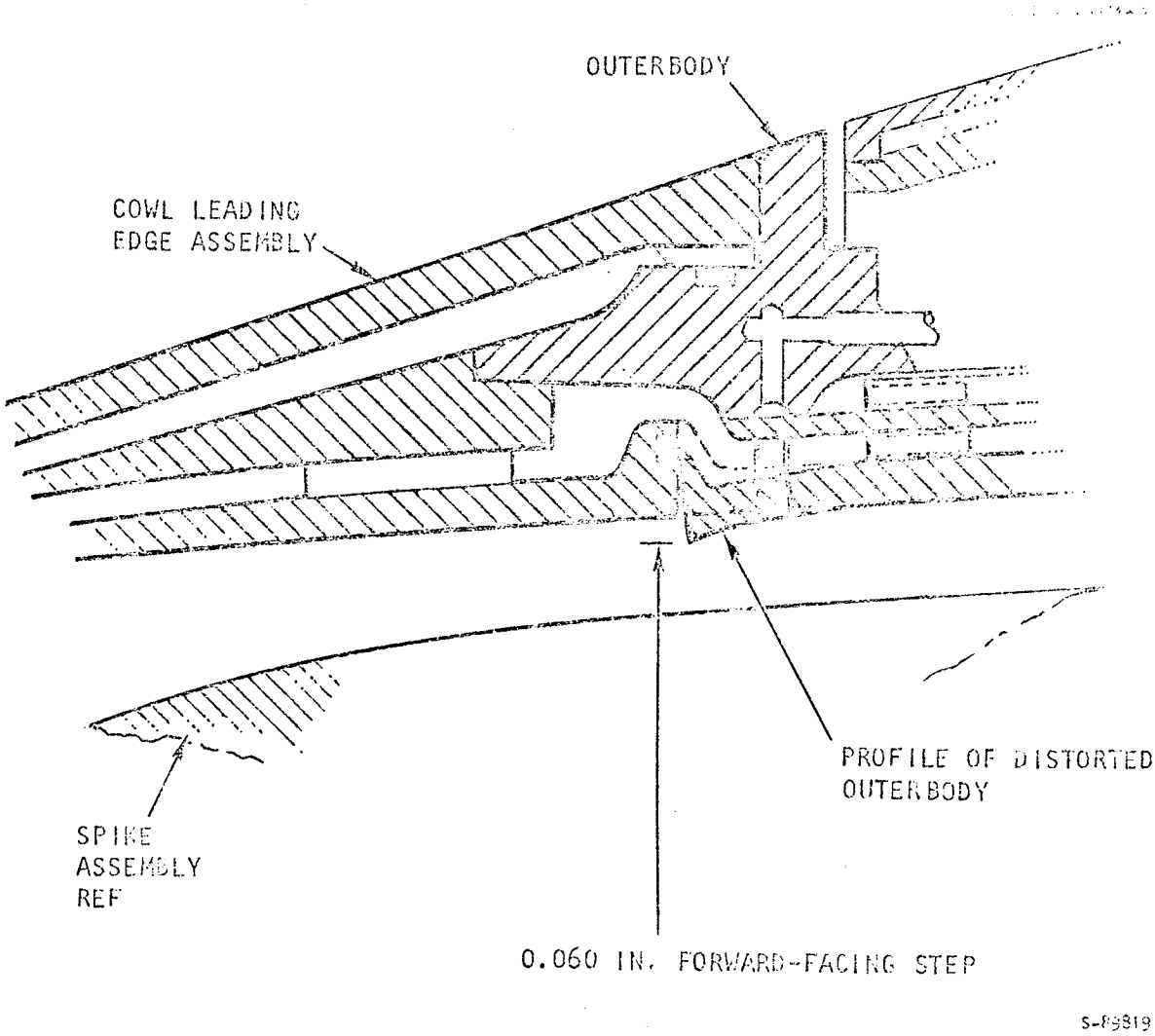

Figure 6-9. Distortion of Outerbody/Cowl Leading Edge Assembly Interface

ORIGINAL PAGE IS
OF POOR QUALITY

expanding mandrel was designed and fabricated, and the repair operation was performed following test reference reading No. 71.

The repair operation consisted of expanding the outerbody hot shell to the desired diameter and adding a restraint to prevent recurrence of the distortion. The expanding tool was designed to expand only the forward section of the outerbody hot wall to prevent further damage to the fuel injector transfer tube. Inspection following the repair operation indicated that the hot wall at Station 40.5 was within 0.004 in. of its nominal drawing dimension (reference Drawing 950610). Pressurizing the coolant passage following this repair indicated that the repair operation was accomplished without further damage to the fuel transfer tubes.

6.3.4 Foreign Object Damage

The surface of the HRE/AIM was noted to change from the shiny, machined finish to a satin finish after the start of the test program. It is believed that fine carbon particles from the heater and the hot train liner were in the hypersonic air stream. The nickel plating on the copper section of the cowl leading edge assembly and the copper tip of the inlet spike assembly were noted to erode as testing progressed. The particle size was small and was not detectable in the television monitor or in the Schlieren system. Later in the test program, the carbon particles became large enough to be visible in the TV monitor (see Figure 6-10). Then, during test reference reading No. 88, greater quantity and larger particles were noted to impinge on the HRE/AIM. Inspection following this run revealed that the leading edge of the outer cowl body support was damaged (see Figure 6-11). It was observed that the damaged area was hit by foreign objects at a higher concentration than other sections of the HRE/AIM. Cursory analyses of the projected path of a foreign object in the hypersonic airstream hitting the conical section of the inlet spike assembly, indicated that the foreign particles could be concentrated into the damaged area (see Figure 6-12). A wedge-shaped, water-cooled protector was designed, fabricated, and installed. Sizable foreign objects were noted to impact the HRE/AIM on tests following installation of this wedge-shaped protector. Enough protection was obtained, however, to complete the test program.

6.3.5 Photographic Record

Photographic record of damaged areas and of areas showing aerodynamic heating were obtained when possible. The configuration of the HRE/AIM was such that in many areas it was difficult to obtain good photographic records, even with studio-type equipment. Photographic service at Plum Brook Station was limited and was not readily available; hence, a Polaroid camera was utilized when necessary. Copies of photos taken by NASA Plum Brook, Polaroid pictures taken by AiResearch on site, and photos taken at AiResearch have been transmitted to NASA/LaRC and are on file at the HRE Project Office.

Major-subject list of photos obtained are:

Installation of AIM in test chamber

Heating of outer cowl body

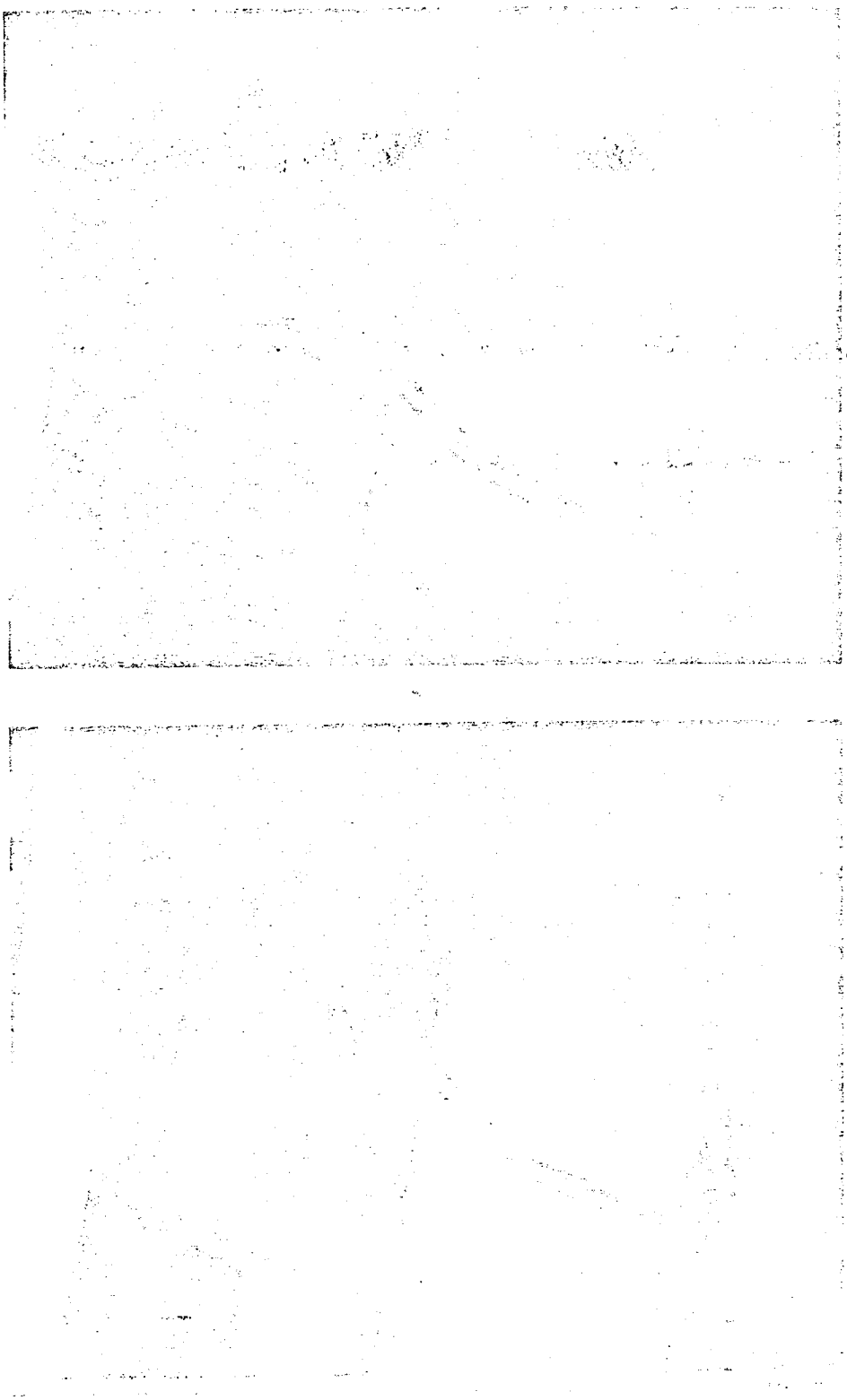

Figure 6-10. HRE/AIM Carbon Particles in Tunnel Flow; AIM F.O.D. (M = 7)

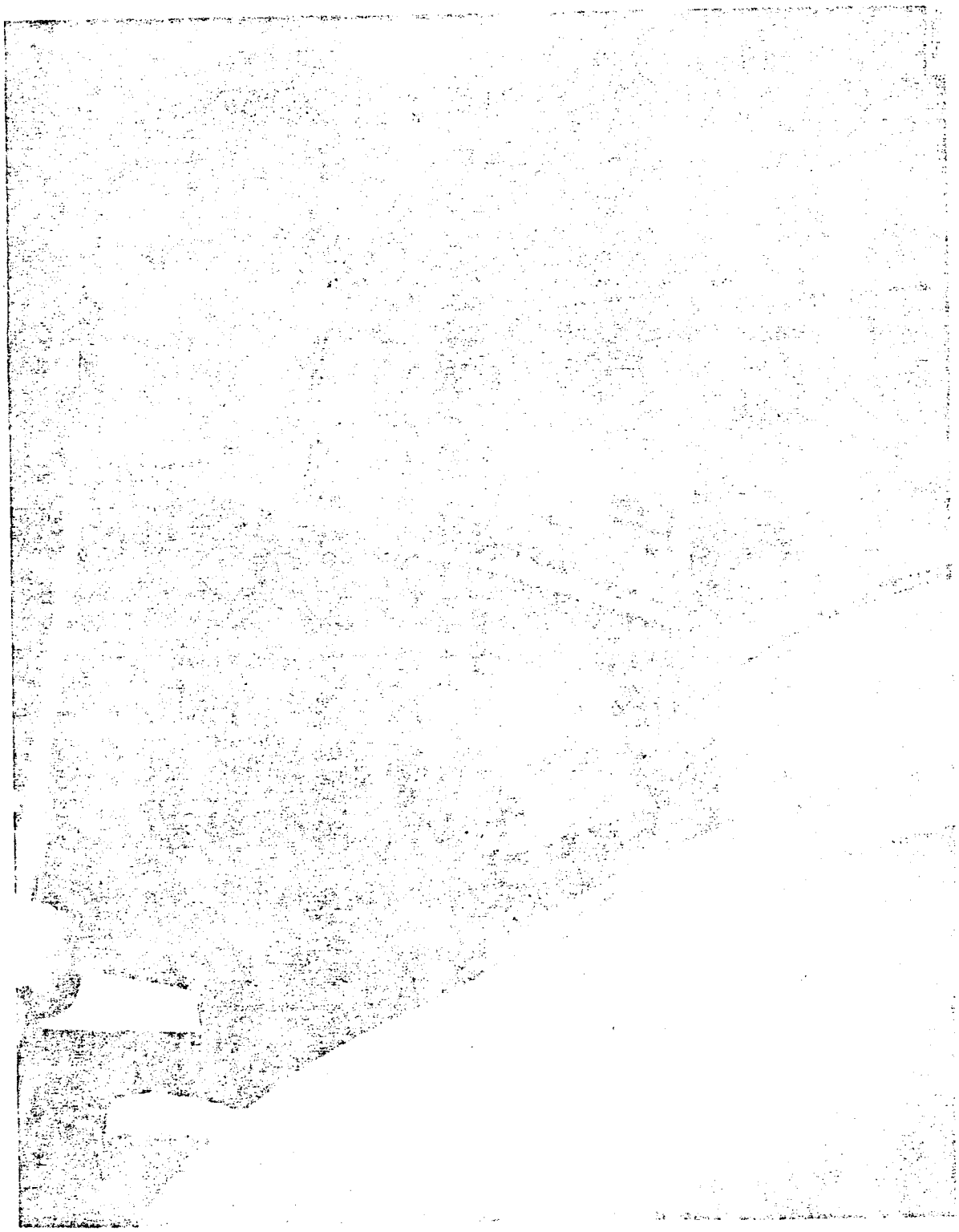

Figure 6-11. Damage to Leading Edge of Outer Coil Body Supports

ORIGINAL PAGE IS
OF POOR QUALITY

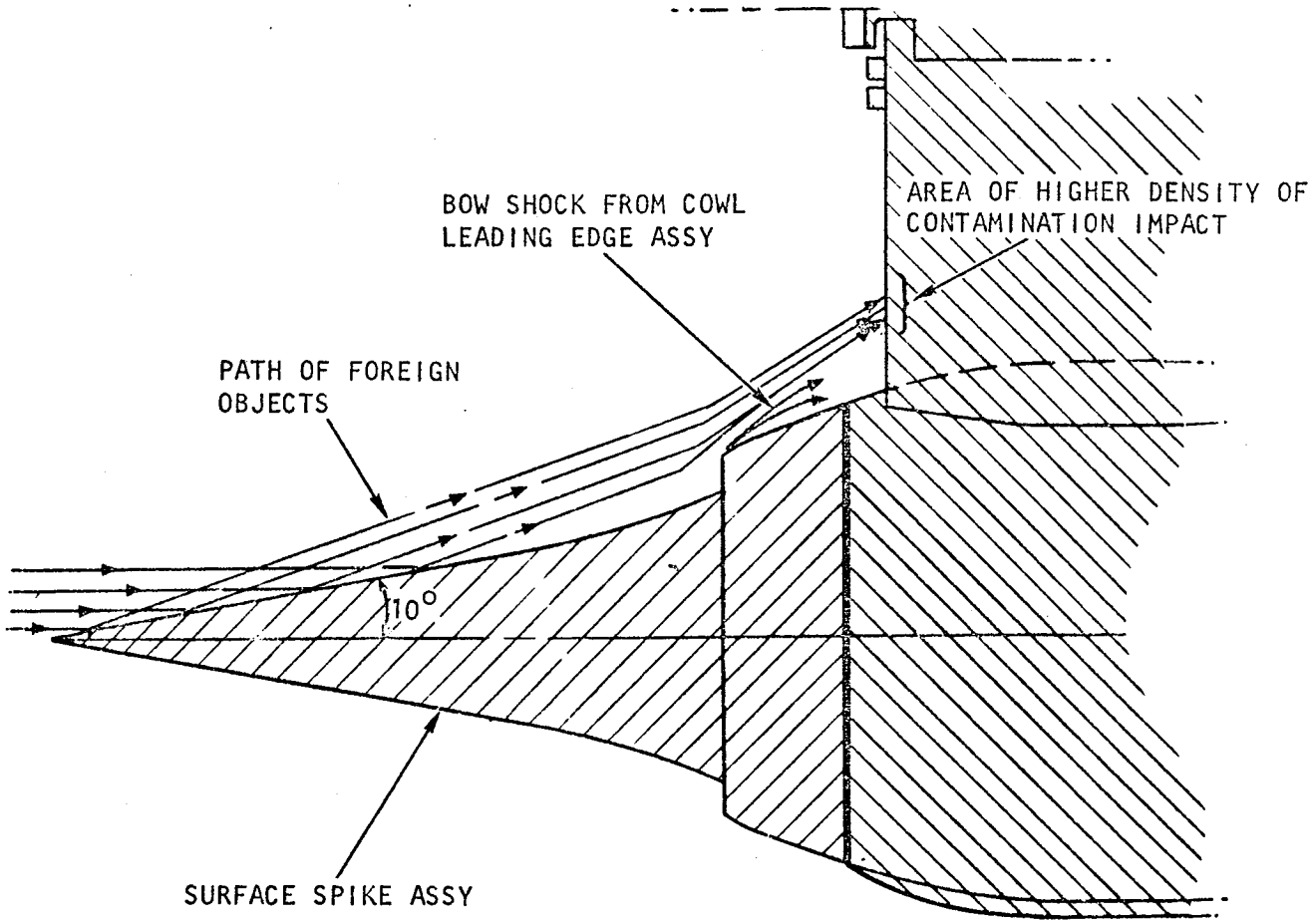

Figure 6-12. Foreign Particles Impinging on Inlet Spike Assembly

Braze failure at the ignitor

Foreign objects in hypersonic airstream

Foreign object damage to cowl leading edge assembly

Foreign object damage to leading edge of the outer cowl body assembly

Heat pattern on the instrumentation rig

Heating pattern aft of the leading edge of the strut assembly

Heating pattern aft of the fuel injector IA and IB

Bow shock, and heating pattern in the combustor zone.

REFERENCES

5-1. Molloy, J. K.; Mackley, E. A.; Keyes, J. W., Effect of Diffusers, Shrouds, and Mass Injection on the Starting and Operating Characteristics of a Mach 5 Free Jet Tunnel, NASA TND-6377, 1971.

5-2. Wieting, A. R., Experimental Blockage Study of a Ramjet Engine (HRE-AIM) Using the Langley 7-Inch Mach 7 Pilot Tunnel, NASA LWP 888, 1970. (Unpublished Langley Working Paper).

APPENDIX A

FUEL CONTROL SYSTEM GH_2

DESIGN CONDITIONS AND CALCULATIONS

TABLE A-1

HFT GH_2 DESIGN CONDITIONS FOR HRE

Sta No.	Req Flow Range, lb/sec		Venturi Flow Range, lb/sec		ΔP Range		Reynold's Number		Upstrm Dia, in.	Throat Dia, in.	β	Approach Factor	TI, °R	PI, psia
	Min	Max	Min	Max	Min	Max	Min	Max	D_1	D_2	D_2/D_1	$1/\sqrt{1-\beta}$		
1A	0.021	.580	.008	.752	.01	100	1.3×10^4	1.2×10^6	1.5	0.750	.500	1.0328		
1B	0.026	.152	.008	.247	.10	100	7.6×10^3	$7. \times 10^5$	1.5	0.450	.300	1.0040		
2A	0.021	.580	.0078	.736	.01	100	1.3×10^4	1.2×10^6	2.3	0.750	.3260	1.0057		
3 (Sub)	0.021	.580	.0078	.736	.01	100	1.3×10^4	1.2×10^6	2.3	0.750	.3260	1.0057		
3A&B (Sub)	0.158	1.518	.068	2.00	.10	100	7.1×10^4	2.1×10^6	2.3	1.22	.5304	1.0420		
4	0.026	.152	.008	.247	.10	100	7.6×10^3	$7. \times 10^5$	1.5	0.45	.300	1.0040		

1600°R* (TI, °R)

900 Psia* (PI, psia)

*see page A-3

S-89717

From ASME "Fluid Meters, Their Theory and Application"
Fifth Edition 1959 Pg 64 Par. 190 Eq 104

$$W = .525 \times C \times F \times E \times YA \times d2^2 \times \sqrt{\rho \Delta P}$$

W = Weight flow (lb/sec)

C = Discharge coefficient (.810 expected-rerange 2×10^3 to 2.5×10^6)*

F = Approach factor $1/\sqrt{1-\beta^4}$

$\beta = d2/d1$

d1 = Upstream diameter (inches)

d2 = Throat diameter (inches)

E = Metal expansion or contraction factor (Pg 424 Vol 1 Mat'l Handbook)

YA = Adiabatic expansion factor (Pg 126)

$$YA = \left[RR^{2/K} \left(\frac{K}{K-1} \right) \left(\frac{1-RR^{\frac{K-1}{K}}}{1-RR} \right) \left(\frac{1-\beta^4}{1-\beta^4 \times RR^{2/K}} \right) \right]^{1/2}$$

RR = P2/P1

P2 = P1 - ΔP

P1 = Upstream press (psia)

P2 = Throat press (psia)

ρ = Density = $\frac{P1 \times 144}{Z \times Rm \times T1}$ (lb /ft^3)

P1 = Upstream press (psia)

Z = Compressibility factor

Rm = R/m

R = Universal gas constant $\left(1545 \frac{\text{ft-lb}}{\text{lb mole } ^\circ R}\right)$

M = Molecular weight (hydrogen-2.016 lb/lb mole)

T1 = Upstream temp $^\circ R$ ($1600^\circ R$)

*References -

1. Discharge Measurements at Low Reynolds Numbers - Special Devices, by A.L. Jorissen ASME Paper No. 54-A-190
2. Discharge Measurements by Means of Cylindrical Nozzles, by A.L. Jorissen and H.T. Newton ASME Paper No 51-A-63
3. A Reassessment of Metering Orifices for Low Reynold's Numbers, by Professor L.J. Kastner and J.C. McVeigh, Process Instn Engr, 1965-1966
4. Bif, Unit of General Signal Corp-Data Sheet Ref No. 160-201-1

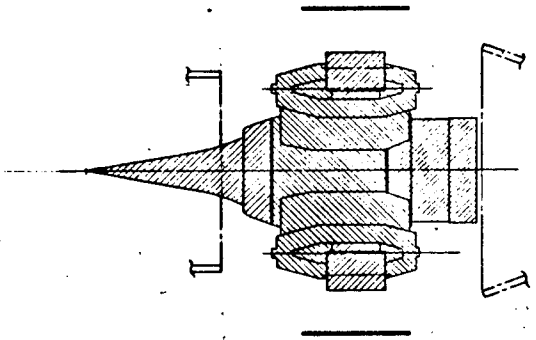

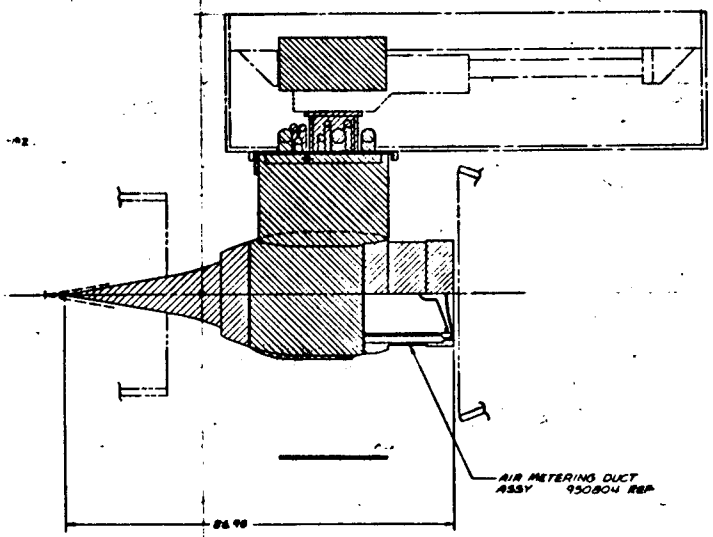

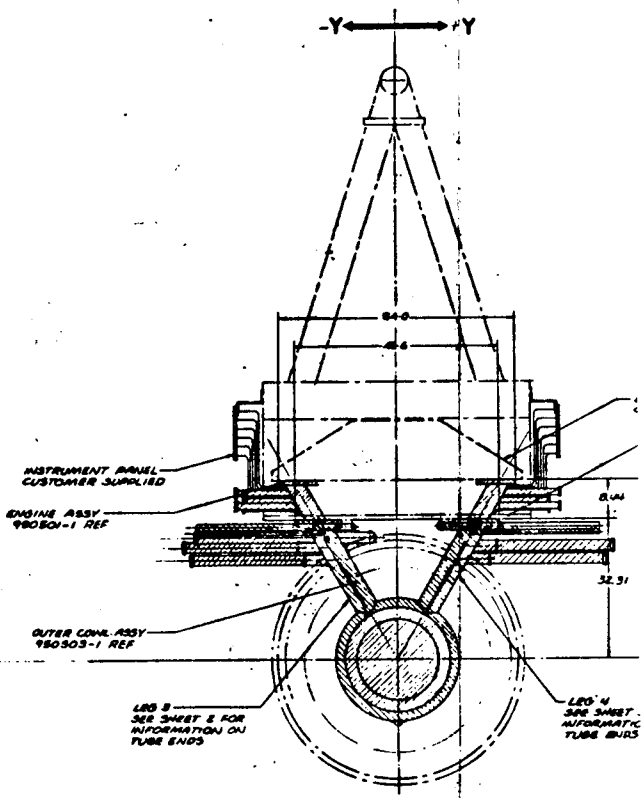

FOLDOUT FRAME 1

FOLDOUT FRAME 2

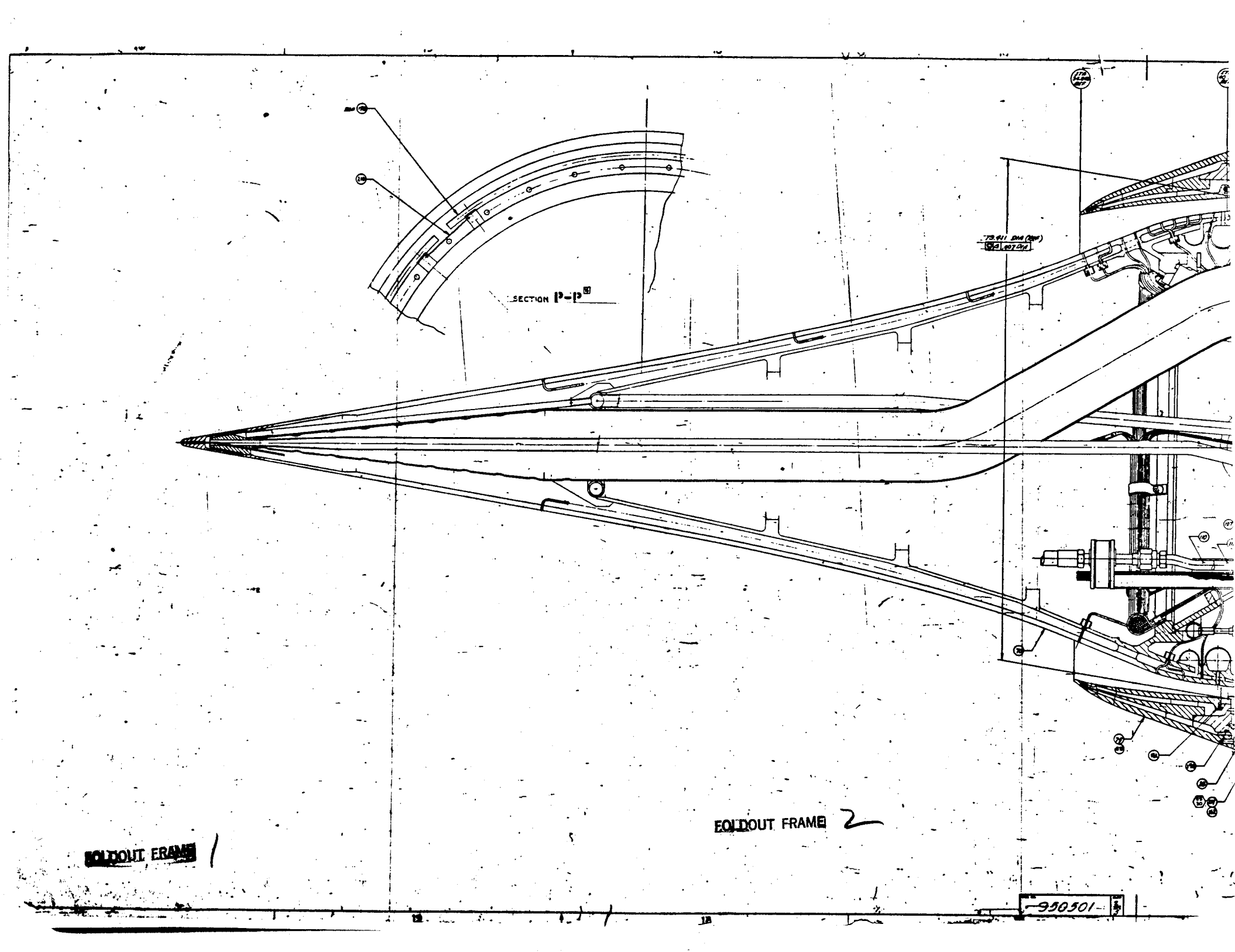
SECTION P-P
FOLDOUT FRAME 1
FOLDOUT FRAME 2
950501

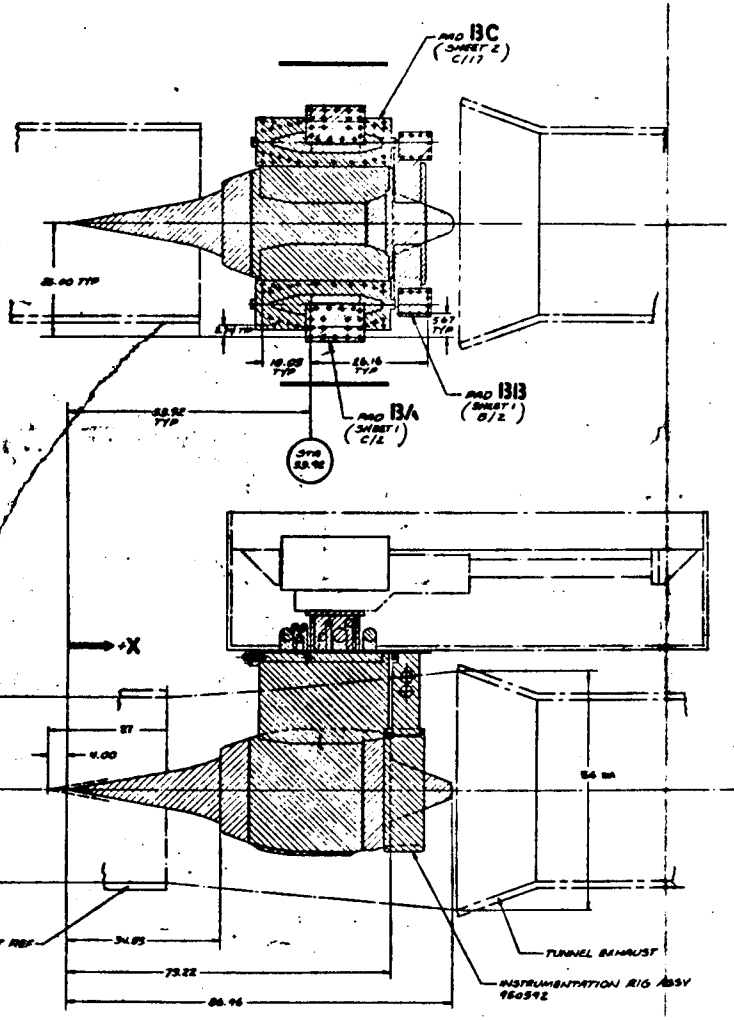

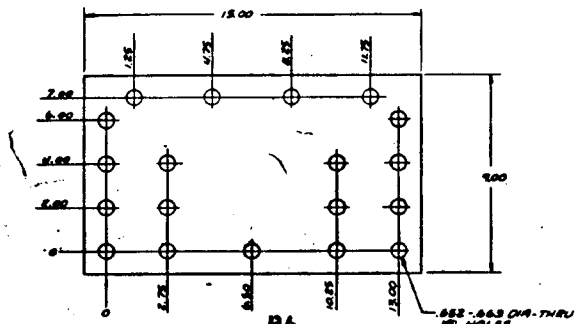

PAD BA
SCALE 1/2
OPPOSITE FOR LEG 8
(SHEET 1)
C/3

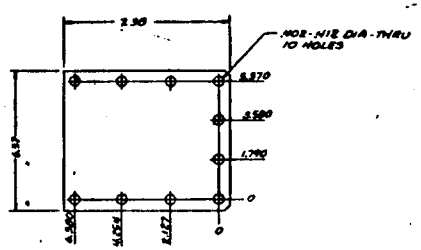

PAD BB
SCALE 1/2
OPPOSITE FOR LEG 3
(SHEET 1)
C/3

FOLDOUT FRAME 4

FOLDOUT FRAME 3

2. STATION 2880 IS VIRTUAL ORIGIN OF INLET SPIKE.

1. PARTS SHOWN SHADED WILL BE SUPPLIED BY AIRESEARCH

OUTLINE-HYPERSONIC RESEARCH ENGINE, AERO-THERMO INTEGRATION MODEL

J | 70210 | 950500

950500

FOLDOUT FRAME 3

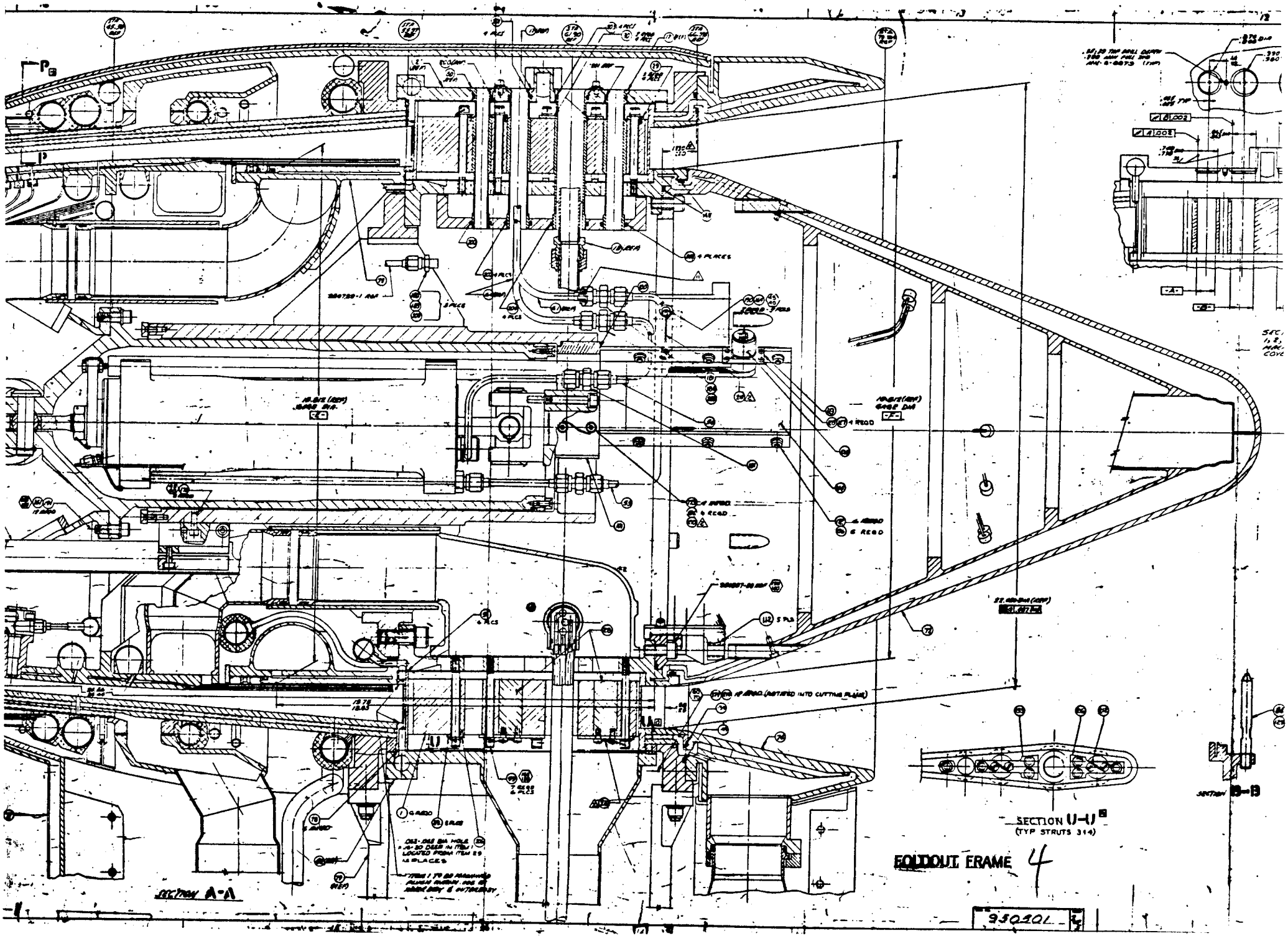

FOLDOUT FRAME 4

950201

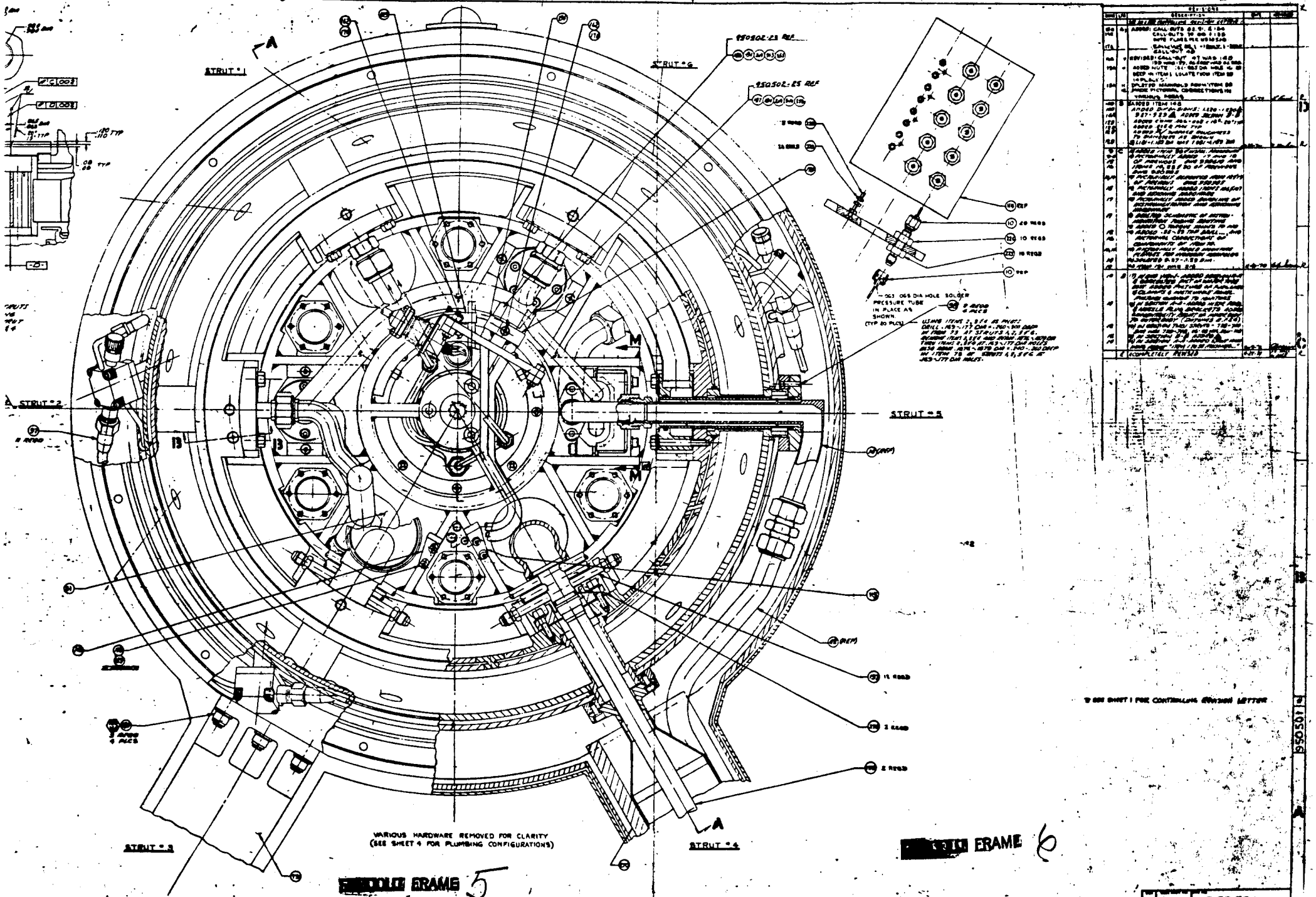

J	70210	950501